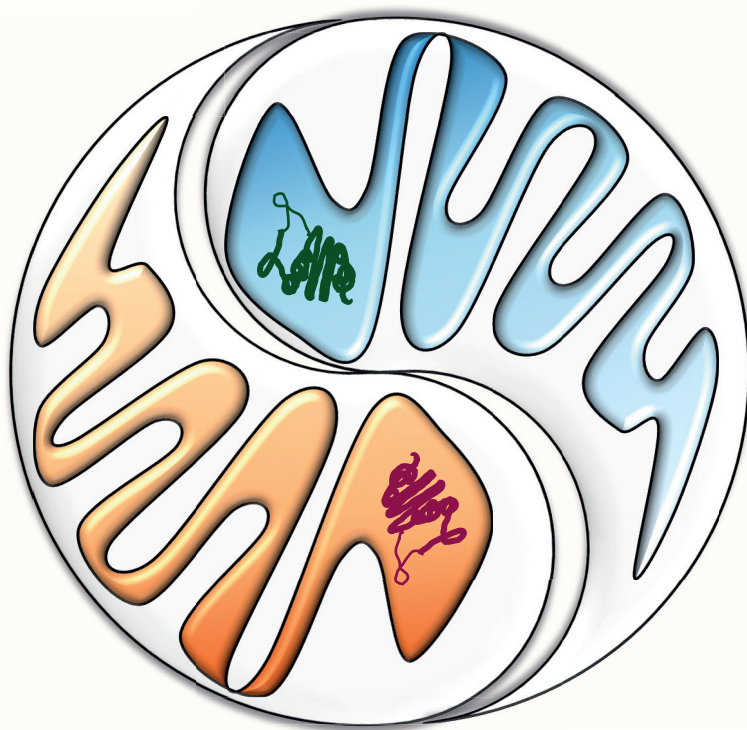


**Small change, big impact:
Functional characterization of human SIRT5 variants**



Taolin Yuan

袁桃林

Propositions

1. Loss-of-function variants of the NAD⁺-dependent deacylase SIRT5 associate with human mitochondrial disease.
(this thesis)
2. SIRT5 is critical for the regulation of human redox homeostasis.
(this thesis)
3. Human beings play a significant role in directing their own evolution through irreversible impacts on climate.
4. Genetic diagnosis of diseases promotes our understanding of the function of proteins.
5. The programming language R makes data visualization fun by incorporating the creativity of the researcher.
6. Technique development is a rate-limiting step in biology research.
7. News should be peer reviewed like scientific papers.
8. The most beautiful thing about research is the dopamine burst elicited by fascinating results.

Propositions belonging to the thesis, entitled
“Small change, big impact: Functional characterization of human SIRT5 variants”

Taolin Yuan
Wageningen, 9 June 2021

**Small change, big impact:
Functional characterization of human SIRT5 variants**

Taolin Yuan

Thesis committee

Promotor

Prof. Dr Jaap Keijer

Professor of Human and Animal Physiology

Wageningen University & Research

Co-promotor

Dr Vincent C. J. de Boer

Assistant professor, Human and Animal Physiology

Wageningen University & Research

Other members

Prof. Dr Ivonne Rietjens, Wageningen University & Research

Prof. Dr Thierry Arnould, University of Namur, Belgium

Prof. Dr Hubert Smeets, Maastricht University, Maastricht

Dr Merel Adjobo-Hermans, Radboud University Medical Center, Nijmegen

This research was conducted under the auspices of the Graduate School VLAG (Advanced studies in Food Technology, Agrobiotechnology, Nutrition and Health Sciences).

**Small change, big impact:
Functional characterization of human SIRT5 variants**

Taolin Yuan

Thesis

submitted in fulfilment of the requirements for the degree of doctor
at Wageningen University
by the authority of the Rector Magnificus,
Prof. Dr A.P.J. Mol,
in the presence of the
Thesis Committee appointed by the Academic Board
to be defended in public
on Wednesday 9 June 2021
at 1.30 p.m. in the Aula

Taolin Yuan

Small change, big impact: Functional characterization of human SIRT5 variants

PhD thesis, Wageningen University, Wageningen, the Netherlands (2021)

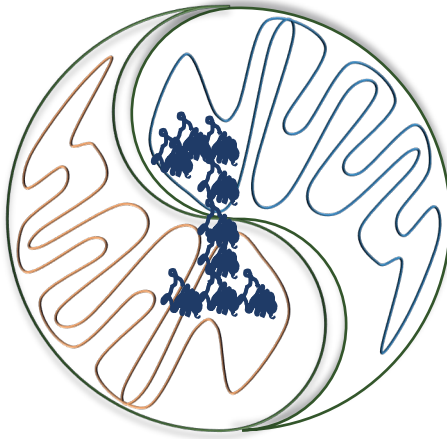
With references, with summary in English

ISBN: 978-94-6395-721-2

DOI: <https://doi.org/10.18174/542143>

Table of contents

Chapter 1	General Introduction	9
Chapter 2	An optimized desuccinylase activity assay reveals a difference in desuccinylation activity between proliferative and differentiated cells	37
Chapter 3	Profiling SIRT5 loss-of-function in humans identifies its critical role in redox homeostasis	63
Chapter 4	Human SIRT5 variant fibroblasts display an impaired glutathione system associated with disrupted Glutathione-Thioredoxin balance	101
Chapter 5	Bayesian hierarchical modelling for Seahorse extracellular flux oxygen consumption rate data analysis	129
Chapter 6	General Discussion	149
Appendices	Summary	171
	Acknowledgements	177
	About the author	
	Curriculum vitae	181
	Education statement	182



General Introduction

Mitochondria are critical for cellular metabolism and health

Mitochondria are double membrane-bound organelles located in the cytoplasm. They are critical to cellular metabolism and organismal health through their numerous functions in bioenergetics, biosynthesis and intracellular signalling^{1, 2}. The most well-known role for mitochondria is their bioenergetic capacity. Mitochondria are responsible for generating the majority of cellular ATP in differentiated cells through integration of nutrients catabolism and ATP generation processes. Fuel sources, including pyruvate, fatty acids and amino acids, are imported into mitochondria^{3, 4, 5, 6} and further metabolized in the tricarboxylic acid (TCA) cycle, where reducing equivalents (NADH and FADH₂) are generated and the reducing equivalents flow through electron transport complexes, embedded in the mitochondrial inner membrane^{7, 8}. The electron transport is coupled to proton transfer from the mitochondrial matrix to the inner membrane space, generating a chemo-electrical potential. This is force that drives ATP synthesis by F1FoATPase (Complex V) also located in the inner membrane. Electron transport couples to ATP synthesis is called oxidative phosphorylation (OXPHOS)⁹. In addition, mitochondria evolved as biosynthetic centres as they are either partly or predominantly involved in the synthesis pathway of nucleotides, amino acids, glucose, fatty acids, cholesterol, iron-sulphur clusters and heme^{2, 10, 11}. For example, mitochondrial citrate, an intermediary metabolite of the TCA cycle, is required for fatty acid and cholesterol synthesis as carbon source. Mitochondrial citrate is first exported to the cytosol by the malate-citrate antiporter¹², and then converted to acetyl-CoA, the building block of fatty acids, by ATP citrate lyase^{13, 14}. Beyond their bioenergy production and biosynthesis functions, mitochondria developed signalling functions to communicate with other parts of cells, such as initiating cell death by releasing mitochondrial cytochrome C¹⁵, and activating transcription of hypoxic genes under limited oxygen condition via reactive oxygen species (ROS)¹⁶, a type of highly reactive molecules generated through electron leak mainly from the electron transport complexes¹⁷. These findings highlight the central role of mitochondria in cellular metabolic networks. In line with this, mitochondrial dysfunction is associated with many common diseases including genetic mitochondrial diseases, cancer, and neurodegenerative disease^{18, 19, 20}.

Genetic mitochondrial disease

Mitochondrial diseases, one of the most complex genetic metabolic disorders, are caused by mutations in either mitochondrial genes or nuclear genes that encode mitochondrial proteins^{21, 22}. Mitochondrial DNA (mtDNA) is a relatively small multicopy genome. Hundred to thousand mitochondria are estimated to be present

per cell, and each mitochondrion contains two to ten copies of mtDNA^{23, 24}. The circular 16569 bp mtDNA contains 37 genes encoding 2 rRNAs, 22 tRNAs and only 13 polypeptides, essential for OXPHOS complexes I, III, IV and V. All other proteins, approximately 1250, are nuclear DNA encoded. MtDNA can be homoplasmic (all mtDNA molecules have the same genotype) or heteroplasmic (coexistence of a mix of mutant and wild type (WT) mtDNA). MtDNA mutations causing mitochondrial diseases are mostly maternally inherited (~75% of the cases) or arise de novo (~25% of the cases)^{21, 25}. The ratio of mutant to WT mtDNA impacts on the severity of clinical symptoms, with higher mutation loads leading to more severe clinical manifestations^{22, 26}. The mtDNA heteroplasmy level is highly variable and can differ between tissue and during the course of life. This contributes to the large variation in the disease onset as well as the clinical abnormalities. Mitochondrial diseases can occur at any phase of a life, including neonatal phase, childhood, or adulthood²⁷. A myriad of different clinical symptoms has been seen in patients with mitochondrial diseases. In these patients, organs with high energy demands, such as brain, skeletal muscle, and heart, are most often affected, and pathologies in brain and muscle are the predominant features^{28, 29}.

At molecular level, OXPHOS dysfunction is present in most, but not all, mitochondrial disease patients. Deficiency in each of five OXPHOS complexes has been seen due to mutations in nuclear or mitochondrial genes encoding complex structural subunits for OXPHOS complexes or assembly factors, but also proteins involved in, mtDNA maintenance and mitochondrial gene translation^{30, 31, 32, 33}. In some cases, mitochondrial disease patients had no evidence of respiratory deficiency, but exhibited neuropathy and multisystem dysfunction. As is, for example, the case for mutations in aconitase 2 (ACO2), a TCA cycle enzyme³⁴. In addition, mitochondrial diseases are commonly paralleled by oxidative stress^{35, 36}. Oxidative stress has been proposed as a potential pathomechanism for mitochondrial disease^{37, 38}. For instance, Friedreich's ataxia (FA), one type of mitochondrial disease caused by mutation in frataxin gene³⁹, has been shown to enhance patients' fibroblasts sensitivity to oxidants, accompanied with reduction in the abundance as well as enzymatic activities of antioxidant enzymes^{40, 41}. Elevated oxidative damage of DNA was detected in multiple common mitochondrial diseases and could be reduced by antioxidant treatment^{36, 42, 43}.

Although there is no cure for mitochondrial diseases so far, advances in development of treatments, such as small molecules, mitochondrial transplantation, and genetic therapies to prevent germline transmission, have been reported and hold promise. Given the close connection between oxidative stress and mitochondrial diseases, restoring redox homeostasis in the patients' fibroblasts is one of the promising

strategies and multiple clinical trials for antioxidants have been performed or are in progress^{44, 45, 46, 47}. The prevalence of oxidative stress phenotypes in the mitochondrial diseases highlight the importance of redox homeostasis for mitochondrial biology.

Apart from the primary mitochondrial diseases caused by genetic defects, mitochondrial dysfunctions have been shown to be associated with other human metabolic disorders such as diabetes^{48, 49}. Both citrate synthase activity as the marker of mitochondrial content and NADH:O₂ oxidoreductase (complex I) activity were significantly reduced in skeletal muscle in type 2 diabetic subjects⁴⁸. Citrate synthase activity was significantly lower in white adipose tissue in obese human and in old mice (age of 72 weeks)^{50, 51}. In addition, mitochondrial dysfunction plays a central role in the development of age-related neurodegeneration disease, such as Parkinson's disease, Alzheimer's disease, and Huntington's disease^{52, 53}. Collectively, the facts that mitochondrial defects cause primary inherited mitochondrial diseases and the involvement of mitochondria in multiple metabolic disorders emphasize that mitochondria play a critical role for human health.

Protein posttranslational modification expands functional proteome

Posttranslational modification (PTM) of proteins refers to the biological process in which proteins undergo either enzymatic cleavage or covalent addition of chemical groups after translation⁵⁴. These modifications can affect protein physical and chemical properties, including structure, stability and localization^{55, 56, 57, 58}. Conformational changes induced by PTM can affect the biological activity of proteins. Therefore, PTM is an important fundamental mechanism of cellular regulation. Together with the capacity of alternative splicing of mRNAs at the translational level⁵⁹, it expands the proteome that is encoded by the genome.

More than 200 types of PTMs have been identified in proteins so far⁶⁰, and some PTMs are reversible. The reversible PTMs, which can be added and removed dynamically, function as a mechanism by which cells can rapidly respond to environmental changes⁶¹. This nature of reversible PTMs makes it important in cellular response and signalling. For instance, phosphorylation is one of the best-established reversible modifications, dephosphorylation at specific amino acids can affect protein functions as well as modulate gene transcription⁶².

Lysine acylations are prevalent protein PTMs and are closely connected with cellular metabolism

Protein acylation is one of the PTMs that are currently highly studied^{63, 64, 65, 66}. It is the covalent attachment of an acyl moiety to one or more amino acid residues of a

protein, and N-acylation of lysine (lysine acylation) is the most abundant acylation modification⁶⁷, although it is worthwhile to note that other types of modifications, such as O-acylation and C-acylation, exist and are required for certain proteins to function properly⁶⁸.

Advances in proteomics have allowed identification of a variety of lysine acylations. Lysine residues can be modified by acyl groups varying in length and charge^{69, 70, 71, 72}. Lysine is positively charged on its ϵ -amino group at physiological pH, and addition of an acyl group could neutralize the residue or even shift it to a negatively charged residue. Due to these changes in chemical properties, lysine acylation plays an important role in regulating protein structure and function as well as protein-protein interactions^{67, 73, 74}. In addition, lysine acylation abundance is closely associated with corresponding acyl-CoA concentrations. Acyl-CoAs are important intermediary metabolites, and they are also substrates for lysine acylations. Indeed, aberrant acyl-CoAs accumulation due to genetic diseases were accompanied with increased lysine acylation levels^{72, 75, 76, 77}. Proteins can also be acylated by acyl-CoAs *in vitro* in a dose- and pH-dependent manner^{75, 78, 79}. This close association between acylation and acyl-CoAs underlies the potentially regulatory role for acylation in cellular metabolism.

Lysine acylation is a rapidly growing field with a huge number of target proteins identified and its physiological relevance starts to be revealed. Besides lysine *acetylation*, the most studied lysine *acylation*, our understanding on relatively novel modifications, such as lysine succinylation, malonylation and glutarylation, is still emerging.

Acetylation

Lysine acetylation is observed on both histones and non-histone proteins. It was first discovered on histones around half a century ago by Allfrey and colleagues⁸⁰. Histone acetylation plays a critical role in regulating virtually all processes involving DNA, including replication, repair, transcription, and heterochromatin formation^{81, 82}. Acetylation of histones can remodel chromatin structures, alter subnuclear localization, and neutralize lysine positive charge, which may loosen interactions between DNA and histones and consequently regulate the genes transcription^{83, 84, 85}.

Due to limitations in the methods for detecting acetylation sites, the first non-histone acetylation target, tubulin⁸⁶, was discovered around 20 years after the discovery of histone acetylation. In the past decades, development in high-resolution mass spectrometry (MS)-based proteomics technologies facilitated our understanding of lysine acylation hugely. As a result, thousands of acetylated sites

were identified. Interestingly, the majority of acetylation events were shown to occur on non-nuclear proteins. In particular, lysine acetylation was detected in many metabolic enzymes in central metabolic pathways, such as glycolysis, gluconeogenesis, the TCA cycle and fatty acid oxidation^{87, 88, 89}. The connection between this modification and cellular metabolism is therefore increasingly appreciated. This is also further supported by evidence from different studies showing that acetyl-CoA levels regulate acetylation levels *in vivo*. Acetyl-CoA is a metabolic intermediate which can be generated from several major carbon catabolic pathways, including glycolysis, pyruvate oxidation and fatty acid oxidation. In eukaryotic cells, it is distinctly present in mitochondrial and non-mitochondrial pools^{90, 91}. Global acetylation levels have also been shown to be correlated with acetyl-CoA concentrations in a compartment-specific manner. For example, global histone acetylation was dependent on the extra-mitochondrial acetyl-CoA pool produced from citrate by adenosine triphosphate-citrate lyase (ATP citrate lyase) in mammalian cells⁹¹. In addition, mitochondrial acetyl-CoA derived from fatty acid oxidation was demonstrated to be the direct donor for mitochondrial protein acetylation⁹². Thus, acetylation responds to metabolic status and its abundance is dynamic *in vivo*. Physiologically, global acetylation levels have been shown to be altered in the context of metabolic stress such as fasting, calorie restriction and high fat diet^{93, 94}.

Besides the important role in gene regulation, acetylation can affect many other biological processes through altering enzymatic activities, protein-protein interactions and protein localization⁷⁴.

Succinylation, malonylation and glutarylation

In addition to acetylation, several other PTMs involving short-chain acyl-groups have been discovered, such as succinylation^{70, 95}, malonylation^{71, 95}, and glutarylation⁷². Succinyl-, malonyl-, and glutaryl- moieties are structurally similar, all dicarboxylic groups, but differ in the number of methylene groups. They impose two negative charges on a lysine residue, altering the charge from + 1 to -1 at physiological pH at a specific residue. It is because of this that they can influence protein properties in different ways as compared to acetylation which merely neutralizes the lysine residue. In addition, these three acidic acyl moieties are bulkier as compared to acetylation; succinylation, malonylation, and glutarylation add four, three, and five carbons to lysine, respectively, while only two carbons are added in case of acetylation. Together, they can affect the protein structure as well as protein-protein interactions and overall cellular physiology, distinctly from acetylation.

Lysine succinylation was first reported to occur on the active site of homoserine trans-succinylase in *E. coli*, identified using Q-TOF mass spectrometry⁹⁶. Succinyl- was covalently bound to lysine 45 or 46, and the modified lysine residues were shown to be critical for the enzymatic activity, because the enzymatic activity was abolished when the lysine residues were replaced with alanine. About one decade ago, the widespread presence of succinylation as well as malonylation was discovered using an antibody-based enrichment strategy in combination with MS-based proteomics, followed by comprehensive validation with a variety of chemical biological or biochemical methods such as competition assays, isotopic labelling, and the use of synthetic peptides^{95, 97}. Lysine glutarylation was recently discovered and validated in a similar fashion⁷².

From the global overview of the cellular succinylome, malonylome, and glutarylome, provided by several proteomics studies, it is clear that they share features as a protein modification. First, they are all evolutionarily conserved modifications, since each of them have been discovered ranging from prokaryotes, such as *E. coli*, to eukaryotes, including in *S. cerevisiae*, *Drosophila*, mouse and human^{72, 95, 98, 99}. Second, they are prevalent modifications throughout the cells. Each of the three modifications show a wide spectrum of substrates, ranging from histones to cytosolic and mitochondrial metabolic enzymes, although the distribution within cells is different for each of these modifications. Enrichment analyses showed that proteins containing either lysine succinylation or lysine glutarylation were largely found within mitochondria^{72, 100, 101}, in contrast, malonylated proteins appeared to be more abundant in cytosolic fraction than the mitochondrial fraction¹⁰². The targets of malonylation were also shown to be different than succinylation in mouse liver. This suggests that these structurally similar acylations could play a role in protein function in different ways. Third, these three acylations occur at a low stoichiometry, i.e. modification site occupancy, *in vivo*. Antibody-based enrichment of acylation of interest is required prior to MS detection and succinylated peptides cannot be detected without enrichment⁹⁹. In addition, Meyer *et al.* found in *E. coli* that at most of the lysine succinylation sites, occupancies were low (< 1% - 5%)¹⁰³.

Since the establishment of these three acylations, the question “what is the mechanism by which the succinylation, malonylation, or glutarylation occur *in vivo*” has been posed. So far, no major acyltransferase has been discovered for catalysing the transfer of succinyl-, malonyl-, or glutaryl- groups to lysine residues *in vivo*, although a few enzymes with other major enzymatic activities were reported to have a lysine succinyltransferase activity. Carnitine palmitoyltransferase 1A (CPT1A) knockdown led to decreased succinylation level and its overexpression increased the succinylation level in several cell lines (HEK293T, T47D, and Ba/F3), and CPT1A can

succinylate and inhibit enolase 1¹⁰⁴. In addition, *in vitro* α -ketoglutarate dehydrogenase was shown to be able to succinylate itself as well as isocitrate dehydrogenase with α -ketoglutarate as a cofactor¹⁰⁵. Histone 4 was acylated by incubating it with recombinant histone acetyltransferase p300 in the presence of succinyl-CoA or glutaryl-CoA⁷². Further studies are needed to elucidate relevance of these chemical reactions for acylations *in vivo*.

While enzymatic mechanism of transfer cannot be excluded, increasing evidence suggests that acyl-CoA species are able to acylate proteins non-enzymatically under the physiological conditions. Acyl-CoAs, important intermediary metabolites, are inherently reactive CoA esters. *In vitro*, incubation of non-acylated BSA with either succinyl-CoA or glutaryl-CoA caused a pH-dependent increase in respective lysine acylation level^{78, 106}. Especially the dicarboxylic acyl-CoAs are reactive, because they can undergo intramolecular catalysis to form high-energy cyclic anhydride intermediates which robustly react with lysine residues and lead to protein acylation⁷⁸. Acylations occurs more at higher pH^{78, 107}, which could explain the widespread succinylation and glutarylation in mitochondrial proteins, since the mitochondrial matrix has a distinct more alkaline environment (pH 7.8) as compared to the cytosol and nuclei, where pH is maintained at 7.0-7.4¹⁰⁸. Moreover, this idea of lysine being modified by acyl-CoA independent of enzymatic catalysts, is strengthened by a strong relationship between acyl-CoA levels and abundance of acyl-lysine modifications in the setting of genetic diseases. Inherited acyl-CoA metabolism disorders are characterized with accumulation of acyl-CoAs *in vivo*. Consequently, aberrant increases in protein butyrylation, malonylation and propionylation were observed in fibroblasts derived from patients with inborn errors of butyryl-CoA, malonyl-CoA, and propionyl-CoA metabolism, respectively^{75, 77}. Similarly, in a mouse model of human glutaric acidemia type I disease, glutaryl-CoA level was increased with a concomitant increase in lysine glutarylation level⁷². Very recently, Gut and colleagues reported a human genetic disease caused by succinyl-CoA ligase (SCL) deficiency due to mutation in succinyl-CoA ligase GTP-specific β -subunit (SUCLA2)⁷⁶. SCL catalyses the conversion of succinyl-CoA to succinate, and its deficiency caused an accumulation of succinyl-CoA in patients' fibroblasts, which was associated with a global increase in protein succinylation⁷⁶. Together, these results point to a mechanism of chemical lysine acylation by acyl-CoAs in cells.

Various protein targets of succinylation, malonylation as well as glutarylation were uncovered in cells and include a large number of metabolic enzymes. The acidic modifications were shown to affect the proteins' enzymatic activities. For example, increased succinylation induced by genetic manipulation reduced enzymatic activity of uncoupling protein 1 and mitochondrial trifunctional enzyme α -subunit (ECHA) in

mice^{100, 109}, while the pyruvate dehydrogenase complex and succinate dehydrogenase displayed an increased activity with higher succinylation level¹⁰¹. Consistent with the influences on protein activity or stability, disruption in multiple biological pathways have been shown in the context of hyperacylation in combination with environmental challenges. For instance, hypersuccinylated mice heart showed deficient fatty acid oxidation and consequently developed hypertrophic cardiomyopathy in aged mice¹⁰⁹, or inability to respond to cold stress due to hypersuccinylated brown adipose tissue¹⁰⁰. Additionally, pathophysiological relevance of global protein hypersuccinylation level was shown for mitochondrial encephalomyopathy⁷⁶. Together, these acyl-lysine modifications emerge as important players in regulating cellular metabolism and physiology.

Sirtuins regulate lysine acylations levels by removing various acyllysine modifications

The involvement of lysine acylation on large numbers of proteins ranging from histones, transcription factors to metabolic enzymes, highlights the importance of maintaining lysine acylation stoichiometry. Lysine acylation level is balanced by the process of adding and removing acyl-groups from the lysine residues. Although it is not clear whether the processes of adding acyl-groups such as succinyl, malonyl, and glutaryl to lysine residues are catalysed by enzymes, it has been established that removal of these acyl- groups from proteins *in vivo* is performed by enzymes, generally called lysine deacylases.

There are two families of lysine deacylases with distinct biochemical characteristics. One is the classical histone *deacetylase* (HDACs) family with eleven protein members which use Zn^{2+} as a cofactor¹¹⁰. These HDACs were initially identified as nuclear histone *deacetylases*¹¹¹, further studies showed they also located in cytosol and their substrates were expanded to numerous non-histone proteins^{112, 113}.

The other class of lysine *deacylases* is the sirtuin family of proteins. The first sirtuin discovered was silent information regulator 2 (Sir2) in yeast^{114, 115}. Sirtuins are highly conserved enzymes found in a diverse array of organisms, including *E. coli*, *S. cerevisiae*, *Drosophila*, *C. elegans*, mouse, and human¹¹⁶. Importantly, their activities are dependent on nicotinamide adenosine dinucleotide (NAD^+)¹¹⁷, which distinguishes sirtuins from conventional HDACs. NAD^+ acts as a classical coenzyme for various oxidoreductases¹¹⁸, the dependence of sirtuins on NAD^+ indicates their activities could be coupled with intracellular metabolism via NAD^+ .

In mammals, there are seven sirtuins (SIRT1-7). They are homologs of Sir2 and share a conserved central catalytic machinery with differences in the flanking N- and C-

termini¹¹⁹. Structurally, they contain a zinc-binding motif in connection with a NAD⁺-binding Rossmann fold domain¹²⁰. These seven mammalian sirtuin members occupy different subcellular compartments. Specifically, SIRT1 can shuttle between the nucleus and cytoplasm, SIRT2 mainly resides in the cytoplasm and can also translocate to nucleus, SIRT6 and 7 were found predominantly in nucleus, SIRT3-5 are primarily found in mitochondria^{121, 122, 123, 124}. These localizations determine a significant part of their substrate targets. The seven sirtuins also possess distinct deacetylase activities. Although sirtuins were initially known as *deacetylases* and/or ADP-ribosylases^{121, 125, 126}, some of them have been demonstrated to de-*acylate* other acyl-modifications than acetyllysine. SIRT4 was shown to efficiently remove methylglutaryl, hydroxymethylglutaryl, and 3-methylglutaconyl modifications from lysines¹²⁷. SIRT5 prefers removing dicarboxylic groups including succinyl-, malonyl-, and glutaryl-groups. SIRT6 hydrolyses long-chain fatty acyl-modifications such as myristoyl and palmitoyl groups¹²⁸. Differences in the cellular compartmentalization as well as enzymatic activities account for the wide scope of substrate targets and the non-redundant biological roles of sirtuin family members *in vivo*¹²⁹.

Mitochondrial sirtuins are important for cellular function in response to metabolic stress

Three of the mammalian sirtuins, SIRT3-5, reside predominantly in the mitochondrial matrix^{101, 124, 130}, the hub of cellular metabolism. Recently, the mitochondrial sirtuins have emerged as a novel mechanism to regulate cell function and health by regulating lysine acylations on numerous protein targets from a variety of metabolic pathways, especially in the context of mitochondria responding to environmental challenges^{63, 123, 127, 131, 132}. Consistently, they are widely expressed in mammals with the highest protein levels in metabolically active tissues including brain, liver, kidney, and heart^{121, 123, 133}. In recent years, regulatory roles for the mitochondrial sirtuins on mitochondrial physiology have become clear due to the availability of genetic-engineered mouse models in combination with developments in high resolution proteomics. Interestingly, ablation of each of the three sirtuins in mice led to metabolic syndromes under stressor conditions, such as fasting, calorie restriction, long-term high fat diet or cold challenges and in ageing, whereas they were metabolically and physiologically unremarkable under basal conditions^{100, 127, 131, 134, 135, 136}. These findings point out the key roles for mitochondrial sirtuins in adaptive response to environmental changes and maintaining metabolic homeostasis.

SIRT3

SIRT3 is the most studied mitochondrial sirtuin till now. It is a major mitochondrial deacetylase, as knockout (KO) of SIRT3, but not SIRT4 or SIRT5, led to dramatic increase in the abundance of lysine acetylated proteins in mitochondria in mice¹³⁷. Although mitochondrial proteins were hyperacetylated in the absence of SIRT3, SIRT3 KO mice did not show apparent metabolic abnormalities under basal conditions and they could also tolerate certain (mild) environmental challenges^{137, 138}. For example, SIRT3 KO mice displayed comparable metabolism as WT littermates, with respect to oxygen consumption, respiratory exchange ratio, during the last 6 hours (hrs) of a 24-hr fast¹³⁷. In the same study, SIRT3-deficient mice displayed undistinguishable thermogenic capacity compared to WT counterparts and maintained their core temperature after 6-hr exposure to 4°C. Nevertheless, SIRT3 KO mice showed metabolic disorders when subjected to stressors such as chronic high-fat diet, calorie restriction and cold exposure during fasting^{131, 139, 140}. SIRT3-deficient mice showed an accelerated obesity and developed insulin resistance and hepatic steatosis upon 13-week high-fat diet¹³⁹. They failed to activate the urea cycle during calorie restriction¹⁴⁰, and exhibited a striking cold intolerance combined with a fasting challenge¹³¹. Mitochondrial fatty acid β -oxidation and ketogenesis are the major metabolic pathways that needed to be activated in response to those metabolic stresses and were impaired in case of SIRT3 deficiency^{131, 141}. SIRT3 has been demonstrated to regulate fatty acid oxidation and ketogenesis via deacetylating and activating long-chain acyl-CoA dehydrogenase and 3-hydroxy-3-methylglutaryl-CoA synthase 2, respectively^{131, 141}. In addition to its role as a regulator for metabolic adaptation to stressors, SIRT3 has been shown to delay the onset of age-associated pathology such as cardiac hypertrophy through suppressing ROS level via deacetylating FoxO3A¹⁴². It was also showed to mediate the prevention of age-related hearing loss in mice subjected to calorie restriction¹⁴³.

SIRT4

In contrast to the large number of acetylated proteins targeted by SIRT3, relatively little is known for SIRT4, as its main enzymatic activity remained unclear for a long time. Although deacetylase, ADP-ribosyltransferase and lipoamidase activities have been detected for SIRT4^{133, 144, 145}, they might not be its main activities, as these activities are either very weak or cannot be detected in some studies^{127, 146}. The ADP-ribosyltransferase activity, first considered the main activity, is now also proposed to be an inefficient side reaction and only very few targets, among them glutamate dehydrogenase, have been established^{133, 147}. Using a phylogenetic analysis as an identification strategy with enzymology for validation, SIRT4 was recently shown to

prefer removal of several negatively charged dicarboxyacyl modifications, 3-hydroxy-3-methylglutaryl- (HMG), glutaryl-, and 3-methylglutaryl- (MG), and 3-methylglutaconyl- (MGc), from lysine residues¹²⁷. The removal of HMG-lysine modification by SIRT4 was also reported in another study¹⁴⁸.

Metabolic characterization of SIRT4 KO mice revealed that SIRT4 plays a role in amino acid catabolism and amino acid-stimulated insulin secretion. Haigis *et al.* reported that SIRT4 acted as a negative regulator of insulin secretion¹³³. SIRT4-deficient mice displayed 30% higher circulating insulin levels during *ad libitum* feeding condition and significantly higher insulin levels after an overnight fast. Plasma insulin levels in SIRT4 KO mice, but not in WT littermates, was increased substantially upon intraperitoneal injection (IP) of glutamine. Moreover, isolated SIRT4 KO islets also showed increase in glutamine-stimulated insulin secretion in a dose-dependent manner, in contrast to WT islets that did not respond. The authors attributed these phenotypes to the role for SIRT4 in repressing glutamate dehydrogenase activity by ADP-ribosylation. The role for SIRT4 regulation of insulin secretion was supported in another study by Anderson and colleagues¹²⁷, who showed that a whole-body deletion of SIRT4 in mice caused elevated basal and leucine-stimulated insulin secretion, which progressively developed into glucose intolerance and insulin resistance as mice aged. SIRT4 was shown to promote leucine metabolism by controlling the acylation status (MG-, HMG-, MGc-lysine) of enzymes in the pathway. Interestingly, a very recent study showed that β -cell-specific SIRT4 KO mice did not show perturbations in insulin secretion¹⁴⁹. More work is required to investigate the mechanism by which SIRT4 regulates and coordinates insulin metabolism in different organs across the whole organism.

SIRT5 regulates cellular metabolism and health via its novel deacylase activities

SIRT5 was first discovered as a predominant mitochondrial matrix sirtuin^{123,124}. Later, extra-mitochondrial localization was also detected in other cellular compartments, including cytosol, nucleus and peroxisomes^{101, 150, 151} (Fig. 1).

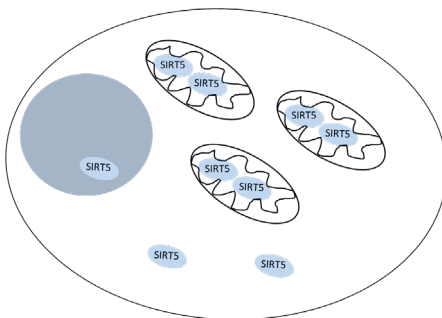


Figure 1. Subcellular localization of SIRT5 in mammalian cells. SIRT5 is primarily present in mitochondria and can be found in cytosol, nucleus and peroxisome as well^{123, 151}.

SIRT5 was the first sirtuin that was discovered to possess several robust NAD⁺-dependent *deacylase* activities other than *deacetylase* activities by Lin and colleagues around one decade ago¹⁵². They demonstrated that SIRT5 prefers removing dicarboxylic acyl groups, succinyl and malonyl, from lysine residues (Fig. 2). This novel substrate preference compared to other sirtuins members, was shown to be due to the presence of arginine and tyrosine in the substrate binding pocket. In addition, SIRT5 was also shown to catalyse deglutarylation from lysine⁷². SIRT5 has received great attention since its unique biochemical activities were elucidated.

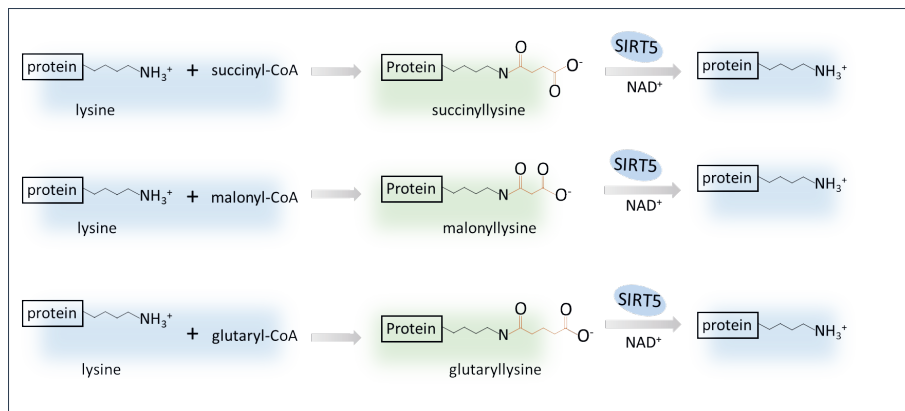


Figure 2. Illustration of SIRT5 biochemical enzymatic activities. Cellular protein lysine residues undergo succinylation, malonylation, and glutarylation modifications with their respective acyl-CoA as donors^{75, 78}. SIRT5 is a robust NAD⁺-dependent desuccinylase, demalonylase, and deglutarylase *in vivo*^{72, 152}.

Our understanding with regard to the protein substrates, biological function, and physiological relevance of SIRT5 has been expanded significantly. Global lysine succinylation, malonylation, and glutarylation levels, but not acetylation, were increased strikingly upon either whole-body or tissue-specific SIRT5 deletion in mice and human cell lines^{100, 101, 135, 153}, and their levels were decreased upon SIRT5 overexpression in mice^{154, 155}. This demonstrated that SIRT5 is responsible for regulating the levels of these three modifications *in vivo*. Multiple large-scale proteomics studies in mice revealed that SIRT5 targets many proteins involved in various key metabolic pathways, including glycolysis, fatty acid β -oxidation, TCA cycle, and ROS management (Fig. 3). In this way SIRT5 can contribute to metabolic and cellular function. Like the other two mitochondrial sirtuins, SIRT5 was demonstrated in different mouse studies to play a critical role in adaptive response to various metabolic stressors by regulating diverse biological processes^{100, 109, 123}, and no obvious phenotypes were shown in SIRT5 KO mice under normal metabolic circumstances^{134, 137}. This again supports the concept that SIRT5 as well as other

sirtuins plays a critical role in maintaining cellular homeostasis in response to environmental stress.

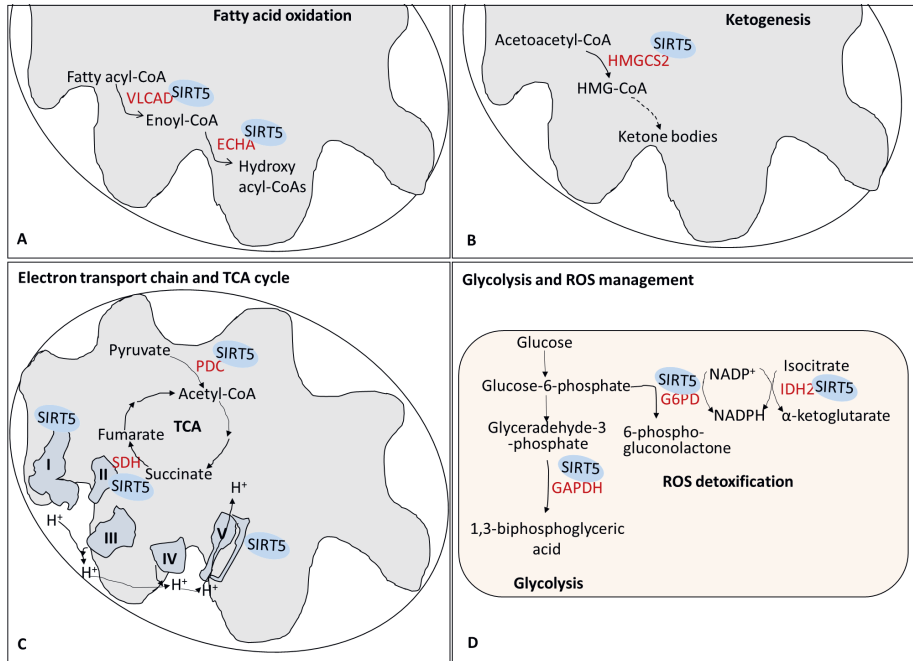


Figure 3. SIRT5 plays a role in maintaining metabolism homeostasis by regulating enzymes involved in multiple biological processes. (A) SIRT5 regulates fatty acid oxidation by desuccinylating and activating ECHA¹⁰⁹, and by desuccinylating and promoting the activity as well as the membrane localization of VLCAD¹⁵⁶. (B) SIRT5 desuccinylates and activates HMGCS2¹³⁵. (C) SIRT5 is involved in the TCA cycle and mitochondrial respiration by regulating activities of enzymes PDC, complex I, complex II, and complex V^{101, 136}. (D) SIRT5 plays a regulatory role in glycolysis through demalonylation and activation of GAPDH and in ROS detoxification through affecting NADPH-generation enzymes G6PD and IDH2^{102, 157}. VLCAD: Very long-chain acyl-CoA dehydrogenase, ECHA: Enoyl-coenzyme A hydratase, HMGCS2: 3-hydroxy-3-methylglutaryl CoA synthase 2, PDC: Pyruvate dehydrogenase complex, SDH: Succinate dehydrogenase, GAPDH: Glyceraldehyde phosphate dehydrogenase, G6PD: Glucose-6-phosphate dehydrogenase, IDH2: Isocitrate dehydrogenase 2.

A reducing environment is necessary for cell survival and proper functioning¹⁵⁸. Given that cells are exposed to both exogenous and endogenous oxidants continuously, it is essential to maintain cellular redox homeostasis for cellular health. The cellular redox environment is influenced by multiple redox couples, such as NAD⁺/NADH and NADP⁺/NADPH, of which concentrations are intimately influenced by the cellular metabolism. Moreover, ROS, the endogenous oxidants, are physiological by-products of the mitochondrial OXPHOS process. Notably, SIRT5 has been shown to be involved in the redox regulation by several independent groups¹⁵¹,

^{157, 159}. Roles for SIRT5 in metabolism such as mitochondrial respiration have been supported by evidence as well.

SIRT5 regulates bioenergetics through multiple pathways

SIRT5 promotes fatty acid β -oxidation

Multiple independent studies pointed towards a role for SIRT5 in fatty acid oxidation in several metabolic important organs liver, muscle, and heart, especially under metabolic challenging contexts. Rardin *et al.* reported that SIRT5-ablated mice had impaired fatty acid oxidation¹³⁵, as evidenced by significantly lower oxidation rates of deuterium-labelled palmitate in primary hepatocytes isolated from SIRT5 KO mice as compared to WT counterparts, and by higher levels of medium- and long-chain acylcarnitines in the SIRT5 KO mice livers and muscles. In another study, accumulation of long-chain CoA esters (after 30 min exercise), significantly reduced oxidation rate of palmitoyl-L-carnitine, and lower ATP levels (after 24 hrs fasting) were observed in SIRT5 KO mice heart¹⁰⁹. Fatty acids are a major energy source for sustaining a proper function of the heart. Induced hypertrophic cardiomyopathy in aged SIRT5-deficient mice was attributed to a constant deficiency in fatty acid oxidation and subsequent inadequate ATP supply¹⁰⁹. Likewise, whole-body deletion of SIRT5 caused a significantly higher mortality in mice upon cardiac stress imposed by transverse aortic constriction¹⁶⁰. This was associated with a decreased fatty acid oxidation and an impaired TCA cycle, which ultimately led to energetic crisis in the SIRT5 KO mice. Of note, heart specific SIRT5 KO mice did not replicate the mortality phenotype, which highlights the complexity of SIRT5 biology.

The involvement of SIRT5 in fatty acid oxidation was also supported by the observation that brown adipose tissue (BAT) specific SIRT5 KO mice failed to maintain core body temperature, when they were subject to fasting for 18 hrs followed by exposure to 7°C¹⁰⁰. Isolated BAT mitochondria from overnight fasted SIRT5 KO mice showed significantly lower fatty acid oxidation rate compared to their WT littermates. These findings connect SIRT5 with fatty acid β -oxidation.

SIRT5 affects ketone body production, TCA cycle and glycolysis

Ketone bodies are important energy sources for organs such as brain, under glucose deprived conditions. SIRT5, as a stress-response protein, has been shown to promote ketone body production¹³⁵ (Fig. 3). Mice without SIRT5 displayed insufficient ketone body production, as evidenced by significantly lower plasma β -hydroxybutyrate and β -hydroxybutyrylcarnitine levels in fasted SIRT5 KO livers compared to those from WT littermates¹³⁵. In addition, the authors demonstrated that the rate-limiting

ketogenic enzyme, 3-hydroxy-3-methylglutaryl-CoA synthase 2 (HMGCS2), was targeted and regulated by SIRT5 both *in vitro* and *in vivo*.

Upon nutrient catabolism, intermediary metabolites enter the TCA cycle and subsequently feed OXPHOS by which mitochondria generate ATP for cellular energy expenditure. Many proteomics studies have shown that enzymes in the TCA cycle, such as the pyruvate dehydrogenase complex (PDC), and many subunits of the electron transport complexes are targets of SIRT5. They were hyperacetylated in SIRT5 KO mice. Although Park *et al.* reported that SIRT5 suppressed the enzymatic activity of, and cellular respiration through, PDC and succinate dehydrogenase in mice¹⁰¹, multiple studies importantly also discovered an inhibitory role of SIRT5 absence towards the activity of OXPHOS complexes as well as mitochondrial respiration^{100, 136, 161}.

Glycolysis represents another important route for ATP production *in vivo*, and SIRT5 has been shown to promote the glycolysis pathway through, primarily, its demalonylation activity¹⁰². Primary hepatocytes derived from SIRT5 KO mice showed lower oxidation rate of deuterium-labelled glucose than WT controls. Consistently, lactic acid levels in culture media of SIRT5 KO hepatocytes were lower. These phenotypes could be explained by suppressed activity of glyceraldehyde 3-phosphate dehydrogenase (GAPDH) by hypermalonylation resulting from knockout of SIRT5¹⁰².

SIRT5 maintains cellular redox balance

Maintenance of redox homeostasis is critical for cell biology and survival, as a reducing environment is required for numerous biochemical reactions *in vivo*¹⁵⁸. Imbalanced redox states have been linked with many diseases or disorders^{38, 162}. ROS are by-products of mitochondrial respiration when electrons flow through the electron transport complexes¹⁶³. Escape of electrons from the electron transport complex I and III, that are considered the main sites of ROS production^{164, 165}, can lead to the formation of the highly reactive superoxide radical. This is rapidly converted to hydrogen peroxide (H₂O₂) by superoxide dismutase 1 in the intermembrane space and the cytoplasm and by superoxide dismutase 2 in mitochondria. H₂O₂ is less reactive compared to superoxide and can act as a second messenger, but it is deleterious for the cells at higher levels. In the mitochondria H₂O₂ is detoxified by glutathione (GSH)- and thioredoxin-dependent systems, which are regenerated by NADPH. Antioxidant systems protect cells from oxidative damage through detoxifying cellular free radicals, organic hydroperoxides and reducing protein disulfides, maintaining their function^{166, 167}. SIRT5 has been shown to be important for sustaining redox homeostasis, affecting ROS production and NADPH

generation. For example, SIRT5 was shown to deacylate and activate two NADPH-producing enzymes, isocitrate dehydrogenase 2 (IDH2) and glucose-6-phosphate dehydrogenase (G6PDH)¹⁵⁷. NADPH is essential for maintaining antioxidant such as glutathione in reduced form. As a result, SIRT5 deletion caused significantly higher ROS levels in mouse embryonic fibroblasts (MEFs), and SIRT5 KO mice brain showed higher oxidative damage upon paraquat, an oxidant, treatment¹⁵⁷. In addition, mRNA expression of several antioxidant genes, such as glutamate-cysteine ligase catalytic subunit, glutathione reductase, and glutathione peroxidase 2, were significantly reduced upon SIRT5 knockdown in human lung carcinoma cells (A549)¹⁶⁸. SIRT5 has also been shown to regulate ROS production via desuccinylating acyl-CoA oxidase 1 (ACOX1) in peroxisomes, decreasing its activity¹⁵¹. ACOX1 is a rate-limiting enzyme in fatty acid β -oxidation in peroxisome and is also an important source of H_2O_2 . Knockdown of SIRT5 in HepG2 cells led to increase in succinylation level as well as activity of peroxisomal ACOX1, which was accompanied with increased H_2O_2 level. Collectively, these results obtained from either mouse or cancer cell lines-based studies show that SIRT5 can regulate redox balance. However, the physiological relevance of SIRT5 in redox homeostasis in humans remains elusive and needs further investigation.

Research gap

To conclude, SIRT5 stands out among the (mito)sirtuin members, based on its unique biochemical activities. Its robust deacylase activity, especially desuccinylase activity, is clear and has been demonstrated in a number of studies. Although SIRT5 has been demonstrated to play an important regulatory role in cellular metabolism, the complexity of its biology is increasingly appreciated, as evidenced by discrepancies in its effects on metabolic enzymatic activities and by the fact that tissue specific SIRT5 deletion cannot reproduce phenotypes observed in the whole-body SIRT5 KO mice. More importantly, all fundamental studies reported so far addressing SIRT5 biological functions were conducted using animal or cell line models. The direct evidence for a role of SIRT5 in human physiology or pathology is lacking. To find such evidence we made use of recently identified SIRT5 variants (mutations) in patients that were diagnosed for mitochondrial disease. To elucidate the human physiological relevance of SIRT5, novel analytical methods that were needed to understand cellular SIRT5 function had to be optimized and comprehensive biochemical, molecular, and functional analyses needed to be performed.

Aim and outlines

My overall aim was to improve our knowledge of the biological function of SIRT5 and to provide evidence for the physiological relevance of SIRT5 in human health and disease.

The specific aims of this thesis were:

- (1). To better understand the biological function of SIRT5 and how human SIRT5 variants relate to human disease.
- (2). To optimize an enzymatic assay for gaining better insights into cellular SIRT5 biochemical activity under different metabolic conditions.
- (3). To develop a novel statistical model to better analyse effects of SIRT5 on the mitochondrial bioenergetic function as assessed by Seahorse extracellular flux analysis.

Since SIRT5 has demonstrated a highly context-dependent functioning, the intracellular environment could influence SIRT5 enzymatic activity significantly. In **Chapter 2**, I optimized a desuccinylase activity assay in order to analyse the desuccinylase in a whole cell lysate context. In **Chapter 3**, I investigated the biochemistry of the SIRT5 variants identified in patients and the biological impact. My data highlighted an altered redox homeostasis in the patients' fibroblasts harbouring the SIRT5 variants. In **Chapter 4**, I further looked into redox systems to understand how the redox balance was affected by the SIRT5 variants. This substantiated the findings in **Chapter 3** and established that two main thiol antioxidant defence systems were strongly affected by the SIRT5 variants. In **Chapter 5**, a Bayesian hierarchical model was proposed to better analyse cellular mitochondrial respiration capacity from Seahorse extracellular flux analysis data. This model took systematic/measurement errors from different experimental levels within one assay into account, and therefore increase the power of these assays, which is important for my studies related to SIRT5 role in regulating mitochondrial function. In **Chapter 6**, all findings from **Chapter 2-5** were combined and further discussed to unravel the biological function of SIRT5 and relations between SIRT5 different regulatory roles, a pathogenic model for the SIRT5 variants was proposed. In addition, I will discuss possible strategies to ameliorate the symptoms in the patients and implications for SIRT5 in other physiological perspectives. Future research direction for better understanding roles for SIRT5 in human health and disease will be recommended.

References

1. Chandel, N.S. Evolution of Mitochondria as Signaling Organelles. *Cell Metab.* **22**, 204-206 (2015).
2. Spinelli, J.B. & Haigis, M.C. The multifaceted contributions of mitochondria to cellular metabolism. *Nat. Cell Biol.* **20**, 745-754 (2018).
3. Herzig, S., *et al.* Identification and functional expression of the mitochondrial pyruvate carrier. *Science* **337**, 93-96 (2012).
4. Sastrasinh, S. & Sastrasinh, M. Glutamine transport in submitochondrial particles. *Am. J. Physiol.* **257**, F1050-1058 (1989).
5. McGarry, J.D. & Brown, N.F. The mitochondrial carnitine palmitoyltransferase system. From concept to molecular analysis. *Eur. J. Biochem.* **244**, 1-14 (1997).
6. Houten, S.M. & Wanders, R.J. A general introduction to the biochemistry of mitochondrial fatty acid beta-oxidation. *J. Inher. Metab. Dis.* **33**, 469-477 (2010).
7. Walsh, C.T., Tu, B.P. & Tang, Y. Eight Kinetically Stable but Thermodynamically Activated Molecules that Power Cell Metabolism. *Chem. Rev.* **118**, 1460-1494 (2018).
8. Sousa, J.S., D'Imprima, E. & Vonck, J. Mitochondrial Respiratory Chain Complexes. In: *Membrane Protein Complexes: Structure and Function* (eds Harris JR, Boekema EJ). Springer Singapore (2018).
9. Watt, I.N., Montgomery, M.G., Runswick, M.J., Leslie, A.G. & Walker, J.E. Bioenergetic cost of making an adenosine triphosphate molecule in animal mitochondria. *Proc. Natl. Acad. Sci. U. S. A.* **107**, 16823-16827 (2010).
10. Palmieri, F. The mitochondrial transporter family SLC25: identification, properties and physiopathology. *Mol. Aspects Med.* **34**, 465-484 (2013).
11. Kory, N., *et al.* SFXN1 is a mitochondrial serine transporter required for one-carbon metabolism. *Science* **362**, (2018).
12. Sun, J., *et al.* Mitochondrial and Plasma Membrane Citrate Transporters: Discovery of Selective Inhibitors and Application to Structure/Function Analysis. *Mol. Cell. Pharmacol.* **2**, 101-110 (2010).
13. Chypre, M., Zaidi, N. & Smans, K. ATP-citrate lyase: a mini-review. *Biochem. Biophys. Res. Commun.* **422**, 1-4 (2012).
14. Watson, J.A., Fang, M. & Lowenstein, J.M. Tricarballoylate and hydroxycitrate: substrate and inhibitor of ATP: citrate oxaloacetate lyase. *Arch. Biochem. Biophys.* **135**, 209-217 (1969).
15. Liu, X., Kim, C.N., Yang, J., Jemmerson, R. & Wang, X. Induction of apoptotic program in cell-free extracts: requirement for dATP and cytochrome c. *Cell* **86**, 147-157 (1996).
16. Chandel, N.S., *et al.* Mitochondrial reactive oxygen species trigger hypoxia-induced transcription. *Proc. Natl. Acad. Sci. U. S. A.* **95**, 11715-11720 (1998).
17. Muller, F. The nature and mechanism of superoxide production by the electron transport chain: Its relevance to aging. *J. Am. Aging Assoc.* **23**, 227-253 (2000).
18. Cenini, G., Lloret, A. & Cascella, R. Oxidative Stress in Neurodegenerative Diseases: From a Mitochondrial Point of View. *Oxid. Med. Cell. Longev.* **2019**, 2105607 (2019).
19. Ramachandran, A., *et al.* Mitochondria, nitric oxide, and cardiovascular dysfunction. *Free Radic. Biol. Med.* **33**, 1465-1474 (2002).
20. Breuer, M.E., *et al.* The role of mitochondrial OXPHOS dysfunction in the development of neurologic diseases. *Neurobiol. Dis.* **51**, 27-34 (2013).
21. Alston, C.L., Rocha, M.C., Lax, N.Z., Turnbull, D.M. & Taylor, R.W. The genetics and pathology of mitochondrial disease. *J. Pathol.* **241**, 236-250 (2017).

22. Craven, L., Alston, C.L., Taylor, R.W. & Turnbull, D.M. Recent Advances in Mitochondrial Disease. *Annu. Rev. Genomics Hum. Genet.* **18**, 257-275 (2017).
23. Robin, E.D. & Wong, R. Mitochondrial DNA molecules and virtual number of mitochondria per cell in mammalian cells. *J. Cell. Physiol.* **136**, 507-513 (1988).
24. Keogh, M.J. & Chinnery, P.F. Mitochondrial DNA mutations in neurodegeneration. *Biochim. Biophys. Acta* **1847**, 1401-1411 (2015).
25. Sallevelt, S.C., *et al.* De novo mtDNA point mutations are common and have a low recurrence risk. *J. Med. Genet.* **54**, 73-83 (2017).
26. Hellebrekers, D.M., *et al.* PGD and heteroplasmic mitochondrial DNA point mutations: a systematic review estimating the chance of healthy offspring. *Hum. Reprod. Update* **18**, 341-349 (2012).
27. Alston, C.L., *et al.* Biallelic Mutations in TMEM126B Cause Severe Complex I Deficiency with a Variable Clinical Phenotype. *Am. J. Hum. Genet.* **99**, 217-227 (2016).
28. McFarland, R., Taylor, R.W. & Turnbull, D.M. A neurological perspective on mitochondrial disease. *Lancet. Neurol.* **9**, 829-840 (2010).
29. Taylor, R.W., Schaefer, A.M., Barron, M.J., McFarland, R. & Turnbull, D.M. The diagnosis of mitochondrial muscle disease. *Neuromuscul. Disord.* **14**, 237-245 (2004).
30. Swalwell, H., *et al.* Respiratory chain complex I deficiency caused by mitochondrial DNA mutations. *Eur. J. Hum. Genet.* **19**, 769-775 (2011).
31. Ghezzi, D., *et al.* SDHAF1, encoding a LYR complex-II specific assembly factor, is mutated in SDH-defective infantile leukoencephalopathy. *Nat. Genet.* **41**, 654-656 (2009).
32. Mordaunt, D.A., *et al.* Phenotypic variation of TTC19-deficient mitochondrial complex III deficiency: a case report and literature review. *Am. J. Med. Genet. A* **167**, 1330-1336 (2015).
33. Jaksch, M., *et al.* Cytochrome c oxidase deficiency due to mutations in SCO2, encoding a mitochondrial copper-binding protein, is rescued by copper in human myoblasts. *Hum. Mol. Genet.* **10**, 3025-3035 (2001).
34. Metodiev, M.D., *et al.* Mutations in the tricarboxylic acid cycle enzyme, aconitase 2, cause either isolated or syndromic optic neuropathy with encephalopathy and cerebellar atrophy. *J. Med. Genet.* **51**, 834-838 (2014).
35. Wu, S.B., Ma, Y.S., Wu, Y.T., Chen, Y.C. & Wei, Y.H. Mitochondrial DNA mutation-elicited oxidative stress, oxidative damage, and altered gene expression in cultured cells of patients with MERRF syndrome. *Mol. Neurobiol.* **41**, 256-266 (2010).
36. Schulz, J.B., *et al.* Oxidative stress in patients with Friedreich ataxia. *Neurology* **55**, 1719-1721 (2000).
37. Pastore, A., *et al.* Actin glutathionylation increases in fibroblasts of patients with Friedreich's ataxia: a potential role in the pathogenesis of the disease. *J. Biol. Chem.* **278**, 42588-42595 (2003).
38. Hayashi, G. & Cortopassi, G. Oxidative stress in inherited mitochondrial diseases. *Free. Radic. Biol. Med.* **88**, 10-17 (2015).
39. Durr, A., *et al.* Clinical and genetic abnormalities in patients with Friedreich's ataxia. *N. Engl. J. Med.* **335**, 1169-1175 (1996).
40. Tozzi, G., *et al.* Antioxidant enzymes in blood of patients with Friedreich's ataxia. *Arch. Dis. Child.* **86**, 376-379 (2002).
41. Chantrel-Groussard, K., *et al.* Disabled early recruitment of antioxidant defenses in Friedreich's ataxia. *Hum. Mol. Genet.* **10**, 2061-2067 (2001).
42. Yen, M.Y., Kao, S.H., Wang, A.G. & Wei, Y.H. Increased 8-hydroxy-2'-deoxyguanosine in leukocyte DNA in Leber's hereditary optic neuropathy. *Invest. Ophthalmol. Vis. Sci.* **45**, 1688-1691 (2004).

43. Koopman, W.J., *et al.* Mitigation of NADH: ubiquinone oxidoreductase deficiency by chronic Trolox treatment. *Biochim. Biophys. Acta* **1777**, 853-859 (2008).
44. Janssen, M.C.H., *et al.* The KHENERGY Study: Safety and Efficacy of KH176 in Mitochondrial m.3243A>G Spectrum Disorders. *Clin. Pharmacol. Ther.* **105**, 101-111 (2019).
45. Klopstock, T., *et al.* Persistence of the treatment effect of idebenone in Leber's hereditary optic neuropathy. *Brain* **136**, e230 (2013).
46. Karaa, A., *et al.* Randomized dose-escalation trial of elamipretide in adults with primary mitochondrial myopathy. *Neurology* **90**, e1212-e1221 (2018).
47. Russell, O.M., Gorman, G.S., Lightowlers, R.N. & Turnbull, D.M. Mitochondrial Diseases: Hope for the Future. *Cell* **181**, 168-188 (2020).
48. Kelley, D.E., He, J., Menshikova, E.V. & Ritov, V.B. Dysfunction of mitochondria in human skeletal muscle in type 2 diabetes. *Diabetes* **51**, 2944-2950 (2002).
49. Petersen, K.F., Dufour, S., Befroy, D., Garcia, R. & Shulman, G.I. Impaired mitochondrial activity in the insulin-resistant offspring of patients with type 2 diabetes. *N. Engl. J. Med.* **350**, 664-671 (2004).
50. Duivenvoorde, L.P., van Schothorst, E.M., Swarts, H.J. & Keijer, J. Assessment of metabolic flexibility of old and adult mice using three noninvasive, indirect calorimetry-based treatments. *J. Gerontol. A Biol. Sci. Med. Sci.* **70**, 282-293 (2015).
51. Christe, M., *et al.* Obesity affects mitochondrial citrate synthase in human omental adipose tissue. *ISRN Obes.* **2013**, 826027 (2013).
52. Nunomura, A., *et al.* Oxidative damage is the earliest event in Alzheimer disease. *J. Neuropathol. Exp. Neurol.* **60**, 759-767 (2001).
53. Lin, M.T. & Beal, M.F. Mitochondrial dysfunction and oxidative stress in neurodegenerative diseases. *Nature* **443**, 787-795 (2006).
54. Farley, A.R. & Link, A.J. Identification and quantification of protein posttranslational modifications. *Methods Enzymol.* **463**, 725-763 (2009).
55. Johnson, L.N. & Lewis, R.J. Structural basis for control by phosphorylation. *Chem. Rev.* **101**, 2209-2242 (2001).
56. Hershko, A. & Ciechanover, A. The ubiquitin system. *Annu. Rev. Biochem.* **67**, 425-479 (1998).
57. Inuzuka, H., *et al.* Acetylation-dependent regulation of Skp2 function. *Cell* **150**, 179-193 (2012).
58. Matsuzaki, H., *et al.* Acetylation of Foxo1 alters its DNA-binding ability and sensitivity to phosphorylation. *Proc. Natl. Acad. Sci. U. S. A.* **102**, 11278-11283 (2005).
59. Maniatis, T. & Tasic, B. Alternative pre-mRNA splicing and proteome expansion in metazoans. *Nature* **418**, 236-243 (2002).
60. Qausain, S., Srinivasan, H., Jamal, S., Nasiruddin, M. & Khan, M.K.A. Chapter 3 - Phosphorylation and Acetylation of Proteins as Posttranslational Modification: Implications in Human Health and Associated Diseases. In: *Protein Modificomics* (eds Dar TA, Singh LR). Academic Press (2019).
61. Uversky, V.N. Posttranslational Modification. In: *Brenner's Encyclopedia of Genetics (Second Edition)* (eds Maloy S, Hughes K). Academic Press (2013).
62. Humphrey, S.J., James, D.E. & Mann, M. Protein Phosphorylation: A Major Switch Mechanism for Metabolic Regulation. *Trends Endocrinol. Metab.* **26**, 676-687 (2015).
63. Carrico, C., Meyer, J.G., He, W., Gibson, B.W. & Verdin, E. The Mitochondrial Acylome Emerges: Proteomics, Regulation by Sirtuins, and Metabolic and Disease Implications. *Cell Metab.* **27**, 497-512 (2018).
64. Hirsche, M.D. & Zhao, Y. Metabolic Regulation by Lysine Malonylation, Succinylation, and Glutarylation. *Mol. Cell. Proteomics* **14**, 2308-2315 (2015).

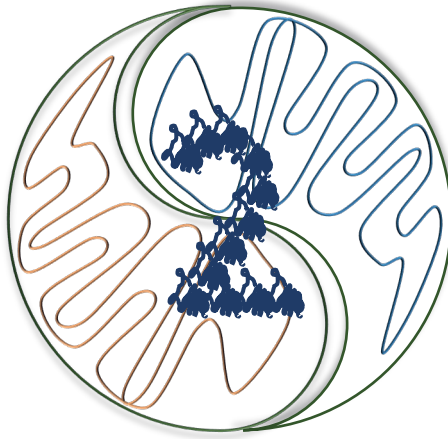
65. Yang, Y. & Gibson, G.E. Succinylation Links Metabolism to Protein Functions. *Neurochem. Res.* **44**, 2346-2359 (2019).
66. Narita, T., Weinert, B.T. & Choudhary, C. Functions and mechanisms of non-histone protein acetylation. *Nat. Rev. Mol. Cell Biol.* **20**, 156-174 (2019).
67. Pougovkina, O. & de Boer, V.C.J. Protein Lysine Acylation: Abundance, Dynamics and Function. In: *Sirtuins* (ed Houtkooper RH). Springer Netherlands (2016).
68. Kojima, M., *et al.* Ghrelin is a growth-hormone-releasing acylated peptide from stomach. *Nature* **402**, 656-660 (1999).
69. Jiang, T., Zhou, X., Taghizadeh, K., Dong, M. & Dedon, P.C. N-formylation of lysine in histone proteins as a secondary modification arising from oxidative DNA damage. *Proc. Natl. Acad. Sci. U. S. A.* **104**, 60-65 (2007).
70. Zhang, Z., *et al.* Identification of lysine succinylation as a new post-translational modification. *Nat. Chem. Biol.* **7**, 58-63 (2011).
71. Peng, C., *et al.* The first identification of lysine malonylation substrates and its regulatory enzyme. *Mol. Cell. Proteomics* **10**, M111 012658 (2011).
72. Tan, M., *et al.* Lysine glutarylation is a protein posttranslational modification regulated by SIRT5. *Cell Metab.* **19**, 605-617 (2014).
73. Lv, L., *et al.* Acetylation targets the M2 isoform of pyruvate kinase for degradation through chaperone-mediated autophagy and promotes tumor growth. *Mol. Cell* **42**, 719-730 (2011).
74. Choudhary, C., Weinert, B.T., Nishida, Y., Verdin, E. & Mann, M. The growing landscape of lysine acetylation links metabolism and cell signalling. *Nat. Rev. Mol. Cell Biol.* **15**, 536-550 (2014).
75. Pougovkina, O., Te Brinke, H., Wanders, R.J., Houten, S.M. & de Boer, V.C. Aberrant protein acylation is a common observation in inborn errors of acyl-CoA metabolism. *J. Inherit. Metab. Dis.* **37**, 709-714 (2014).
76. Gut, P., *et al.* SUCLA2 mutations cause global protein succinylation contributing to the pathomechanism of a hereditary mitochondrial disease. *Nat. Commun.* **11**, 5927 (2020).
77. Colak, G., *et al.* Proteomic and Biochemical Studies of Lysine Malonylation Suggest Its Malonic Aciduria-associated Regulatory Role in Mitochondrial Function and Fatty Acid Oxidation. *Mol. Cell. Proteomics* **14**, 3056-3071 (2015).
78. Wagner, G.R., *et al.* A Class of Reactive Acyl-CoA Species Reveals the Non-enzymatic Origins of Protein Acylation. *Cell Metab.* **25**, 823-837. e8 (2017).
79. Simic, Z., Weiwad, M., Schierhorn, A., Steegborn, C. & Schutkowski, M. The varepsilon-Amino Group of Protein Lysine Residues Is Highly Susceptible to Nonenzymatic Acylation by Several Physiological Acyl-CoA Thioesters. *ChemBioChem* **16**, 2337-2347 (2015).
80. Allfrey, V.G., Faulkner, R. & Mirsky, A.E. Acetylation and Methylation of Histones and Their Possible Role in the Regulation of Rna Synthesis. *Proc. Natl. Acad. Sci. U. S. A.* **51**, 786-794 (1964).
81. Kurdistani, S.K. & Grunstein, M. Histone acetylation and deacetylation in yeast. *Nat. Rev. Mol. Cell Biol.* **4**, 276-284 (2003).
82. Kouzarides, T. Chromatin modifications and their function. *Cell* **128**, 693-705 (2007).
83. Brown, C.R., Kennedy, C.J., Delmar, V.A., Forbes, D.J. & Silver, P.A. Global histone acetylation induces functional genomic reorganization at mammalian nuclear pore complexes. *Genes Dev.* **22**, 627-639 (2008).
84. Clayton, A.L., Hazzalin, C.A. & Mahadevan, L.C. Enhanced histone acetylation and transcription: a dynamic perspective. *Mol. Cell* **23**, 289-296 (2006).
85. Schneider, R. & Grosschedl, R. Dynamics and interplay of nuclear architecture, genome organization, and gene expression. *Genes Dev.* **21**, 3027-3043 (2007).

86. L'Hernault, S.W. & Rosenbaum, J.L. Chlamydomonas alpha-tubulin is posttranslationally modified by acetylation on the epsilon-amino group of a lysine. *Biochemistry* **24**, 473-478 (1985).
87. Zhao, S., *et al.* Regulation of cellular metabolism by protein lysine acetylation. *Science* **327**, 1000-1004 (2010).
88. Kim, S.C., *et al.* Substrate and functional diversity of lysine acetylation revealed by a proteomics survey. *Mol. Cell* **23**, 607-618 (2006).
89. Wang, Q., *et al.* Acetylation of metabolic enzymes coordinates carbon source utilization and metabolic flux. *Science* **327**, 1004-1007 (2010).
90. Takahashi, H., McCaffery, J.M., Irizarry, R.A. & Boeke, J.D. Nucleocytosolic acetyl-coenzyme A synthetase is required for histone acetylation and global transcription. *Mol. Cell* **23**, 207-217 (2006).
91. Wellen, K.E., *et al.* ATP-citrate lyase links cellular metabolism to histone acetylation. *Science* **324**, 1076-1080 (2009).
92. Pougovkina, O., *et al.* Mitochondrial protein acetylation is driven by acetyl-CoA from fatty acid oxidation. *Hum. Mol. Genet.* **23**, 3513-3522 (2014).
93. Hebert, A.S., *et al.* Calorie restriction and SIRT3 trigger global reprogramming of the mitochondrial protein acetylome. *Mol. Cell* **49**, 186-199 (2013).
94. Schwer, B., *et al.* Calorie restriction alters mitochondrial protein acetylation. *Aging Cell* **8**, 604-606 (2009).
95. Xie, Z., *et al.* Lysine succinylation and lysine malonylation in histones. *Mol. Cell. Proteomics* **11**, 100-107 (2012).
96. Rosen, R., *et al.* Probing the active site of homoserine trans-succinylase. *FEBS Lett.* **577**, 386-392 (2004).
97. Zhang, Q., *et al.* Identification of histone malonylation in the human fetal brain and implications for diabetes-induced neural tube defects. *Mol. Genet. Genomic Med.* **8**, e1403 (2020).
98. Colak, G., *et al.* Identification of lysine succinylation substrates and the succinylation regulatory enzyme CobB in Escherichia coli. *Mol. Cell. Proteomics* **12**, 3509-3520 (2013).
99. Weinert, B.T., *et al.* Lysine succinylation is a frequently occurring modification in prokaryotes and eukaryotes and extensively overlaps with acetylation. *Cell Rep.* **4**, 842-851 (2013).
100. Wang, G., *et al.* Regulation of UCP1 and Mitochondrial Metabolism in Brown Adipose Tissue by Reversible Succinylation. *Mol. Cell* **74**, 844-857 e847 (2019).
101. Park, J., *et al.* SIRT5-mediated lysine desuccinylation impacts diverse metabolic pathways. *Mol. Cell* **50**, 919-930 (2013).
102. Nishida, Y., *et al.* SIRT5 Regulates both Cytosolic and Mitochondrial Protein Malonylation with Glycolysis as a Major Target. *Mol. Cell* **59**, 321-332 (2015).
103. Meyer, J.G., *et al.* Quantification of Lysine Acetylation and Succinylation Stoichiometry in Proteins Using Mass Spectrometric Data-Independent Acquisitions (SWATH). *J. Am. Soc. Mass Spectrom.* **27**, 1758-1771 (2016).
104. Kurmi, K., *et al.* Carnitine Palmitoyltransferase 1A Has a Lysine Succinyltransferase Activity. *Cell Rep.* **22**, 1365-1373 (2018).
105. Gibson, G.E., *et al.* Alpha-ketoglutarate dehydrogenase complex-dependent succinylation of proteins in neurons and neuronal cell lines. *J. Neurochem.* **134**, 86-96 (2015).
106. Wagner, G.R. & Payne, R.M. Widespread and enzyme-independent Nepsilon-acetylation and Nepsilon-succinylation of proteins in the chemical conditions of the mitochondrial matrix. *J. Biol. Chem.* **288**, 29036-29045 (2013).

107. Tanner, K.G., *et al.* Catalytic mechanism and function of invariant glutamic acid 173 from the histone acetyltransferase GCN5 transcriptional coactivator. *J. Biol. Chem.* **274**, 18157-18160 (1999).
108. Casey, J.R., Grinstein, S. & Orlowski, J. Sensors and regulators of intracellular pH. *Nat. Rev. Mol. Cell Biol.* **11**, 50-61 (2010).
109. Sadhukhan, S., *et al.* Metabolomics-assisted proteomics identifies succinylation and SIRT5 as important regulators of cardiac function. *Proc. Natl. Acad. Sci. U. S. A.* **113**, 4320-4325 (2016).
110. de Ruijter, A.J., van Gennip, A.H., Caron, H.N., Kemp, S. & van Kuilenburg, A.B. Histone deacetylases (HDACs): characterization of the classical HDAC family. *Biochem. J.* **370**, 737-749 (2003).
111. Taunton, J., Hassig, C.A. & Schreiber, S.L. A mammalian histone deacetylase related to the yeast transcriptional regulator Rpd3p. *Science* **272**, 408-411 (1996).
112. Hubbert, C., *et al.* HDAC6 is a microtubule-associated deacetylase. *Nature* **417**, 455-458 (2002).
113. Juan, L.J., *et al.* Histone deacetylases specifically down-regulate p53-dependent gene activation. *J. Biol. Chem.* **275**, 20436-20443 (2000).
114. Ivy, J.M., Klar, A.J. & Hicks, J.B. Cloning and characterization of four SIR genes of *Saccharomyces cerevisiae*. *Mol. Cell. Biol.* **6**, 688-702 (1986).
115. Shore, D., Squire, M. & Nasmyth, K.A. Characterization of two genes required for the position-effect control of yeast mating-type genes. *EMBO J.* **3**, 2817-2823 (1984).
116. Frye, R.A. Phylogenetic classification of prokaryotic and eukaryotic Sir2-like proteins. *Biochem. Biophys. Res. Commun.* **273**, 793-798 (2000).
117. Imai, S., Armstrong, C.M., Kaeberlein, M. & Guarente, L. Transcriptional silencing and longevity protein Sir2 is an NAD-dependent histone deacetylase. *Nature* **403**, 795-800 (2000).
118. Houtkooper, R.H., Canto, C., Wanders, R.J. & Auwerx, J. The secret life of NAD+: an old metabolite controlling new metabolic signaling pathways. *Endocr. Rev.* **31**, 194-223 (2010).
119. Frye, R.A. Characterization of five human cDNAs with homology to the yeast SIR2 gene: Sir2-like proteins (sirtuins) metabolize NAD and may have protein ADP-ribosyltransferase activity. *Biochem. Biophys. Res. Commun.* **260**, 273-279 (1999).
120. Sanders, B.D., Jackson, B. & Marmorstein, R. Structural basis for sirtuin function: what we know and what we don't. *Biochim. Biophys. Acta* **1804**, 1604-1616 (2010).
121. Onyango, P., Celic, I., McCaffery, J.M., Boeke, J.D. & Feinberg, A.P. SIRT3, a human SIR2 homologue, is an NAD-dependent deacetylase localized to mitochondria. *Proc. Natl. Acad. Sci. U. S. A.* **99**, 13653-13658 (2002).
122. Cooper, H.M., Huang, J.Y., Verdin, E. & Spelbrink, J.N. A new splice variant of the mouse SIRT3 gene encodes the mitochondrial precursor protein. *PLoS One* **4**, e4986 (2009).
123. Nakagawa, T., Lomb, D.J., Haigis, M.C. & Guarente, L. SIRT5 Deacetylates carbamoyl phosphate synthetase 1 and regulates the urea cycle. *Cell* **137**, 560-570 (2009).
124. Michishita, E., Park, J.Y., Burneskis, J.M., Barrett, J.C. & Horikawa, I. Evolutionarily conserved and nonconserved cellular localizations and functions of human SIRT proteins. *Mol. Biol. Cell* **16**, 4623-4635 (2005).
125. Vaziri, H., *et al.* hSIRT2(SIRT1) functions as an NAD-dependent p53 deacetylase. *Cell* **107**, 149-159 (2001).
126. North, B.J., Marshall, B.L., Borra, M.T., Denu, J.M. & Verdin, E. The human Sir2 ortholog, SIRT2, is an NAD⁺-dependent tubulin deacetylase. *Mol. Cell* **11**, 437-444 (2003).
127. Anderson, K.A., *et al.* SIRT4 Is a Lysine Deacylase that Controls Leucine Metabolism and Insulin Secretion. *Cell Metab.* **25**, 838-855.e815 (2017).
128. Jiang, H., *et al.* SIRT6 regulates TNF-alpha secretion through hydrolysis of long-chain fatty acyl lysine. *Nature* **496**, 110-113 (2013).

129. Cen, Y., Youn, D.Y. & Sauve, A.A. Advances in characterization of human sirtuin isoforms: chemistries, targets and therapeutic applications. *Curr. Med. Chem.* **18**, 1919-1935 (2011).
130. Schwer, B., North, B.J., Frye, R.A., Ott, M. & Verdin, E. The human silent information regulator (Sir)2 homologue hSIRT3 is a mitochondrial nicotinamide adenine dinucleotide-dependent deacetylase. *J. Cell Biol.* **158**, 647-657 (2002).
131. Hirschey, M.D., *et al.* SIRT3 regulates mitochondrial fatty-acid oxidation by reversible enzyme deacetylation. *Nature* **464**, 121-125 (2010).
132. Jing, E., *et al.* Sirtuin-3 (Sirt3) regulates skeletal muscle metabolism and insulin signaling via altered mitochondrial oxidation and reactive oxygen species production. *Proc. Natl. Acad. Sci. U. S. A.* **108**, 14608-14613 (2011).
133. Haigis, M.C., *et al.* SIRT4 inhibits glutamate dehydrogenase and opposes the effects of calorie restriction in pancreatic beta cells. *Cell* **126**, 941-954 (2006).
134. Yu, J., *et al.* Metabolic characterization of a Sirt5 deficient mouse model. *Sci Rep.* **3**, 2806 (2013).
135. Rardin, M.J., *et al.* SIRT5 regulates the mitochondrial lysine succinylome and metabolic networks. *Cell Metab.* **18**, 920-933 (2013).
136. Zhang, Y., *et al.* Lysine desuccinylase SIRT5 binds to cardiolipin and regulates the electron transport chain. *J. Biol. Chem.* **292**, 10239-10249 (2017).
137. Lombard, D.B., *et al.* Mammalian Sir2 homolog SIRT3 regulates global mitochondrial lysine acetylation. *Mol. Cell. Biol.* **27**, 8807-8814 (2007).
138. Fernandez-Marcos, P.J., *et al.* Muscle or liver-specific Sirt3 deficiency induces hyperacetylation of mitochondrial proteins without affecting global metabolic homeostasis. *Sci. Rep.* **2**, 425 (2012).
139. Hirschey, M.D., *et al.* SIRT3 deficiency and mitochondrial protein hyperacetylation accelerate the development of the metabolic syndrome. *Mol. Cell* **44**, 177-190 (2011).
140. Hallows, W.C., *et al.* Sirt3 promotes the urea cycle and fatty acid oxidation during dietary restriction. *Mol. Cell* **41**, 139-149 (2011).
141. Shimazu, T., *et al.* SIRT3 deacetylates mitochondrial 3-hydroxy-3-methylglutaryl CoA synthase 2 and regulates ketone body production. *Cell Metab.* **12**, 654-661 (2010).
142. Sundaresan, N.R., *et al.* Sirt3 blocks the cardiac hypertrophic response by augmenting Foxo3a-dependent antioxidant defense mechanisms in mice. *J. Clin. Invest.* **119**, 2758-2771 (2009).
143. Someya, S., *et al.* Sirt3 mediates reduction of oxidative damage and prevention of age-related hearing loss under caloric restriction. *Cell* **143**, 802-812 (2010).
144. Laurent, G., *et al.* SIRT4 coordinates the balance between lipid synthesis and catabolism by repressing malonyl CoA decarboxylase. *Mol. Cell* **50**, 686-698 (2013).
145. Mathias, R.A., *et al.* Sirtuin 4 is a lipoamidase regulating pyruvate dehydrogenase complex activity. *Cell* **159**, 1615-1625 (2014).
146. Feldman, J.L., Baeza, J. & Denu, J.M. Activation of the protein deacetylase SIRT6 by long-chain fatty acids and widespread deacylation by mammalian sirtuins. *J. Biol. Chem.* **288**, 31350-31356 (2013).
147. Du, J., Jiang, H. & Lin, H. Investigating the ADP-ribosyltransferase activity of sirtuins with NAD analogues and 32P-NAD. *Biochemistry* **48**, 2878-2890 (2009).
148. Pannek, M., *et al.* Crystal structures of the mitochondrial deacylase Sirtuin 4 reveal isoform-specific acyl recognition and regulation features. *Nat. Commun.* **8**, 1513 (2017).
149. Huynh, F.K., *et al.* beta-Cell-specific ablation of sirtuin 4 does not affect nutrient-stimulated insulin secretion in mice. *Am. J. Physiol. Endocrinol Metab.* **319**, E805-E813 (2020).
150. Geng, Y.Q., Li, T.T., Liu, X.Y., Li, Z.H. & Fu, Y.C. SIRT1 and SIRT5 activity expression and behavioral responses to calorie restriction. *J. Cell. Biochem.* **112**, 3755-3761 (2011).

151. Chen, X.F., *et al.* SIRT5 inhibits peroxisomal ACOX1 to prevent oxidative damage and is downregulated in liver cancer. *EMBO Rep.* **19**, (2018).
152. Du, J., *et al.* Sirt5 is a NAD-dependent protein lysine demalonylase and desuccinylase. *Science* **334**, 806-809 (2011).
153. Hershberger, K.A., *et al.* Ablation of Sirtuin5 in the postnatal mouse heart results in protein succinylation and normal survival in response to chronic pressure overload. *J. Biol. Chem.* **293**, 10630-10645 (2018).
154. Du, Y., *et al.* SIRT5 deacylates metabolism-related proteins and attenuates hepatic steatosis in ob/ob mice. *EBioMedicine* **36**, 347-357 (2018).
155. Bentley, N.L., *et al.* Protein hypoacylation induced by Sirt5 overexpression has minimal metabolic effect in mice. *Biochem. Biophys. Res. Commun.* **503**, 1349-1355 (2018).
156. Zhang, Y., *et al.* SIRT3 and SIRT5 regulate the enzyme activity and cardiolipin binding of very long-chain acyl-CoA dehydrogenase. *PLoS One* **10**, e0122297 (2015).
157. Zhou, L., *et al.* SIRT5 promotes IDH2 desuccinylation and G6PD deglutarylation to enhance cellular antioxidant defense. *EMBO Rep.* **17**, 811-822 (2016).
158. Schafer, F.Q. & Buettner, G.R. Redox State and Redox Environment in Biology. In: *Signal Transduction by Reactive Oxygen and Nitrogen Species: Pathways and Chemical Principles* (eds Forman HJ, Fukuto J, Torres M). Springer Netherlands (2003).
159. Lin, Z.F., *et al.* SIRT5 desuccinylates and activates SOD1 to eliminate ROS. *Biochem. Biophys. Res. Commun.* **441**, 191-195 (2013).
160. Hershberger, K.A., *et al.* Sirtuin 5 is required for mouse survival in response to cardiac pressure overload. *J. Biol. Chem.* **292**, 19767-19781 (2017).
161. Hershberger, K.A., Martin, A.S. & Hirschey, M.D. Role of NAD(+) and mitochondrial sirtuins in cardiac and renal diseases. *Nat. Rev. Nephrol.* **13**, 213-225 (2017).
162. Chinta, S.J. & Andersen, J.K. Redox imbalance in Parkinson's disease. *Biochim. Biophys. Acta* **1780**, 1362-1367 (2008).
163. Zorov, D.B., Juhaszova, M. & Sollott, S.J. Mitochondrial reactive oxygen species (ROS) and ROS-induced ROS release. *Physiol. Rev.* **94**, 909-950 (2014).
164. Koopman, W.J., *et al.* Mammalian mitochondrial complex I: biogenesis, regulation, and reactive oxygen species generation. *Antioxid. Redox Signal.* **12**, 1431-1470 (2010).
165. Murphy, Michael P. How mitochondria produce reactive oxygen species. *Biochem. J.* **417**, 1-13 (2009).
166. Beer, S.M., *et al.* Glutaredoxin 2 catalyzes the reversible oxidation and glutathionylation of mitochondrial membrane thiol proteins: implications for mitochondrial redox regulation and antioxidant DEFENSE. *J. Biol. Chem.* **279**, 47939-47951 (2004).
167. Lu, J. & Holmgren, A. The thioredoxin antioxidant system. *Free Radic. Biol. Med.* **66**, 75-87 (2014).
168. Lu, W., Zuo, Y., Feng, Y. & Zhang, M. SIRT5 facilitates cancer cell growth and drug resistance in non-small cell lung cancer. *Tumour Biol.* **35**, 10699-10705 (2014).



An optimized desuccinylase activity assay reveals a difference in desuccinylation activity between proliferative and differentiated cells

Taolin Yuan¹, Jaap Keijer¹, Angela H. Guo², David B. Lombard²,
Vincent C. J. de Boer^{1,*}

¹Human and Animal Physiology, Wageningen University & Research, The Netherlands

²Department of Pathology, University of Michigan, USA

Published in **Scientific Reports** 2020 10(1):17030.

DOI: 10.1038/s41598-020-72833-7

Abstract

Succinylation is a novel post-translational modification identified on many proteins and is involved in multiple biological processes. Succinylation levels are dynamically regulated, balanced by succinylation and desuccinylation processes, and are closely connected to metabolic state *in vivo*. Sirtuins have been shown to possess NAD⁺-dependent desuccinylation activity *in vitro* and *in vivo*, among which the desuccinylation activity of SIRT5 is most extensively studied. Our understanding of the response of succinylation levels to different metabolic conditions, is hampered by the lack of a fast NAD⁺-dependent desuccinylation assay in a physiological context. In the present study, we therefore optimized and validated a fluorescence-based assay for measuring NAD⁺-dependent desuccinylation activity in cell lysates. Our results demonstrated that shorter and stricter reaction time was critical to approach the initial rate of NAD⁺-dependent desuccinylation activity in crude cell lysate systems, as compared to the desuccinylation reaction of purified His-SIRT5. Analysis of desuccinylation activity in SIRT5 knockout HEK293T cells confirmed the relevance of SIRT5 in cellular desuccinylation activity, as well as the presence of other NAD⁺-dependent desuccinylase activities. In addition, we were able to analyse desuccinylation and deacetylation activity in multiple cell lines using this assay. We showed a remarkably higher desuccinylase activity, but not deacetylase activity, in proliferative cultured muscle and adipose cells in comparison with their differentiated counterparts. Our results reveal an alteration in NAD⁺-dependent desuccinylation activity under different metabolic states.

Introduction

Proteins involved in almost all essential life processes undergo different post-translational modifications (PTMs), by which protein structural changes are introduced and the functionality of the proteome is diversified¹⁻³. Post-translational modifications are closely associated with metabolites⁴⁻⁶, and the intimate connections between PTMs and metabolites allow PTMs to integrate different signals to enable rapid responses of the organism to environmental challenges⁷. Lysine succinylation is a relatively new PTM, identified nearly one decade ago¹. It provides a dynamic and relatively abundant network of modifications on both mitochondrial and extra-mitochondrial proteins^{1,8-10}. Lysine residues of many proteins involved in important metabolic processes, such as fatty acid β -oxidation, ketogenesis, tricarboxylic acid (TCA) cycle, branched chain amino acids metabolism, and glycolysis/gluconeogenesis, are subjected to succinylation¹¹⁻¹⁶. In addition, protein succinylation levels respond to metabolic manipulations. For example, succinylation levels in whole cell extracts and mitochondria in mouse liver were increased under a fasting condition¹¹. In contrast, mouse liver succinylation levels were shown to be significantly decreased¹⁷ or variably altered¹⁸ by a high fat diet intervention. These results indicate that protein succinylation levels vary with metabolic contexts and are likely to play a role in various signalling processes and regulatory pathways. Therefore, succinylation levels need to be carefully controlled. Sirtuins, a family of nicotinamide adenine dinucleotide (NAD⁺)-dependent lysine deacylase, regulate acylation levels *in vivo*¹⁹⁻²³. Thus far, sirtuin (SIRT) 5 and SIRT7 have been shown to be able to remove a succinyl adduct from lysine in the presence of the cofactor NAD⁺^{24,25}. SIRT5 was identified as a robust desuccinylase²⁴, but it can also remove malonyl and glutaryl adducts from lysine residues with high affinity^{24,26} and possesses a weak deacetylase activity²⁷. SIRT7 was demonstrated to function as a histone desuccinylase²⁵, and is also able to remove acetyl-group from targets^{28,29}. Since the protein succinylation level can be driven by succinyl-CoA levels^{5,8,30}, as well as NAD⁺ levels or the NAD⁺/NADH balance³¹, it is likely that ultimately a complex interplay between succinyl-CoA, NAD⁺ and desuccinylase activity dictates lysine succinylation levels^{15,16}. Although changes in succinylation levels have been observed with altered metabolism, it is not completely understood how desuccinylation activity responds to metabolic alterations. Improved understanding would be facilitated by the availability of additional options to assay desuccinylase activity.

A fluorescence based, homogenous, NAD⁺-dependent desuccinylation activity assay to study desuccinylase activity in crude cell lysate directly and rapidly is lacking. Its availability would allow for studying desuccinylation in a physiological context.

Fluorogenic assays have been used for identifying activators and inhibitors of recombinant SIRT5 *in vitro*³²⁻³⁴. Only a limited number of studies analysed desuccinylase activity in the more physiological context of a cell lysate^{35,36}. Notably, NAD⁺-dependent desuccinylase activity in a crude cellular extract has not yet been reported to our knowledge. Here, we optimize and validate a fluorescence-based assay for detecting NAD⁺-dependent cellular desuccinylase activity. Moreover, we use this assay to gain insights into NAD⁺-dependent desuccinylase activity in different cellular contexts, as well as its relation to global protein succinylation levels.

Results

Optimization and validation of desuccinylation activity in crude cell lysate

We aimed to measure cellular NAD⁺-dependent desuccinylase activity by using the succinylated-fluorogenic reporter substrate (Fig. 1a). Given the complexity of enzymatic reactions in crude cell lysates, we first optimized and validated the assay with a pure recombinant NAD⁺-dependent desuccinylase protein, His-SIRT5. Levels of desuccinylated peptides increased linearly over time up to 2 hours (Fig. 1b), when incubating His-SIRT5 with 10 μ M succinyl-substrate and 500 μ M NAD⁺. In addition, the desuccinylation rate of the peptide substrate linearly increased with the His-SIRT5 input when the reaction time was fixed (Fig. 1c). In contrast to the substantial desuccinylation activity of His-SIRT5, its deacetylation activity was virtually undetectable (Fig. 1d). In addition, we performed the assay in the presence of nicotinamide (NAM), a well-known inhibitor of sirtuins. As expected, the desuccinylation activity of His-SIRT5 was negatively impacted by NAM, with an IC₅₀ value of 20.2 μ M (Fig. 1e). These results show that NAD⁺-dependent desuccinylation activity of His-SIRT5 can be analysed well using the succinylated-fluorogenic reporter substrate. We next examined whether the assay set-up for pure His-SIRT5 could be applied to measure desuccinylase activity in a crude cell lysate. Linearity of cellular desuccinylation activity with time was assessed in fibroblasts cell lysates. Desuccinylation of the succinylated-substrate was proportional to reaction time up to 15 minutes, after which the reaction rate decreased (Fig. 2a), suggesting that an initial reaction rate was reached in the first 15 minutes. After 15 minutes, desuccinylated adduct amount again increased linearly with time, but at a slower reaction rate. Based on this, we performed further analyses of desuccinylase activity after 10 minutes, i.e. within the first 15 minutes. Desuccinylation by cell lysate after 10 minutes reaction time increased linearly in a protein-dependent manner (Fig. 2b). Inhibition by NAM of the cellular desuccinylation activity was observed at concentrations higher than 0.1 mM, and maximal inhibition was seen at 2 mM (Fig. 2c). Moreover, the desuccinylase activity was lower in HEK293T SIRT5 knockout cell

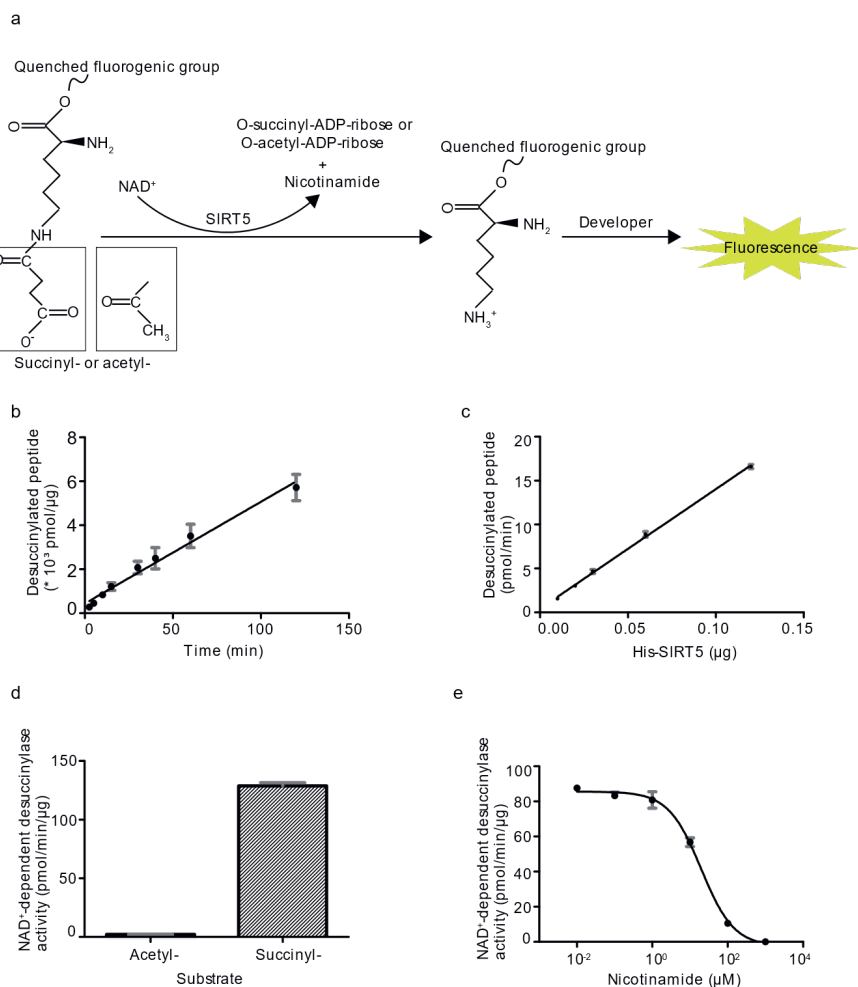


Figure 1. NAD⁺-dependent deacylation activity of human His-SIRT5. (a) Schematic illustration of desuccinylation and deacetylation activity analysis using a fluorogenic reporter assay. (b) Time course NAD⁺-dependent desuccinylation of succinylated-substrate by His-SIRT5 (0.046 μg). The desuccinylation reaction was proceeded for 2.5 - 120 minutes. Data represent mean ± SEM, n = 3. (c) NAD⁺-dependent desuccinylation of succinylated-substrate by increasing His-SIRT5 input (0.03 - 0.12 μg). (d) NAD⁺-dependent deacetylation (left) and desuccinylation activity (right) of His-SIRT5 (0.03 μg). (e) Inhibition of NAD⁺-dependent desuccinylation activity of His-SIRT5 (0.06 μg) by nicotinamide. (b) to (e), fluorescence signal obtained in the negative group (with cell lysates and with acylated-substrate and without NAD⁺) was subtracted from each experiment. Error bars in (c) to (e) represent deviation from the mean of duplicates.

lysates as compared to wild type cell lysates at all tested reaction time, which ranged from 2.5 to 60 minutes (Fig. 2d). This result demonstrates that SIRT5 contributes to

the desuccinylation activity of the crude cell lysate. Of note, the level of desuccinylated adduct increased over time in the absence of SIRT5 (Fig. 2d), indicating the presence of multiple desuccinylation enzymes in the crude cell lysate. Taken together, our results show that cellular desuccinylation activity can be analysed by the fluorescence-based assay, is dependent on NAD^+ and is sensitive to NAM inhibition.

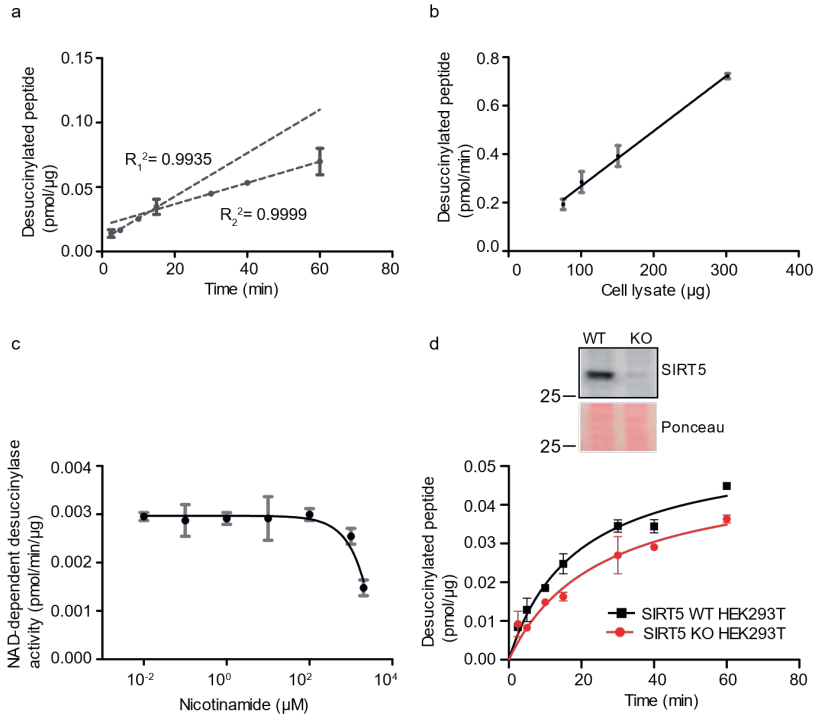


Figure 2. NAD⁺-dependent desuccinylation activity in human fibroblast lysate. (a) Time course NAD⁺-dependent desuccinylation of succinylated-substrate by cell lysate (148.5 μg). The desuccinylation reaction was proceeded for 2.5 - 60 minutes. Two dashed lines represent two different slopes obtained from the first four data points and last three data points, respectively. (b) NAD⁺-dependent desuccinylation of succinylated-substrate by increasing fibroblasts lysate (75.5 - 302 μg). (c) Inhibition of NAD⁺-dependent desuccinylation activity of fibroblasts lysate (187.3 μg) by nicotinamide. (d) Time-course NAD⁺-dependent desuccinylation of succinylated-substrate by SIRT5 WT (140 μg) and SIRT5 KO (140 μg) HEK293T cell lysate, respectively. Blots of SIRT5 and ponceau staining were cropped from the same blot, and the full-length SIRT5 blot and the ponceau image are presented in Supplementary Figure S2. (a) to (d), fluorescence signal obtained in the presence of substrate and absence of NAD^+ was subtracted from each experiment sample. Experiments were done in duplicates, and error bars represent deviation from the mean.

Desuccinylation and deacetylation activities in a range of cells with diverse metabolic states

Cellular succinylation levels were shown to be dynamically affected by metabolism⁸, whereas little is known about NAD⁺-dependent desuccinylation activity in cells with variable metabolic states. To gain insights into the latter, we analysed the desuccinylation activity by applying the fluorescence-based assay in a variety of cell lines that are commonly used. Desuccinylation activities among the different cell lines ranged from 0.0018 to 0.003 pmol/min/μg protein (Fig. 3a), whereas the deacetylation activities in the same cell lines were approximately 10-fold higher (Fig. 3b). Interestingly, desuccinylation activity among the tested cell lines did not differ markedly, whereas differences in the deacetylase activity appeared to be larger between the cell types. The deacetylation activity was highest in Caco2 cells and lowest in fibroblasts (Fig. 3b).

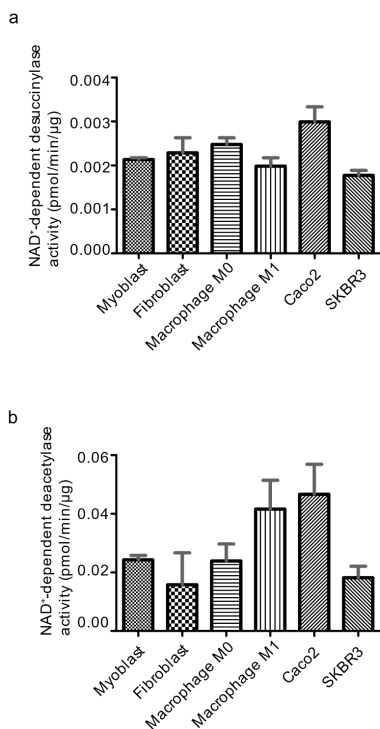


Figure 3. NAD⁺-dependent deacylation activities in various cell lines. (a) NAD⁺-dependent desuccinylase activity, and (b) NAD⁺-dependent deacetylase activity in multiple cell lines. 200 μg of cell lysates, 10 μM of succinyl/acetyl-substrate and 500 μM NAD⁺ were present in the desuccinylation/deacetylation assays. Fluorescence signal obtained in the presence of substrate and absence of NAD⁺ was subtracted from each experiment sample. Experiments were done in duplicates, and error bars represent deviation from the mean.

A difference in desuccinylation activity between proliferative and differentiated cells

Next, we asked whether cellular differentiation alters desuccinylase activity. In myoblasts differentiated into myotubes, metabolic changes occur with a relative increase in mitochondrial mass^{37,38}. Furthermore, differentiation of preadipocytes to adipocytes results in lipid droplets formation and a relative increase in mitochondrial biogenesis and metabolism^{39,40}. Since SIRT5 is mainly localized in mitochondria, and acylations such as acetylation has been shown to be involved in cell differentiation^{41,42}, desuccinylase activity could play a role in differentiation as well. C2C12 mouse myoblasts were successfully differentiated into myotubes, as can be seen from the longer myotubular structures that were observed after differentiation (Fig. 4a). Also, 3T3-L1 mouse preadipocytes were successfully differentiated into adipocytes, as can be seen from the lipid droplet accumulation in the cytosol of the adipocytes (Fig. 4b). Interestingly, desuccinylation activity in myotubes was around 4-fold ($P = 0.0002$) lower than in the myoblasts (Fig. 4c) and desuccinylase activity in adipocytes was around 6-fold ($P = 0.0375$) lower than that in the preadipocytes (Fig. 4d). In contrast, NAD⁺-dependent deacetylase activity displayed comparable in myotubes and adipocytes as compared to that in myoblast and preadipocytes, respectively (Fig. 4e, f). Given that the observed NAD⁺-dependent desuccinylation activities in myotubes and adipocytes were much lower than that in their proliferative counterparts, we aimed to study whether this was reflected in the SIRT5 protein levels. Since mitochondrial biogenesis is closely associated with cell differentiation, and SIRT5 is known to be the non-redundant desuccinylase in mitochondria. We first analysed the expression level of the mitochondrial outer membrane protein, voltage-dependent anion channel (VDAC). As expected, protein levels of VDAC (normalised to histone3 level) were increased by around 4-fold in both myotubes and adipocytes (Fig. 5a). Unexpectedly, the SIRT5 protein levels (normalised to histone3 level) in myotubes and adipocytes were increased by 2-fold as compared to their proliferative counterparts (Fig. 5a). Since total desuccinylase activity decreased (Fig. 4c, d) and SIRT5 protein levels increased, we were interested to see how it was reflected in the protein lysine succinylation levels of undifferentiated and differentiated myocytes and adipocytes. Our results show a distinct pattern of lysine succinylation for each cell type (Fig. 5b, c). Band intensity lane profiling of succinylated proteins on blots showed multiple bands with a higher intensity in the myoblasts compared to myotubes (grey areas, Fig. 5b), indicating that higher lysine succinylation levels of these proteins in myoblasts. However, other protein bands were of lower intensity in the myoblasts as compared to the same

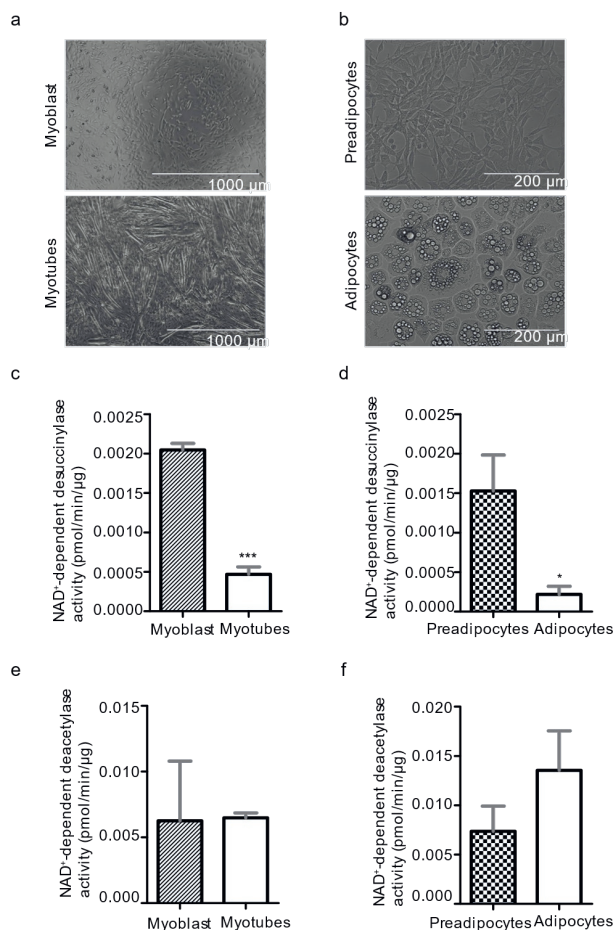


Figure 4. NAD⁺-dependent deacetylase activities in C2C12 and 3T3-L1 cell lysates. (a) Light micrograph of myoblasts (left panel), and myotubes at day 6 of differentiation (right panel); scale bar is 1000 μm. (b) Light micrograph of preadipocytes (left panel), and adipocytes at day 11 of differentiation (right panel); scale bar is 200 μm. NAD⁺-dependent desuccinylase activity in 150 μg lysates of (c) myoblast and myotubes and (d) 180 μg lysates of preadipocytes and adipocytes. NAD⁺-dependent deacetylase activity in lysates (145.6 μg) of (e) myoblasts and myotubes and (f) in lysates (145.6 μg) of preadipocytes and adipocytes. Data represent mean ± SEM. n = 3 for desuccinylation activity assays. Two-tailed unpaired Student's t-test was performed. *, P < 0.05, ***, P < 0.001. n = 2 for deacetylation activity assays.

bands in the myotubes (green areas, Fig. 5b), indicating that lower succinylation levels of these proteins in myoblasts as compared to myotubes. Also when comparing succinylation profiles between preadipocytes and adipocytes, succinylation differences similar to those seen in the muscle cell were observed, with multiple protein bands being of higher intensity in preadipocytes as compared to

adipocytes (grey areas, Fig. 5c), while this was the other way around for other proteins (red areas, Fig. 5c). Taken together, in differentiated myotubes and adipocytes, the overall desuccinylation activity was decreased, the SIRT5 protein level was increased and protein lysine succinylation profiles changed differentially.

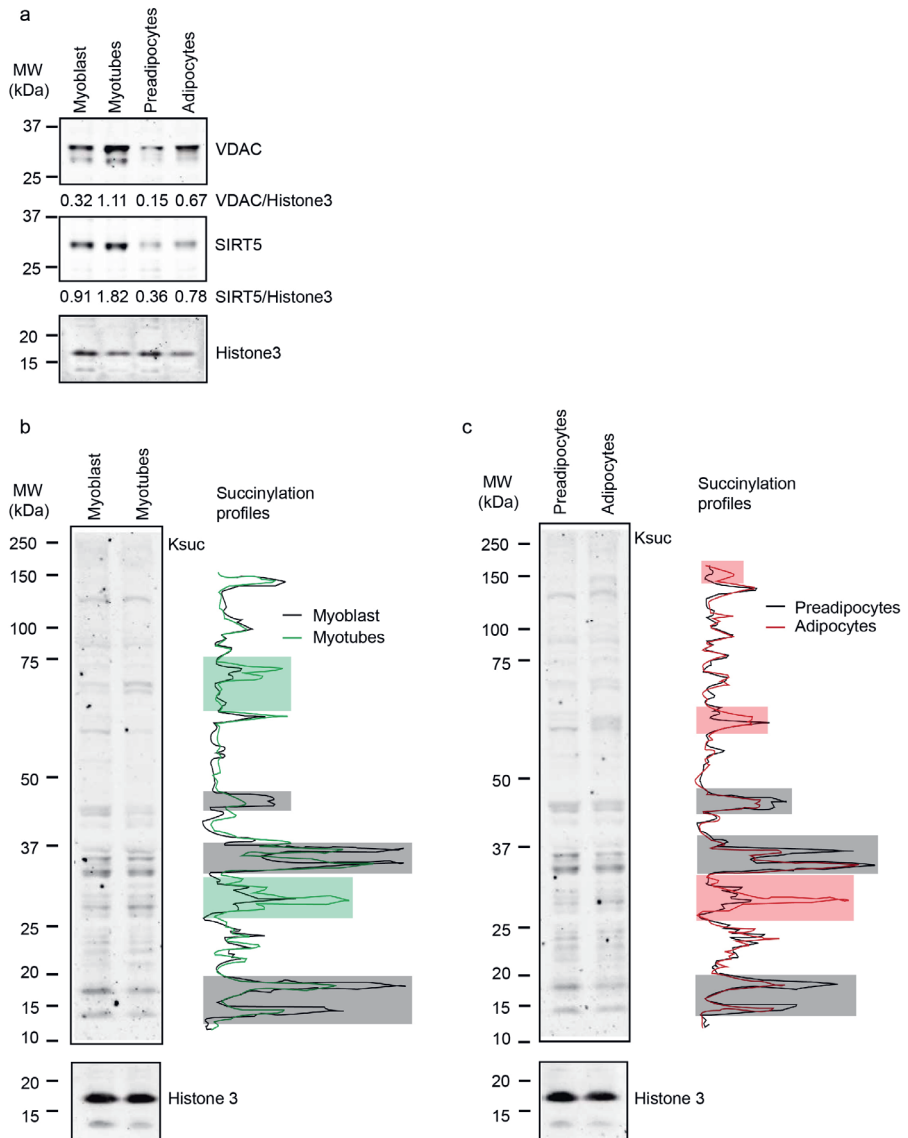


Figure 5. SIRT5 protein and succinylation levels in C2C12 myoblasts and myotubes and in 3T3-L1 preadipocytes and adipocytes. (a) Western blot analysis of voltage-dependent anion channel (VDAC), SIRT5 and histone 3. The numbers represent band intensity relative to histone 3. Blots of VDAC and SIRT5 were cropped from the same gel, and histone 3 was cropped from a different gel. Full-length blots are

presented in Supplementary Figure S3. **(b)** Succinyllysine levels and blot lane profiles of C2C12 myoblasts (black line) and myotubes (green line). Grey areas represent succinyllysine protein bands with higher intensity in myoblasts and green areas represent succinyllysine protein bands with lower intensity in myoblasts. **(c)** Succinyllysine levels and blot lane profiles of 3T3-L1 preadipocytes (black line) and adipocytes (red line). Grey areas represent succinyllysine protein bands with higher intensity in preadipocytes and red areas represent succinyllysine protein bands with lower intensity in adipocytes. In **b** and **c**, blots of succinylation and histone3 were grouped from different gels, and full-length blots for **b** and **c** are presented in Supplementary Figure S4.

Discussion

The complex interplay between metabolite-driven succinylation and NAD⁺-dependent desuccinylation gives opportunities to cells to regulate protein function based on metabolic state of the cells. To get more insights into these processes, we optimized a desuccinylase assay in cell lysates and applied our method to different cell types and conditions. We showed that a stricter reaction time was required to analyse initial rate in crude cell lysates as compared to recombinant His-SIRT5, that SIRT5 was responsible partially for the observed NAD⁺-dependent desuccinylase activity, and that NAD⁺-dependent desuccinylation activity varied with physiologic states. NAD⁺-dependent desuccinylase activity was higher in proliferative myoblasts and preadipocytes as compared to their differentiated counterparts.

Protein acetylation has been demonstrated to act as a regulator of cell differentiation from myoblast to myotubes⁴¹ as well as from preadipocyte to adipocytes⁴². Acetylation of histones is regulated by deacetylases and acetyltransferase to maintain, activate or repress gene transcription programs⁴³⁻⁴⁵. Although succinylation has been identified on histones, and NAD⁺-dependent desuccinylation by SIRT7 of specific histone marks regulated DNA damage repair pathway²⁵, it is not known whether there is a general role for succinylation and desuccinylation in regulating cell differentiation. Our findings that NAD⁺-dependent desuccinylase activities were higher in proliferative cells as compared to their differentiated counterparts, suggest that desuccinylation could play a role in the differentiation process. Interestingly, the NAD⁺-dependent desuccinylase protein, SIRT5, has been shown to support proliferative tumour cell growth in *in vitro* as well as *in vivo* models⁴⁶⁻⁴⁸. SIRT5 has also been found to be upregulated in different tumour types and its increased expression was proposed as marker for recurrence in non-small cell lung cancer (NSCLC)^{49,50}.

In our study, we identified a mismatch between SIRT5 protein expression and NAD⁺-dependent desuccinylase activity. SIRT5 protein was expressed higher in differentiated cells as compared to proliferative cells, whereas desuccinylase activity was lower. The increased SIRT5 protein level in differentiated myotubes and

adipocytes, could be explained by the fact that SIRT5 is primarily located in mitochondria¹¹, and that increased mitochondrial biogenesis is associated with both myogenesis³⁷ as well as adipogenesis³⁹. In support of this, protein levels of VDAC, an abundant mitochondrial outer membrane protein, were increased in differentiated cells as compared to proliferative cells. Interestingly, that the increased protein expression of SIRT5 did not translate into a higher NAD⁺-dependent desuccinylase activity could implicate that mitochondria-localized SIRT5 is post-translationally modified to be inactive. Since we analysed enzymatic activity in cell lysates and added external NAD⁺, NAD⁺ could not be a limitation for the analysed desuccinylase activity. Instead, SIRT5 could be regulated by PTMs or could be inhibited by interaction with other proteins that are part of a SIRT5 regulatory complex. Although only a limited number of SIRT5 protein interactors in the mitochondria have been identified in a large screen for mitochondrial sirtuin interactions⁵¹, it is possible that these interactors could have a role in altering the desuccinylation activity of SIRT5. For SIRT1, post-translational modifications and their impacts have been studied extensively. For example, phosphorylation on several SIRT1 sites could translocate SIRT1 and redirect it to specific targets with enhanced its enzymatic function^{52,53}. Additionally, other PTMs have also been demonstrated to affect SIRT1 level or activity, including sumoylation⁵⁴, carbonylation⁵⁵, and methylation⁵⁶. Another explanation for the mismatch between the SIRT5 expression and the desuccinylase activity could be that mitochondrial SIRT5 is not the main contributor to overall NAD⁺-dependent desuccinylase activity in myoblasts and preadipocytes. Indeed, when analysing NAD⁺-dependent desuccinylase activity in cell lysates of HEK293T SIRT5 KO cells, we observed substantial NAD⁺-dependent desuccinylase activity, whereas SIRT5 protein was not detectable. These findings highlight the importance of analysing NAD⁺-dependent desuccinylase activity, over only analysing expression of the protein or gene.

It has become apparent that sirtuin proteins have versatile deacetylase activity^{21,24,57}. Sirtuin members share deacetylase activities among each other, but also specific deacetylase, ADP-ribosyltransferase^{58,59} and lipoamidase⁶⁰ activities have been identified for sirtuins. Deacetylation activity is shared by SIRT1¹⁹, SIRT2²², and SIRT3²⁰. Desuccinylation has been identified, apart from SIRT5 and SIRT7, for SIRT3 and SIRT4 although these sirtuins only displayed minor desuccinylation activity against a succinylated lysine peptide *in vitro*⁶¹.

The versatility in enzymatic activity of sirtuins is also apparent from studies on SIRT6, which has both deacetylase activity as well as de-fatty acylase activity and ADP-ribosyltransferase activity^{59,62,63}. Specific mutations of SIRT6 identified in tumors could even predispose for one activity over the other⁶⁴. In our cell lines and

physiological conditions tested, the NAD⁺-dependent desuccinylase activities of cell lysates were approximately 10-fold lower than the NAD⁺-dependent deacetylase activities. Interestingly, the deacetylase activity did not change upon differentiation, whereas desuccinylase activity was different. Interestingly, in our study, we even identified two distinct desuccinylation reaction rates in cell lysates, one initial high activity and a second slower one. This could possibly be explained by differential substrate-binding affinity by multiple desuccinylases. Further studies are needed to explore the desuccinylation potential of specific proteins.

Overall, we optimized a fluorescence-based assay for detecting cellular NAD⁺-dependent desuccinylase activity, and demonstrated that NAD⁺-dependent desuccinylase activity was lowered in differentiated myotubes and adipocytes. The observed mismatch between SIRT5 protein expression and NAD⁺-dependent desuccinylase activity highlights the relevance of analysing sirtuin enzymatic activities in physiological contexts. The high desuccinylase activity in proliferating cells is of relevance to analyse how desuccinylase activity contributes to tumor cell function and how sirtuins with NAD⁺-dependent desuccinylase activity are regulated during proliferation and differentiation.

Material and Methods

His-SIRT5 expression and purification

The human His-SIRT5 (6x His) plasmid was a gift from Cheryl Arrowsmith (Addgene plasmid # 25487). Human SIRT5 gene is inserted into the vector pET28a-LIC, and six histidine residues are fused into the SIRT5 protein on N terminal, and the plasmid is resistant to kanamycin. The plasmid was transformed into chemical competent *E. coli* BL21 by heat shock as previously published⁶⁵, with minor modifications. Briefly, 1 µg of plasmid DNA was added to 50 µl competent *E. coli* BL21 cells, incubated for 30 minutes on ice, heat-shocked for 11 s at 42°C and returned to ice for 5 minutes. After the cells were incubated in 950 µL Lysogeny broth (LB) medium for 1 hour at 37°C. 100 µL of the transformation mix was plated on LB agar plates containing 50 µg/mL kanamycin and incubated overnight at 37°C. For His-SIRT5 protein expression, a single colony was inoculated in 3 mL LB medium with 50 µg/mL kanamycin, incubated for 8 hours at 37°C with shaking at 220 rpm using an incubator shaker (G25, New Brunswick Scientific), and the bacterial starter culture was stored at 4°C. Next day, 100 µL of bacterial starter culture was inoculated to 100 mL LB medium with 50 µg/mL kanamycin in a 300 mL Erlenmeyer flask, incubated at 37°C with shaking at 220 rpm until an OD₆₀₀ of 0.25, after which the cultures were placed at 22°C and Isopropyl β- d-1-thiogalactopyranoside (IPTG) was added to a final concentration of 1 mM. Cells were harvested 18 hours after IPTG induction by

centrifugation at 6,000 x *g* for 15 minutes at 4°C. For purification of His-SIRT5, 3 - 4 mg of *E. coli* pellet was resuspended in 3 mL lysis buffer (10 mM Tris/HCl pH 8.0, 500 mM NaCl, and 1 mg/mL lysozyme) and incubated end-over-end for 30 minutes at 4°C. Cells were then sonicated at 40% amplitude (burst of 1 s followed by 3 s interval) for 5 minutes on ice using a digital sonifier (Branson SLPe). Insoluble debris in the cell lysate was removed by centrifugation at 8,500 x *g* and 4°C for 15 minutes. Imidazole/HCl at pH 8.0 was added to the supernatant to a final concentration of 30 mM. Crude His-SIRT5 was purified using HisLink protein purification resin (#V8823, Promega) in combination with a chromatography column (#731-1150, Bio-Rad). The protein purification resin consists of microporous silica resin which contains a high level of tetradentate-chelated nickel and can purify polyhistidine-tagged recombinant proteins efficiently. To purify crude His-SIRT5, 0.4 mL of the HisLink protein purification resin was loaded to a chromatography column, then the resin was first equilibrated by washing five times with washing buffer (25 mM Tris/HCl pH 8.0, 500 mM NaCl, and 30 mM imidazole). *E. coli* lysate was then loaded onto the equilibrated column and was allowed to pass through, and this step was repeated once. Then, the column was washed five times with the washing buffer, and His-SIRT5 was eluted with 200 µL of elution buffer (25 mM Tris/HCl pH 8.0, 100 mM NaCl, and 500 mM imidazole). Elution fractions were checked for SIRT5 content using gel electrophoresis and Coomassie staining (Supplementary Fig. S1). Prior to use in further experiments, imidazole was removed from the eluted His-SIRT5 using ultra-0.5 centrifugal filter units (#UFC501096, Merck Millipore) according to the manufacturer's instruction. Briefly, 50 µL of eluted His-SIRT5 was loaded to a filter column, and 450 µL of exchange buffer (25 mM Tris/HCl pH 8.0 and 100 mM NaCl) was added, followed by centrifugation at 14,000 x *g* for 15 minutes at 4°C. The flow through was discarded and another 450 µL of exchange buffer was added to the column and the same centrifugation step was repeated once. Then the His-SIRT5 was collected by reverse centrifugation in an Eppendorf tube at 1,000 x *g* for 2 minutes at 4°C. The protein concentration of His-SIRT5 was determined using a Bradford protein assay (#23200, Thermo Scientific), after which the His-SIRT5 was preserved in 1x freezing buffer (50 mM Tris/HCl pH 8.0, 500 mM NaCl, 500 mM DTT, and 20% glycerol) and aliquoted with 10 µL/tube and the aliquots were stored at -80°C until use.

Cell culture

Murine 3T3-L1 preadipocytes (ATCC, #CL-173) were cultured at 37°C, 5% CO₂ in 3T3-L1 medium, which consisted of DMEM (#11880-028, Gibco) supplemented with 10% (v/v) foetal bovine serum (FBS, #06Q3501K, Gibco), 4.5 g/L glucose (#G7021, Sigma-

Aldrich), 4 mM l-glutamine (#25030-024, Gibco) and an antibiotic-antimycotic mix (10,000 units/mL of penicillin, 10,000 µg/mL of streptomycin, and 25 µg/mL Amphotericin B, #15240-062, Gibco). For differentiation of preadipocytes into adipocytes, 3T3-L1 preadipocytes (8,000 cells/well) were first seeded in 6-well plates in 3T3-L1 medium, and differentiation was started 48 hours after the preadipocytes reached 100% confluency by switching to 3T3-L1 differentiation medium (2 mL/well) in the same culture plates. The 3T3-L1 differentiation medium consisted of 3T3-L1 medium supplemented with a final concentration of 1 µM insulin (#I0516, Sigma-Aldrich), 0.5 mM 3-isobutyl-1-methylxanthine (#5879, Sigma-Aldrich), 1 µM dexamethasone (#D4902, Sigma-Aldrich) and 1 µM 15-Deoxy- Δ 12,14-prostaglandin J2 (#D8440, Sigma-Aldrich). The cells were cultured in the differentiation medium for 48 hrs, then in differentiation maintaining medium (3T3-L1 medium containing 1 µM insulin) until the cells were harvested at day 11 of differentiation.

Murine C2C12 myoblasts (ATCC, #CRL-1772) were cultured in C2C12 growth medium, consisted of DMEM (#11960-044, Gibco) supplemented with 25 mM HEPES (#15630080, Thermo Scientific), 10% FBS, and antibiotic-antimycotic mix. For differentiation of myoblasts into myotubes, myoblasts (3×10^5 cells/well) were first seeded in a 6-well plate in the C2C12 growth medium, and differentiation of myoblasts was started when the myoblasts reached 90% confluency by switching to C2C12 differentiation medium that contained 2% horse serum (#26050070, Gibco) instead of 10% FBS. Cells were cultured in the C2C12 differentiation medium until harvest at day 6 of differentiation.

Generation of SIRT5 knockout HEK293T cells

SIRT5 knockout HEK293T cells were generated using the CRISPR-Cas9 system following the directions outline in Ran *et. al*⁶⁶. Briefly, sgRNA against SIRT5 oligos (sequence: GGCTGCTGGGTACACCACAG) were resuspended in water, annealed, then phosphorylated using T4 polynucleotide kinase. Then, the ligated oligos and PX459 vector were digested and ligated together using BbsI and the T7 ligase, respectively. HEK293T cells (ATCC, #CRL-11268), cultured following ATCC guidelines, were transfected with the PX459-sgRNA vector using Lipofectamine 3000 according to manufacturer's instructions. Transfected cells were selected using puromycin (3 µg/mL) for 48 hrs. To achieve single-cell colonies, cells remaining after selection were diluted to a density of 50 cells/10 ml of media, and 100 µl of the diluted cell suspension per well was plated to 96-well plates. SIRT5 status in the colonies were assessed using immunoblotting. Colonies lacking SIRT5 protein were then sequenced to confirm Cas9-mediated genomic alterations at the location targeted by the sgRNA.

Colonies with SIRT5 levels comparable to WT HEK293T cells were used as controls for SIRT5 KO cells.

Desuccinylation activity assays

Desuccinylation activity was measured using a fluorogenic reporter assay. Succinylated-substrate (#BML-KI590), assay buffer (#BML-KI286-0020), developer concentrate (20x, #BML-KI105), NAD⁺ (#BML-KI282), and NAM (#BML-KI283-0500) were all purchased from Enzo. Assay reagents were prepared freshly in the assay buffer prior to the assay and were kept on ice until use.

For desuccinylase activity in cells, trypsinized, washed and pelleted cells were resuspended in lysis buffer (50 mM Tris/HCl, pH 8.0, 137 mM NaCl, 2.7 mM KCl, 1 mM MgCl₂, 0.1% Triton X-100, and protease inhibitor (#04693159001, Roche)) and sonicated on ice at 40% amplitude (burst of 1 s followed by 3 s cooling) for 12 bursts using a Branson SLPe digital sonifier. Cell lysates were centrifuged at 10,000 x *g*, 4°C for 10 minutes, and the supernatants were used in further experiments. Samples were equalized with lysis buffer on protein concentration after determination using DC protein assays (#5000116, Bio-Rad). Protein input for each sample in the desuccinylase reaction was indicated in the figure legends. Prior to use in desuccinylation reaction, 28 µL of cell lysates were incubated at a 37°C water bath with shaking at 60 rpm (Shaking water bath, VWR) in 1.5 mL Eppendorf tubes for 10 minutes to degrade endogenous NAD⁺, then 0.6 µL of 50 mM dithiothreitol⁶⁷ dissolved in assay buffer was added to all cell lysates, and incubation continued for an additional 5 minutes. The catalytic reactions were performed at 37°C with shaking at 60 rpm, initiated by adding 28 µL of pre-warmed (37°C) 20 µM succinyl-substrate (final concentration of 10 µM) in combination with either 1 mM NAD⁺ (final concentration of 500 µM) or assay buffer only (negative control). After adding the substrates, the tubes were vortexed at 2200 rpm for 2 seconds with a Minishaker (IKA MS2) and then placed at the 37°C water bath. The reactions were stopped after 10 minutes, unless stated otherwise, by adding 56 µL of 1x developer containing 2 mM NAM, vortexing at 2200 rpm for 2 seconds, then incubating at 25°C for 15 minutes. Finally, 100 µL of each sample was loaded onto half-area black 96-well plates (#3686, Corning) and the fluorescence was read with excitation at 360 nm and emission at 460 nm at 25°C on a BioTek Synergy HT microplate reader. Fluorescence signal of the negative control group was subtracted from each experimental sample. To analyse the desuccinylation activity of His-SIRT5, the same procedure was followed as for cell lysate, but instead of cell lysates, purified recombinant His-SIRT5 was used. The amount of His-SIRT5 used in each assay was indicated in figure legends.

NAM sensitivity of desuccinylation activity

For analysing NAM sensitivity of cellular desuccinylation activity, the assay procedure was the same as desuccinylation assay described above, with a slightly different reaction system composition, as follows: 14 μL cell lysate (187.3 μg), 28 μL of 20 μM succinylated-substrate containing 1 mM NAD^+ , and 14 μL NAM (0.04 - 4000 μM , resulting in a final concentration in the reaction system of 0.01-1000 μM). The reaction was stopped with either 56 μL 1x developer (experimental samples) or 56 μL 1x developer containing 2 mM NAM (negative control sample). The fluorescence signal was subtracted from signal in the negative control group, which consisted of 14 μL cell lysate, 28 μL succinylated-substrate without NAD^+ and 14 μL assay buffer. The same procedure was used to analyse NAM sensitivity of His-SIRT5 desuccinylation activity, except that His-SIRT5 (0.06 μg) was used instead of cell lysate.

Deacetylation activity assay

Deacetylation activities of cell lysates and recombinant His-SIRT5 were determined similarly to the desuccinylation activity, except that an acetylated-fluorogenic substrate (#BML-KI179, Enzo) rather than a succinylated-substrate was used and 1x developer II (#BML-KI176-1250, Enzo) was used to stop the deacetylation reaction.

Western blotting

Cells were lysed in lysis buffer (50 mM Tris/HCl pH 7.4) containing deacylase inhibitors (1 μM trichostatin A and 10 mM NAM) as well as protease inhibitor cocktail (#04693159001, Roche) by sonication on ice, the cell lysate sonication procedure was the same as described in the Desuccinylation activity assays section. Samples were equalized to the same protein level with the lysis buffer following quantification by DC protein assays. Cell lysates (30 μg protein) were separated on NuPAGE 4-12% gradient gels (#NP0322, Thermo Scientific) at 110 V for 35 minutes, followed by 150 V for 40 minutes at room temperature. After which, proteins on the gel were immediately transferred to a nitrocellulose membrane at 300 mA for 1 hour on ice. Antibodies against SIRT5 (#8782, Cell Signaling Technology), succinyllysine (#401, PTM Biolabs), voltage-dependent anion channel (VDAC) (#ab14734, Abcam) and Histone 3 (#9715, Cell Signaling Technology) were used to identify the respective targets. IRDye Donkey anti-rabbit (#926-32213, LI-COR Biosciences) and Goat anti-mouse (#926-32210, LI-COR Biosciences) were used and signals were detected using an Odyssey scanner (LI-COR). Lane profile analyses was performed using Image J 1.51p.

Statistics

Statistical analysis was performed using GraphPad Prism 5.04. Data was compared using the two-tailed unpaired Student's t-test. Data represent mean \pm SEM. P values below 0.05 were considered significant.

Data availability

All data generated or analysed during this study are included in this published article (and its Supplementary Information files).

Acknowledgements

TY has received financial support from the China Scholarship Council (Grant No. 201606350170). AG was supported by T32 AG000114. Generation of the SIRT5 KO cells in the Lombard lab was supported by R01GM101171. His-SIRT5 plasmid was a gift from Cheryl Arrowsmith (Addgene plasmid # 25487).

Author Contributions

TY performed all experiments, analysed all data, drafted and wrote the manuscript. AG and DL generated and provided essential experimental resources. JK and VdB supervised study, discussed data and edited manuscript. All authors commented on the manuscript.

Additional Information

Competing interests. The authors declare no competing interests.

References

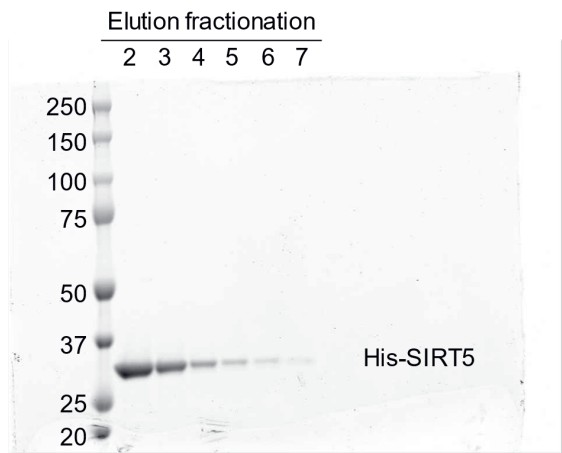
1. Zhang, Z. *et al.* Identification of lysine succinylation as a new post-translational modification. *Nat. Chem. Biol.* **7**, 58-63, doi:10.1038/nchembio.495 (2011).
2. Walsh, C. T., Garneau-Tsodikova, S. & Gatto, G. J., Jr. Protein posttranslational modifications: the chemistry of proteome diversifications. *Angew. Chem. Int. Ed. Engl.* **44**, 7342-7372, doi:10.1002/anie.200501023 (2005).
3. Eshun-Wilson, L. *et al.* Effects of α -tubulin acetylation on microtubule structure and stability. *Proc. Natl. Acad. Sci. U. S. A.* **116**, 10366-10371, doi:10.1073/pnas.1900441116 (2019).
4. Pougovkina, O. *et al.* Mitochondrial protein acetylation is driven by acetyl-CoA from fatty acid oxidation. *Hum. Mol. Genet.* **23**, 3513-3522, doi:10.1093/hmg/ddu059 (2014).
5. Li, F. *et al.* NADP(+)-IDH Mutations Promote Hypersuccinylation that Impairs Mitochondria Respiration and Induces Apoptosis Resistance. *Mol. Cell* **60**, 661-675, doi:10.1016/j.molcel.2015.10.017 (2015).
6. Wagner, G. R. & Payne, R. M. Widespread and enzyme-independent Nepsilon-acetylation and Nepsilon-succinylation of proteins in the chemical conditions of the mitochondrial matrix. *J. Biol. Chem.* **288**, 29036-29045, doi:10.1074/jbc.M113.486753 (2013).
7. Lin, H. & Carroll, K. S. Introduction: Posttranslational Protein Modification. *Chem Rev.* **118**, 887-888, doi:10.1021/acs.chemrev.7b00756 (2018).
8. Weinert, B. T. *et al.* Lysine succinylation is a frequently occurring modification in prokaryotes and eukaryotes and extensively overlaps with acetylation. *Cell Rep.* **4**, 842-851, doi:10.1016/j.celrep.2013.07.024 (2013).
9. Xie, Z. *et al.* Lysine succinylation and lysine malonylation in histones. *Mol. Cell. Proteomics* **11**, 100-107, doi:10.1074/mcp.M111.015875 (2012).
10. Smestad, J., Erber, L., Chen, Y. & Maher, L. J. Chromatin Succinylation Correlates with Active Gene Expression and Is Perturbed by Defective TCA Cycle Metabolism. *iScience* **2**, 63-75, doi:10.1016/j.isci.2018.03.012 (2018).
11. Park, J. *et al.* SIRT5-mediated lysine desuccinylation impacts diverse metabolic pathways. *Mol. Cell* **50**, 919-930, doi:10.1016/j.molcel.2013.06.001 (2013).
12. Rardin, M. J. *et al.* SIRT5 regulates the mitochondrial lysine succinylome and metabolic networks. *Cell Metab.* **18**, 920-933, doi:10.1016/j.cmet.2013.11.013 (2013).
13. Sadhukhan, S. *et al.* Metabolomics-assisted proteomics identifies succinylation and SIRT5 as important regulators of cardiac function. *Proc. Natl. Acad. Sci. U. S. A.* **113**, 4320-4325, doi:10.1073/pnas.1519858113 (2016).
14. Hershberger, K. A. *et al.* Sirtuin 5 is required for mouse survival in response to cardiac pressure overload. *J. Biol. Chem.* **292**, 19767-19781, doi:10.1074/jbc.M117.809897 (2017).
15. Chen, H. *et al.* Mild metabolic perturbations alter succinylation of mitochondrial proteins. *J. Neurosci. Res.* **95**, 2244-2252, doi:10.1002/jnr.24103 (2017).
16. Gibson, G. E. *et al.* Alpha-ketoglutarate dehydrogenase complex-dependent succinylation of proteins in neurons and neuronal cell lines. *J. Neurochem.* **134**, 86-96, doi:10.1111/jnc.13096 (2015).
17. Meyer, J. G. *et al.* Temporal dynamics of liver mitochondrial protein acetylation and succinylation and metabolites due to high fat diet and/or excess glucose or fructose. *PLoS One* **13**, e0208973, doi:10.1371/journal.pone.0208973 (2018).
18. Bentley, N. L. *et al.* Protein hypoacylation induced by Sirt5 overexpression has minimal metabolic effect in mice. *Biochem. Biophys. Res. Commun.* **503**, 1349-1355, doi:10.1016/j.bbrc.2018.07.047 (2018).

19. Vaziri, H. *et al.* hSIR2(SIRT1) functions as an NAD-dependent p53 deacetylase. *Cell* **107**, 149-159, doi:10.1016/s0092-8674(01)00527-x (2001).
20. Onyango, P., Celic, I., McCaffery, J. M., Boeke, J. D. & Feinberg, A. P. SIRT3, a human SIR2 homologue, is an NAD-dependent deacetylase localized to mitochondria. *Proc. Natl. Acad. Sci. U. S. A.* **99**, 13653-13658, doi:10.1073/pnas.222538099 (2002).
21. Anderson, K. A. *et al.* SIRT4 Is a Lysine Deacetylase that Controls Leucine Metabolism and Insulin Secretion. *Cell Metab.* **25**, 838-855.e815, doi:10.1016/j.cmet.2017.03.003 (2017).
22. North, B. J., Marshall, B. L., Borra, M. T., Denu, J. M. & Verdin, E. The human Sir2 ortholog, SIRT2, is an NAD⁺-dependent tubulin deacetylase. *Mol. Cell* **11**, 437-444 (2003).
23. Houtkooper, R. H., Pirinen, E. & Auwerx, J. Sirtuins as regulators of metabolism and healthspan. *Nat. Rev. Mol. Cell Biol.* **13**, 225-238, doi:10.1038/nrm3293 (2012).
24. Du, J. *et al.* Sirt5 is a NAD-dependent protein lysine demalonylase and desuccinylase. *Science* **334**, 806-809, doi:10.1126/science.1207861 (2011).
25. Li, L. *et al.* SIRT7 is a histone desuccinylase that functionally links to chromatin compaction and genome stability. *Nat. Commun.* **7**, 12235, doi:10.1038/ncomms12235 (2016).
26. Tan, M. *et al.* Lysine Glutarylation Is a Protein Posttranslational Modification Regulated by SIRT5. *Cell Metab.* **19**, 605-617, doi:http://dx.doi.org/10.1016/j.cmet.2014.03.014 (2014).
27. Nakagawa, T., Lomb, D. J., Haigis, M. C. & Guarente, L. SIRT5 Deacetylates carbamoyl phosphate synthetase 1 and regulates the urea cycle. *Cell* **137**, 560-570, doi:10.1016/j.cell.2009.02.026 (2009).
28. Ryu, D. *et al.* A SIRT7-dependent acetylation switch of GABPbeta1 controls mitochondrial function. *Cell Metab.* **20**, 856-869, doi:10.1016/j.cmet.2014.08.001 (2014).
29. Yu, J. *et al.* Regulation of Serine-Threonine Kinase Akt Activation by NAD(+)-Dependent Deacetylase SIRT7. *Cell Rep.* **18**, 1229-1240, doi:10.1016/j.celrep.2017.01.009 (2017).
30. Wagner, G. R. *et al.* A Class of Reactive Acyl-CoA Species Reveals the Non-enzymatic Origins of Protein Acylation. *Cell Metab.* **25**, 823-837, doi:10.1016/j.cmet.2017.03.006 (2017).
31. Houtkooper, R. H., Canto, C., Wanders, R. J. & Auwerx, J. The secret life of NAD⁺: an old metabolite controlling new metabolic signaling pathways. *Endocr. Rev.* **31**, 194-223, doi:10.1210/er.2009-0026 (2010).
32. Schuster, S. *et al.* A continuous sirtuin activity assay without any coupling to enzymatic or chemical reactions. *Scientific Rep.* **6**, 22643, doi:10.1038/srep22643 (2016).
33. Madsen, A. S. & Olsen, C. A. Substrates for efficient fluorometric screening employing the NAD-dependent sirtuin 5 lysine deacetylase (KDAC) enzyme. *J. Med. Chem.* **55**, 5582-5590, doi:10.1021/jm300526r (2012).
34. Maurer, B. *et al.* Inhibitors of the NAD(+)-Dependent Protein Desuccinylase and Demalonylase Sirt5. *ACS. Med. Chem. Lett.* **3**, 1050-1053, doi:10.1021/ml3002709 (2012).
35. Pacella-Ince, L., Zander-Fox, D. L. & Lane, M. Mitochondrial SIRT5 is present in follicular cells and is altered by reduced ovarian reserve and advanced maternal age. *Reprod. Fert. Dev.* **26**, 1072-1083, doi:10.1071/RD13178 (2014).
36. Polletta, L. *et al.* SIRT5 regulation of ammonia-induced autophagy and mitophagy. *Autophagy* **11**, 253-270, doi:10.1080/15548627.2015.1009778 (2015).
37. Remels, A. H. *et al.* Regulation of mitochondrial biogenesis during myogenesis. *Mol. Cell. Endocrinol.* **315**, 113-120, doi:10.1016/j.mce.2009.09.029 (2010).
38. Kraft, C. S. *et al.* Control of mitochondrial biogenesis during myogenesis. *Am. J. Physiol. Cell Physiol.* **290**, C1119-1127, doi:10.1152/ajpcell.00463.2005 (2006).
39. Wilson-Fritch, L. *et al.* Mitochondrial biogenesis and remodeling during adipogenesis and in response to the insulin sensitizer rosiglitazone. *Mol. Cell. Biol.* **23**, 1085-1094 (2003).

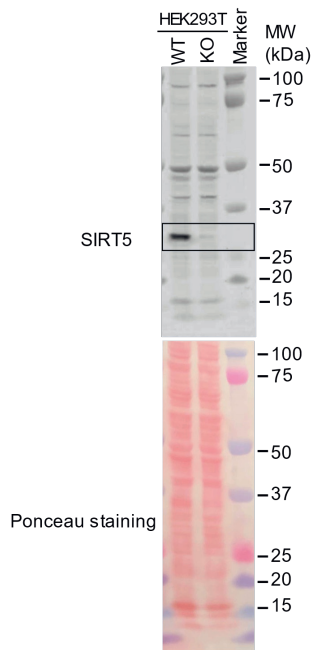
40. Tormos, K. V. *et al.* Mitochondrial complex III ROS regulate adipocyte differentiation. *Cell Metab.* **14**, 537-544, doi:10.1016/j.cmet.2011.08.007 (2011).
41. Mal, A. & Harter, M. L. MyoD is functionally linked to the silencing of a muscle-specific regulatory gene prior to skeletal myogenesis. *Proc. Natl. Acad. Sci. U. S. A.* **100**, 1735-1739, doi:10.1073/pnas.0437843100 (2003).
42. Yoo, E. J., Chung, J. J., Choe, S. S., Kim, K. H. & Kim, J. B. Down-regulation of histone deacetylases stimulates adipocyte differentiation. *J. Biol. Chem.* **281**, 6608-6615, doi:10.1074/jbc.M508982200 (2006).
43. Verdone, L., Agricola, E., Caserta, M. & Di Mauro, E. Histone acetylation in gene regulation. *Brief Funct. Genomic Proteomic* **5**, 209-221, doi:10.1093/bfpg/ell028 (2006).
44. Mehrotra, S. *et al.* Histone hypoacetylation-activated genes are repressed by acetyl-CoA- and chromatin-mediated mechanism. *Biochim. Biophys. Acta* **1839**, 751-763, doi:10.1016/j.bbaggm.2014.05.029 (2014).
45. Brownell, J. E. *et al.* Tetrahymena histone acetyltransferase A: a homolog to yeast Gcn5p linking histone acetylation to gene activation. *Cell* **84**, 843-851, doi:10.1016/s0092-8674(00)81063-6 (1996).
46. Du, Z. *et al.* Targeting a Sirt5-Positive Subpopulation Overcomes Multidrug Resistance in Wild-Type Kras Colorectal Carcinomas. *Cell Rep.* **22**, 2677-2689, doi:10.1016/j.celrep.2018.02.037 (2018).
47. Yang, X. *et al.* SHMT2 Desuccinylation by SIRT5 Drives Cancer Cell Proliferation. *Cancer Res.* **78**, 372-386, doi:10.1158/0008-5472.can-17-1912 (2018).
48. Lv, X. B. *et al.* SUN2 exerts tumor suppressor functions by suppressing the Warburg effect in lung cancer. *Sci Rep.* **5**, 17940, doi:10.1038/srep17940 (2015).
49. Lu, W. D., Zuo, Y., Feng, Y. F. & Zhang, M. SIRT5 facilitates cancer cell growth and drug resistance in non-small cell lung cancer. *Tumor Biol.* **35**, 10699-10705, doi:10.1007/s13277-014-2372-4 (2014).
50. Kumar, S. & Lombard, D. B. Functions of the sirtuin deacylase SIRT5 in normal physiology and pathobiology. *Crit. Rev. Biochem. Mol. Biol.* **53**, 311-334, doi:10.1080/10409238.2018.1458071 (2018).
51. Yang, W. *et al.* Mitochondrial Sirtuin Network Reveals Dynamic SIRT3-Dependent Deacetylation in Response to Membrane Depolarization. *Cell* **167**, 985-1000 e1021, doi:10.1016/j.cell.2016.10.016 (2016).
52. Nasrin, N. *et al.* JNK1 phosphorylates SIRT1 and promotes its enzymatic activity. *PLoS One* **4**, e8414, doi:10.1371/journal.pone.0008414 (2009).
53. Sasaki, T. *et al.* Phosphorylation regulates SIRT1 function. *PLoS One* **3**, e4020, doi:10.1371/journal.pone.0004020 (2008).
54. Yang, Y. *et al.* SIRT1 sumoylation regulates its deacetylase activity and cellular response to genotoxic stress. *Nat. Cell Biol.* **9**, 1253-1262, doi:10.1038/ncb1645 (2007).
55. Caito, S. *et al.* SIRT1 is a redox-sensitive deacetylase that is post-translationally modified by oxidants and carbonyl stress. *FASEB J.* **24**, 3145-3159, doi:10.1096/fj.09-151308 (2010).
56. Liu, X. *et al.* Methyltransferase Set7/9 regulates p53 activity by interacting with Sirtuin 1 (SIRT1). *Proc. Natl. Acad. Sci. U. S. A.* **108**, 1925-1930, doi:10.1073/pnas.1019619108 (2011).
57. Kumar, S. & Lombard, D. B. Mitochondrial sirtuins and their relationships with metabolic disease and cancer. *Antioxid. Redox Signal.* **22**, 1060-1077, doi:10.1089/ars.2014.6213 (2015).
58. Haigis, M. C. *et al.* SIRT4 inhibits glutamate dehydrogenase and opposes the effects of calorie restriction in pancreatic beta cells. *Cell* **126**, 941-954, doi:10.1016/j.cell.2006.06.057 (2006).
59. Liszt, G., Ford, E., Kurtev, M. & Guarente, L. Mouse Sir2 homolog SIRT6 is a nuclear ADP-ribosyltransferase. *J. Biol. Chem.* **280**, 21313-21320, doi:10.1074/jbc.M413296200 (2005).

60. Mathias, R. A. *et al.* Sirtuin 4 is a lipoamidase regulating pyruvate dehydrogenase complex activity. *Cell* **159**, 1615-1625, doi:10.1016/j.cell.2014.11.046 (2014).
61. Feldman, J. L., Baeza, J. & Denu, J. M. Activation of the protein deacetylase SIRT6 by long-chain fatty acids and widespread deacylation by mammalian sirtuins. *J. Biol. Chem.* **288**, 31350-31356, doi:10.1074/jbc.C113.511261 (2013).
62. Michishita, E. *et al.* SIRT6 is a histone H3 lysine 9 deacetylase that modulates telomeric chromatin. *Nature* **452**, 492-496, doi:10.1038/nature06736 (2008).
63. Jiang, H. *et al.* SIRT6 regulates TNF- α secretion through hydrolysis of long-chain fatty acyl lysine. *Nature* **496**, 110-113, doi:10.1038/nature12038 (2013).
64. Kugel, S. *et al.* Identification of and Molecular Basis for SIRT6 Loss-of-Function Point Mutations in Cancer. *Cell Rep.* **13**, 479-488, doi:10.1016/j.celrep.2015.09.022 (2015).
65. Kumar, S. & Lombard, D. B. Generation and Purification of Catalytically Active Recombinant Sirtuin5 (SIRT5) Protein. *Methods Mol. Biol.* **1436**, 241-257, doi:10.1007/978-1-4939-3667-0_16 (2016).
66. Ran, F. A. *et al.* Genome engineering using the CRISPR-Cas9 system. *Nat. Protoc.* **8**, 2281-2308, doi:10.1038/nprot.2013.143 (2013).
67. Hu, J., He, B., Bhargava, S. & Lin, H. A fluorogenic assay for screening Sirt6 modulators. *Org. Biomol. Chem.* **11**, 5213-5216, doi:10.1039/c3ob41138a (2013).

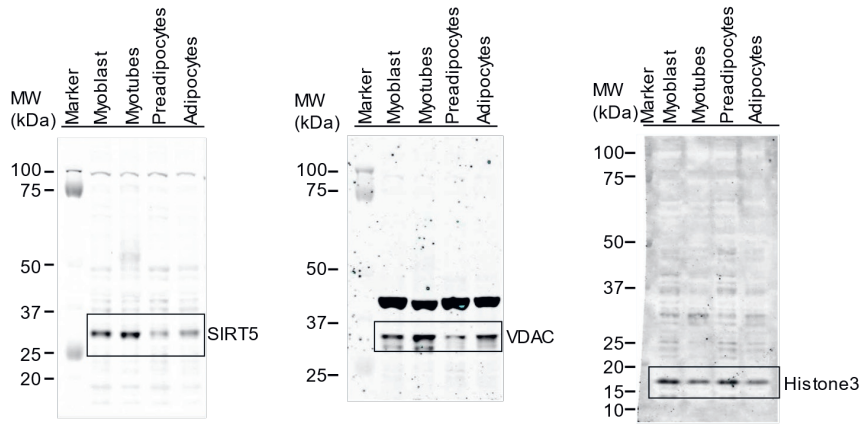
Supplementary Figures



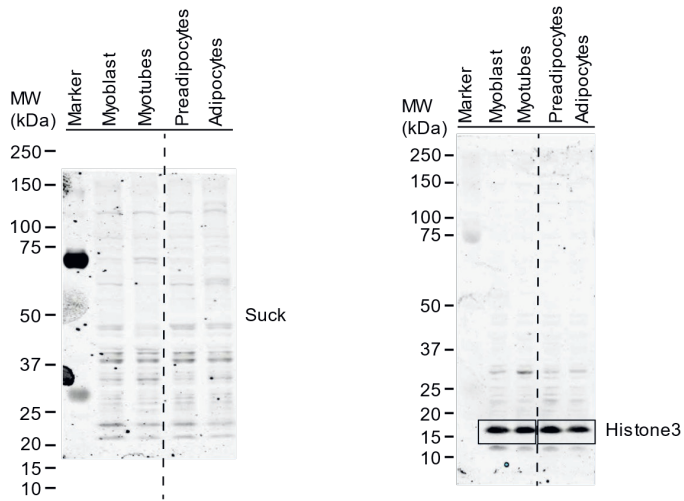
Supplementary Figure S1. Gel electrophoresis result of elution fractionation of His-SIRT5. The elution fractionation 1 was not loaded on gel due to high salt content in the sample.



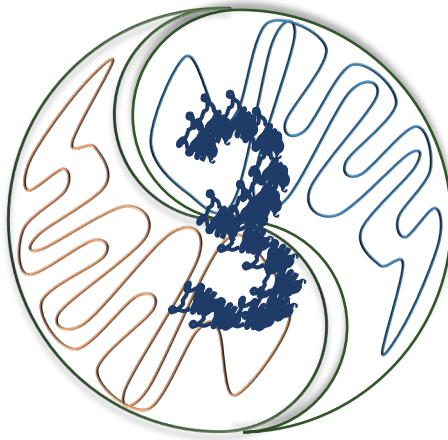
Supplementary Figure S2. Full-length blots for cropped blots shown in Fig. 1e. Ponceau staining shows the equal loading.



Supplementary Figure S3. Full-length blots for cropped blots shown in Fig. 5a.



Supplementary Figure S4. Full-length blots of cropped blots shown in Fig. 5b and Fig. 5c. Blot was cropped along the black dash line. Left side of dash line was shown in Fig. 5b, and right side of dash line was shown in Fig. 5c.



Profiling SIRT5 loss-of-function in humans identifies its critical role in redox homeostasis

Taolin Yuan¹, Jaap Keijer¹, Annelies Bunschoten¹, Werner J. H. Koopman^{1,2}, Nicolas F. van der Hoeven¹, Johannes N. Spelbrink³, Jun Young Hong⁴, Yingling Chiang⁴, Dennis A. Kutateladze⁴, Min Yang⁴, Yizhen Jin⁴, Hening Lin⁵, Fathiya Al-Murshedi⁶, Majid Alfadhel⁷, Richard J. Rodenburg^{3, *}, Vincent C. J. de Boer^{1, *}

¹Human and Animal Physiology, Wageningen University & Research, The Netherlands

²Department of Biochemistry, Radboud University Medical Center, The Netherlands

³Department of Pediatrics, Radboud University Medical Center, The Netherlands

⁴Department of Chemistry and Chemical Biology, Cornell University, USA

⁵Howard Hughes Medical Institute, Cornell University, USA

⁶Department of Genetics, Sultan Qaboos University Hospital, Sultan Qaboos University, Oman

⁷Department of Pediatrics, King Abdulaziz Medical City, Saudi Arabia

In Revision

Abstract

SIRT5 is a primarily mitochondria-located, NAD⁺-dependent desuccinylase. Based on functional studies in cells and mice, SIRT5 has emerged as an important regulator of metabolic health, especially during cellular and metabolic stress. However, direct evidence for a role of SIRT5 in human physiology or pathology is lacking. Here, we describe two different homozygous loss-of-function variants of *SIRT5* identified in two unrelated individuals by whole exome sequencing. The affected individuals present clinical mitochondrial disorder manifestations, including mitochondrial encephalopathy. In patients-derived fibroblasts, SIRT5 protein levels were markedly reduced, and global lysine succinylation levels were significantly higher than in control fibroblasts. Immunofluorescence staining showed for control and *SIRT5* variant fibroblasts that succinylation localized primarily to mitochondria. Functional analyses demonstrated that SIRT5 loss-of-function did not affect mitochondrial oxidative phosphorylation enzymology and cellular oxygen consumption rate. Instead, SIRT5 loss altered redox homeostasis. We identified that cells with each of the two loss-of-function *SIRT5* variants had an elevated mitochondrial proton leak rate and the NADPH/NADP⁺ redox couple ratio was decreased 2-fold. In addition, intracellular ROS levels increased to a higher level in the *SIRT5* variant fibroblasts upon acute H₂O₂ application. Combined, we conclude that human SIRT5 loss-of-function caused by the *SIRT5* variants establishes the critical role of SIRT5 in maintaining redox homeostasis.

Introduction

Mitochondria are essential for maintaining health of eukaryotes, through their distinct functioning as bioenergetic, biosynthetic and signalling organelles¹. Consequently, mitochondria are vital for normal tissue function and mitochondrial dysfunctions lead to a myriad of diseases^{2, 3, 4}. In general, organs with high energy requirements, such as brain, liver and heart, are more sensitive to defective mitochondria and display severe clinical phenotypes⁵. Mitochondrial disease has been shown for genetic variation in proteins involved in oxidative phosphorylation (OXPHOS) complex assembly, in mitochondrial structure, mtDNA maintenance, or other aspects of mitochondrial functioning^{2, 6, 7, 8, 9}. At the cellular level, mitochondrial dysfunction is often paralleled by increased reactive oxygen species (ROS) levels^{10, 11, 12, 13}. This has led to the hypothesis that targeting these ROS and/or redox homeostasis might be a valid intervention strategy in mitochondrial disease, and various clinical trials have been performed or are ongoing^{14, 15, 16, 17}.

SIRT5, a robust NAD⁺-dependent desuccinylase belonging to the mammalian sirtuin family, is primarily localized in mitochondria^{18, 19, 20}. It not only removes succinyl-adducts, but can also catalyse the removal of malonyl- and glutaryl- groups from lysine residues of proteins^{18, 21}. SIRT5 depletion is paralleled by increased global levels of succinylation, malonylation and glutarylation, and most of the modified proteins are metabolic enzymes^{20, 22, 23, 24, 25, 26}. Based on its numerous physiological substrates and widespread tissue distribution *in vivo*, SIRT5 has been speculated as an important regulator of metabolic health. While the phenotype of SIRT5 knockout (KO) mice remained largely normal under basal condition^{27, 28}, in different physiologically challenging contexts, mice with SIRT5 KO revealed roles of SIRT5 in metabolic pathways as well as pathways related to stress response^{25, 26, 29}. SIRT5 KO mice were shown to be more sensitive to paraquat-induced damage in the brain³⁰. Furthermore, SIRT5 KO in mice resulted in increased infarct size upon ischemia-reperfusion injury³¹. In contrast, SIRT5 KO mice brains were less sensitive to ischemia/reperfusion injury as compared to wild-type (WT) mice³² and heart-specific SIRT5 KO did not replicate the heart pathology that was found in the whole body SIRT5 KO mice^{33, 34}. These studies highlight a role for SIRT5 in regulating mouse stress responses depending on the physiological context. However, more insight is needed on the potential role of SIRT5 function in human (patho)physiology, especially during stress conditions.

In this study, we analysed two novel *SIRT5* variants detected in patients with a mitochondrial disease-like pathology. We show that each of the two *SIRT5* variants results in a loss of SIRT5 protein level, loss of NAD⁺-dependent desuccinylase activity,

and increased global protein succinylation levels. Patient fibroblasts displayed a disrupted redox homeostasis, characterized by reduced NADPH/NADP⁺ ratios during OXPHOS-stimulating conditions and increased ROS levels during exogenous oxidant addition. Our findings reveal a functional relevance of SIRT5 in humans via affecting redox homeostasis.

Results

Whole exome sequencing identifies *SIRT5* variants in two patients with mitochondrial disease-like pathology

Whole exome sequencing (WES) of DNA from two unrelated patients that presented with severe mitochondrial-like pathology resulted in the identification of two predicted-pathogenic *SIRT5* variants. These patients did not have common copy number genetic variants according to CGH microarray analysis or major chromosomal aberrations that could associate these patients with other mitochondrial genetic variants. In the first patient, we identified a *SIRT5* homozygous missense variant (c.340C>A, NM_012241.3) that led to a proline114 substitution to threonine (P114T) in the SIRT5 protein. In the second patient, a different homozygous *SIRT5* missense variant was identified. In this patient, the variation in the *SIRT5* gene (c.382C>G, NM_012241.3) resulted in leucine128 to valine change (L128V).

Clinically, the first patient (a 7-year-old boy) presented with a profound global developmental delay, seizures, spastic quadriparesis, optic atrophy, blindness and deafness (Fig. 1a). An MRI of the brain at 2 years of age, showed global cerebral and cerebellar atrophy with a marked reduction of white matter volume, as well as a delayed myelination pattern (Fig. 1b, left panel). Besides these severe physical anomalies, echocardiography indicated a normal function of the heart and investigations in plasma and urine metabolites were largely non-remarkable. The patient was born to first cousin parents. He has an older healthy sister, and two sisters born after him who died in early infancy (age of 3 months) with progressive hypoalbuminemia and nephrotic range proteinuria, a phenotype different from patient 1. Both sisters did not have visual tracking nor responding to sounds right from the beginning. One of the sisters was heterozygous for the *SIRT5* variant and WES on her was negative. There was no DNA available on the second sister. He has a seven-month-old brother who is homozygous for the *SIRT5* c.340C>A (p.P114T) variant. Thus far, this child has appropriate development and neurological examination (sitting unsupported, grasping, and transferring objects and is babbling). The second patient (a 30-year-old female) presented clinically with

neuroregression, dysarthria, and dystonia (Fig. 1a). At the age of 22 years, patient 2 started to have ataxia and proptosis, and shortly thereafter developed tremors, that gradually resulted in loss of motor skills until she became bedridden. An MRI of the brain at age of 25 years showed bilateral symmetrical signal abnormalities in the basal ganglia, as well as in the posterior limb of the internal capsule and brain stem (Fig. 1b, right panel).

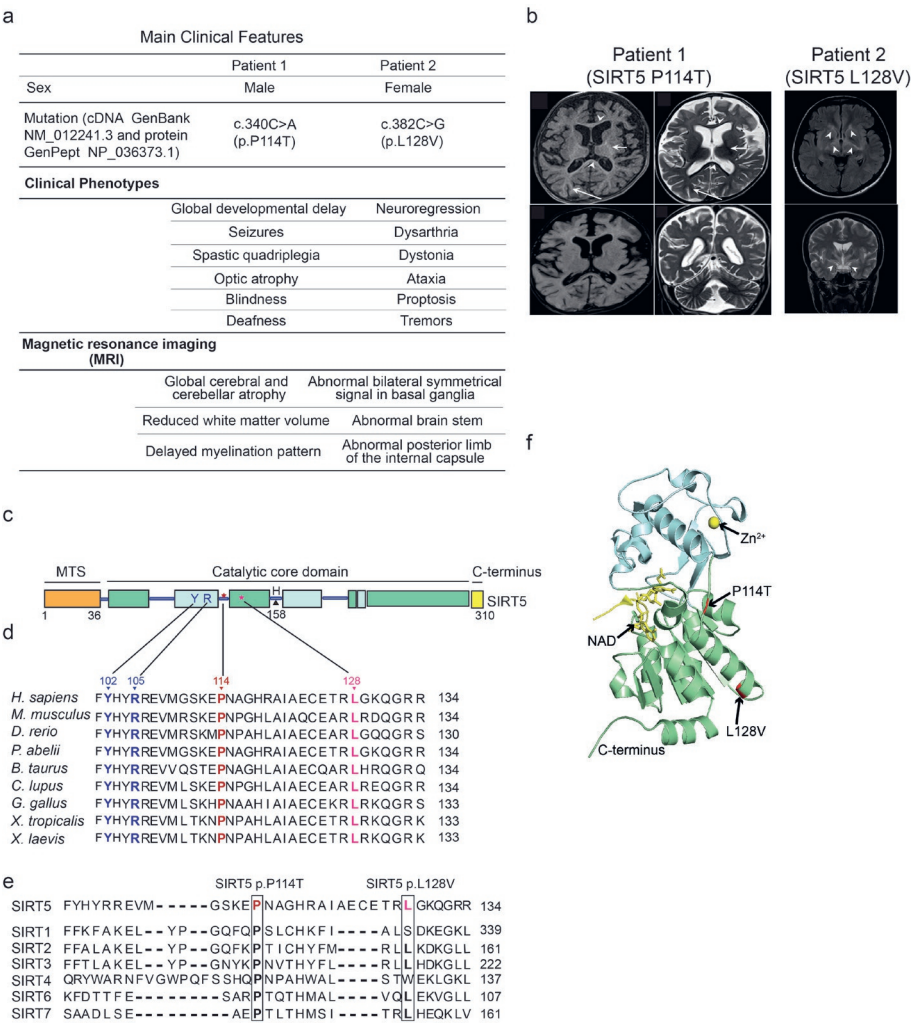


Figure 1. Two SIRT5 homozygous variants were identified in patients with mitochondrial-like disease. (a) Clinical symptoms of the two patients. (b) MRI images of brains of the patient 1 (at the age of 2 years) and patient 2 (at the age of 25 years). (c) Schematic representation of the human SIRT5 protein structure. The catalytic core domain consists of Rossmann-fold domain (green box) and zinc-binding domain (cyan box), flanked by a mitochondrial target sequence (MTS, orange box) and the C-terminal region (yellow box).

box). Three sites known important for catalytic activity Y102, R105, and H158 are indicated. Two altered residues P114 (patient 1), and L128 (patient 2) are represented as star symbols. Evolutionary conservation of two mutated sites SIRT5 P114 and L128V across (d) different species, and across (e) human sirtuin family. Substrate specificity-defining residues Y102 and R105 are indicated in blue; P114 and L128 are highlighted in dark red and pink, respectively. (f) Spatial position of the altered amino acids P114 and L128 in human SIRT5. The structure was generated based on the crystal structure of human SIRT5 (PDB: 3RIY). Affected residues P114 and L128 are indicated in red. The zinc-binding domain and Rossmann-fold domain are in blue and green, respectively. The Zinc atom is included as a yellow sphere.

As was also apparent in patient 1, the severe clinical manifestations were not associated with biochemical abnormalities in plasma and urine. The only indication of affected biochemical characteristics was a borderline complex IV deficiency (229 mU/UCS versus control range 228-1032 mU/UCS) in a skeletal muscle biopsy (Supplementary Table S1, lower panel).

To gain insight into the two missense *SIRT5* variants identified in the patients, we first investigated characteristics of the two affected residues, P114 and L128, in the SIRT5 protein. Both P114 and L128 are located in the catalytic core domain of SIRT5 (Fig. 1c). Moreover, the two residues appear highly evolutionarily conserved across species (Fig. 1d) as well as within the human sirtuin family (Fig. 1e). In addition, both P114 and L128 locate close to the well-established enzymatic active site residues Y102 and R105 (Fig. 1d), which have been demonstrated to be critical for substrate binding¹⁸. Structurally, P114 lies in the flexible loop which connects the helix of the zinc-binding domain and helix $\alpha 6$ of the NAD⁺-binding Rossmann fold domain, and L128 is positioned in $\alpha 6$ helix of the NAD⁺-binding Rossmann domain (Fig. 1f). The evolutionary conservations as well as nearly coinciding positions of these two altered residues, P114 and L128, suggest their importance for SIRT5 functioning *in vivo*. Indeed, both variants P114T and L128V are predicted to be pathogenic using Polyphen. Both variants have been detected at very low frequency in heterozygous states (10 out of 280,762 alleles for P114T, and 5 out of 250,928 alleles for L128V in Genome Aggregation Database) but have never been reported before in homozygous forms.

***SIRT5* variants cause loss of SIRT5 protein levels and increased global succinylation levels in human fibroblasts**

To understand what the consequences are of the P114T (patient 1) and L128V (patient 2) genetic variation for the SIRT5 protein and function, we used primary skin fibroblasts from the two patients and compared them to fibroblasts from healthy controls. Whole cell lysate SIRT5 protein levels were remarkably reduced in patient 1 and 2 as compared to controls (Fig. 2a), despite normal mRNA expression levels (Fig. 2b). To rule out the possibility that lower SIRT5 protein levels detected in

patients' fibroblasts were caused by a lower antibody affinity due to amino acids substitution, we confirmed reduction of SIRT5 protein level using two different SIRT5 antibodies with different antigen-binding regions (Supplementary Fig. S1a). Contrary to the reduced SIRT5 level, protein levels of SIRT3 and SIRT4 remained unchanged (Fig. 2a). Moreover, complex V (ATP5A subunit) protein levels were not different between patients and controls indicating that the total level of mitochondria was not affected in the *SIRT5* variant cell lines (Fig. 2a). Next, we introduced the P114T mutation in another human cell line (HEK293T) to confirm that the loss of SIRT5 protein was due to the *SIRT5* variant. Indeed, upon a knock-in of the *SIRT5* variant (c.340C>A) using CRISPR/Cas9 in HEK293T cells, SIRT5 protein level was clearly reduced in comparison to the WT cells (Fig. 2c). Combined, these results demonstrate that the *SIRT5* variants identified in the two patients caused a loss of the SIRT5 protein.

Next, we determined whether SIRT5 function in cells was affected by the *SIRT5* variants. Because SIRT5 possesses efficient desuccinylase, demalonylase and deglutarylase activities^{18, 21}, we first analysed these three SIRT5 related acylation levels by Western blotting. Succinyllysine levels were increased in patient 1 and 2 fibroblasts as compared to controls (Fig. 2d), whereas no clear differences in malonyllysine and glutaryllysine levels were detected (Supplementary Fig. S1b and S1c). Upon exposure to dimethyl succinate-ester, a cell permeable succinate analogue, we observed an increase in succinylation levels in both control and patients' fibroblasts (Supplementary Fig. S1d), indicating that the succinylation machinery in the cells was not affected, and increased succinylation level in patients' fibroblasts was due to SIRT5 dysfunction.

Then, it was investigated whether localization of succinyllysine was influenced. Localization of intracellular succinyllysine was visualized using immunofluorescence staining. Exposure of fibroblasts to dimethyl succinate-ester confirmed that protein succinylation was apparent most in mitochondria of cells (Fig. 2e). Consistent with the Western blot result, a significantly higher succinyllysine fluorescence signal was detected in both patients' fibroblasts in comparison with succinyllysine fluorescence in controls (Fig. 2e, f). Furthermore, the intracellular localization of succinyllysine did not appear to be altered. Overlay images of succinyllysine and MitoTracker showed that succinylation was present in both mitochondria and cytosol. Together, these results demonstrate that each of the two *SIRT5* variants markedly reduced SIRT5 protein level and significantly increased global succinyllysine level in patient cells.

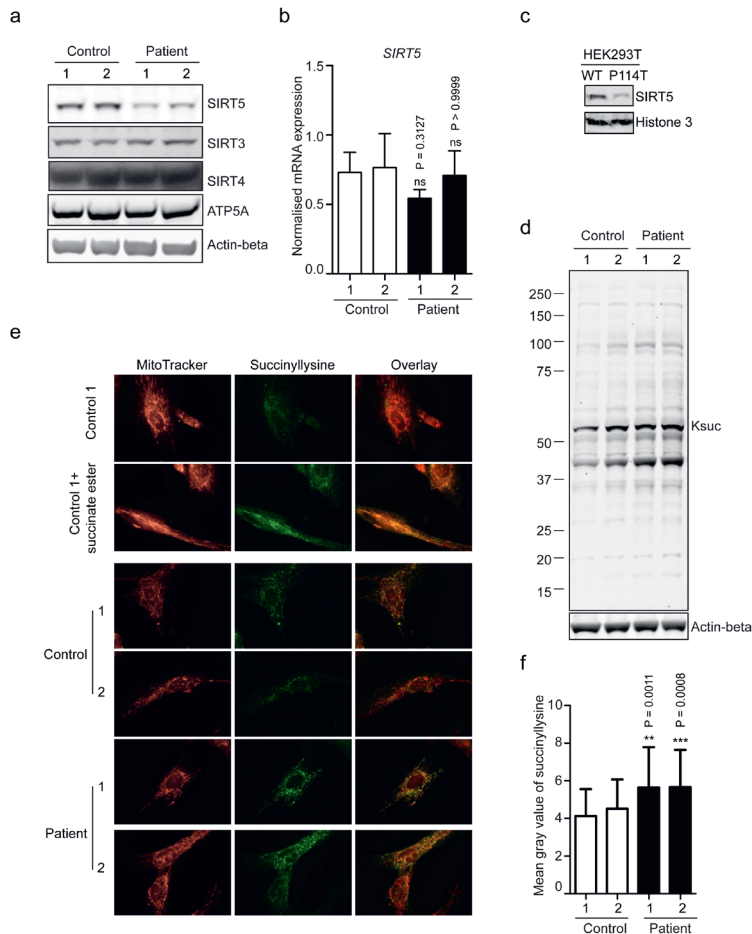


Figure 2. Each of the two *SIRT5* variants leads to reduced *SIRT5* protein level and increased global succinylation in human fibroblasts. (a) Western blots for SIRT5, SIRT3, and SIRT4 in whole cell lysates from control and patients' fibroblasts. ATP5A and Actin-beta were used as loading control. (b) SIRT5 mRNA normalised expression level in control and patients' fibroblasts. Three reference genes were used for expression normalisation. $n = 3$ independent experiments and duplicates in each experiment. (c) Western blot for SIRT5 in WT and SIRT5 P114T HEK293T cells. Histone3 was used as loading control. (d) Western blots for succinyllysine and loading control Actin-beta of control and patients' fibroblasts. (e) Representative immunofluorescence staining images of control and patients' fibroblasts. Cells were stained with succinyllysine antibody and with Mitotracker orange. Control fibroblast exposed to 4 mM cell-permeable dimethyl succinate-ester was used as positive control for succinyllysine staining. (f) Quantification of immunofluorescence staining for succinyllysine in control and patients' fibroblasts. $n = 46$ images were analysed for each cell line. Data represent mean \pm SD. Statistical analyses in (b) and (f) were performed using one-way ANOVA, followed by Bonferroni's multiple comparison test. Each patient fibroblast was tested against average of controls. ** indicates $P < 0.01$. *** indicates $P < 0.001$. ns, not significant.

SIRT5 variants result in loss of SIRT5 thermal stability and desuccinylase activity

To gain more insight into the mechanism why the patient *SIRT5* variants result in lower SIRT5 protein levels and higher succinylation levels, we biochemically characterized the SIRT5 protein variants *in vitro*. The patient SIRT5 protein variants, P114T and L128V, were generated using site-directed mutagenesis (Fig. 3a) and these His-tagged SIRT5 recombinant proteins were purified with Ni²⁺-affinity resin columns (Supplementary Fig. S2a).

Considering that SIRT5 protein levels were decreased without significant alteration in mRNA levels, we first assessed whether protein stability was disturbed in any of the two SIRT5 variants. Thermal stability analysis demonstrated that the P114T as well as the L128V SIRT5 variant exhibited a lower denaturation temperature than WT SIRT5 (Fig. 3b). This suggests an impaired SIRT5 variants' protein stability, which could contribute to the reduced SIRT5 protein levels at physiological temperature. Next, we investigated whether enzymatic kinetics in SIRT5 variants were altered. Since succinylation levels, and not glutarylation and malonylation levels, were increased in patients' fibroblasts, we focused on desuccinylase activity. The Michaelis-Menten constant (K_m) of desuccinylation of a succinyl-peptide by SIRT5 P114T was 74% higher, and catalytic efficiency (K_{cat}/K_m) was 42% lower compared to WT (Fig. 3c). For the SIRT5 L128V, the K_m for the succinyl-substrate was 30% higher, and catalytic efficiency was 20% lower compared to WT (Fig. 3c). Additionally, the K_m for NAD⁺ was 53% higher for SIRT5 P114T, and the catalytic efficiency was 35% lower compared to WT (Fig. 3d). No evident difference in catalytic efficiency with regards to NAD⁺ was observed between L128V and WT (Fig. 3d). Also, no difference was found in the IC₅₀ value of the general sirtuin inhibitor, nicotinamide (NAM), for the P114T and L128V variants as compared to WT recombinant SIRT5 (Fig. 3e).

Since SIRT5 desuccinylase kinetics were only mildly decreased in the recombinant SIRT5 variants, we analysed whether desuccinylase activity was affected to a greater extent under lower substrate conditions, which could be physiologically relevant, because locally in the mitochondria NAD⁺ levels can change dramatically in response to altered metabolic conditions. Under these substrate limiting conditions, with 10 μ M of succinyl-substrate and a NAD⁺ concentration of 500 μ M, desuccinylase activity was reduced by 30% in the P114T and in the L128V SIRT5 variant relative to WT (Fig. 3f). WT SIRT5 as well as two variants had a neglectable deacetylation activity (Fig. 3f). In the context of limitation of the level of NAD⁺ to 10 μ M, the desuccinylase activity of each of the SIRT5 patients' variants was decreased further, to 50% of the activity of WT (Supplementary Fig. S2b). Together, these results indicate that likely the reduced SIRT5 protein thermal stability as well as NAD⁺-dependent desuccinylase

activity of each of the two *SIRT5* variants contributed to the significant decrease in SIRT5 protein levels and increase in succinylation levels observed in the patients' fibroblasts.

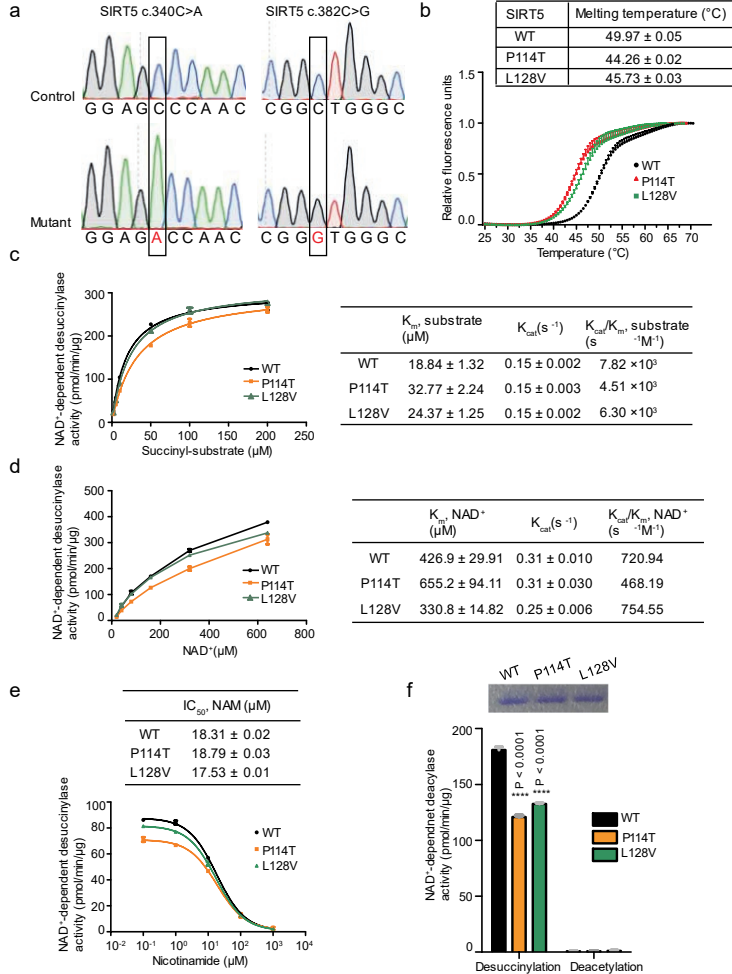


Figure 3. Recombinant SIRT5 P114T and SIRT5 L128V variants decrease protein thermal stability and NAD⁺-dependent desuccinylase activity. (a) Sanger sequencing confirmed correct amino acid substitution in recombinant SIRT5, SIRT5 c.340C>A (p. P114T) represents SIRT5 variant identified in patient 1 and c.382C>G (p. L128V) represents SIRT5 variant identified in patient 2. (b) Thermal shift assay of recombinant SIRT5 WT and two variants. Triplicates for each sample. Representative for 3 independent experiments. (c) Steady-state kinetics of desuccinylation was determined by varying succinyl-peptide (2–200 μM) in the presence of 1 mM NAD⁺ and 0.03 μg of recombinant SIRT5 protein. Duplicates for each data point. (d) Steady-state kinetics of desuccinylation was measured by varying NAD⁺ (20–640 μM) in the presence of 120 μM of succinyl-peptide and 0.03 μg recombinant SIRT5 protein. Duplicates for each data

point. (e) IC_{50} value of nicotinamide (NAM) for NAD^+ -dependent desuccinylase activity was assessed for recombinant WT and two SIRT5 variants. Triplicates for each data point. (f) Steady-state desuccinylase and deacetylase activities were measured in recombinant WT and two SIRT5 variants, using 10 μ M acyl-peptide and 500 μ M NAD^+ . Triplicates for desuccinylation and duplicates for deacetylation activity. Representative for 2 independent experiments. Data represent mean \pm SD.

SIRT5 dysfunction in human fibroblasts causes oxidative stress

SIRT5 has been shown to play a role in OXPHOS, mitochondrial intermediary metabolism, ROS detoxification, and glycolysis³⁵. Since biochemical analyses of OXPHOS complexes (complex I, II, III, IV and V) activities were largely normal in the two patients' fibroblasts and in the muscle biopsy from patient 2 (Supplementary Table S1), we reasoned that a more comprehensive assessment with variable metabolic challenges would allow us to unravel an underlying disruption in bioenergetics. For this, extensive metabolic stress tests were applied and quantified using the Seahorse metabolic flux analyzer (Fig. 4a). In these stress tests, we forced cells to strongly rely on either the glycolytic pathway, by applying $CoCl_2$ as a HIF1A mediated inducer of glycolysis³⁶, or on oxidative phosphorylation, by applying galactose and low glucose conditions. Furthermore, we applied a cell-permeable succinate-ester to induce cellular succinylation stress (Fig. 4a). When combining all bioenergetic parameters obtained under different metabolic stress conditions, patients' fibroblasts exhibited consistent and evident alterations on OXPHOS-related phenotypes in the context of all galactose conditions tested, as compared to control fibroblasts (Fig. 4b). Also, glycolytic parameters were altered in glycolysis-stimulated conditions but only in patient 1 (Fig. 4b).

Integration of these cellular bioenergetics data demonstrated that the strongest increase of all parameters tested was that for the proton leak rate (Fig. 4b). Rates of proton leak were around 2-fold higher in the fibroblasts of the two patients as compared to control fibroblast cell lines (Fig. 4c). In addition, basal oxygen consumption rates were slightly elevated in patients' cells, which was very likely due to the increased proton leak rate. We found no differences in other aspects of bioenergetics. No remarkable difference in mitochondrial ATP generation capacity, as well as in maximal mitochondrial respiration rate between control and patients' cells was found (Fig. 4c). Contribution of mitochondrial ATP to total cellular ATP generation, presented as ATP rate index, did not differ either (Fig. 4c). Apart from the increase in proton leak rate, we observed that cell growth rate of patients' fibroblasts was reduced by 50% as compared to that of controls (Fig. 4d).

To validate that the increased proton leak rate phenotype arises from SIRT5 dysfunction, we made use of a SIRT5-specific small molecule inhibitor (DK1-04e) that effectively blocks SIRT5 function in cells. As a control compound, we used an

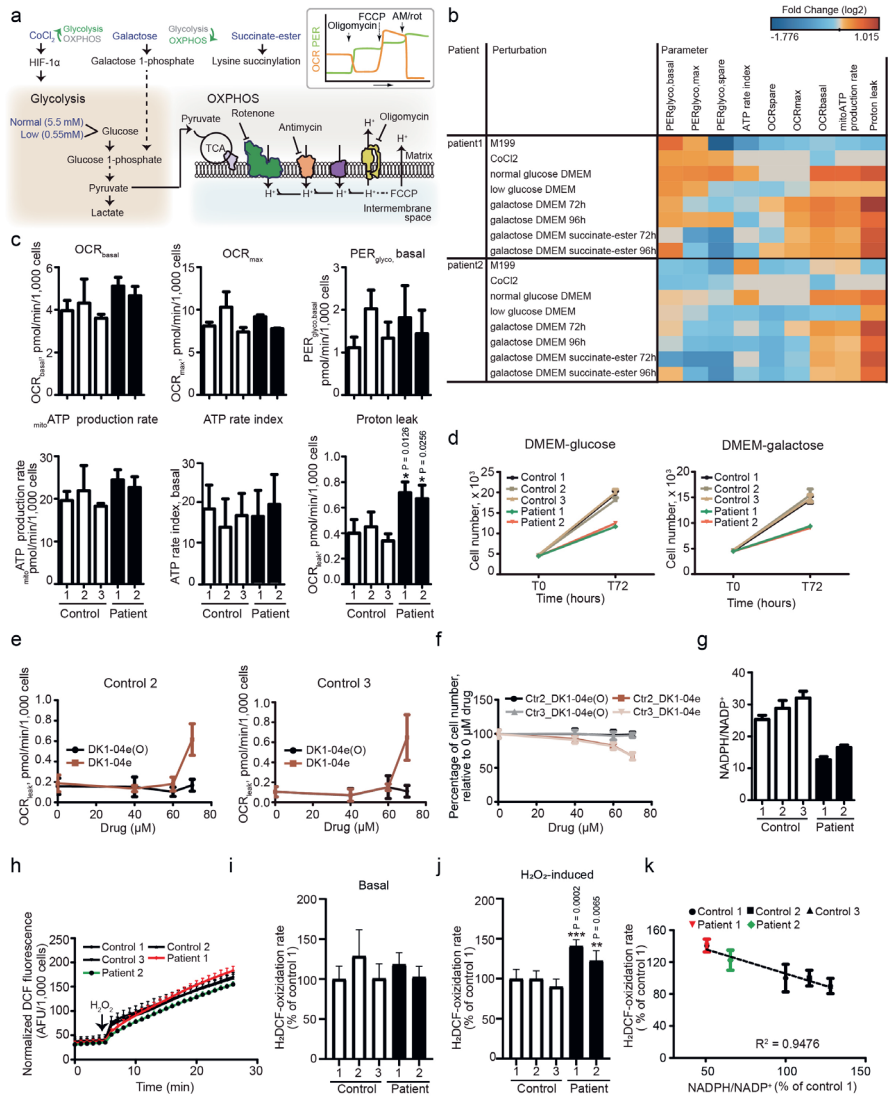


Figure 4. Each of the two *SIRT5* variants causes oxidative stress in human fibroblasts without overt bioenergetic deficits. **(a)** Schematic representation of pathways and metabolic conditions (in blue characters) used for fibroblast bioenergetics characterization. **(b)** A heatmap visualization of fold changes in glycolytic and OXPHOS parameters of patient 1 and patient 2 fibroblasts relative to average of control fibroblasts ($n = 2 - 3$ controls) under different metabolic stress conditions. **(c)** Seahorse metabolic flux parameters in human fibroblasts in galactose medium (measured at 72 hrs; $n = 3$ independent experiments, 6 - 8 technical replicates in each experiment). **(d)** Growth curve of human fibroblasts under glucose and galactose media ($n = 8$ technical replicates), representative for 3 independent experiments. **(e)** Proton leak rate and **(f)** growth curve of two control fibroblasts exposed to galactose medium containing either *SIRT5* inhibitor DK1-04e or control compound DK1-04e(O) (measured at 72 hrs, $n = 8$ -

10 technical replicates). Representative for 2 and 3 independent experiments for control 2 and 3, respectively. 0 μ M of drug refers to DMSO control (0.14% in medium). (g) NADPH/NADP⁺ ratio in human fibroblasts under galactose medium (measured at 72 hrs; n = 2 independent experiments, and duplicates in each experiment). (h) A representative (for 4 independent experiments) real-time normalized DCF fluorescence signal trace of fibroblasts after 72 hrs-exposure to galactose medium. H₂O₂ (100 μ M) was performed after basal measurement. (i) Basal and (j) H₂O₂-induced relative H₂DCF oxidation rate in fibroblasts after 72 hrs-exposure to galactose medium. In both (i) and (j), n = 4 independent experiments, 3 - 6 technical replicates in each experiment. (k) Correlation analysis between NADPH/NADP⁺ versus H₂O₂-induced H₂DCF-oxidation rate. Data from (g) and (j) were used in the correlation analysis. 5.5 mM glucose and 5.5 mM galactose were used throughout the study. Data represent mean \pm SD. (c), (i) and (j), one-way ANOVA, followed by Bonferroni post-doc testing, and each patient fibroblast was tested against average of three control cell lines. * indicates $P < 0.05$, ** indicates $P < 0.01$, *** $P < 0.001$.

analogous compound (DK1-04e(O)) that also enters cells, but cannot effectively inhibit SIRT5 activity, because one atom has been changed from S to O, which substantially increases its IC₅₀. DK1-04e dose-dependently increased proton leak in two normal fibroblast cell lines, with a strikingly higher proton leak observed at the concentration of 70 μ M (Fig. 4e). Importantly, the absolute level of proton leak induced by SIRT5 inhibitor in these control fibroblasts was comparable to that detected in the patients' fibroblasts. By contrast, the effects of the control drug DK1-04e(O) were negligible at any given concentration tested. As observed in patients' fibroblasts, cell proliferation was negatively impacted upon exposure to the SIRT5 inhibitor DK1-04e in a dose-dependent manner, but not by the control compound DK1-04e(O) (Fig. 4f). This indicates that chemical inhibition of SIRT5 in human fibroblasts phenocopies the cellular physiology that we observed in the patients' fibroblasts.

Since the *SIRT5* variants lead to higher proton leak rates without other major bioenergetics defects, and elevated proton leak has been proposed to be a result of elevated oxidative stress³⁷, we hypothesized that elevated proton leak rate was an adaptive mechanism by which fibroblasts respond to underlying dysfunctions in handling of redox homeostasis. To test this, we first analysed NADPH/NADP⁺ ratio, a redox couple with a critical role in maintaining intracellular redox homeostasis³⁸. Under galactose conditions, the NADPH/NADP⁺ ratios were reduced 2-fold in whole cell lysates of the two patients as compared to that in controls (Fig. 4g), suggesting a more oxidative stress-favoured state in the SIRT5-deficient patients' fibroblasts. Next, we analysed whether ROS levels were affected by *SIRT5* variants in human fibroblasts using the intracellular oxidation of the non-fluorescent 2',7'-Dichlorodihydrofluorescein diacetate (H₂DCFDA) to its fluorescent analogue (DCF) over time. DCF fluorescence increased linearly over time for all fibroblasts (Fig. 4h and Supplementary Fig. S3a), indicating that the amount of non-fluorescent H₂DCF was not rate-limiting and intracellular oxidant levels were the only factor

determining the rate of H₂DCF oxidation. Consistent with previous reports³⁹, basal H₂DCF-oxidizing ROS levels were higher in the galactose conditions than under glucose conditions in the patients' fibroblasts and control cells (Supplementary Fig. S3b). Although basal H₂DCF-oxidation rates were similar in patients' and control cells (Fig. 4i and Supplementary Fig. S3c), acute exogenous H₂O₂ (100 μ M) addition induced significant higher H₂DCF-oxidation rate in patients' relative to control cells (Fig. 4j). This strongly suggest that higher ROS levels are reached in SIRT5-mutated patients' cells upon extracellular oxidant addition. Of note, this higher ROS level was only observed under galactose but not under glucose conditions (Supplementary Fig. S3d). This was in line with the observed increase in proton leak in galactose, but not in glucose conditions. Interestingly, NADPH/NADP⁺ ratios and H₂O₂-induced H₂DCF-oxidizing ROS levels displayed a strong negative correlation (Fig. 4k; $R^2 = 0.9476$). This suggests a mechanistic link between NADPH/NADP⁺ ratio and oxidant detoxification in our cell model and combined with the observed effects on proton leak, highlights a role for human SIRT5 in redox homeostasis.

Discussion

In the present study, we identified two novel homozygous *SIRT5* variants in two unrelated patients with mitochondrial disease-like pathologies. Comprehensive biochemical and molecular analyses revealed that each of the two loss-of-function variants in *SIRT5* led to a reduction in SIRT5 protein level and NAD⁺-dependent desuccinylase activity, as well as significantly higher succinylation levels in patients-derived fibroblasts. Moreover, we established that each *SIRT5* variant led to elevated levels of ROS upon exposure to extracellular H₂O₂, implicating a critical role for SIRT5 in regulating redox homeostasis in humans.

The role of SIRT5 in metabolic health and biology has been supported in previous studies by evidence generated using cells and genetically engineered mouse models, showing mainly the failure of SIRT5 KO mice to respond to challenging conditions^{25, 26, 34}. However, discrepancies in biological impacts of SIRT5 absence have been observed among different studies^{27, 33, 40}, which rendered SIRT5 physiological relevance elusive. Our observations that human *SIRT5* genetic variants cause imbalances in redox homeostasis emphasizes the direct relevance of the SIRT5 protein for human health. In line with our findings, in mice it has been shown that SIRT5 was needed for protein kinase C epsilon-induced protection from cerebral ischemia⁴¹. SIRT5 KO mice were more sensitive to paraquat-induced neurodegeneration, associated with lowering of NADPH/NADP⁺ ratio, glutathione status and increases in ROS levels³⁰. Furthermore, reduced ROS levels and improved

cell viability upon H₂O₂ exposure has been observed following SIRT5 overexpression in neuroblastoma cells⁴².

One of the most pronounced bioenergetic parameters we identified in a screen for stress-induced extracellular flux analysis, was an increase in the proton leak rate in patients with the *SIRT5* variants. Proton leak is a natural process during which protons flow back into the mitochondrial matrix independent of ATP synthase. It occurs in intact cells and tissues^{43, 44, 45} and requires mitochondrial inner membrane located proteins, like adenine nucleotide translocase (ANT)⁴⁶. Additionally, proton influx into mitochondria, independent of ATP generation, can drive the mitochondrial inner membrane protein nicotinamide nucleotide dehydrogenase (NNT) to generate NADPH⁴⁷. Previous studies have demonstrated that the mitochondrial proton leak physiologically responds to alterations in ROS levels^{48, 49}. In addition, increased proton leak was shown to decrease ROS production^{50, 51}, indicating that proton leak could exist as a cytoprotective strategy to counteract oxidative stress^{52, 53}. Elevated proton leak rate in turn, supports the notion that oxidative stress was induced in the *SIRT5* variant fibroblasts. Interestingly, oxidative stress is a common feature in multiple human diseases associated with mitochondrial dysfunction⁵⁴, including type II diabetes, cardiovascular diseases and neurodegenerative disease^{55, 56, 57}. Furthermore, altered ROS levels, antioxidants, and oxidative damages have been observed in patients and animal models for genetic mitochondrial disease^{12, 13, 58}, highlighting that oxidative stress has been especially suspected as pathological mechanism for mitochondrial diseases^{10, 17, 59}. Although there is no cure for genetic mitochondrial diseases to date, progress has been made regarding development of treatment for mitochondrial diseases based on targeting imbalances in redox homeostasis. Notably, clinical trials of several promising antioxidants are ongoing¹⁷.

SIRT5 protein levels were markedly reduced by the *SIRT5* variants, with consequent increases in succinylation levels in cytosol and mitochondria. Previous research showed that the predominant subcellular distribution of succinylation in humans was mitochondrial⁶⁰, but succinylation was also observed outside of the mitochondria²⁰. SIRT5, as the most effective desuccinylase in mammals established so far, also localized primarily in the mitochondria^{29, 61}, but also non-mitochondrial localization of SIRT5 and its target proteins have been identified^{20, 24}, indicating that SIRT5 could have multiple roles in cells. Interestingly, SIRT5 displays a broad tissue distribution in multiple species with the highest protein levels in brain, heart, kidney and liver^{29, 35}. Analysis of expressed sequence tags (ESTs) in human tissues even demonstrated a pronounced overrepresentation of SIRT5 transcripts in the brain, as

compared to other tissues⁶², which could possibly explain why patients with the *SIRT5* variants have primarily brain pathologies.

In line with abundant expression of SIRT5 in mitochondria and metabolically active tissues, SIRT5 has been suggested to play a role in mitochondrial energy metabolism^{22, 25, 33}. We identified higher rates of glycolysis in patient 1-derived fibroblasts. Although we did not find impaired mitochondrial respiratory capacity in *SIRT5* variant fibroblasts, the induction of glycolytic rate could be a response to impaired mitochondrial function. Previous studies showed that effect of SIRT5 on cellular respiration was highly context-dependent and different phenotypes have been observed. For example, decreased succinate-drive respiration rate in SIRT5 KO mice liver homogenates was reported²³, while oppositely, Park *et al.* found that deletion of SIRT5 increased pyruvate- as well as succinate-driven respiration rates in mice liver mitochondria²⁰. Decreased mitochondrial respiration of fatty acids²⁵ or decreased ATP contents have been detected in SIRT5 KO heart mitochondria⁴⁰. Contrary, respiration profiles of heart mitochondria were unaffected by SIRT5 ablation when subjected to the mitochondrial substrates glutamate/malate or pyruvate/malate⁶³. Thus, physiological effects of SIRT5 deficiency in mice and consequent increase in succinylation are likely multifactorial. Similar apparently contradictory findings have been reported for the role of acetylation in the mitochondria in cells and mice, where acetylation can either limit mitochondrial energy homeostasis^{64, 65, 66} but can also increase mitochondrial respiratory function^{67, 68} depending on the model system and conditions that have been used. Interestingly, Williams *et al.* found that hyperacetylation, induced by knockout both the mitochondrial deacetylase SIRT3 and the acetyl-CoA lowering protein, carnitine acetyltransferase (CRAT), did not influence muscle mitochondrial respiration, but instead, similar to our findings, redox balance was significantly disturbed by hyperacetylation⁶⁷. It is intriguing to speculate that redox-regulating pathways are common pathways that are sensitive to increased acylation levels induced by sirtuin defects. Our finding that SIRT5 plays a critical role in regulating cellular redox homeostasis in humans underlines the importance of SIRT5 for regulating human health and disease.

Material and Methods

Patient ethics

Informed consent for diagnostic and research studies was obtained for both subjects in accordance with the Declaration of Helsinki and following the regulations of the local medical ethics committee.

Cell Culture

Fibroblasts from skin biopsies of healthy subjects and two patients with *SIRT5* variants were used in this study. Control fibroblasts included: #13370, #MW28, #14308, and #14321; patients fibroblasts harbouring *SIRT5* variants included: #13395 and #13706. Human primary skin fibroblasts were routinely cultured in fibroblast growth medium that consisted of medium 199 (#M3769, Sigma-Aldrich, which is formulated with 5.5 mM glucose) supplemented with 10% foetal bovine serum (FBS, #06Q3501K, Gibco), 2 mM Glutamine-Max (#35050038, Gibco), and 1x antibiotic-antimycotic mix (100 IU/ml penicillin/streptomycin, and 25 µg/mL Amphotericin B, #15240062, Gibco). Cells were incubated at 37°C and were maintained in an atmosphere containing 5% CO₂. Cells were passaged once every 4-5 days when reaching 90% confluency by trypsinization (#15400054, Gibco) for 2 min at 37°C. All fibroblast cell lines were tested mycoplasma-free (MycoSensor QPCR assay, #302107, Agilent Technologies).

Western Blotting

After harvest by trypsinization and centrifugation (5 min, 300 x *g*, 4°C), cell pellets were lysed in lysis buffer (50 mM Tris/HCl pH 7.4, 2 mM NAM, 1 µM trichostatin A and protease inhibitor cocktail (#04693159001, Roche)), followed by sonication on ice. Protein concentrations were determined with BioRad DC assay (#5000116, BioRad), and equalized to the same level with lysis buffer, after which NuPAGE LDS Sample Buffer (#NP0007, Invitrogen) and 50 mM dithiothreitol were added followed by heating at 95°C for 5 min. Protein samples (50 µg for human fibroblasts lysates; 30 µg for HEK293T lysates) were run through a 4-12% Bis-Tris Gel (#NW04125BOX, Invitrogen) and electroblotted onto a nitrocellulose membrane (#88018, Invitrogen). The membrane was then probed with anti-SIRT5, anti-SIRT3, anti-SIRT4, anti-succinyllysine, anti-glutaryllysine, anti-malonyllysine, anti-complex V, anti-actin beta or anti-histone3, followed by appropriate secondary antibody (IRDye 800CW or HRP-linked IgG). Images were obtained using the Odyssey or Bio-Rad ChemiDoc XRS Systems. Antibodies information is listed in Table 1.

Immunofluorescence

Fibroblasts were seeded on sterile 24 mm cover glasses in 6-well plates. Cells were cultured in fibroblast growth medium and allowed to grow for 48 hrs before the start of the assay. For succinate exposure, cells were cultured in fibroblast growth medium supplemented with 4 mM dimethyl succinate-ester (#112755, Sigma-Aldrich). Mitochondria were visualized with 400 nM MitoTracker Orange (#M7510, Molecular Probes) diluted in medium 199 (#M3769, which is formulated phenol red free). Cells

were fixed with 4% formaldehyde solution (#252549, Sigma-Aldrich) at 37°C for 20 min, then were permeabilized by 0.2% Triton X-100 (#T8787, Sigma-Aldrich) in Tris-buffered saline (TBS) for 30 min at room temperature. After permeabilization, cells were washed with TBS containing 0.05% Tween 20 (#P7949, Sigma-Aldrich) three times, followed by blocking for 90 min at room temperature in blocking buffer consisted of 2% BSA (#A7907, Sigma-Aldrich) in TBS, 2% goat serum (#S-1000, Vector laboratories), 0.1% Triton X-100, 0.05% Tween 20 and 50 mM glycine (#G8898, Sigma-Aldrich). Then, they were incubated with either pan anti-succinyllysine or rabbit IgG diluted in TBS at room temperature for 90 min, washed and incubated with the secondary AlexaFluor488 conjugated goat anti-rabbit antibody diluted in TBS at room temperature for 60 min. Finally, cells were counterstained with 1 µg/ml of 4',6-diamidino-2-phenylindole (DAPI, #D9564, Sigma-Aldrich) and mounted with Fluoromount G (#0100-01, SouthernBiotech). Images were taken by a Leica DM6b upright microscope and quantification was performed by ImageJ 1.52 (National Institutes of Health). Forty-six images of each cell line were quantified. Antibodies information is listed in Table 1.

Mutagenesis of SIRT5 plasmid

His-SIRT5 WT expression plasmid was obtained from Addgene (plasmid #25487). Site-directed mutagenesis of WT SIRT5 was performed using the QuickChange Lightning site-directed mutagenesis kit (#210518, Agilent Technologies), according to the manufacturer's instruction. Briefly, the SIRT5 mutagenic primers were designed using web-based QuickChange Primer Design Program (www.agilent.com/genomics/qcpd). Each of the two *SIRT5* variants was synthesized by 2 min at 95°C, 18 cycles of (20 seconds at 95°C, 10 seconds at 60°C, and 4.5 min at 68°C), and followed by 5 min at 68°C. Then, Dpn I was directly added to the amplification reaction and incubated at 37°C for 5 min to digest the parental SIRT5 plasmids. Dpn I-treated plasmids were transformed into XL10-Gold ultracompetent cells and grown in NYZ⁺ broth at 37°C for 1 hr. Then, the cells were spread on Luria broth (LB) agar plates containing 50 µg/ml kanamycin and allowed to grow at 37°C for 16 hrs. Single colony was streaked once more in another LB/kanamycin agar plate, followed by amplification in liquid LB with kanamycin at 37°C with shaking at 220 rpm overnight. The plasmids were isolated and purified using an Endofree plasmid max kit (#12362, Qiagen) according to manufacturer's instruction, and stored at -20°C. Plasmids were sent for Sanger sequencing to confirm the introduced *SIRT5* variants (BaseClear, the Netherlands). Mutagenesis primers are listed in Table 2.

Expression and Purification of Recombinant His-SIRT5

His-tagged WT and variant SIRT5 proteins were expressed in the BL21(DE3) *E. coli* strain. The transformed BL21DE3 cultures were grown in LB medium containing kanamycin (50 µg/ml) at 37°C until OD₆₀₀ of 0.25 was reached, after which the culture was allowed to cool down to 22°C. SIRT5 expression was induced with 500 mM isopropyl β-d-1-thiogalactopyranoside (IPTG) and the cells were harvested 18 hrs after the induction by centrifugation at 6,000 x *g* for 15 min at 4°C, and cell pellet aliquots were snap frozen with liquid nitrogen and stored at -80°C. To purify His-SIRT5, the *E. coli* pellet was resuspended in 10 mM Tris/HCl pH 8.0, 500 mM NaCl supplemented with 1 mg/ml lysozyme (#L6876, Sigma-Aldrich), and sonicated on ice. After centrifugation at 12,000 x *g* for 15 min at 4°C, SIRT5 WT and variants were purified by Ni²⁺-affinity resin (#V8823, Promega), and eluted with 25 mM Tris/HCl pH 8.0, 100 mM NaCl, and 500 mM imidazole. Prior to use in further experiments, imidazole was removed from the eluted His-SIRT5 using ultra-0.5 centrifugal filter units (#UFC501096, Merck Millipore). Protein concentrations were then determined by Bradford assay (#23200, Thermo Scientific).

SIRT5 enzymatic assay and steady-state kinetic analyses

Desuccinylation activity of recombinant His-SIRT5 WT, P114T and L128V variants was analysed with fluor de lys SIRT5 fluorometric drug discovery assay kit (#BML-AK5130001, Enzo). Reaction reagents including succinyl-substrate, NAD⁺, NAM, developer and assay buffer were provided in the kit. To assess the Michaelis-Menten constant (*K_m*) of SIRT5 for succinyl-peptides, steady-state rates were measured by varying succinyl-substrate (2-200 µM) in the presence of 1 mM NAD⁺. For the determination of *K_m*, NAD⁺, activity was measured under a range of NAD⁺ (20-320 µM) and 120 µM of succinyl-substrate. The enzymatic reaction took place at 37°C water bath with shaking (60 rpm) for 10 min. The reaction was stopped after 10 min by incubating with 1x developer and 2 mM NAM at 25°C for 15 min. The fluorescence was read in half-area black 96-well plate (#3686, Corning) with excitation at 360 nm and emission at 460 nm on a Biotek Synergy HT microplate reader. For analysis of His-SIRT5 sensitivity to NAM, fixed concentration of succinyl-substrate (10 µM) and NAD⁺ (500 µM) and varying concentration of NAM (0.1 - 1000 µM) were present in the reaction system. For analysis of His-SIRT5 desuccinylation activity under limiting conditions, succinyl-peptide was fixed at 10 µM, and NAD⁺ input was used as indicated in the figure legends. Deacetylation activity of His-SIRT5 was determined similarly to the desuccinylation activity, except that acetylated substrate (#BML-KI179-0005, Enzo) and developer II (#BML-KI176-1250, Enzo) were used. Fluorescence signal of negative control (acyl-substrate without NAD⁺ in the reaction

system) was subtracted from each experimental sample. 0.03 µg of freshly purified His-SIRT5 (WT, P114T, and L128V SIRT5) were used in all the experiments. For kinetic parameter calculations, data were fitted to the Michaelis-Menten equation in GraphPad Prism 6.01. For IC₅₀ of NAM for each His-SIRT5, data were fitted to the log(inhibitor) vs response (three parameters) equation in GraphPad Prism 6.01.

Protein thermal shift assay

Recombinant His-SIRT5 protein concentrations were equalized to 320 µg/ml with thermal assay buffer (25 mM Tris/HCl pH 8.0 and 100 mM NaCl), and 20x Sypro Orange (#S5692, Sigma-Aldrich, delivered at 5000x) was added. Samples were added to qPCR plate and analysed with Bio-Rad CFX96 Real-Time System C1000 thermal cycler. The temperature was increased at a rate of 0.5°C/min ranging from 25-95°C, and fluorescence signal was monitored in the FRET channel of the thermal cycler. Melting temperature was determined by performing non-linear fitting of normalised thermal denaturation fluorescence signal, using Boltzmann Sigmoidal curves in GraphPad Prism 6.01.

RNA extraction and cDNA synthesis

Total RNA was extracted using RNeasy mini kit (#74106, Qiagen) according to the manufacturer's instruction. Total RNA was dissolved in DNase/RNase-free water, and concentration was measured by a Nanodrop spectrophotometer (IsoGen Life Science). RNA quality was checked on an Agilent 2200 TapeStation (Agilent Technologies Inc.) with an RNA ScreenTape (Agilent). Subsequently, 1 µg of total RNA was reverse-transcribed to cDNA by using an iScript kit (#1708891, Bio-Rad) on a Mastercycler (Eppendorf), with 5 min at 25°C, 30 min at 42°C, and 5 min at 85°C.

Real-Time RT-PCR Analysis

Transcript expression was measured using iQ SYBR Green Supermix (#1725006CUST, Bio-Rad), and the fluorescence signal was monitored with a CFX96 Real-Time PCR Detection System. The PCR reaction program was 3 min at 95°C, 40 cycles of (15 s at 95°C and 45 s at 60°C), followed by the melt-curve analysis. The low-level expressed gene ribosomal protein S15 (RPS15) was preamplified with SsoAdvanced PreAmp Supermix (#1725160, Bio-Rad), with 3 min at 95°C, and 12 cycles of (15 s at 95°C and 4 min at 58°C). A negative control (a sample without reverse transcriptase) was included in the preamplification. cDNA from all (preamplified) samples was pooled and serial dilutions were made for standard curves. Samples were diluted 100-fold for the PCR reaction, and two negative controls (DNase/RNase-free water and a sample without reverse transcriptase) were also included. SIRT5 gene expression level was normalised to expression level of three reference genes, beta-2

microglobulin (B2M), RPS15, and erbb2 interacting protein (ERBB2IP) in each fibroblast cell line. RNA of each fibroblast cell line was isolated from three independent batches of cultures, and all the samples were analysed in the same RT-PCR run. Duplicates were used for each sample. The primer sequences are listed in Table 2.

Seahorse metabolic flux analyses

Respiration of fibroblasts was measured using a Seahorse XFe96 Extracellular Flux Analyzer (Agilent Technologies) following the manufacturer's protocols. Fibroblasts were seeded in XFe96 V3 PS cell culture microplates (#101085-004, Agilent Technologies), and cultured in fibroblast growth medium overnight. Sixteen hours post seeding, medium was switched to exposure medium as detailed in Table 3. On the day of the Seahorse assay, pH of freshly prepared assay medium (detailed compositions are described in Table 3) and all injection solutions were checked and adjusted to 7.4 if needed, subsequently, they were filtered through 0.2 µm cellulose acetate membranes (#28145477, VWR) and kept at 37°C until use. Prior to the Seahorse run, exposure medium was replaced with Seahorse assay medium, first for 1 hr in a 37°C non-CO₂ incubator with normal air. Then, the fresh Seahorse assay medium was applied to cells again just before the Seahorse run. For bioenergetic determinations, two different injection strategies were applied separately within one assay after basal measurement. Final concentration of the compounds used in strategy 1: i) 1 µM oligomycin (#O4876, Sigma-Aldrich), ii) 2.5 µM antimycin (#A8674, Sigma-Aldrich) plus 1.25 µM rotenone (#R8875, Sigma-Aldrich), iii) 100 mM 2-deoxyglucose (2-DG, #D8375, Sigma-Aldrich). For injection strategy 2: i) 1 µM carbonyl cyanide-4-(trifluoromethoxy) phenylhydrazone (FCCP, #C2920, Sigma-Aldrich), ii) 2.5 µM antimycin plus 1.25 µM rotenone, iii) 20 µM monensin (#M5273, Sigma-Aldrich). The Seahorse analyser was maintained at 37°C for all Seahorse assays. The assay procedure consisted of a 12 min equilibration period followed by 3 cycles to measure the basal rate, comprising of a 2 min mix, and a 3 min measurement period. Injection of compounds was followed by 3 cycles, except for 2-DG injection, which was followed by 5 cycles. After Seahorse assays, cells in plate were stained with 4 µM of 2'-(4-ethoxyphenyl)-5-(4-methyl-1-piperazinyl)-2,5'-bi-1H-benzimidazole trihydrochloride trihydrate (Hoechst 33342, #B2261, Sigma-Aldrich) dissolved in assay medium, for 1 hr at 37°C non-CO₂ incubator. Images were taken by Cytation 1 Imaging Reader (BioTek) and cell number was determined by ImageJ 1.52. Seahorse data were normalised to cell number in each well. For determining buffer factor capacity of Seahorse assay medium, either Seahorse assay medium or 5.0 mM HCl in assay medium was injected at port A, B and C, followed by

3 measurement cycles after each. Dulbecco's Modified Eagle's Medium (DMEM, #A1443001, Gibco) and L-glutamine (L-Gln, #25030024, Gibco) were used in all exposure media throughout this study. Galactose (#G0625), dimethyl succinate-ester (#112755) and CoCl_2 (#C8661) were all from Sigma-Aldrich. XF DMEM (pH 7.4, #27518004), XF L-Gln (#103579-100), and XF glucose (#103577-100) were all from Agilent Technologies.

Whole exome sequencing

Whole exome sequencing (WES) and data analysis were performed as described before^{69, 70}. Briefly, exome enrichment was performed using the SureSelect Human All Exon 50 Mb Kit V5 (Agilent), and sequencing was done using a HiSeq4000 (Illumina). The minimum median coverage was 80-fold. The alignment of sequencing reads to the human reference genome (GrCH37/hg19) and variant calling was performed at BGI (Copenhagen) using BWA and GATK software, respectively. The annotation of sequence variants was performed using an in-house designed annotation software. Patient data were first analysed using a custom-made virtual gene panel containing mitochondrial disease genes (as described in OMIM). As no disease-causing variants were detected, the entire exome was investigated for rare, protein damaging variants based on the GnomAD dataset, dbSNPv132 and our in-house variant database.

Cell growth curve

For cell growth curve analysis, either 2500/well or 7000/well of fibroblasts were seeded in 96-well cell culture plates and cultured in fibroblasts growth medium overnight. Next, cells were switched to either glucose or galactose exposure medium. Glucose exposure medium consisted of DMEM supplemented with 10% FBS, 2 mM L-Gln and 5.5 mM glucose. For galactose exposure medium, 5.5 mM galactose was used instead of glucose and the rest were the same as glucose exposure medium. At the time of exposure, cells in a parallel plate were stained with 4 μM of hoechst dissolved in fibroblasts growth medium, for 1 hr at 37°C and images were taken using the Cytation 1. After 72 hrs-exposure, cells in the experimental plate were stained and imaged. For cell growth curve analysis of the SIRT5 inhibitor DK1-04e, cells were exposed to galactose exposure medium containing different concentration of DK1-04e or DK1-04e(O) as indicated in the figure. Galactose exposure medium containing DMSO (0.14% in medium) was used as a no drug control. All exposure media were filtered through 0.2 μm cellulose acetate membranes after preparation before application to the cells.

Measurement of intracellular NADPH/NADP⁺ ratio

Intracellular NADPH/NADP⁺ ratio was determined using the luminescence-based NADP⁺/NADPH-Glo Assay kit (#G9081, Promega). 3.5×10^5 of human fibroblasts were seeded in T75 flasks and cultured in fibroblast growth medium. After 18 hrs, fibroblast growth medium was replaced with galactose exposure medium. After 72 hrs of exposure, cells were washed twice with 1x Dulbecco's phosphate-buffered saline (DPBS) (#14200067, Gibco) and harvested by trypsinization. The cell suspension was immediately split into two equal fractions and centrifuged for 5 min at 4°C, 300 x g. Cell pellet from one fraction was then immediately lysed in 400 µl of an ice-cold 1:1 mixture of PBS and 0.2 M NaOH with 1% dodecyltrimethylammonium bromide (DTAB). Cell pellet from the other fraction was resuspended in 400 µl of fibroblast growth medium and cell counting was performed. Volume of the lysate fraction was then adjusted to have 3.2×10^5 cells/ml and was kept on ice until further use. To analyse NADPH and NADP⁺ separately, the cell lysate was immediately divided into two 100 µl fractions. For NADP⁺ analysis, one fraction of the cell lysate was supplemented first with 1 µl of 1 M ascorbic acid and then with 50 µl of 0.4 M HCl containing 10 mM ascorbic acid, then the mixture was heated at 60°C for 15 min and put at room temperature for 10 min to cool down, after which the sample was neutralized with 50 µl of 0.5 M TRIS-base. For NADPH analysis, the other cell lysate fraction was maintained in the original lysis buffer with basic condition, heated at 60°C for 15 min and also put at room temperature for 10 min and neutralized with 100 µl of a 1:1 mixture of TRIS base and 0.4 M HCl with 10 mM ascorbic acid. Then, 50 µl of each sample was loaded onto a white flat bottom 96-well plate (#CLS3912, Corning) and NADPH/NADP⁺ levels were determined according to the manufacturer's instruction. Luminescence was measured by a Biotek Synergy HT microplate reader. Average luminescence signal from blank wells (reaction without cell lysates) was subtracted from experimental samples. NADPH/NADP⁺ ratio was determined by dividing the relative luminescence unit (RLU) values of base-treated samples by the RLU values of acid-treated samples.

Measurement of intracellular ROS level

Intracellular ROS generation was determined using the cell-permeable probe 2',7'-dichlorofluorescein diacetate (H₂DCFDA) (#D6883, Sigma-Aldrich). 7000 human fibroblasts were seeded in black 96-well plates with clear bottom (#CLS3603, Sigma-Aldrich) in fibroblast growth medium. After 18 hrs, cells were switched to either glucose or galactose exposure medium. After 72 hrs of exposure, cells were washed once with 1x DPBS and protected from light. Cells were incubated in HEPES/Tris buffer (HT, 132 mM NaCl, 4.2 mM KCl, 1 mM CaCl₂, 1 mM MgCl₂, either glucose (5.5

mM) or galactose (5.5 mM), and 10 mM HEPES, pH 7.4) containing 10 μ M of H₂DCFDA in the dark for 15 min at 37°C. Next, cells were washed twice with 1x DPBS, and HT buffer containing either glucose (5.5 mM) or galactose (5.5 mM) was added. Fluorescence was detected with excitation at 485 nm and emission at 530 nm on a Biotek Synergy HT microplate reader. After basal ROS measurement, 100 μ M of fresh H₂O₂ (#HI01351000, Scharlab) diluted in 1x DPBS was added and fluorescence measured. Cells in HT buffer without H₂DCFDA dye were used for background correction. After the assay, cells were stained with 4 μ M hoechst at 37°C for 1 hr. Images were made with Cytation 1. Cell number was counted using ImageJ 1.52. ROS levels were normalised to cell number.

Generation of *SIRT5* variant (c.340C>A) HEK293T cells by CRISPR/Cas9 editing

A stable HEK293T cell line expressing *SIRT5* variant (c.340C>A, p.P114T) was generated by homology directed repair (HDR) after CRISPR/Cas9-induced double strand breaks in the *SIRT5* gene, using the CRISPR Nuclease Orange fluorescence protein (OFP) reporter Kit (#21174, Invitrogen), according to manufacturer's instruction. The *SIRT5*-targeted gRNA was designed using the Zhang lab "optimized CRIPSR Design" web tool (<https://crispr.mit.edu/>), and ligated into the CRISPR Nuclease vector. The *SIRT5* P114T CRISPR nuclease construct was produced in *E. coli* and amplified by inoculating single cell colonies in liquid LB media with ampicillin and grown overnight at 37°C with shaking (220 rpm). Plasmids were purified using Endofree Plasmid Maxi kit (#12362, Qiagen) and sequences were confirmed by Sanger sequencing (BaseClear, the Netherlands). The donor DNA was designed using Horizon webtool "Edit-R HDR Donor Designer-oligo". *SIRT5* variant (c.340C>A) as well as a silent mutation in the PAM site were made in the donor DNA sequence. The oligos/primers used are listed in Table 2.

HEK293T cells were co-transfected with the *SIRT5*-P114T CRISPR nuclease construct and donor DNA, using lipofectamine 3000 according to manufacturer's instruction (#L3000015, Invitrogen). Forty-eight hours after the start of transfection, cells were trypsinized and plated at a limiting dilution in routine culture media to obtain single cell grown colonies. *SIRT5* P114T modification in HEK293T cells were verified using restriction fragment analysis. For this, the HDR-targeted fragment of *SIRT5* gene was amplified using AmpliTaq Gold 360 (#4398881, Thermo Fischer Scientific) and restriction analysis of the amplified *SIRT5* fragment was performed using *EaeI* and *BanII*. The restriction fragment lengths were checked by capillary electrophoresis using Agilent D1000 ScreenTape on the TapeStation 2200. Homozygous *SIRT5* P114T variant and WT were further confirmed with Sanger sequencing (BaseClear, the Netherlands).

Statistical Analysis

Data are expressed as mean \pm standard deviation (SD). For SIRT5 mRNA normalised expression, succinylation fluorescence levels, His-SIRT5 desuccinylation activity, Seahorse metabolic flux parameters, basal and H₂O₂-induced ROS levels data, one-way analysis of variance (ANOVA) of the means was used, followed by Bonferroni post-hoc testing. Statistical analysis was performed using GraphPad Prism 6.01. P values less than 0.05 were considered statistically significant (* P < 0.05, ** P < 0.01; *** P < 0.001).

Data Availability

The data that support the findings of this study are available from the corresponding authors VdB and RJR upon reasonable request.

Acknowledgements

We want to thank Maurice Henquet for kindly providing HEK293T cells, and we also would like to acknowledge the Genome Technology Center at the Radboudumc and BGI Copenhagen for technical support of the exome sequencing. His-SIRT5 plasmid was a gift from Cheryl Arrowsmith (Addgene plasmid # 25487). Taolin Yuan has received financial support from the China Scholarship Council (Grant No. 201606350170).

Author Contributions

TY designed and performed experiments, analysed data, drafted and wrote the manuscript. AB, NvdH, JYH, YC, DAK, MY, YJ, HL, WK, FAM and MA contributed to experimental procedures and/or generating and providing essential experimental resources. JK supervised study, edited manuscript and discussed data. JNS, RJR and VdB initiated study, analysed data and discussed data. VdB edited the manuscript, analysed data, designed, supervised and coordinated study. All authors commented on the paper.

Competing Interests

WJHK is a scientific advisor of Khondrion BV (Nijmegen, the Netherlands) and of Fortify Therapeutics (Palo Alto, USA). These SMEs had no involvement in the data collection, analysis and interpretation, writing of the manuscript, and in the decision to submit the manuscript for publication.

Materials and Correspondence

Material requests and correspondence should be addressed to VdB and RJR.

References

1. Chandel, N.S. Evolution of Mitochondria as Signaling Organelles. *Cell Metab.* **22**, 204-206 (2015).
2. Koopman, W.J., Willems, P.H. & Smeitink, J.A. Monogenic mitochondrial disorders. *N. Engl. J. Med.* **366**, 1132-1141 (2012).
3. Breuer, M.E., *et al.* The role of mitochondrial OXPHOS dysfunction in the development of neurologic diseases. *Neurobiol. Dis.* **51**, 27-34 (2013).
4. Coskun, P., *et al.* A mitochondrial etiology of Alzheimer and Parkinson disease. *Biochim. Biophys. Acta* **1820**, 553-564 (2012).
5. Wallace, D.C. Mitochondrial diseases in man and mouse. *Science* **283**, 1482-1488 (1999).
6. Schapira, A.H.V. Mitochondrial disease. *The Lancet* **368**, 70-82 (2006).
7. Scaglia, F. Nuclear gene defects in mitochondrial disorders. *Methods Mol. Biol.* **837**, 17-34 (2012).
8. Gorman, G.S., *et al.* Prevalence of nuclear and mitochondrial DNA mutations related to adult mitochondrial disease. *Ann. Neurol.* **77**, 753-759 (2015).
9. Smeitink, J., van den Heuvel, L. & DiMauro, S. The genetics and pathology of oxidative phosphorylation. *Nat. Rev. Genet.* **2**, 342-352 (2001).
10. Hayashi, G. & Cortopassi, G. Oxidative stress in inherited mitochondrial diseases. *Free Radic. Biol. Med.* **88**, 10-17 (2015).
11. Wu, S.B., Ma, Y.S., Wu, Y.T., Chen, Y.C. & Wei, Y.H. Mitochondrial DNA mutation-elicited oxidative stress, oxidative damage, and altered gene expression in cultured cells of patients with MERRF syndrome. *Mol. Neurobiol.* **41**, 256-266 (2010).
12. Esposito, L.A., Melov, S., Panov, A., Cottrell, B.A. & Wallace, D.C. Mitochondrial disease in mouse results in increased oxidative stress. *Proc. Natl. Acad. Sci. U. S. A.* **96**, 4820-4825 (1999).
13. Schulz, J.B., *et al.* Oxidative stress in patients with Friedreich ataxia. *Neurology* **55**, 1719-1721 (2000).
14. Janssen, M.C.H., *et al.* The KHENERGY Study: Safety and Efficacy of KH176 in Mitochondrial m.3243A>G Spectrum Disorders. *Clin. Pharmacol. Ther.* **105**, 101-111 (2019).
15. Klopstock, T., *et al.* Persistence of the treatment effect of idebenone in Leber's hereditary optic neuropathy. *Brain* **136**, e230 (2013).
16. Karaa, A., *et al.* Randomized dose-escalation trial of elamipretide in adults with primary mitochondrial myopathy. *Neurology* **90**, e1212-e1221 (2018).
17. Russell, O.M., Gorman, G.S., Lightowlers, R.N. & Turnbull, D.M. Mitochondrial Diseases: Hope for the Future. *Cell* **181**, 168-188 (2020).
18. Du, J., *et al.* Sirt5 is a NAD-dependent protein lysine demalonylase and desuccinylase. *Science* **334**, 806-809 (2011).
19. Zhou, Y., *et al.* The bicyclic intermediate structure provides insights into the desuccinylation mechanism of human sirtuin 5 (SIRT5). *J. Biol. Chem.* **287**, 28307-28314 (2012).
20. Park, J., *et al.* SIRT5-mediated lysine desuccinylation impacts diverse metabolic pathways. *Mol. Cell* **50**, 919-930 (2013).
21. Tan, M., *et al.* Lysine glutarylation is a protein posttranslational modification regulated by SIRT5. *Cell Metab.* **19**, 605-617 (2014).
22. Rardin, M.J., *et al.* SIRT5 regulates the mitochondrial lysine succinylome and metabolic networks. *Cell Metab.* **18**, 920-933 (2013).
23. Zhang, Y., *et al.* Lysine desuccinylase SIRT5 binds to cardiolipin and regulates the electron transport chain. *J. Biol. Chem.* **292**, 10239-10249 (2017).

24. Nishida, Y., *et al.* SIRT5 Regulates both Cytosolic and Mitochondrial Protein Malonylation with Glycolysis as a Major Target. *Mol. Cell* **59**, 321-332 (2015).
25. Sadhukhan, S., *et al.* Metabolomics-assisted proteomics identifies succinylation and SIRT5 as important regulators of cardiac function. *Proc. Natl. Acad. Sci. U. S. A.* **113**, 4320-4325 (2016).
26. Wang, G., *et al.* Regulation of UCP1 and Mitochondrial Metabolism in Brown Adipose Tissue by Reversible Succinylation. *Mol. Cell* **74**, 844-857 e847 (2019).
27. Yu, J., *et al.* Metabolic characterization of a Sirt5 deficient mouse model. *Sci Rep.* **3**, 2806 (2013).
28. Lombard, D.B., *et al.* Mammalian Sir2 homolog SIRT3 regulates global mitochondrial lysine acetylation. *Mol. Cell. Biol.* **27**, 8807-8814 (2007).
29. Nakagawa, T., Lomb, D.J., Haigis, M.C. & Guarente, L. SIRT5 Deacetylates carbamoyl phosphate synthetase 1 and regulates the urea cycle. *Cell* **137**, 560-570 (2009).
30. Zhou, L., *et al.* SIRT5 promotes IDH2 desuccinylation and G6PD deglutarylation to enhance cellular antioxidant defense. *EMBO Rep.* **17**, 811-822 (2016).
31. Boylston, J.A., *et al.* Characterization of the cardiac succinylome and its role in ischemia-reperfusion injury. *J. Mol. Cell Cardiol.* **88**, 73-81 (2015).
32. Diaz-Canestro, C., *et al.* Sirtuin 5 as a novel target to blunt blood-brain barrier damage induced by cerebral ischemia/reperfusion injury. *Int. J. Cardiol.* **260**, 148-155 (2018).
33. Hershberger, K.A., *et al.* Ablation of Sirtuin5 in the postnatal mouse heart results in protein succinylation and normal survival in response to chronic pressure overload. *J. Biol. Chem.* **293**, 10630-10645 (2018).
34. Hershberger, K.A., *et al.* Sirtuin 5 is required for mouse survival in response to cardiac pressure overload. *J. Biol. Chem.* **292**, 19767-19781 (2017).
35. Kumar, S. & Lombard, D.B. Functions of the sirtuin deacylase SIRT5 in normal physiology and pathobiology. *Crit. Rev. Biochem. Mol. Biol.* **53**, 311-334 (2018).
36. Ullah, M.S., Davies, A.J. & Halestrap, A.P. The plasma membrane lactate transporter MCT4, but not MCT1, is up-regulated by hypoxia through a HIF-1alpha-dependent mechanism. *J. Biol. Chem.* **281**, 9030-9037 (2006).
37. Divakaruni, A.S. & Brand, M.D. The regulation and physiology of mitochondrial proton leak. *Physiology (Bethesda)* **26**, 192-205 (2011).
38. Ying, W. NAD⁺/NADH and NADP⁺/NADPH in cellular functions and cell death: regulation and biological consequences. *Antioxid. Redox Signal.* **10**, 179-206 (2008).
39. Iannetti, E.F., Smeitink, J.A.M., Willems, P., Beyrath, J. & Koopman, W.J.H. Rescue from galactose-induced death of Leigh Syndrome patient cells by pyruvate and NAD⁺. *Cell Death Dis.* **9**, 1135 (2018).
40. Zhang, M., *et al.* SIRT5 deficiency suppresses mitochondrial ATP production and promotes AMPK activation in response to energy stress. *PLoS One* **14**, e0211796 (2019).
41. Morris-Blanco, K.C., *et al.* Protein Kinase C Epsilon Promotes Cerebral Ischemic Tolerance Via Modulation of Mitochondrial Sirt5. *Sci Rep.* **6**, 29790 (2016).
42. Liang, F.Y., Wang, X., Ow, S.H., Chen, W.X. & Ong, W.C. Sirtuin 5 is Anti-apoptotic and Anti-oxidative in Cultured SH-EP Neuroblastoma Cells. *Neurotox. Res.* **31**, 63-76 (2017).
43. Brand, M.D. Uncoupling to survive? The role of mitochondrial inefficiency in ageing. *Exp. Gerontol.* **35**, 811-820 (2000).
44. Nobes, C.D., Brown, G.C., Olive, P.N. & Brand, M.D. Non-ohmic proton conductance of the mitochondrial inner membrane in hepatocytes. *J. Biol. Chem.* **265**, 12903-12909 (1990).
45. Rolfe, D.F., Newman, J.M., Buckingham, J.A., Clark, M.G. & Brand, M.D. Contribution of mitochondrial proton leak to respiration rate in working skeletal muscle and liver and to SMR. *Am. J. Physiol.* **276**, C692-699 (1999).

46. Brand, M.D., *et al.* The basal proton conductance of mitochondria depends on adenine nucleotide translocase content. *Biochem. J.* **392**, 353-362 (2005).
47. Olausson, T., Fjellstrom, O., Mueller, J. & Rydström, J. Molecular biology of nicotinamide nucleotide transhydrogenase--a unique proton pump. *Biochim. Biophys. Acta* **1231**, 1-19 (1995).
48. Brookes, P.S., Land, J.M., Clark, J.B. & Heales, S.J. Peroxynitrite and brain mitochondria: evidence for increased proton leak. *J. Neurochem.* **70**, 2195-2202 (1998).
49. Echtaý, K.S., *et al.* Superoxide activates mitochondrial uncoupling proteins. *Nature* **415**, 96-99 (2002).
50. Hoerter, J., *et al.* Mitochondrial uncoupling protein 1 expressed in the heart of transgenic mice protects against ischemic-reperfusion damage. *Circulation* **110**, 528-533 (2004).
51. Teshima, Y., Akao, M., Jones, S.P. & Marbán, E. Uncoupling protein-2 overexpression inhibits mitochondrial death pathway in cardiomyocytes. *Circul. Res.* **93**, 192-200 (2003).
52. Cadenas, S. Mitochondrial uncoupling, ROS generation and cardioprotection. *Biochim. Biophys. Acta Bioenerg.* **1859**, 940-950 (2018).
53. Brookes, P.S. Mitochondrial H(+) leak and ROS generation: an odd couple. *Free Radic. Biol. Med.* **38**, 12-23 (2005).
54. Stepien, K.M., *et al.* Evidence of Oxidative Stress and Secondary Mitochondrial Dysfunction in Metabolic and Non-Metabolic Disorders. *J. Clin. Med.* **6**, (2017).
55. Bhatti, J.S., Bhatti, G.K. & Reddy, P.H. Mitochondrial dysfunction and oxidative stress in metabolic disorders - A step towards mitochondria based therapeutic strategies. *Biochim. Biophys. Acta Mol. Basis Dis.* **1863**, 1066-1077 (2017).
56. Ramachandran, A., *et al.* Mitochondria, nitric oxide, and cardiovascular dysfunction. *Free Radic. Biol. Med.* **33**, 1465-1474 (2002).
57. Cenini, G., Lloret, A. & Cascella, R. Oxidative Stress in Neurodegenerative Diseases: From a Mitochondrial Point of View. *Oxid. Med. Cell Longev.* **2019**, 2105607 (2019).
58. Haugen, A.C., *et al.* Altered gene expression and DNA damage in peripheral blood cells from Friedreich's ataxia patients: cellular model of pathology. *PLoS Genet.* **6**, e1000812 (2010).
59. Frazier, A.E., Thorburn, D.R. & Compton, A.G. Mitochondrial energy generation disorders: genes, mechanisms, and clues to pathology. *J. Biol. Chem.* **294**, 5386-5395 (2019).
60. Weinert, B.T., *et al.* Lysine succinylation is a frequently occurring modification in prokaryotes and eukaryotes and extensively overlaps with acetylation. *Cell Rep.* **4**, 842-851 (2013).
61. Michishita, E., Park, J.Y., Burneskis, J.M., Barrett, J.C. & Horikawa, I. Evolutionarily conserved and nonconserved cellular localizations and functions of human SIRT proteins. *Mol. Biol. Cell* **16**, 4623-4635 (2005).
62. Du, Y., Hu, H., Hua, C., Du, K. & Wei, T. Tissue distribution, subcellular localization, and enzymatic activity analysis of human SIRT5 isoforms. *Biochem. Biophys. Res. Commun.* **503**, 763-769 (2018).
63. Fisher-Wellman, K.H., *et al.* Respiratory Phenomics across Multiple Models of Protein Hyperacetylation in Cardiac Mitochondria Reveals a Marginal Impact on Bioenergetics. *Cell Rep.* **26**, 1557-1572.e1558 (2019).
64. Ahn, B.H., *et al.* A role for the mitochondrial deacetylase Sirt3 in regulating energy homeostasis. *Proc. Natl. Acad. Sci. U. S. A.* **105**, 14447-14452 (2008).
65. Horton, J.L., *et al.* Mitochondrial protein hyperacetylation in the failing heart. *JCI Insight* **2**, (2016).
66. Hirschey, M.D., *et al.* SIRT3 regulates mitochondrial fatty-acid oxidation by reversible enzyme deacetylation. *Nature* **464**, 121-125 (2010).

67. Williams, A.S., *et al.* Disruption of Acetyl-Lysine Turnover in Muscle Mitochondria Promotes Insulin Resistance and Redox Stress without Overt Respiratory Dysfunction. *Cell Metab.* **31**, 131-147 e111 (2020).
68. Shi, T., Wang, F., Stieren, E. & Tong, Q. SIRT3, a mitochondrial sirtuin deacetylase, regulates mitochondrial function and thermogenesis in brown adipocytes. *J. Biol. Chem.* **280**, 13560-13567 (2005).
69. Wortmann, S.B., Koolen, D.A., Smeitink, J.A., van den Heuvel, L. & Rodenburg, R.J. Whole exome sequencing of suspected mitochondrial patients in clinical practice. *J. Inherit. Metab. Dis.* **38**, 437-443 (2015).
70. Neveling, K., *et al.* A post-hoc comparison of the utility of sanger sequencing and exome sequencing for the diagnosis of heterogeneous diseases. *Hum. Mutat.* **34**, 1721-1726 (2013).

Table 1 List of antibodies

Antibody	Company	Catalogue number
Rabbit monoclonal anti-SIRT5	Cell Signaling Technology	#8782
Rabbit polyclonal anti-SIRT5	Sigma-Aldrich	#HPA022002
Rabbit polyclonal anti-SIRT3	Cell Signaling Technology	#5490s
Goat polyclonal anti-SIRT4	Abcam	#ab10140
Rabbit polyclonal pan anti-succinyllysine (western blot)	PTM BioLabs	#PTM-401
Mouse monoclonal pan anti-succinyllysine (Immunofluorescence)	PTM BioLabs	#PTM-419
Mouse monoclonal anti-actin beta	Abcam	#ab6276
Anti-Histone H3	Cell Signaling Technology	#9715
Rabbit monoclonal mix anti-malonyllysine	Cell Signaling Technology	#14942
Rabbit polyclonal anti-glutaryllysine	PTM BioLabs	#PTM-1151
Mouse monoclonal anti-total OXPHOS Human Cocktail	Abcam	#ab110411
Rabbit IgG	Vector Laboratories	#I-1000
Monoclonal goat anti-rabbit IgG, Alexa Fluor 488	Invitrogen, Thermo Fisher Scientific	#A11008
Anti-rabbit IgG, HRP-linked	Cell Signaling Technology	#7074
IRDye 800CW Goat anti-Rat IgG (H + L)	LI-COR	#925-32219
IRDye 800CW Donkey anti-Goat IgG (H + L)	LI-COR	#926-32214

Table 2 List of primers/oligos

Oligonucleotides for recombinant SIRT5 variant proteins	
Mutagenesis primer for <i>SIRT5</i> (c.340C>A, p.P114T)	Forward: 5'-GCCCCGGCGTTGGTCTCCTTGCTCCC-3'
	Reverse: 5'-GGGAGCAAGGAGACCAACGCCGGGC-3'
Mutagenesis primer for <i>SIRT5</i> (c.382C>G, p.L128V)	Forward: 5'-CCTGCTTGCCACCCGGGTCTCACA-3'
	Reverse: 5'-TGTGAGACCCGGGTGGGCAAGCAGG-3'
Oligonucleotides for knock-in SIRT5 variant in HEK293T	
Single-stranded DNA encoding guide RNA	5'-GGAGCAAGGAGCCCAACGCC-3'
Donor DNA	5'-GGGTGTGGGAGTTCTACCACTACCGCGGGAGGTCATGGGGA GCAAGGAGACCAACGCCGGCCACCGGCCATAGCCGAGTGTGAG ACCCGGCTGGGCAAGCAGGGCCGGCG-3'
Primers for SIRT5 variant amplification/s equencing	Forward: 5'-GATGGGGACGTAGGCTGGTA-3'
	Reverse: 5'-AAGCTGGTTCCTGAATGGG-3'
Primer for gene expression in fibroblasts	
<i>SIRT5</i>	Forward: 5'-AAATGGCAAGCCCAGGACC-3'
	Reverse: 5'-GGTCTCACACTCGGCTATGG-3'
<i>B2M</i>	Forward: 5'-TGCCGTGTGAACCATGTG-3'
	Reverse: 5'-GCGGCATCTTCAAACCTC-3'
<i>ERBB2IP</i>	Forward: 5'-TGTGGCTCTCAGATAATCAGTCC-3'
	Reverse: 5'-ACATAACATCCTCAGTCCTTGGC-3'
<i>RPS15</i>	Forward: 5'-AGAAGCCGGAAGTGGTGAAGAC-3'
	Reverse: 5'-AGAGGGATGAAGCGGGAGGAG-3'

Table 3 Detailed description of exposure media and seahorse assay media applied in seahorse experiments

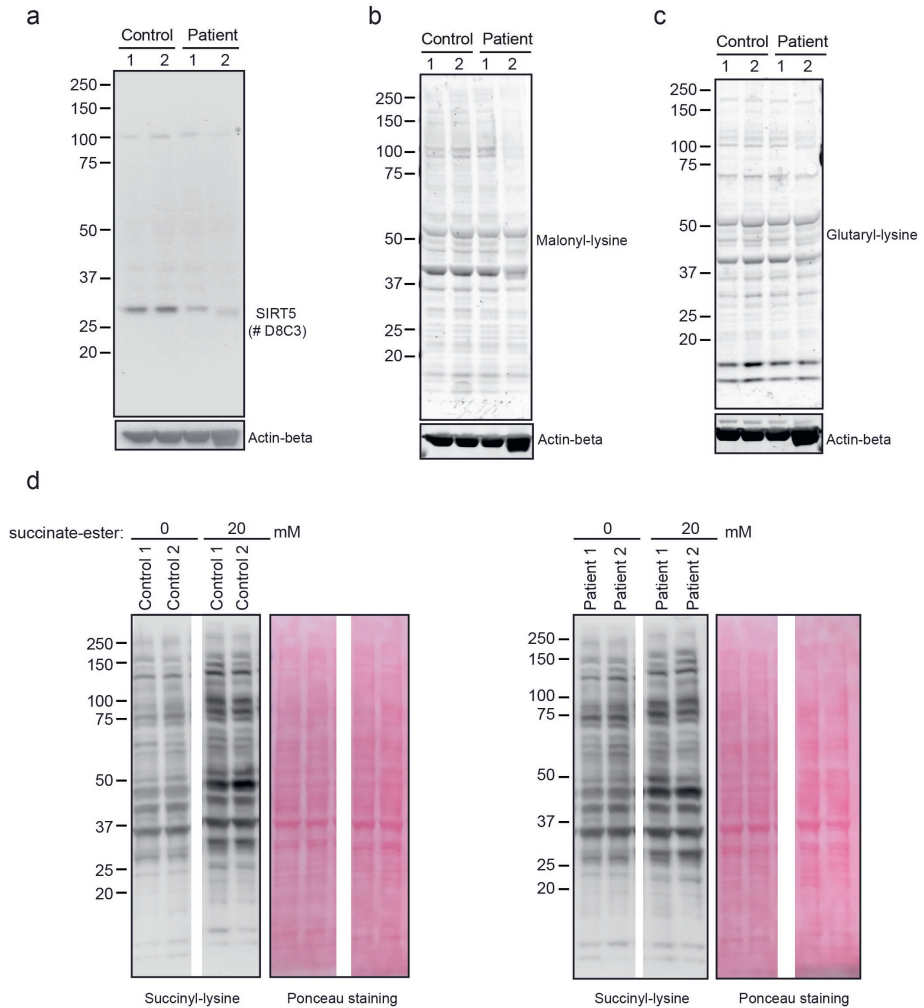
Perturbation	Exposure media composition	Exposure time	Seahorse assay media
M199	Normal culture medium 199	overnight	XF DMEM, supplemented with 2 mM XF L-Gln and 5.5 mM XF glucose
CoCl ₂	DMEM, supplemented with 10% FBS, 2 mM L-Gln and 5.5 mM XF glucose, and 100 µM CoCl ₂	6 hrs	XF DMEM, supplemented with 2 mM XF L-Gln, 5.5 mM XF glucose and 100 µM CoCl ₂
Glucose DMEM	DMEM, supplemented with 10% FBS, 2 mM L-Gln and 5.5 mM XF glucose	72 hrs	XF DMEM, supplemented with 2 mM XF L-Gln and 5.5 mM XF glucose
galactose DMEM 72h	DMEM, supplemented with 10% FBS, 2 mM L-Gln and 5.5 mM galactose	72 hrs	XF DMEM, supplemented with 2 mM XF L-Gln and 5.5 mM galactose
galactose DMEM 96h	DMEM, supplemented with 10% FBS, 2 mM L-Gln and 5.5 mM galactose	96 hrs	XF DMEM, supplemented with 2 mM XF L-Gln and 5.5 mM galactose
galactose DMEM succinate-ester 72h	DMEM, supplemented with 10% FBS, 2 mM L-Gln, 5.5 mM galactose and 4 mM dimethyl succinate-ester	72 hrs	XF DMEM, supplemented with 2 mM XF L-Gln and 5.5 mM galactose
galactose DMEM succinate-ester 96h	DMEM, supplemented with 10% FBS, 2 mM L-Gln, 5.5 mM galactose and 4 mM dimethyl succinate-ester	96 hrs	XF DMEM, supplemented with 2 mM XF L-Gln and 5.5 mM galactose

Supplementary Material

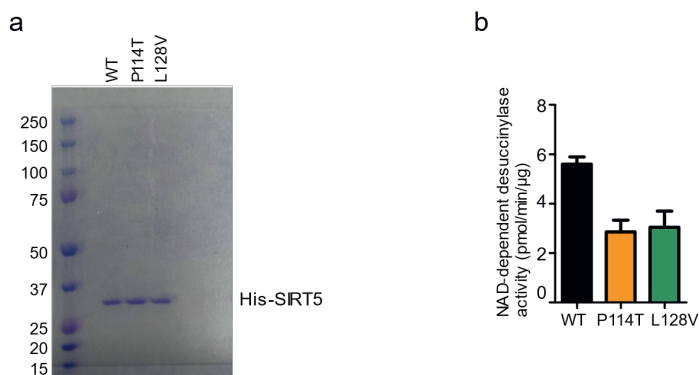
Supplementary Table S1 Enzymatic activity of OXPHOS complexes in fibroblasts and muscle biopsy of patients

Enzyme activities (human fibroblasts)	Activity		Control range	Unit
	Patient 1	Patient 2		
Complex I	565	770	279 - 1076	mU/UCOX
Complex II	978	956	375 - 2692	mU/UCOX
Complex III	1576	1327	623 - 3534	mU/UCOX
Complex II + III (succ.: cyt.c oxidoreductase; SCC)	565	522	269 - 781	mU/UCOX
Complex IV	377	541	288 - 954	mU/UCS
Complex V (ATPase)	1261	1434	480 - 2705	mU/UCOX
Citrate synthase	428	435	151 - 499	mU/mg

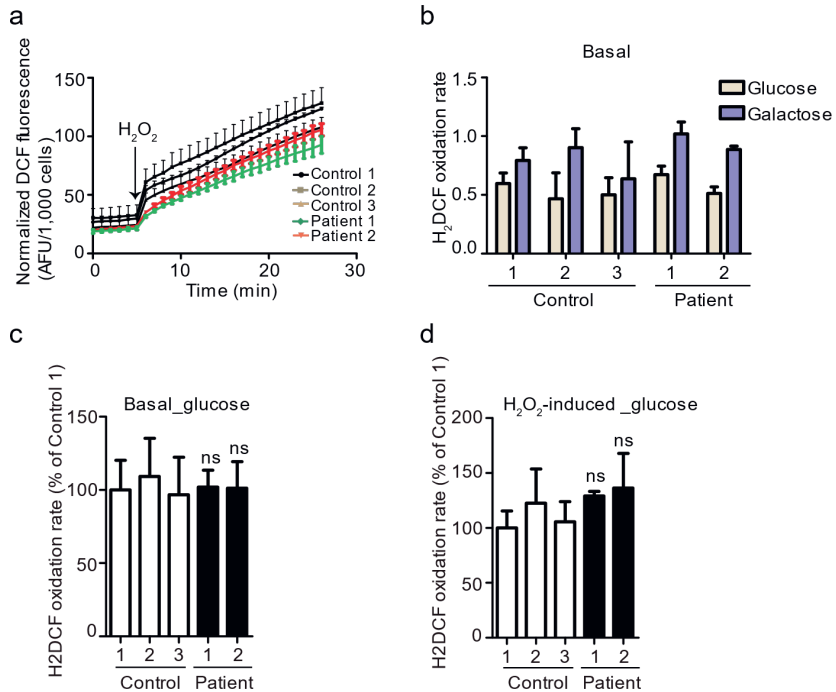
Enzyme activities (skeletal muscle)	Activity		Control range	Unit
	Patient 1	Patient 2		
Complex I	ND	107	68 - 230	mU/UCS
Complex II	ND	216	76 - 281	mU/UCS
Complex III	ND	244	182 - 1421	mU/UCS
Complex II + III (succ.: cyt.c oxidoreductase; SCC)	ND	56	30 - 263	mU/UCS
Complex IV	ND	229	228 - 1032	mU/UCS
Citrate synthase	ND	299	111 - 604	mU/mg



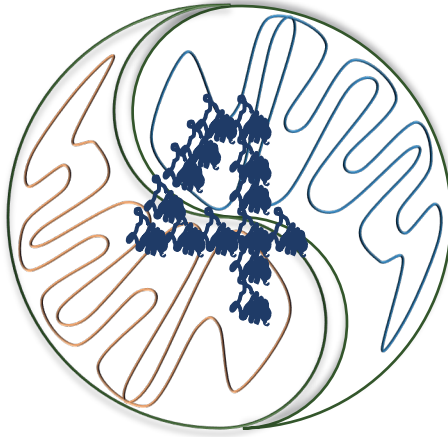
Supplementary Figure S1. (a) Confirmation of SIRT5 protein level in whole cell lysates of controls and patients-derived fibroblasts with SIRT5 antibody (#D8C3), Actin-beta was loading control. Western blot detection of (b) malonyllysine and (c) glutaryllysine in lysates of controls and patients-derived fibroblasts. Actin-beta was loading control in (b) and (c). (d) Western blot detection of succinyllysine in lysates of controls and patients-derived fibroblasts, with and without succinate-ester exposure, and ponceau staining demonstrating equal loading.



Supplementary Figure S2. (a) Confirmation of recombinant His-SIRT5s purification. The gel was stained by Coomassie staining. (b) NAD⁺-dependent desuccinylase activity of recombinant SIRT5 WT, SIRT5 P114T and SIRT5 L128V in the context of 10 μM succinyl-substrate with 10 μM NAD⁺. Duplicates, representative for 2 independent experiments. Data represent mean ± SD.



Supplementary Figure S3. (a) A representative normalised real-time DCF fluorescence signal traces of human fibroblasts after 72 hrs-exposure to glucose medium. Acute application of H₂O₂ (100 μ M) was performed after basal treatment. (b) A representative basal H₂DCF-oxidation rate of human fibroblasts exposed to either glucose (5.5 mM) or galactose (5.5 mM) medium for 72 hrs. (c) Basal and (d) H₂O₂-induced relative H₂DCF oxidation rate of human fibroblasts cultured in glucose medium for 72 hrs. In both (c) and (d), n = 4 independent experiments, and 3-6 technical replicates in each experiment. Data represent mean \pm SD. (a) and (b), representative for 4 independent experiments. (c) and (d), one-way ANOVA, followed by Bonferroni post-hoc testing, and each patient fibroblast was tested against average of three control cell lines. ns, not significant. The concentrations of both glucose and galactose used here were 5.5 mM.



Human SIRT5 variant fibroblasts display an impaired glutathione system associated with disrupted Glutathione-Thioredoxin balance

Taolin Yuan, Inge van der Stelt, Vincent C. J. de Boer,
Jaap Keijer*

Human and Animal Physiology, Wageningen University & Research, The Netherlands

In preparation

Abstract

Cells need a balanced redox environment to maintain proteins functionality and survival. Thiol-dependent antioxidant systems play a significant role in maintaining mitochondrial cellular redox homeostasis. Sirtuin5 (SIRT5) is a primarily mitochondria-located, versatile NAD⁺-dependent deacylase. We previously showed that SIRT5 was critical for human redox homeostasis using primary skin fibroblasts of two independent patients harbouring a dysfunctional SIRT5 protein as a result of a *SIRT5* gene variant. It was, however, unclear how SIRT5 deficiency led to redox perturbation. Here, we demonstrated a disrupted GSH antioxidant system in the patients' fibroblasts by analysing key components in the system, including GSH, glutathione reductase and glutathione peroxidase 4. The perturbation in GSH system resulted in blunted response of patients' fibroblasts to BSO-induced GSH deprivation, in contrast, enhanced sensitivities to inhibition of thioredoxin system were observed. Since both the GSH and the thioredoxin system play a critical role in protecting cells from oxidative stress, the impaired GSH system and consequential imbalance between the two thiol systems may play a role in physiopathology in the patients.

Introduction

A reducing intracellular redox environment is critical for cellular survival and health because it protects cells from endogenous oxidants that are continuously generated in various physiological processes^{1, 2, 3, 4, 5}. Oxidants have important physiological functions, but their reactivity, especially at high levels, can cause damage to cellular macromolecules such as DNA, lipids, and proteins, leading to cell injury, including genome modifications, lipid peroxidation and inactivation of enzymes^{6, 7, 8}. Antioxidant defence mechanisms are in place to protect against oxidative damage and keep signalling oxidants at physiological levels, maintaining redox homeostasis. Indeed, dysregulated redox homeostasis has been linked to multiple human diseases, including mitochondrial diseases and neurodegenerative diseases^{9, 10}.

Mitochondria are cell organelles that perform a number of essential functions, including ATP production by oxidative phosphorylation. This process is driven by a proton gradient that is generated by electron transport, with electrons provided by NADH and via FADH₂. Escape of electrons leads to the generation of so-called reactive oxygen species (ROS). Because of the high rate of ATP generation, the electron transport complexes, and other enzymes that donate electrons for oxidative phosphorylation, are considered as significant sources of cellular ROS in mammalian cells^{2, 11}. Superoxide, resulting from the addition of an electron to molecular oxygen, which occurs mostly at electron transport complexes I and III, is the initial ROS^{2, 12}. It is highly reactive, but it is usually rapidly converted to hydrogen peroxide (H₂O₂) by superoxide dismutases. H₂O₂ is less reactive compared to superoxide and, at physiological levels, acts as a signalling molecule^{13, 14}. It is, however, deleterious for cells at higher levels and can cause damage to DNA, lipids and proteins^{15, 16, 17}. To prevent oxidative stress imposed by H₂O₂ and other oxidants, cells have evolved sets of non-enzymatic and enzymatic antioxidant systems in a compartmentalized manner^{18, 19, 20}. In the mitochondria, ROS is detoxified by glutathione (GSH)- and thioredoxin-dependent systems^{21, 22, 23}. GSH is the most abundant low molecular weight thiol peptide in most cells, present in millimolar concentrations^{24, 25}. It plays an important role in maintaining cellular redox balance via its thiol-disulfide exchange reactions and is considered to be a major redox buffer^{26, 27}. GSH exhibits its antioxidant role through either directly removing free radicals or acting as a cofactor for antioxidant enzymes^{28, 29}. For instance, glutathione peroxidases reduce H₂O₂ and lipid hydroperoxides with GSH serving as an electron donor^{30, 31}. In addition to detoxifying free radical species, GSH also plays an important role in reducing protein disulfides and maintaining their functions^{32, 33}. The thioredoxin system, another important thiol-based antioxidant system, consists of thioredoxin,

thioredoxin reductase, peroxiredoxins and reducing equivalent NADPH. Thioredoxins, ubiquitous small proteins, play an important role in reducing protein disulfides³⁴, and the oxidized thioredoxin is reduced back by thioredoxin reductase in a NADPH-dependent manner³⁵. Additionally, thioredoxin works along with peroxiredoxins to efficiently reduce H₂O₂ as well as other hydroperoxides *in vivo*^{36,37}. The GSH and thioredoxin antioxidant system share some functions and work in collaboration to protect the cells from oxidative stress.

Sirtuin 5 (SIRT5), a robust NAD⁺-dependent desuccinylase³⁸, demalonylase³⁸ and deglutarylase³⁹. It is primarily located in the mitochondrial matrix and extramitochondrial localization was seen in the cytosol and nucleus^{40,41}. Increasing evidence, obtained from mouse models and *in vitro* studies, points to a regulatory role for SIRT5 in redox homeostasis. Absence of SIRT5 exacerbated oxidative damage in SIRT5 knockout mice upon exogenous paraquat injection, as shown by increased lipid peroxide levels in the brain, accompanied with decreased levels of GSH and NADPH, as compared to SIRT5 wild-type littermates⁴². Additionally, the potential involvement of SIRT5 in redox regulation is also suggested by data obtained in multiple cell lines. For example, ROS levels were increased upon SIRT5 knockdown in ovarian cancer cell lines and neuroblastoma cells, whereas the levels were diminished by overexpression of SIRT5^{43,44}. Furthermore, in cancer cell lines at the gene expression level, SIRT5 positively correlated with glutathione reductase (*GSR*) as well as nuclear factor erythroid 2-related factor 2 (*NRF2*), a master transcription factor for antioxidant defence^{43,45}. Together, these data indicate a role for SIRT5 in redox biology. However, direct evidence showing the physiological relevance of SIRT5 in redox regulation, especially in humans, is still lacking.

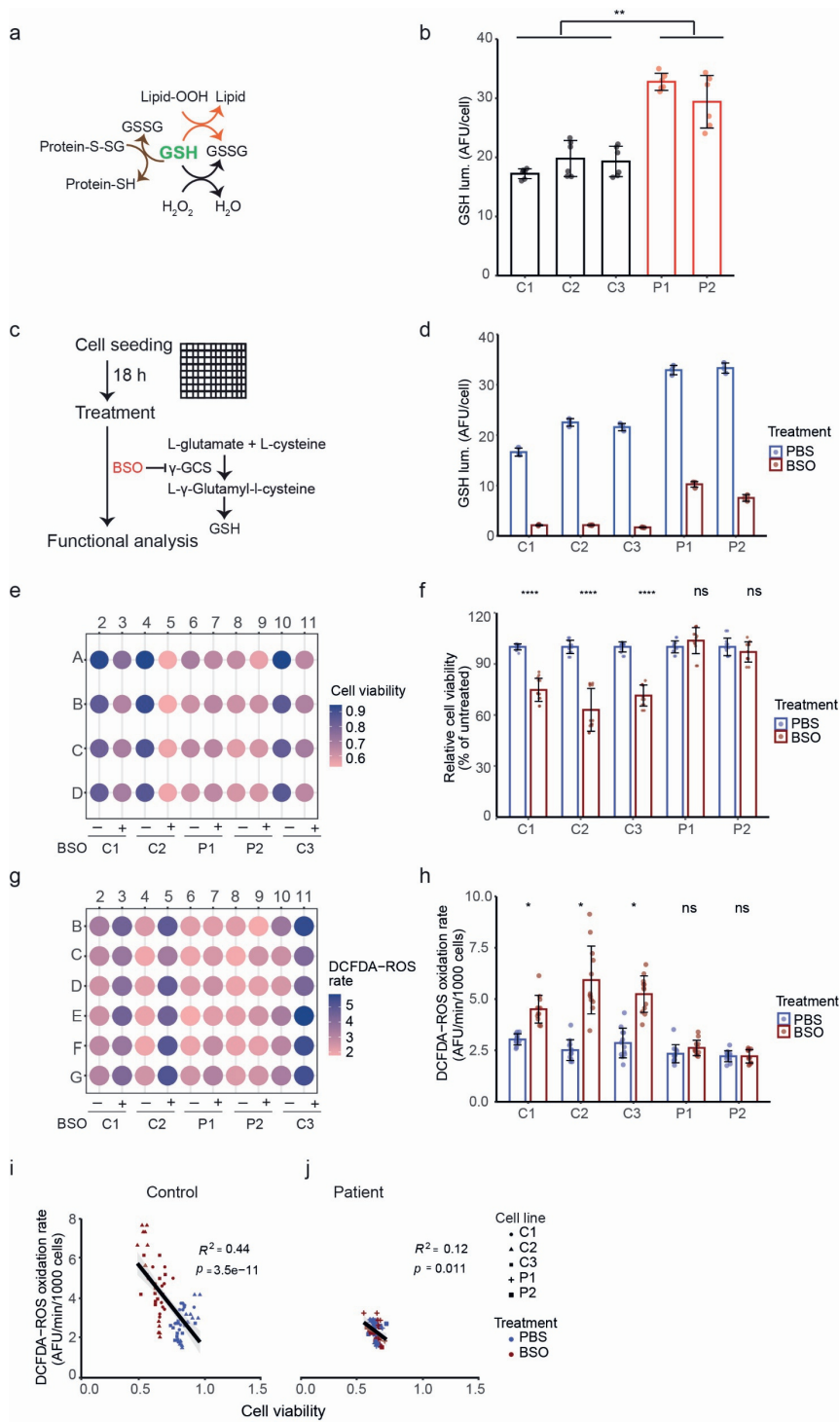
Very recently, we showed the critical role for SIRT5 in human redox homeostasis by investigating two patients with loss-of-function *SIRT5* variants. The two patients manifested clinical mitochondrial disease-like symptoms such as neuroregression, global cerebral and cerebellar atrophy, and seizures (Chapter 3). In that study, we observed that a disrupted redox homeostasis was the most pronounced phenotype in the primary skin fibroblasts derived from the patients. Significantly higher ROS accumulation rates were present in patients' fibroblasts upon acute application of exogenous H₂O₂, but not under basal conditions, which suggested to us an impairment in antioxidant systems. In this study, we set out to understand how redox balance was affected by the SIRT5 variants, with a focus on the two mitochondrial thiol antioxidant systems, using the SIRT5 patients' primary skin fibroblasts as a model.

Results

Patient fibroblasts show increased GSH, but a blunted response to inhibition of the glutathione system

Given that GSH is an important cellular antioxidant and plays a critical role in multiple antioxidant defence pathways (Fig. 1a), we decided to analyse intracellular levels of reduced glutathione. Significantly higher GSH levels were observed in two fibroblast cell lines derived from patients with SIRT5 variant (P1 and P2) as compared to three human control fibroblast cell lines (C1, C2, and C3) (Fig. 1b). We previously showed increased sensitivity of these patients' fibroblasts to exogenous H₂O₂ (Chapter 3), and the increase in GSH observed here was interpreted as an adaptive response. We therefore hypothesized that glutathione, as well as its related antioxidant system, was critical for survival of the patients' fibroblasts, and disruption might sensitize them to cell death. To test this, fibroblasts were subjected to buthionine sulfoximine (BSO) treatment, an established chemical compound that elicits GSH depletion by inhibiting γ -glutamylcysteine synthetase (γ -GCS)^{46, 47}, followed by cell viability and ROS level analysis (Fig. 1c).

GSH levels decreased dramatically upon BSO treatment for 8 hrs (short-term) without morphological changes in both control and patient fibroblasts cell lines (Fig. 1d and Supplementary Fig. S1a). The absolute decrease was similar in patient and control cells, resulting in significantly higher GSH levels in SIRT5 variant cells as compared to control cells (Fig. 1d). BSO-induced GSH deprivation caused a 30% decrease in cell viability in control cells, but not in the SIRT5 variant fibroblasts (Fig. 1e and 1f). The reduced cell viability was concomitant with a 2-fold increase in cellular ROS level in control fibroblasts. In contrast, no changes in ROS levels were detected in two SIRT5 variant fibroblasts exposed to BSO (Fig. 1g and 1h). A negative correlation was observed between the cell viability and DCFDA-oxidizing ROS level in control fibroblasts (Fig. 1i), which indicates that a BSO-induced increase in cellular ROS levels contributes to the decreased cell viability. Furthermore, control fibroblasts were grouped into two populations according to BSO exposure when analysed for cell viability and intracellular ROS level. However, the short-term BSO challenge did not affect these parameters in SIRT5 variant fibroblasts (Fig. 1j). A blunted response of SIRT5 variant fibroblasts to BSO treatment, was further supported by a longer time needed for patients' fibroblasts to show BSO-induced cell morphological damage (Supplemental Fig. 1b). Detrimental effects of BSO on cell morphology were observed in controls' cells after 22-hr exposure, but not in the two patients' fibroblasts, which required a longer exposure (28 hrs) to induce



damage. Together, these results show a blunted sensitivity of SIRT5 variant fibroblasts to glutathione deprivation.

Patient fibroblasts are sensitive to inhibition of thioredoxin system

In mammalian cells, the thioredoxin antioxidant system, another key antioxidant system, works along with the glutathione system to maintain cellular redox homeostasis. Importantly, the two thiol-dependent systems have been found to serve as a backup system for each other^{48, 49}. The blunted responses of patients' fibroblasts to glutathione inhibition may suggest a more essential role for the thioredoxin system in survival of these cells. To test our hypothesis, we used a well-characterized inhibitor of thioredoxin reductases, auranofin (AFN), to inhibit cytosolic and mitochondrial thioredoxin reductases^{48, 50} (Fig. 2a). After exposure to AFN for 5 hrs, altered fibroblast morphology was observed in both patients' fibroblasts, whereas controls' fibroblasts maintained the morphology (Fig. 2b). Cell number can affect the response to exogenous stimuli, as cells are more tolerant to environmental stresses at higher cell number as compared to lower cell number⁵¹. To rule out the possibility that increased sensitivity of SIRT5 variant fibroblasts to AFN-induced thioredoxin inhibition was caused by changes in cell number, we stained the cell nuclei to determine cell numbers. Results showed that cell numbers were comparable among cell lines and were not affected by the AFN treatment during the 5-hour exposure time (Fig. 2c). This supports our conclusion that the AFN-induced alteration in patients' fibroblast morphology was due to inherent biological properties.

Figure 1. Patient fibroblasts but not control fibroblasts display blunt response to BSO-induced glutathione deprivation. (a) GSH participates in multiple antioxidant defence pathways *in vivo*. (b) GSH level in fibroblasts of either PBS (0.1%) or DMSO (0.06%) control group. Data were pooled from two independent experiments. (c) An experimental scheme of human fibroblasts undergoing BSO challenge. (d) Intracellular GSH level in fibroblasts in control PBS group and BSO group. The datapoints in PBS group were also used in (a). (e) A representative plate heatmap visualization of cell viability in fibroblasts subject to either PBS (vehicle control) or BSO. The colour represents the absorbance at 440 nm for WST-1 assay. The letters and numbers were the labels for row and columns of a 96-well plate, respectively. (f) Cell viability of each fibroblast exposed to BSO relative to its own PBS control group. Data from three independent experiments were pooled. (g) A representative plate heatmap visualization of DCFDA-oxidizing ROS level in fibroblasts subject to either PBS (vehicle control) or BSO. (h) DCFDA-oxidizing ROS rate in fibroblasts in PBS or BSO group. Data from three independent experiments were pooled. A correlation analysis between cell viability and DCFDA-ROS oxidizing rate in control (i) and patients' fibroblasts (j). Within each cell type (control or patient), media treatment was distinguished with different colour. Cell viability and DCFDA-ROS rate data corresponds to the data used in (f) and (h), respectively. In all panels, fibroblasts were exposed to either PBS (0.1%) or BSO (100 μ M, 8 hr). Data represent mean \pm SD. For statistical analysis, in (b) and (f), unpaired t-test were used. In (d) and (h), Two-way ANOVA followed by Bonferroni post-test was used. *P < 0.05, **P < 0.01, ***P < 0.001, ****P < 0.0001, ns, not

significant. Pearson method was used for the correlation analysis. Related information can be found in Supplementary Fig. S1a and S1b.

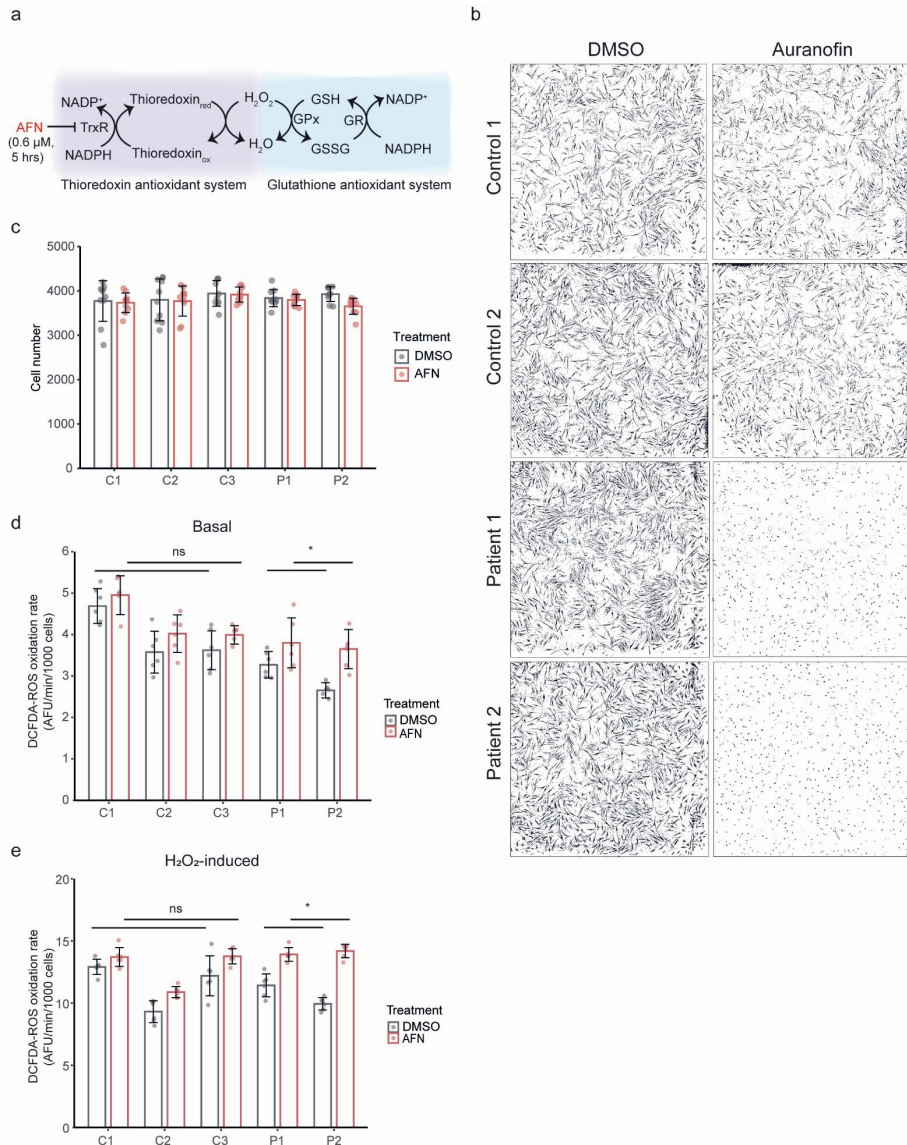


Figure 2. Enhanced sensitivity of patients' fibroblast to auranofin (AFN)-induced thioredoxin system inhibition. (a) An experimental protocol used to challenge fibroblasts with AFN. (b) Representative (for three independent experiments) processed images of fibroblasts after 5-hr exposure to DMSO (0.06%) or AFN. (c) Cell number after exposure to DMSO or AFN for 5 hrs. DCFDA-ROS oxidizing rate in fibroblasts under basal (d) and upon acute 100 μ M H_2O_2 application (e) condition. Two-way ANOVA followed by Bonferroni correction was used for statistical analysis in d and e. * $P < 0.05$, ns, not significant.

Consistently, a significant increase in intracellular ROS levels induced by AFN was observed in patients' fibroblasts (Fig. 2d), and this difference was further increased upon acute exogenous H_2O_2 application (Fig. 2e). In contrast, AFN did not significantly affect the intracellular ROS levels in the control fibroblasts under both basal and H_2O_2 challenging condition (Fig. 2d and 2e). Together, these results demonstrated that patients' fibroblasts were intolerant to inhibition of the thioredoxin system.

Involvement of impaired glutathione system in the imbalanced antioxidant systems in patient fibroblasts

The patients' fibroblasts tolerated BSO-induced GSH deprivation, but displayed enhanced sensitivity to AFN-induced thioredoxin system inhibition. This triggered us to speculate that in the patients' fibroblasts the GSH-dependent system was somehow impaired, seeming reduced in use of GSH, leading to a consequently increased dependence on the thioredoxin system.

To gain further insights, we examined the mRNA expression of several antioxidant defence genes. Superoxide dismutase 2 (*SOD2*), a mitochondrial antioxidant defence enzyme that is critical for detoxifying superoxide radicals to H_2O_2 , did not differ between DMSO vehicle control and AFN treatment at transcriptional level. A trend of higher *SOD2* mRNA level in patients' fibroblasts compared to controls under AFN condition was seen ($p = 0.0708$) (Fig. 3a), possibly indicating a higher oxidative stress in the SIRT5 variant fibroblasts. On the other hand, a significant increase in thioredoxin reductase 1 (*TXNRD1*), but not thioredoxin reductase 2 (*TXNRD2*), was observed in all fibroblasts upon AFN treatment (Fig. 3b and 3c). Since AFN has been reported to inhibit cellular thioredoxin reductase 1 activity⁵², the increase in *TXNRD1* mRNA level can be explained as a compensatory upregulation in our human AFN-treated fibroblasts. Similarly, the gene expression of *GSR* was significantly increased in both control and patients' fibroblasts in the presence of AFN (Fig. 3d), likely also as a compensatory action of the inhibitory effects of AFN on the thioredoxin system. *GSR* plays a critical role in glutathione antioxidant system by converting oxidized glutathione (GSSG) to the reduced form (GSH). In line with the AFN-induced increase in *GSR* gene expression level, we also observed a significant 10-20% increase in GSH levels in controls' as well as in patients' fibroblasts subjected to AFN treatment (Fig. 3e). Moreover, SIRT5 variant fibroblasts consistently displayed higher intracellular GSH level as compared to controls (Fig. 3e). NADPH is a key component in the thiol-antioxidant systems acting as a reducing molecule and the gene expression level of nicotinamide nucleotide transhydrogenase (*NNT*), a significant contributor of

mitochondrial NADPH pool⁵³, was not altered by AFN treatment, nor did it differ between control and SIRT5 variant fibroblasts (Fig. 3f).

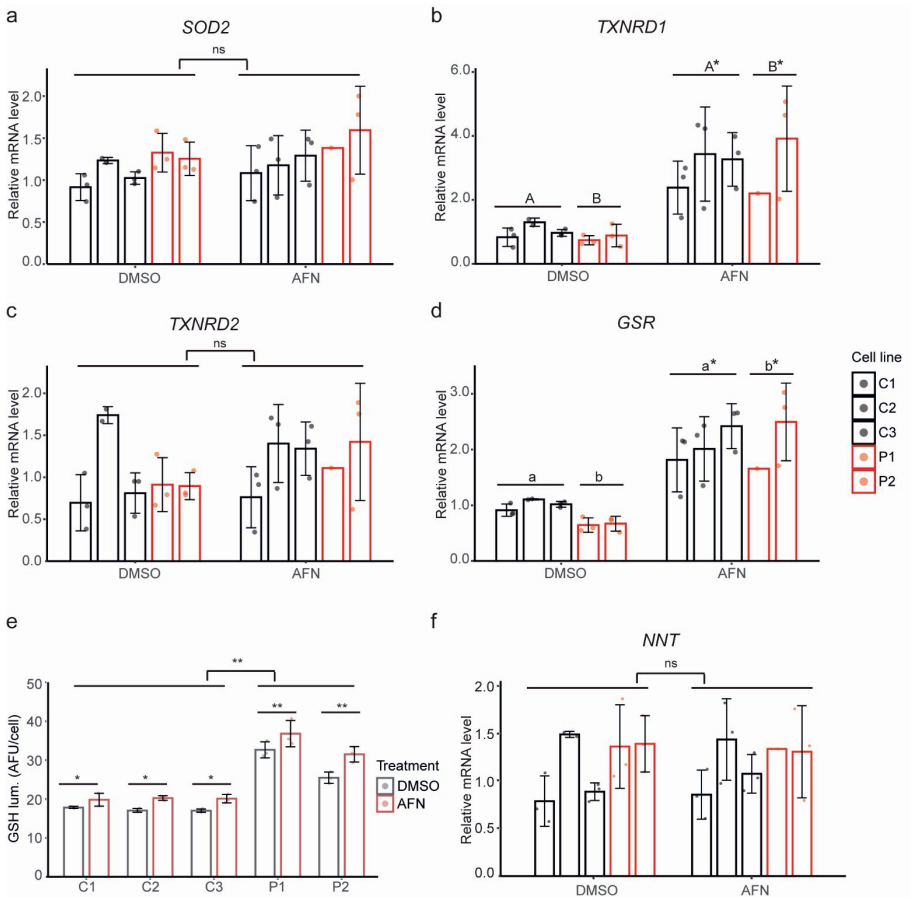


Figure 3. Both control and patients' fibroblasts were able to increase antioxidants level in response to AFN exposure. (a) Relative gene expression level of sodium dismutase 2 (*SOD2*), (b) thioredoxin reductase 1 (*TXNRD1*), (c) thioredoxin reductase 2 (*TXNRD2*), (d) glutathione reductase (*GSR*) and (f) nicotinamide nucleotide transhydrogenase (*NNT*) in fibroblasts under either DMSO or AFN condition. (e) Intracellular GSH level in fibroblasts under DMSO or AFN condition, respectively. The datapoints for DMSO group were also used in Fig.1a. In (a-d, f), each data point represents an averaged value from duplicates in one batch of cells, and mRNA of each cell line were isolated from three different batches of cells. Two reference genes were used for gene expression normalization. The mRNA level for each gene on interest in each cell line was relative to the averaged expression level of three control cell lines. Two-way ANOVA followed by Bonferroni post-hoc testing was used for statistical analysis. In (b) and (d), the significance was relative to the marked condition (A and B). Condition A, control fibroblast group consisted of three biologically independent human primary fibroblasts cell lines. Condition B, patient fibroblast group consisted of two biologically independent patients' fibroblasts cell lines. *P < 0.05, **P < 0.01. ns, not significant. In all

exposure experiments, DMSO (0.06%) was used vehicle control, and cells were exposed to AFN (0.6 μ M, 8 hrs).

Despite of the fact that patients' fibroblasts responded to AFN treatment by upregulating of *TXNRD1* and *GSR* gene expression and by increasing GSH levels similarly compared to controls' fibroblasts, they displayed higher sensitivity to the AFN-induced thioredoxin inhibition. Moreover, GSH levels were consistently higher in the SIRT5 variant fibroblasts in all conditions.

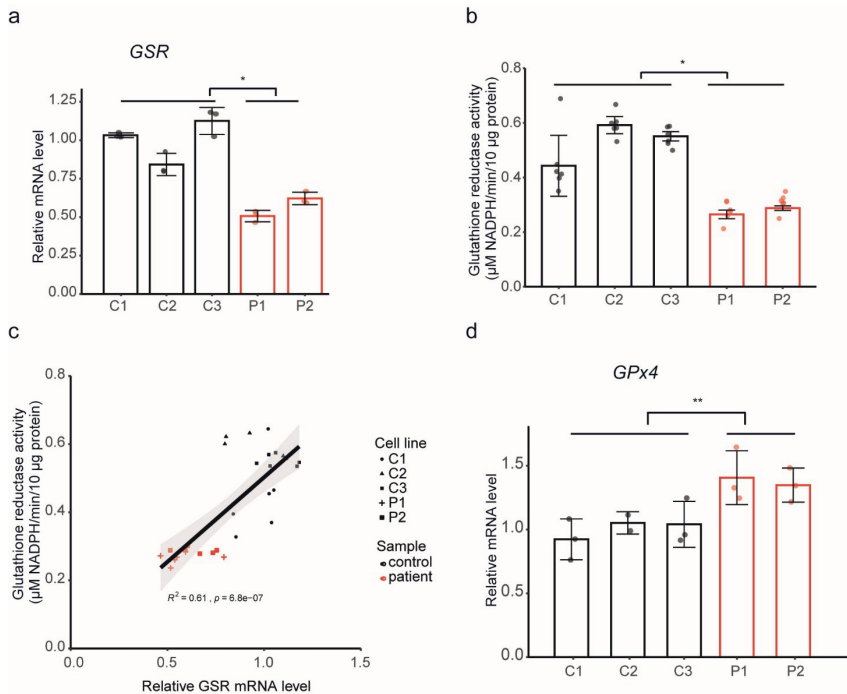


Figure 4. Impaired GSH-dependent antioxidant system in patients' fibroblasts. (a) Relative gene expression level of glutathione reductase (*GSR*) in fibroblasts under PBS (0.1%) control condition. (b) Glutathione reductase activity in the total cell lysates. Data from two independent experiments were pooled. (c) A correlation analysis between relative *GSR* mRNA level and glutathione reductase activity in fibroblasts. (d) Glutathione peroxidase 4 (*GPx4*) mRNA level in the fibroblasts under DMSO (0.06%) control conditions. For gene expression analysis in (a) and (d), each data point represents an averaged value from duplicates in one batch of cells, mRNAs were isolated from three different batches of cells, and mRNA of each cell line were isolated from three different batches of cells. Two reference genes were used for gene expression normalization. The mRNA level for each gene on interest in each cell line was relative to the averaged expression level of three control cell lines. Unpaired t-test was used for statistical analysis. * $P < 0.05$, ** $P < 0.01$. Pearson correlation analysis was used in (c).

We reasoned these phenotypes together point to a defect in the glutathione system in the SIRT5 variant cells. In support of this, *GSR* mRNA level was found to be reduced 2-fold in the patients' fibroblasts under basal non-exposed condition (Fig. 4a).

Likewise, total intracellular glutathione reductase (GR) activity was 2-fold lower in the patients' fibroblasts (Fig. 4b). The strong positive correlation of intracellular GR activity with *GSR* mRNA level (Fig. 4c) suggests that the lower GR levels lead to the reduced GR activity in SIRT5 variant fibroblasts. In living cells, GSH level is determined by a dynamic reduction-oxidation cycle. GSH is oxidized to GSSG, during the glutathione peroxidases-mediated reduction of hydroperoxides, and GSSG is reduced back to GSH by GR. Given that SIRT5 variant fibroblasts displayed increased GSH levels, but with reduced GSR levels, we postulate a defect in the oxidation process of GSH by glutathione peroxidase. To test this, we focused on glutathione peroxidase 4 (GPx4), because of its key role in chronic metabolic stress induced non-apoptotic cell death, ferroptosis⁵⁴. Gpx4 gene expression was significantly, 1.5-fold, increased in SIRT5 variant fibroblasts in comparison to controls (Fig. 4d). The alteration in the GPx4 mRNA level, which we interpret as an adaptive response, substantiates our hypothesis of a disrupted glutathione antioxidant system in the SIRT5 variant fibroblasts, i.e., as a consequence of dysfunctional SIRT5.

Discussion

In this study, we showed that glutathione antioxidant system was functionally affected in human SIRT5 deficient fibroblasts derived from patients. We used primary skin fibroblasts of two independent patients with SIRT5 variants, which resulted in significantly reduced SIRT5 protein levels and increased global succinylation levels (Chapter 3). Here, we found that in the SIRT5 variant fibroblasts, intracellular GSH level was strikingly high, while GR activity was low, suggesting a downstream defect in the use of GSH, supported by a compensatory increased GPx4 gene expression. These changes explain the blunted sensitivity to BSO treatment and enhanced intolerance to the AFN treatment in the SIRT5 variant fibroblasts. Thus, redox imbalance ensues from the disrupted glutathione system due to SIRT5 malfunction. Together our findings highlight the importance of SIRT5 in redox homeostasis by regulation of glutathione antioxidant defence system.

Both the glutathione and the thioredoxin system require the major cellular reducing equivalent NADPH as a cofactor. Previously, SIRT5 has been shown to play a role in ROS detoxification via deacylating and activating NADPH-generation enzymes isocitrate dehydrogenase 2 and glucose-6-phosphate dehydrogenase⁴². However, the similar molecular response of the thioredoxin system in the patients' and the controls' fibroblasts argue against overall dysfunctional NADPH generation in our study. In addition, the gene expression level of NNT, an important mitochondrial NADPH-production enzyme, did not alter between control the SIRT5 variant

fibroblasts, which in turn, further supported that NADPH production was not affected by SIRT5 deficiency in the patients' fibroblasts.

Instead, our results point to the concept that glutathione antioxidant system specifically is more likely to be regulated by SIRT5. The enzymatic activity of GR, which is responsible for maintaining the reduced glutathione pool within cells, was decreased by 50% in the SIRT5 variant fibroblasts. In spite of this low GR activity, 1.5-fold higher intracellular GSH levels were observed in the patients' fibroblasts. This phenotype strongly indicates an impairment in the process of GSH oxidation. GSH is oxidized to GSSG by glutathione peroxidases, which catalyse the reduction of H_2O_2 and peroxides. Indeed, glutathione metabolism has been shown to be one of the significantly enriched succinylated pathways in SIRT5 KO mouse models⁵⁵. Multiple SIRT5-targeted succinylated sites of glutathione peroxidase 1 were identified in several mouse studies^{40, 56}. Although we did not investigate glutathione peroxidase 1 in this study, the possibility, that SIRT5 deficiency decreased enzymatic activity of GPx1 and consequently contributed to the high GSH levels and impaired GSH antioxidant system, cannot be excluded. We chose to examine the GPx4 because it was only known glutathione peroxidase that is pivotal for organism survival. Ablation of GPx4 in mice resulted in lethal phenotypes^{57, 58}. GPx4 catalyses the reduction of H_2O_2 and uniquely reduces lipid hydroperoxides and protects cells from lipid peroxidation^{59, 60, 61}. GPx4 mRNA levels were found to be increased by 1.5-fold in SIRT5 fibroblasts. Given the observation of significantly higher global succinylation levels in SIRT5 variant fibroblasts (Chapter 3), and increase in protein lysine succinylation levels resulted from SIRT5 deficiency has been shown to primarily exert an inhibitory effect on the enzymatic activities of the targeted proteins^{42, 56, 62}, we speculated that increased GPx4 mRNA levels were a compensatory response to potentially inhibited GPx4 enzymatic activity in the SIRT5 variant fibroblasts. Finally, the reduced GPx4 activity contributed to the high GSH level. In support of this, total GSH has been shown to be significantly higher in cells with an inactive GPx4 mutant⁶³.

The impaired GSH antioxidant system suggests a lower efficiency to detoxify oxidants in the patients, which can induce oxidative stress *in vivo* especially in highly metabolically active organs, such as brain and muscle. Oxidative stress has been well documented to negatively affect cell components^{6, 7, 8} and has been proposed to be a pathogenic factor for multiple human disease such as mitochondrial diseases and neurodegenerative diseases^{10, 64}. At molecular level, fundamental macromolecules including DNA, proteins, lipids are susceptible to oxidants. For instance, protein can be oxidatively modified by ROS and form protein disulfides, protein carbonyl- and hydroxyl-derivatives^{16, 65}. Accumulation of these modifications impairs the structure

of the targeted proteins, resulting in loss of enzymatic activities and/or interference with protein-protein interactions^{66, 67}. In addition, lipids, especially polyunsaturated fatty acids (PUFAs), are easily oxidized by ROS and form lipids peroxides. Membranes are rich in PUFAs and can undergo lipid peroxidation which interferes membrane assembly and fluidity^{68, 69, 70}. Thus, oxidative stress resulted from SIRT5 dysfunction in the patients can affect many critical biological processes, which may ultimately contribute to the disease pathogenesis.

Notably, the alteration in GPx4 suggests that lipid peroxidation as well as lipid peroxidation-elicited ferroptosis resulted from potential GPx4 impairment may play a significant role in the pathogenesis in the SIRT5 patients. Deregulation of lipid peroxidation is detrimental for life. Depletion of GPx4 led to massive lipid peroxidation in cells⁷¹ and renal failure in mice⁷², neuron specific GPx4 inactivation caused cerebellar hypoplasia, seizures and ataxia^{71, 73}. Cardiolipin, an inner mitochondrial membrane specific phospholipid as well as a preferred substrate for GPx4, is particularly susceptible to peroxidation by excessive ROS, which negatively affects mitochondrial membrane fluidity, interaction between cardiolipin and electron transport complexes, resulting in mitochondrial dysfunction. Collectively, based on our results and findings from literatures, it is intriguing to speculate that SIRT5 dysfunction negatively affects GPx4 enzymatic activity, leading to accumulation of lipid peroxidation and impaired mitochondrial function, which partly contribute to the encephalopathy observed in the patients (Chapter 3) because brain is highly sensitive to lipid peroxidation due to its high PUFAs content. In support of this proposed model, SIRT5 ablation in mice increased brain lipid peroxide levels and caused degradation of dopaminergic neurons after exogenous injection of oxidant paraquat, although the underlying mechanism remained elusive⁴².

SIRT5 is known to play a critical role in the adaptive response of organism to environmental stresses^{74, 75}. In this context, a role for SIRT5 in the regulation of GSH antioxidant system also has a physiological significance in relation to other known regulatory roles for SIRT5 to maintain overall cellular metabolic homeostasis. For instance, SIRT5 is required to sustain energy supply under fasting conditions by promoting fatty acid oxidation⁶². Fatty acids are the major energy sources and are oxidized in mitochondria during fasting. Apart from providing ATP, to satisfy the cellular energy demand, fatty acid oxidation is accompanied with high mitochondrial ROS production, because electrons generated from β -oxidation enter the respiratory chain at multiple sites, such as complex I and coenzyme Q. The electron donation to coenzyme Q leads to a high reduced to oxidized coenzyme Q ratio, which, together with potential electron leaks at several sites, ultimately increase ROS levels at

complex I, II and complex III^{76, 77, 78, 79}. Moreover, the intracellular NAD⁺ level is increased in response to fasting⁸⁰, providing the cellular conditions that would activate SIRT5 to potentially facilitate the activation of the GSH-dependent antioxidant system, counteracting the elevated ROS levels and its damaging consequences.

In conclusion, we have established a key role for SIRT5 in redox homeostasis, which fits its role as an adaptive regulator of metabolism. We also showed an impaired glutathione antioxidant system underlying redox imbalance in the cells of both patients with SIRT5 variants, which may have contributed to the mitochondrial disease phenotype of these patients.

Material and methods

Patient ethics

Informed consent for diagnostic and research studies was obtained for both subjects in accordance with the Declaration of Helsinki and following the regulations of the local medical ethics committee.

Cell culture

Human primary skin fibroblasts were routinely cultured in fibroblast growth medium. This medium contained medium 199 (#M3769, Sigma-Aldrich, which is formulated with 5.5 mM glucose) supplemented with 10% foetal bovine serum (FBS, #06Q3501K, Gibco), 2 mM Glutamine-Max (#35050038, Gibco), and 1x antibiotic-antimycotic mix (100 IU/ml penicillin/streptomycin, and 25 µg/ml Amphotericin B, #15240062, Gibco). Cells were incubated at 37°C with 5% CO₂ and passaged every 4-5 days with 0.05% trypsin (#15400054, Gibco) for 2 min at 37°C. All fibroblast cell lines were tested mycoplasma negative with qPCR (MycoSensor QPCR assay, #302107, Agilent Technologies). Cell lines were used in experiments until they reached passage number 20.

Exposure media

In Buthionine sulfoximine (BSO) and Auranofin (AFN) exposure experiments, DMEM medium (#A1443001, Gibco) without glucose, glutamine, pyruvate, and phenol red was used. Based on this DMEM, a glucose medium was prepared by supplementing with 5.5 mM glucose (#103577-100, Agilent Technologies), 2 mM L-glutamine (#25030024, Gibco), and 10% FBS. To make BSO exposure medium, a 100 mM BSO (#19176, Sigma-Aldrich) stock in 1x PBS was made and diluted with glucose medium to reach 100 µM BSO exposure medium. The glucose medium with 1x PBS (0.1% final concentration) was used as a vehicle control. To prepare AFN exposure

media, AFN (#BML-EI206-0100, Enzo Life Sciences) was dissolved in DMSO (#276855, Sigma-Aldrich) to make a 1 mM stock solution, and 1 mM stock was further diluted in glucose medium to 0.6 μ M AFN exposure medium. For solvent controls, the glucose medium with DMSO (0.06% final concentration) was used. All exposure media were filtered through 0.2 μ m cellulose acetate membranes (#28145477, VWR) after preparation, before application to cells. All media were prepared fresh on the day of use.

Cell viability assay

Fibroblasts were suspended in fibroblast growth medium and seeded in transparent 96-well plates (#3599, Corning) at a density of 3000 cells/well and incubated in a humidified atmosphere at 37°C, 5 % CO₂. 18 hrs after seeding, growth medium was switched to exposure medium and cell viability was tested after 7 hrs. Cell viability was assessed using a WST-1 assay (#5015944001, Sigma-Aldrich) according to manufacturer's instruction. To make WST-1 working solution, WST-1 reagent was diluted in either glucose or galactose medium at 1:10 ratio and was warmed up to 37°C prior to use. Exposure medium was removed, and cells were wash once with 1x Dulbecco's phosphate-buffered saline (DPBS, #14200067, Gibco). Then, the WST-1 working solution was added to cells (100 μ l/well) and the cells were incubated at 37°C with 5% CO₂. The absorbance at 440 nm was measured using a Biotek Synergy HT microplate reader. Average absorbance signal from blank wells (without cells) was subtracted from experimental samples.

Reactive oxygen species measurement

The levels of cellular reactive oxygen species (ROS) were measured using the cell-permeable probe 2',7'-dichlorofluorescein diacetate (H₂DCFDA) (#D6883, Sigma-Aldrich). Fibroblasts were seeded in black 96-well plates (#CLS3603, Sigma-Aldrich) at a density of 3000 cells/well in fibroblast growth medium. After 18 hrs, growth medium was removed, and exposure media was added to cells. ROS measurement was performed after 8 hrs of exposure. Cells were washed once with 1x DPBS and protected from light onwards. Cells were incubated in HEPES/TRIS (HT) buffer (132 mM NaCl, 4.2 mM KCl, 1 mM CaCl₂, 1 mM MgCl₂, 5.5 mM glucose, and 10 mM HEPES, adjust pH to 7.4 with Tris) containing 10 μ M H₂DCFDA in the dark for 15 min at 37°C. Cells were washed twice with 1x DPBS, and incubated in HT buffer during fluorescence measurement. Fluorescence was detected with excitation at 485 nm and emission at 530 nm on a Biotek Synergy HT microplate reader. After basal ROS measurement, 100 μ M fresh H₂O₂ (#HI01351000, Scharlab) diluted in HT buffer was added and fluorescence measurement continued. Average fluorescence signals of cells in HT buffer without H₂DCFDA dye were used for background correction. After

the assay, cells' nuclei were stained with 4 μ M 2'-(4-ethoxyphenyl)-5-(4-methyl-1-piperazinyl)-2,5'-bi-1H-benzimidazole trihydrochloride trihydrate (Hoechst 33342, #B2261, Sigma-Aldrich) at 37°C for 1 hr, and thereafter images were made with BioTek Cytation 1. Cell number was counted based on the nuclei images using ImageJ 1.52 (National Institutes of Health). ROS levels were normalized to cell number. Linear increase in fluorescence signals were obtained over the measurement for all cell lines. The intracellular ROS level was represented as the rate of fluorescence signal increase per min per 1000 cells.

Quantification of total cellular GSH

Fibroblasts were seeded in white 96-well plates (#734-1665, VWR) as well as transparent 96-well plates (#3599, Corning) in parallel at a density of 3000 cells/well. The parallel transparent plates were used for cell number determination using Hoechst staining. The cells were allowed to grow in fibroblast growth medium for 18 hrs until they were treated with either BSO or AFN. The cells were incubated under 5% CO₂ at 37°C for 8 hrs. The exposure medium was removed, cells were washed once with 1x DPBS, and GSH levels of cells were quantified using a luminescence-based assay kit (#V6911, Promega). The luminescence signals were monitored with an integration time of 0.5 s at 22°C using the Biotek Synergy HT microplate reader. Average signals in blank wells (without cells) were subtracted from experimental samples. Cells seeded in the parallel transparent plates were handled the same as that in white plate until cells were washed with 1x DPBS after 8 hrs exposure, and thereafter cells were stained with 4 μ M Hoechst and incubated at 37°C for 1 hr. The GSH levels were corrected for cell number.

Glutathione reductase activity assay

Human fibroblasts (1.0×10^6 cells) were seeded in 150 mm dishes (#734-1711, VWR) and grew in fibroblast growth medium until the cell confluency reached 90%. Culture media was discarded, and cells were washed twice with ice-cold 1x Hanks' Balanced Salt Solution (HBSS, #14175129, Gibco), harvested by scraper (#734-1527, VWR), and collected by centrifugation (300 x g) at 4°C for 5 min. Cell pellets were lysed in lysis buffer (50 mM Tris/HCl, pH 7.60, 1% Triton), followed by sonication on ice at 40% amplitude (burst of 1 s followed by 3 s cooling) for 12 bursts using a Branson SLPe digital sonifier. Cell lysates were then centrifuged at 10,000 x g, 4°C for 10 minutes, and the supernatants were used in the downstream analysis. Protein concentrations were determined with DC protein assay (#5000116, Bio-Rad). Protein concentrations among different cell lines were equalized with the lysis buffer and 50 μ g of protein were used for glutathione reductase activity assessment. The cellular glutathione reductase activity was measured by monitoring the absorbance of NADPH which was

a co-enzyme in the reaction converting oxidized glutathione (GSSG) to reduced glutathione (GSH) by the glutathione reductase present in the cell lysates. Reagents required in this reaction include: (1) potassium phosphate/EDTA assay buffer (100 mM/3.4 mM, pH 7.40), (2) 0.33 mM NADPH (#N1630, Sigma-Aldrich) in potassium phosphate/EDTA buffer (NADPH-mix, pH 7.40), (3) 5.5 mM GSSG (#G4376, Sigma-Aldrich) in ultrapure water. All reagents were prewarmed to 37°C prior to use. The reaction took place in 96-well plates. The following reagents were added to 96-well plates in order: 50 µl ultrapure water; 125 µl 0.33 mM NADPH-mix; 25 µl cell lysates. The absorbance of NADPH was measured at 340 nm in a Biotek Synergy HT microplate reader at 37°C for 10 min. Then, the chemical reaction was initiated by adding 50 µl GSSG solution to each well. The absorbance of NADPH was then monitored for another 30 min at an interval of 13 s. A negative control (without cell lysates) and a positive control (glutathione reductase enzyme (#G3664, Sigma-Aldrich)) were included as quality controls of the assay. The cellular glutathione reductase activity was represented as µmol NADPH oxidized/min/10 µg protein.

RNA extraction and cDNA synthesis

Fibroblasts were seeded in transparent 96-well plates (3000 cells/well) in fibroblast growth medium for 18 hrs. Cells were exposed to either BSO or AFN exposure media for 8 hrs. Medium was removed, and cells were washed with ice-cold 1x DPBS twice. Total cellular RNA was extracted using RNeasy mini kit (#74106, QIAGEN) according to the manufacturer's instructions. RNA was dissolved in DNase/RNase-free water, and concentration was determined by a Nanodrop spectrophotometer (ND1000, IsoGen Life Science). RNA integrity and quality were checked on an Agilent 2200 TapeStation (Agilent Technologies Inc.) with high sensitivity RNA Screen Tapes (#172-5160, Bio-Rad). Subsequently, 100 ng RNA was reverse transcribed to cDNA using an iScript kit (#1708890, Bio-Rad) on a CFX96 Touch Real-Time PCR system (Bio-Rad) for 5 min at 25°C, 20 min at 46°C, and 1 min at 95°C according to the manufacturer's instructions. A no reverse transcriptase (minRT) reaction was included to function as a negative control for the downstream qPCR analysis, and a combined RNA randomly selected from four samples was used for minRT reaction. For each condition, RNA was isolated from three independent batches of fibroblasts.

Preamplification and Real-Time PCR (RT-qPCR) analysis

Prior to qPCR measurement, cDNA was preamplified in the presence of all primers (for genes of interest and reference genes) using the SsoAdvanced PreAmp Supermix (#1725160, Bio-Rad) on a C1000 Thermal Cyclers (Bio-Rad), with 3 min at 95°C, 12 cycles of 15 s at 95°C and 4 min at 58°C. A cDNA pool was made using preamplified cDNA from all samples and serial dilutions were made for standard curves in qPCR

measurement. Samples were diluted 100-fold for qPCR reaction, and two negative controls (DNase/RNase-free water and minRT) were also included. The qPCR reactions were performed with iQ SYBR Green Supermix (#1725006, Bio-Rad) using the C1000 PCR detection system (Bio-Rad). The qPCR reaction consisted of 3 min at 95°C, 40 cycles of 15 s at 95°C and 45 s at 60°C, followed by 1 min at 95°C, and 1 min at 65°C. Melting curve analysis was done from 65°C to 95°C with a temperature increment of 0.5°C/min. Individual samples were measured in duplicates. Standard curves of pooled samples, negative controls, melting curve profiles, R^2 and PCR efficiency were used for validation of each run according to the MIQE guidelines¹⁰. Each gene expression level was normalized against two reference genes (B2M and ERBB2IP that were selected for stability), and relative gene expression level for each sample was expressed as its expression level relative to the mean expression of the three control fibroblast cell lines. An overview of primers for all genes tested can be found in Supplementary Table S1.

Bright field image analysis

The bright field images were imaged using the BioTek Cytation 1, and processed with R^{11,12} and ImageJ. The original bright field images underwent background subtraction and invert in R, followed by Auto Threshold with default method in ImageJ.

Data analysis

Data analysis and visualization were performed using R^{13,14,15} and Adobe Illustrator 2020. Data represent mean \pm standard deviation (SD). For GSH levels, DCFDA-ROS oxidation rates, and gene expression analyses in control and patients' fibroblasts treated with and without inhibitors, two-way ANOVA with Bonferroni correction was used for statistical analysis. For other experiments, statistical analysis was performed using unpaired t-test with GraphPad Prism 5. P values less than 0.05 were considered statistically significant (* $P < 0.05$, ** $P < 0.01$, *** $P < 0.001$). Pearson correlation analysis was performed for testing correlation coefficient.

Acknowledgements

We would like to thank Zhou Wu for the help in R programming for data visualization. We also want to thank Joelle Janssen for setting up the glutathione reductase enzymatic assay which was adapted by Taolin Yuan for human fibroblasts. Taolin Yuan has received financial support from the China Scholarship Council (Grant No. 201606350170).

Author Contributions

TY designed and performed all experiments, analysed data, drafted and wrote the manuscript. IvdS performed the gene expression experiments, analysed and discussed data, and edited manuscript. VdB discussed the data, edited manuscript and wrote the R script for bright field image analysis and TY adapted it. JK supervised the study, discussed the data and edited the manuscript.

Competing Interests

The authors declare there is no conflicts of interests.

References

1. Schafer, F.Q. & Buettner, G.R. Redox State and Redox Environment in Biology. In: *Signal Transduction by Reactive Oxygen and Nitrogen Species: Pathways and Chemical Principles* (eds Forman HJ, Fukuto J, Torres M). Springer Netherlands (2003).
2. Murphy, Michael P. How mitochondria produce reactive oxygen species. *Biochem. J.* **417**, 1-13 (2009).
3. Gross, E., *et al.* Generating disulfides enzymatically: reaction products and electron acceptors of the endoplasmic reticulum thiol oxidase Ero1p. *Proc. Natl. Acad. Sci. U. S. A.* **103**, 299-304 (2006).
4. Murphy, M.P. Mitochondrial thiols in antioxidant protection and redox signaling: distinct roles for glutathionylation and other thiol modifications. *Antioxid. Redox Signal.* **16**, 476-495 (2012).
5. Sbarra, A.J. & Karnovsky, M.L. The biochemical basis of phagocytosis. I. Metabolic changes during the ingestion of particles by polymorphonuclear leukocytes. *J. Biol. Chem.* **234**, 1355-1362 (1959).
6. Ghosh, R. & Mitchell, D.L. Effect of oxidative DNA damage in promoter elements on transcription factor binding. *Nucleic Acids Res.* **27**, 3213-3218 (1999).
7. Keller, J.N., *et al.* 4-Hydroxynonenal, an aldehydic product of membrane lipid peroxidation, impairs glutamate transport and mitochondrial function in synaptosomes. *Neuroscience* **80**, 685-696 (1997).
8. Fucci, L., Oliver, C.N., Coon, M.J. & Stadtman, E.R. Inactivation of key metabolic enzymes by mixed-function oxidation reactions: possible implication in protein turnover and ageing. *Proc. Natl. Acad. Sci. U. S. A.* **80**, 1521-1525 (1983).
9. Nakamura, T. & Lipton, S.A. Redox modulation by S-nitrosylation contributes to protein misfolding, mitochondrial dynamics, and neuronal synaptic damage in neurodegenerative diseases. *Cell Death Differ.* **18**, 1478-1486 (2011).
10. Hayashi, G. & Cortopassi, G. Oxidative stress in inherited mitochondrial diseases. *Free Radic. Biol. Med.* **88**, 10-17 (2015).
11. Koopman, W.J., *et al.* Mammalian mitochondrial complex I: biogenesis, regulation, and reactive oxygen species generation. *Antioxid. Redox Signal.* **12**, 1431-1470 (2010).
12. Miller, D.M., Buettner, G.R. & Aust, S.D. Transition metals as catalysts of "autoxidation" reactions. *Free Radic. Biol. Med.* **8**, 95-108 (1990).
13. Burdon, R.H. & Rice-Evans, C. Free radicals and the regulation of mammalian cell proliferation. *Free Radic. Res. Commun.* **6**, 345-358 (1989).
14. Burke, T.M. & Wolin, M.S. Hydrogen peroxide elicits pulmonary arterial relaxation and guanylate cyclase activation. *Am. J. Physiol.* **252**, H721-732 (1987).

15. Dizdaroglu, M. & Jaruga, P. Mechanisms of free radical-induced damage to DNA. *Free Radic. Res.* **46**, 382-419 (2012).
16. Sitte, N. Oxidative Damage to Proteins. In: *Aging at the Molecular Level* (ed von Zglinicki T). Springer Netherlands (2003).
17. Refsgaard, H.H., Tsai, L. & Stadtman, E.R. Modifications of proteins by polyunsaturated fatty acid peroxidation products. *Proc. Natl. Acad. Sci. U. S. A.* **97**, 611-616 (2000).
18. Cohen, G. & Hochstein, P. Glutathione Peroxidase: The Primary Agent for the Elimination of Hydrogen Peroxide in Erythrocytes. *Biochemistry* **2**, 1420-1428 (1963).
19. Rhee, S.G., Woo, H.A., Kil, I.S. & Bae, S.H. Peroxiredoxin functions as a peroxidase and a regulator and sensor of local peroxides. *J. Biol. Chem.* **287**, 4403-4410 (2012).
20. Hu, J., Dong, L. & Outten, C.E. The redox environment in the mitochondrial intermembrane space is maintained separately from the cytosol and matrix. *J. Biol. Chem.* **283**, 29126-29134 (2008).
21. Mari, M., Morales, A., Colell, A., Garcia-Ruiz, C. & Fernandez-Checa, J.C. Mitochondrial glutathione, a key survival antioxidant. *Antioxid. Redox Signal.* **11**, 2685-2700 (2009).
22. Rabilloud, T., *et al.* The mitochondrial antioxidant defence system and its response to oxidative stress. *Proteomics* **1**, 1105-1110 (2001).
23. Aon, M.A., *et al.* Glutathione/thioredoxin systems modulate mitochondrial H₂O₂ emission: an experimental-computational study. *J. Gen. Physiol.* **139**, 479-491 (2012).
24. Meister, A. Glutathione metabolism and its selective modification. *J. Biol. Chem.* **263**, 17205-17208 (1988).
25. Forman, H.J., Zhang, H. & Rinna, A. Glutathione: overview of its protective roles, measurement, and biosynthesis. *Mol. Aspects Med.* **30**, 1-12 (2009).
26. Schafer, F.Q. & Buettner, G.R. Redox environment of the cell as viewed through the redox state of the glutathione disulfide/glutathione couple. *Free Radic. Biol. Med.* **30**, 1191-1212 (2001).
27. Gilbert, H.F. Redox control of enzyme activities by thiol/disulfide exchange. *Methods Enzymol.* **107**, 330-351 (1984).
28. Lushchak, V.I. Glutathione homeostasis and functions: potential targets for medical interventions. *J. Amino Acids* **2012**, 736837 (2012).
29. Sagone, A.L., Jr., Husney, R.M., O'Dorisio, M.S. & Metz, E.N. Mechanisms for the oxidation of reduced glutathione by stimulated granulocytes. *Blood* **63**, 96-104 (1984).
30. Toppo, S., Flohe, L., Ursini, F., Vanin, S. & Maiorino, M. Catalytic mechanisms and specificities of glutathione peroxidases: variations of a basic scheme. *Biochim. Biophys. Acta* **1790**, 1486-1500 (2009).
31. Mills, G.C. Hemoglobin catabolism. I. Glutathione peroxidase, an erythrocyte enzyme which protects hemoglobin from oxidative breakdown. *J. Biol. Chem.* **229**, 189-197 (1957).
32. Beer, S.M., *et al.* Glutaredoxin 2 catalyzes the reversible oxidation and glutathionylation of mitochondrial membrane thiol proteins: implications for mitochondrial redox regulation and antioxidant DEFENSE. *J. Biol. Chem.* **279**, 47939-47951 (2004).
33. Kil, I.S. & Park, J.W. Regulation of mitochondrial NADP⁺-dependent isocitrate dehydrogenase activity by glutathionylation. *J. Biol. Chem.* **280**, 10846-10854 (2005).
34. Maeda, K., Hagglund, P., Finnie, C., Svensson, B. & Henriksen, A. Structural basis for target protein recognition by the protein disulfide reductase thioredoxin. *Structure* **14**, 1701-1710 (2006).
35. Zhong, L., Arner, E.S. & Holmgren, A. Structure and mechanism of mammalian thioredoxin reductase: the active site is a redox-active selenolthiol/selenenylsulfide formed from the conserved cysteine-selenocysteine sequence. *Proc. Natl. Acad. Sci. U. S. A.* **97**, 5854-5859 (2000).

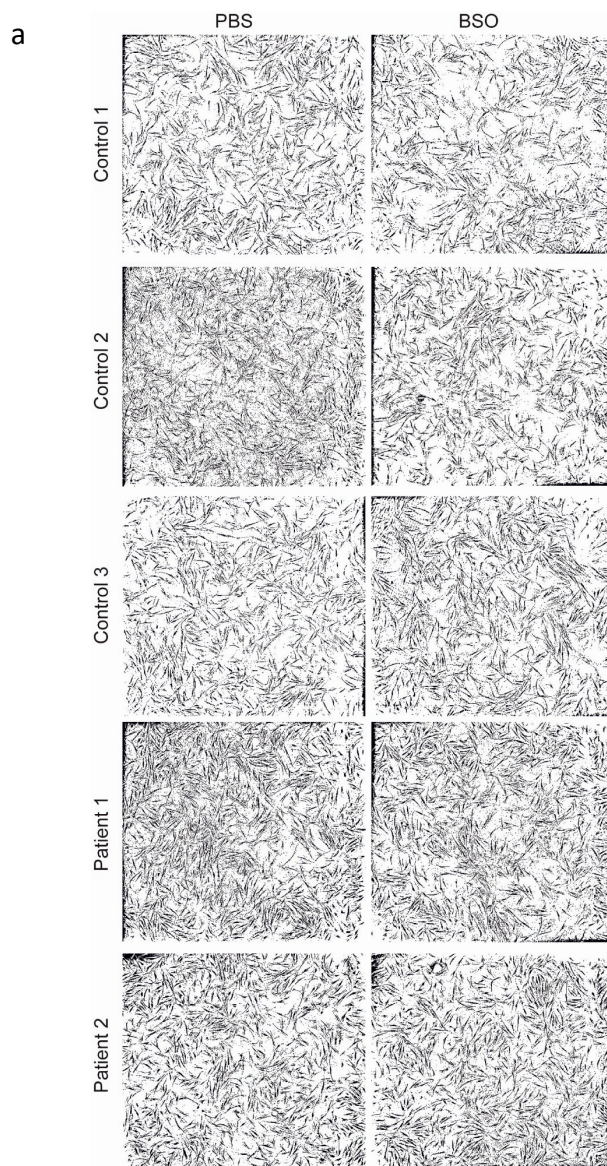
36. Holmgren, A. Reduction of disulfides by thioredoxin. Exceptional reactivity of insulin and suggested functions of thioredoxin in mechanism of hormone action. *J. Biol. Chem.* **254**, 9113-9119 (1979).
37. Lu, J. & Holmgren, A. The thioredoxin antioxidant system. *Free Radic Biol Med* **66**, 75-87 (2014).
38. Du, J., *et al.* Sirt5 is a NAD-dependent protein lysine demalonylase and desuccinylase. *Science* **334**, 806-809 (2011).
39. Tan, M., *et al.* Lysine glutarylation is a protein posttranslational modification regulated by SIRT5. *Cell Metab.* **19**, 605-617 (2014).
40. Park, J., *et al.* SIRT5-mediated lysine desuccinylation impacts diverse metabolic pathways. *Mol. Cell* **50**, 919-930 (2013).
41. Nakagawa, T., Lomb, D.J., Haigis, M.C. & Guarente, L. SIRT5 Deacetylates carbamoyl phosphate synthetase 1 and regulates the urea cycle. *Cell* **137**, 560-570 (2009).
42. Zhou, L., *et al.* SIRT5 promotes IDH2 desuccinylation and G6PD deglutarylation to enhance cellular antioxidant defense. *EMBO Rep.* **17**, 811-822 (2016).
43. Sun, X., *et al.* SIRT5 Promotes Cisplatin Resistance in Ovarian Cancer by Suppressing DNA Damage in a ROS-Dependent Manner via Regulation of the Nrf2/HO-1 Pathway. *Front. Oncol.* **9**, 754 (2019).
44. Liang, F.Y., Wang, X., Ow, S.H., Chen, W.X. & Ong, W.C. Sirtuin 5 is Anti-apoptotic and Anti-oxidative in Cultured SH-EP Neuroblastoma Cells. *Neurotox. Res.* **31**, 63-76 (2017).
45. Lu, W., Zuo, Y., Feng, Y. & Zhang, M. SIRT5 facilitates cancer cell growth and drug resistance in non-small cell lung cancer. *Tumour Biol.* **35**, 10699-10705 (2014).
46. Griffith, O.W. & Meister, A. Glutathione: interorgan translocation, turnover, and metabolism. *Proc. Natl. Acad. Sci. U. S. A.* **76**, 5606-5610 (1979).
47. Drew, R. & Miners, J.O. The effects of buthionine sulfoximine (BSO) on glutathione depletion and xenobiotic biotransformation. *Biochem. Pharmacol.* **33**, 2989-2994 (1984).
48. Du, Y., Zhang, H., Lu, J. & Holmgren, A. Glutathione and glutaredoxin act as a backup of human thioredoxin reductase 1 to reduce thioredoxin 1 preventing cell death by aurothioglucose. *J. Biol. Chem.* **287**, 38210-38219 (2012).
49. Tan, S.X., *et al.* The thioredoxin-thioredoxin reductase system can function in vivo as an alternative system to reduce oxidized glutathione in *Saccharomyces cerevisiae*. *J. Biol. Chem.* **285**, 6118-6126 (2010).
50. Gromer, S., Arscott, L.D., Williams, C.H., Jr., Schirmer, R.H. & Becker, K. Human placenta thioredoxin reductase. Isolation of the selenoenzyme, steady state kinetics, and inhibition by therapeutic gold compounds. *J. Biol. Chem.* **273**, 20096-20101 (1998).
51. Iannetti, E.F., Smeitink, J.A.M., Willems, P., Beyrath, J. & Koopman, W.J.H. Rescue from galactose-induced death of Leigh Syndrome patient cells by pyruvate and NAD(.). *Cell Death Dis.* **9**, 1135 (2018).
52. Oh, B.M., *et al.* Cystatin SN inhibits auranofin-induced cell death by autophagic induction and ROS regulation via glutathione reductase activity in colorectal cancer. *Cell Death Dis.* **8**, e2682 (2017).
53. Fisher-Wellman, K.H., *et al.* Pyruvate dehydrogenase complex and nicotinamide nucleotide transhydrogenase constitute an energy-consuming redox circuit. *Biochem. J.* **467**, 271-280 (2015).
54. Zheng, J. & Conrad, M. The Metabolic Underpinnings of Ferroptosis. *Cell Metab.* **32**, 920-937 (2020).
55. Weinert, B.T., *et al.* Lysine succinylation is a frequently occurring modification in prokaryotes and eukaryotes and extensively overlaps with acetylation. *Cell Rep.* **4**, 842-851 (2013).
56. Rardin, M.J., *et al.* SIRT5 regulates the mitochondrial lysine succinylome and metabolic

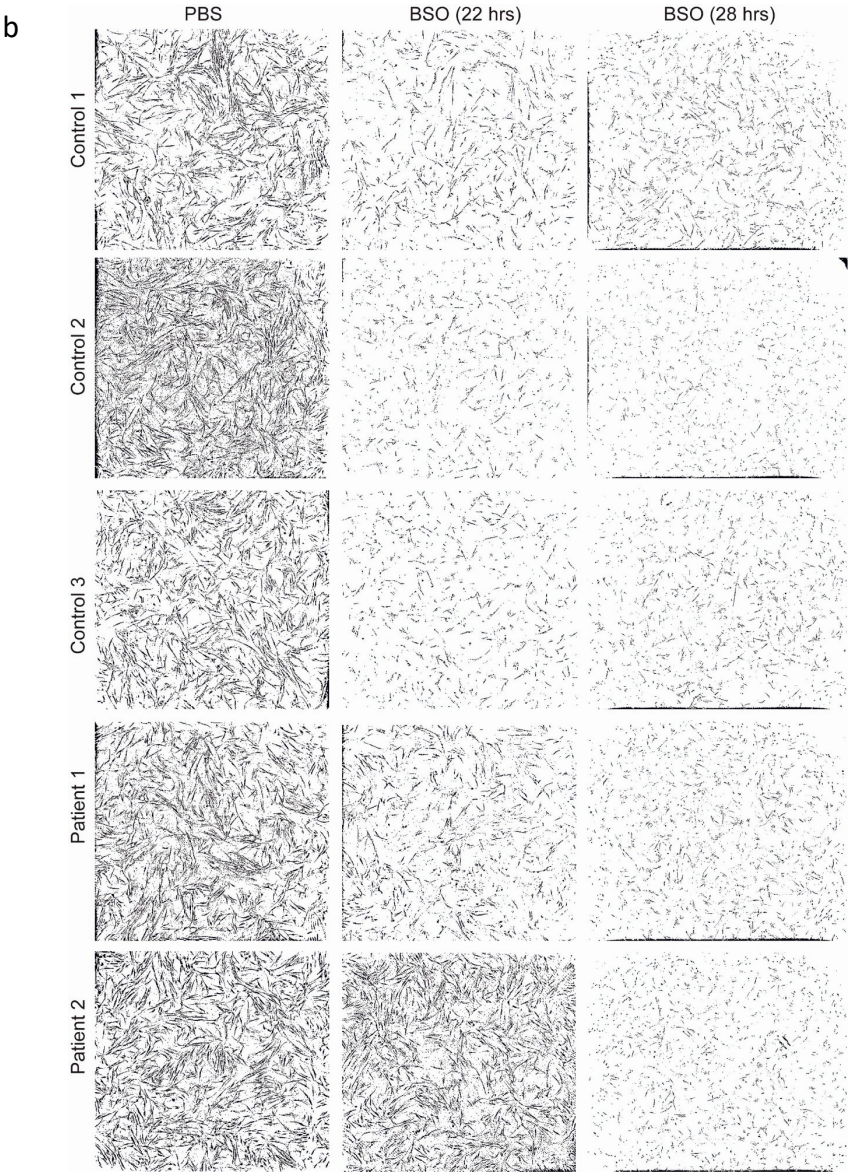
- networks. *Cell Metab.* **18**, 920-933 (2013).
57. Yant, L.J., *et al.* The selenoprotein GPX4 is essential for mouse development and protects from radiation and oxidative damage insults. *Free Radic. Biol. Med.* **34**, 496-502 (2003).
58. Yoo, S.E., *et al.* Gpx4 ablation in adult mice results in a lethal phenotype accompanied by neuronal loss in brain. *Free Radic. Biol. Med.* **52**, 1820-1827 (2012).
59. Ursini, F., Maiorino, M., Valente, M., Ferri, L. & Gregolin, C. Purification from pig liver of a protein which protects liposomes and biomembranes from peroxidative degradation and exhibits glutathione peroxidase activity on phosphatidylcholine hydroperoxides. *Biochim. Biophys. Acta* **710**, 197-211 (1982).
60. Yang, W.S., *et al.* Regulation of ferroptotic cancer cell death by GPX4. *Cell* **156**, 317-331 (2014).
61. Yang, W.S., *et al.* Peroxidation of polyunsaturated fatty acids by lipoxygenases drives ferroptosis. *Proc. Natl. Acad. Sci. U. S. A.* **113**, E4966-4975 (2016).
62. Sadhukhan, S., *et al.* Metabolomics-assisted proteomics identifies succinylation and SIRT5 as important regulators of cardiac function. *Proc. Natl. Acad. Sci. U. S. A.* **113**, 4320-4325 (2016).
63. Ingold, I., *et al.* Selenium Utilization by GPX4 Is Required to Prevent Hydroperoxide-Induced Ferroptosis. *Cell* **172**, 409-422 e421 (2018).
64. Chinta, S.J. & Andersen, J.K. Redox imbalance in Parkinson's disease. *Biochim. Biophys. Acta* **1780**, 1362-1367 (2008).
65. Cremers, C.M. & Jakob, U. Oxidant sensing by reversible disulfide bond formation. *J. Biol. Chem.* **288**, 26489-26496 (2013).
66. Berlett, B.S. & Stadtman, E.R. Protein oxidation in aging, disease, and oxidative stress. *J. Biol. Chem.* **272**, 20313-20316 (1997).
67. Morgan, P.E., Dean, R.T. & Davies, M.J. Inhibition of glyceraldehyde-3-phosphate dehydrogenase by peptide and protein peroxides generated by singlet oxygen attack. *Eur. J. Biochem.* **269**, 1916-1925 (2002).
68. Chen, J.J. & Yu, B.P. Alterations in mitochondrial membrane fluidity by lipid peroxidation products. *Free Radic. Biol. Med.* **17**, 411-418 (1994).
69. Wong-Ekkabut, J., *et al.* Effect of lipid peroxidation on the properties of lipid bilayers: a molecular dynamics study. *Biophys. J.* **93**, 4225-4236 (2007).
70. Borst, J.W., Visser, N.V., Kouptsova, O. & Visser, A.J. Oxidation of unsaturated phospholipids in membrane bilayer mixtures is accompanied by membrane fluidity changes. *Biochim. Biophys. Acta* **1487**, 61-73 (2000).
71. Seiler, A., *et al.* Glutathione peroxidase 4 senses and translates oxidative stress into 12/15-lipoxygenase dependent- and AIF-mediated cell death. *Cell Metab.* **8**, 237-248 (2008).
72. Friedmann Angeli, J.P., *et al.* Inactivation of the ferroptosis regulator Gpx4 triggers acute renal failure in mice. *Nat. Cell Biol.* **16**, 1180-1191 (2014).
73. Wirth, E.K., *et al.* Neuronal selenoprotein expression is required for interneuron development and prevents seizures and neurodegeneration. *FASEB J.* **24**, 844-852 (2010).
74. Wang, G., *et al.* Regulation of UCP1 and Mitochondrial Metabolism in Brown Adipose Tissue by Reversible Succinylation. *Mol. Cell* **74**, 844-857 e847 (2019).
75. Kumar, S. & Lombard, D.B. Functions of the sirtuin deacylase SIRT5 in normal physiology and pathobiology. *Crit. Rev. Biochem. Mol. Biol.* **53**, 311-334 (2018).
76. Anderson, E.J., Yamazaki, H. & Neuffer, P.D. Induction of endogenous uncoupling protein 3 suppresses mitochondrial oxidant emission during fatty acid-supported respiration. *J. Biol. Chem.* **282**, 31257-31266 (2007).
77. Seifert, E.L., Estey, C., Xuan, J.Y. & Harper, M.E. Electron transport chain-dependent and -independent mechanisms of mitochondrial H₂O₂ emission during long-chain fatty acid oxidation. *J. Biol. Chem.* **285**, 5748-5758 (2010).

- 78. St-Pierre, J., Buckingham, J.A., Roebuck, S.J. & Brand, M.D. Topology of superoxide production from different sites in the mitochondrial electron transport chain. *J. Biol. Chem.* **277**, 44784-44790 (2002).
- 79. Fisher-Wellman, K.H. & Neuffer, P.D. Linking mitochondrial bioenergetics to insulin resistance via redox biology. *Trends Endocrinol. Metab.* **23**, 142-153 (2012).
- 80. Rodgers, J.T., *et al.* Nutrient control of glucose homeostasis through a complex of PGC-1alpha and SIRT1. *Nature* **434**, 113-118 (2005).

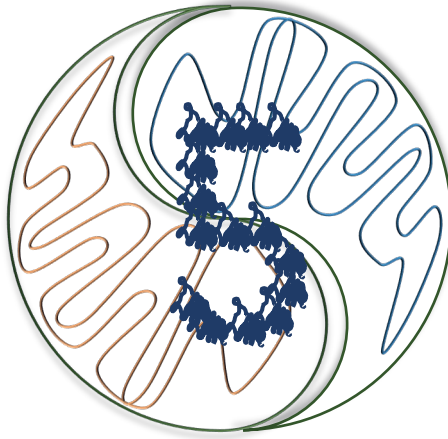
Supplementary Material**Supplementary Table S1** List of primers

Gene	Forward	Reverse
<i>Gene of interest</i>		
SOD2	TGGACAAACCTCAGCCCTAACG	GCCGTCAGCTTCTCCTTAAACTTG
TXNRD1	CAGGTTCCACTGTCAAGTGTG	TGGACCCAGTACGTGAAAGC
TXNRD2	CTTTGTTGACGAGCACACGG	CCCGACCACCAACGTTTTTC
GSR	TCAAACCGATGACAAGGGTC	CAGCAGCTATTGCAACTGGA
GPX4	AGGAGCCAGGGAGTAACGAA	CCACTTGATGGCATTTCACAG
<i>Reference genes</i>		
B2M	TGCCGTGTGAACCATGTG	GCGGCATCTTCAAACCTC
ERBB2IP	TGTGGCTCTCAGATA ATCAGTCC	ACATAACATCCTCAGTCCTTGGC





Supplementary Fig. S1 Time-course effects of BSO exposure on fibroblasts morphology (Related to Fig.1). Processed images of fibroblasts under (a) PBS vehicle control (0.1%) or BSO (100 μ M, 7 hrs) group, and (b) after exposure to BSO (100 μ M) for 22 hrs or 28 hrs.



Bayesian hierarchical modelling for Seahorse extracellular flux oxygen consumption rate data analysis

Xiang Zhang, Taolin Yuan, Jaap Keijer, Vincent C. J. de Boer*

Human and Animal Physiology, Wageningen University & Research, The Netherlands

In Preparation

Abstract

Mitochondrial dysfunction is involved in many complex diseases. Efficient and accurate evaluation of mitochondrial functionality is crucial for understanding pathology as well as for facilitating development of novel therapeutics. As a reliable platform, the Seahorse extracellular flux (XF) analyzer is widely used for measuring mitochondrial oxygen consumption rate (OCR) in living cells. A hidden feature of XF OCR data is that it has a complex data structure, caused by nesting and crossing between multiple factors. Surprisingly, statistical analysis of XF data has received little attention, and current methods completely ignore the complex data structure, impairing the robustness of statistical inference. To rigorously incorporate the complex structure into data analysis, we here developed a Bayesian hierarchical modelling framework and demonstrated its applicability for analysing XF OCR data with two experimental data sets. We showed that our approach can incorporate uncertainty in the OCR measurements into the posterior estimation of bioenergetic measures and is flexible to be applied to analyse experimental data with various experimental designs and sample sizes.

Introduction

Mitochondria are double-membrane cellular organelles that are central hubs in regulating energy generation and partitioning. Since defects in mitochondrial function have been found to be involved in cardiovascular diseases¹, type II diabetes², neurodegenerative disease³, aging⁴ and cancer⁵, restoring mitochondrial function is emerging as a therapeutic target for common diseases⁶.

Mitochondria produce energy primarily by transferring electrons along the electron transport complexes I-IV (ETC) in the mitochondrial inner membrane (MIM). During electron transport, protons are pumped over the MIM, building up an electrochemical proton gradient that is ultimately used by ATP synthase to generate ATP. Since oxygen is the final electron acceptor at complex IV and is reduced to H₂O, the activity of the ETC can be assessed by measuring oxygen consumption rate (OCR). As a reliable and efficient platform, the Seahorse XF analyzer is a multi-well plate based respirometry assay that is widely used to quantify OCR in living cells⁷. Typically, the Seahorse XF analyzer measures the OCR of cells in a 96-well plate (or 24-well plate) under different ETC perturbation scenarios, used for assessing mitochondrial functionality, such as maximal respiration, leak respiration and ATP-linked respiration. One of the assessment scenarios, encompassed in the Seahorse XF Cell Mito Stress Test, consists of four phases including an initial phase, followed by three consecutive injections with oligomycin, carbonyl cyanide-4-(trifluoromethoxy) phenylhydrazone (FCCP) and a mixture of rotenone and antimycin A. In the initial phase, no compound is injected and the ETC are not perturbed. Once oligomycin is injected in the assay, proton translocation through ATP synthase is blocked, leading to a reduction in OCR. Next, injection of FCCP allows protons to move into the mitochondrial matrix independent of the ATP synthase, pushing the oxygen consumption to the maximum level. In the end, a mixture of rotenone and antimycin A is injected to inhibit complex I and III, shutting down mitochondrial respiration.

A standard Seahorse run includes three measurement cycles for each phase. Every measurement cycle starts by lowering the cartridge and creating a temporary semi-closed 4-7 μ L chamber⁸. During a measurement cycle, fluorescent oxygen sensors capture oxygen concentration changes in the chamber and generate output OCR. The Seahorse XF analyzer measures OCR of tens to hundreds of thousands of cells per well and typically requires 4–5 replicate wells per experimental group⁹. A single 96-well plate can contain multiple experimental groups. Since measurements are nested within scenarios (i.e., the initial measurement or one of the injections), scenarios are crossed with wells, and wells are nested in experimental groups, a very complex structure is inherently embedded in the Seahorse XF OCR data (Fig. 1a).

Surprisingly, current Seahorse XF data analyses most often ignore this complex structure, and by default, data sets are often chopped into subgroups followed by performing ANOVA-like statistical tests. Other Seahorse XF data analysis tools such as OCR-Stats¹⁰, SHORE¹¹ and Bioenergetic Health Index¹² do not take the complexity of the data structure into account either.

A direct and rigorous way to incorporate the complex structure into data analysis is to use hierarchical modelling. Hierarchical models have been extensively developed for analysing gene expression data^{13, 14}. Here, we developed a Bayesian hierarchical modelling framework for the Seahorse XF OCR data. Our modelling framework is based on a fully Bayesian approach, chosen because of its flexibility and convenience for constructing hierarchical models. Briefly, in the fully Bayesian approach, we focus on estimating posterior distributions for all parameters conditional on prior distributions and data. We used two research cases to demonstrate the applicability of our approach for analysing Seahorse XF OCR data.

Results

Bayesian hierarchical modelling framework for Seahorse OCR data analysis

In this study, we developed a Bayesian hierarchical modelling framework for the Seahorse XF OCR data. We applied a fully Bayesian approach because of its flexibility and convenience for constructing hierarchical models. The mathematical description of our Bayesian hierarchical modelling framework is as follows:

$$\text{OCR}_{\text{obs}}[i] \sim \text{Lognormal}(\log\text{OCR}_{\text{true}}[W[i], I[i]], \log\text{OCR}_{\text{se}}[W[i], I[i]]) \text{ (Equation 6)}$$

$$\exp(\log\text{OCR}_{\text{true}}[W[i], I[i]]) = \text{OCR}_{\text{per 1k cells}}[G[i], I[i]] \times N_{\text{cells}}[W[i]] \text{ (Equation 7)}$$

$$\text{OCR}_{\text{per 1k cells}}[G[i], I[i]] \sim \text{Normal}(\mu[i], \sigma) \text{ (Equation 8)}$$

$$\mu[i] = \text{Regression model depending on the experimental design (Equation 9)}$$

$$\sigma \sim \text{Exponential}(1) \text{ (Equation 10)}$$

$$\log\text{OCR}_{\text{se}}[i] \sim \text{prior distribution (Equation 11)}$$

In Equation 6, we used a lognormal distribution with the true OCR value at the log scale ($\log\text{OCR}_{\text{true}}$) and the measurement uncertainty (also at the log scale, $\log\text{OCR}_{\text{se}}$) to model each observed OCR value (OCR_{obs}), because OCR values must be positive. OCR_{obs} is a vector of length $N_{\text{wells}} \times N_{\text{injections}} \times N_{\text{measurement}}$, where N_{wells} , $N_{\text{injections}}$ and $N_{\text{measurement}}$ are number of wells, injections and measurement cycles, respectively. The $\log\text{OCR}_{\text{true}}$ and $\log\text{OCR}_{\text{se}}$ are matrices of N_{wells} rows and $N_{\text{injections}}$ columns.

In Equation 7, we modelled the true OCR value as a function of the cell number. N_{cells} is a vector of length N_{wells} , and every entry represents the cell number in that well. $\text{OCR}_{\text{per 1k cells}}$ is a matrix with N_{Groups} rows and $N_{\text{injections}}$ columns. Every entry of this matrix represents the OCR value per 1000 cells that received the same treatment (or from the same group) and injection.

In Equation 8 and 9, we applied a linear regression model in which the OCR value per 1000 cells was used as the response (or dependent) variable to estimate effect sizes of various factors (e.g., treatment, group). Since experimental design and plate set-up are not uniform between studies, regression models need to be constructed accordingly. The parameter σ represented the residual that cannot be explained by the regression model. To make a Bayesian model run, prior distributions are needed for all the parameters. We used a weakly informative prior distribution (Exponential (1)) for σ .

In this study, since our case studies focused on human fibroblast cells, we used an informative prior distribution for $\log\text{OCR}_{\text{se}}$. We estimated the prior distribution based on the Seahorse XF OCR data in OCR-stats¹⁰ by running the `fitdistr` function (maximum likelihood) built in the MASS R package. As a result, the Lognormal (-3.11, 0.81) was used as the prior distribution for $\log\text{OCR}_{\text{se}}$.

Case studies

To demonstrate how our Bayesian hierarchical modelling approach can be used for Seahorse XF OCR data analysis, we used two data sets that investigate mitochondrial function alteration due to either treatment with a novel inhibitor targeting SIRT5¹⁵ (case 1) or a SIRT5 variant (case 2).

Case study 1: Factorial design with no biological replicates

In the first case study, we assessed if the SIRT5 inhibitor DK1-04e could lead to mitochondrial dysfunction in human fibroblasts. This study used a factorial design with two factors: treatment and injection. In addition, a concentration escalation was applied in this study (Fig. 1b). Here, we treated the concentration factor as a continuous variable. Based on the experimental design of this study, we composed the regression model as:

$$\mu[i] = \beta_0 + \beta_T[T[i]] + \beta_D[D[i]] + \beta_I[I[i]] \text{ (Equation 12)}$$

β_0 is the overall average of OCR per 1000 cells in all wells and across different injections. Based on the OCR-stats data, we estimated the prior distribution for β_0 as Lognormal (0.54, 0.32). β_T is the deviation in OCR due to treatment, DK1-04e (SIRT5 inhibitor) or DK1-04e(O) ("placebo").

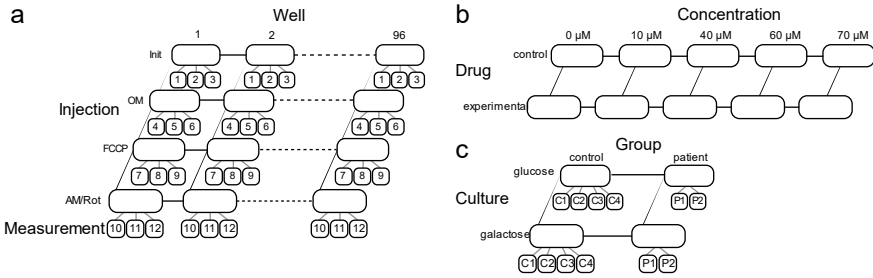


Figure 1. (a) An Overview of the complex data structure of a typical mito-stress test performed using a Seahorse 96-well plate extracellular flux analyzer, Init = Initial phase (before first injection), OM = oligomycin (injection 1), FCCP = carbonyl cyanide-4-(trifluoromethoxy) phenylhydrazone (injection 2), AM/Rot = antimycin A/rotenone (injection 3). (b) Overview of data structure of Case study 1. (c) Overview of data structure of Case study 2, C1, C2, C3, C4 = control cell line 1, 2, 3 and 4; P1, P2 = patient cell line 1 and 2.

β_D is the effect when the concentration increases with 10 μ M. We assume that the higher concentration, the larger effect will be. β_I is the deviation in OCR due to injection, including initial, oligomycin, FCCP and rotenone/antimycin A.

Our analysis showed that in dimethyl sulfoxide (DMSO)-treated fibroblasts, the median basal respiration, ATP-linked respiration, proton leak, spare respiratory capacity and maximal respiration were 3.23 [95% credible interval: 3.009, 3.34] pmol/min, 3.14 [2.99, 3.25] pmol/min, 0.0955 [0.0258, 0.158] pmol/min, -0.890 [-1.05, -0.705] pmol/min, and 2.34 [2.22, 2.48] pmol/min, respectively (Fig. 2). In general, treatment of fibroblasts with 10-60 μ M SIRT5 inhibitor DK1-04e or “placebo” DK1-04e(O) resulted in similar basal respiration, ATP-linked respiration, proton leak, spare respiratory capacity and maximal respiration. We found that the proton leak in 10 μ M DK1-04e treated fibroblasts was 0.114 [0.0143, 0.203] pmol/min, whereas in the “placebo” group (10 μ M Dk104[O]) that proton leak was 0.368 [0.101, 0.469] pmol/min. However, the difference was not statistically significant (mean difference -0.255 [-0.387, 0.0185]) (Fig. 2). In contrast, we found that at 60 μ M the proton leak in DK1-04e treated fibroblasts was 0.144 [0.113, 0.181] pmol/min, 0.0736 [0.00898, 0.143] pmol/min higher than the proton leak (0.0711 [0.0124, 0.128]) in DK1-04e(O) treated fibroblasts (Fig. 2). At 70 μ M, DK1-04e treated fibroblasts showed significant increases in basal respiration (1.45 [1.19, 1.68] pmol/min), ATP-linked respiration (0.793 [0.537, 1.08]), proton leak (0.662 [0.446, 0.784] pmol/min) and maximal respiration (1.09 [0.775, 1.40] pmol/min) in comparison with DK1-04e(O) group (Fig. 2).

Case study 2: Split-plot design

The second study was an experiment in which fibroblasts derived from two patients with *SIRT5* mutations were compared to fibroblasts derived from four healthy

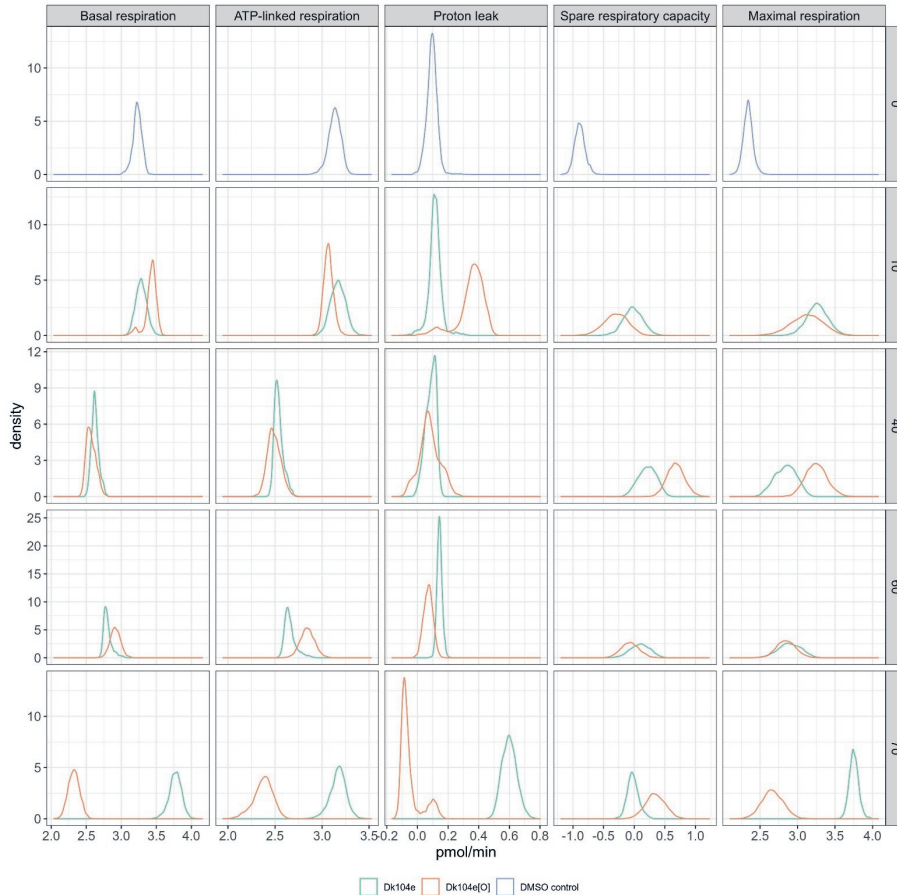


Figure 2. Posterior distributions of basal respiration, ATP-linked respiration, proton leak, spare respiratory capacity and maximal respiration in galactose-cultured fibroblasts treated with either *SIRT5* inhibitor DK1-04e or with the control compound DK1-04e(O).

individuals. The goal of this study was to identify mitochondrial dysfunction in the *SIRT5* mutation carriers. In this study, subjects were nested in group factor (healthy control or patient). Meanwhile, treatment factor (galactose and glucose) and injection factor were crossed with subjects (Fig. 1c). With both nested and crossed factors, this experiment essentially has a split-plot design. The split plot design was originally invented in agricultural experiments in order to deal with randomization of hard-to-change factors. Accordingly, we specified the regression model as:

$$\mu[i] = \beta_0 + \beta_G[G[i]] + \beta_T[T[i]] + \beta_I[I[i]] + \beta_{IT}[I[i], T[i]] + \beta_{GT}[G[i], T[i]] + \beta_{GI}[G[i], I[i]] + \beta_S[S[i]] \text{ (Equation 13)}$$

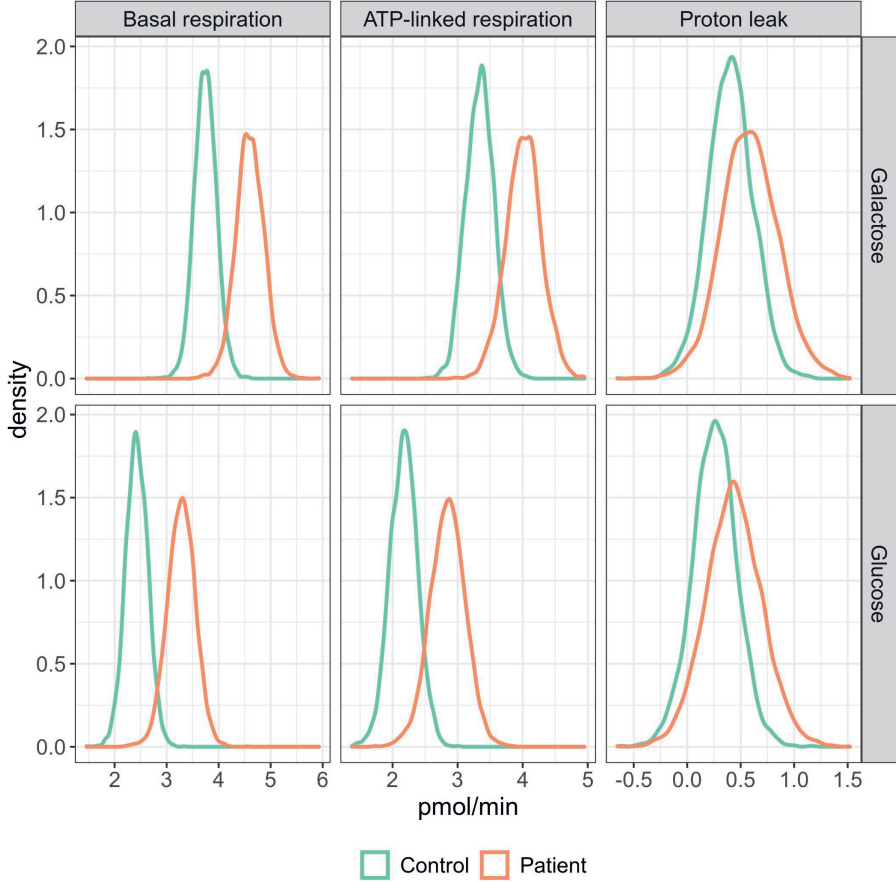


Figure 3. Posterior distributions of basal respiration, ATP-linked respiration and proton leak of galactose or glucose-treated fibroblasts derived from healthy subjects and patients with genetic SIRT5 variants.

β_0 is the overall average OCR per 1000 cells in all wells and across injections. As before, we used Lognormal (0.54, 0.32) as the prior distribution. β_G , β_T and β_I are OCR deflections due to group (healthy or patient), treatment (glucose or galactose), and injections, respectively. To take into account the fact that cell lines derived from the same subject were used for all levels of treatments and injections, β_S is used to estimate the deflection due to subject factor. The interaction term, β_{IT} denotes whether deflection due to injections is dependent on treatment factor. Similarly, the other two interaction terms, β_{GT} and β_{GI} denote whether deflection caused by treatment and injection factor are dependent on group factor.

Our analysis showed that on average fibroblasts treated with galactose had higher basal respiration (1.31 [0.801, 1.86] pmol/min) and ATP-linked respiration (1.17 [0.649, 1.71] pmol/min) than glucose-treated fibroblasts (Fig. 3). In contrast, proton leak was similar between galactose and glucose-treated fibroblasts (median difference 0.149 [-0.371, 0.687]). Interestingly, our analysis showed that on average the basal respiration of galactose-treated fibroblasts was 3.75 [3.33, 4.17] pmol/min in healthy controls and 4.60 [4.07, 5.13] pmol/min in patients with *SIRT5* mutations (Fig. 3). In glucose-treated fibroblasts, the basal respiration of healthy controls was 2.42 [2.01, 2.84] pmol/min, whereas the basal respiration of patient-derived fibroblasts was 3.29 [2.75, 3.79] pmol/min. The basal respiration difference between patients and controls is 0.861 [0.293, 1.41] and was independent of treatment of glucose or galactose. The ATP-linked respiration in galactose-treated fibroblasts derived from healthy controls and patients with *SIRT5* mutations were 3.35 [2.94, 3.76] and 4.02 [3.47, 4.54], respectively. In glucose-treated fibroblasts, the ATP-linked respiration in healthy controls and patients were 2.17 [1.75, 2.59] pmol/min and 2.85 [2.29, 3.38] pmol/min, respectively (Fig. 3). Similar to basal respiration, the difference in ATP-linked respiration between patients and controls was 0.682 [0.0998, 1.24] pmol/min, and this difference was independent of treatment of glucose or galactose. The proton leak of galactose-treated fibroblasts in healthy controls was 0.404 [-0.0152, 0.819] pmol/min whereas in patients the proton leak was 0.579 [0.0657, 1.12] pmol/min. In glucose-treated fibroblasts, healthy controls had proton leak 0.258 [-0.164, 0.665] pmol/min, and patients had proton leak 0.434 [-0.0804, 0.962] pmol/min (Fig. 3). The proton leak difference between patients and controls was 0.176 [-0.363, 0.736] pmol/min and was independent of treatment of glucose or galactose.

Discussion

Although the Seahorse XF analyzer is widely used in bioenergetic profiling, its data analysis has received little attention¹⁰. In the current study, we developed a Bayesian hierarchical modelling approach, which accounts for the complex structure of Seahorse OCR data. The complexity of Seahorse OCR data is due to the fact that XF measurements are nested within injections, injections are crossed with wells, and wells are nested in experimental groups. The data structure can be even more complex when a study has a complicated experimental design with multiple factors. From our perspective, there are three levels in the Seahorse XF OCR data. These levels are the 1) measurement, 2) well, and 3) group.

At the lowest level, the measurement level, the variation within an injection phase is assumed to be caused by measurement error. This is because there are multiple

measurement cycles during each injection phase, and every measurement cycle starts with a mixing and waiting steps to ensure the same baseline of cell values, therefore cell physiology should not substantially change within an injection phase. Since OCR data must be positive values, we used the lognormal distribution as the likelihood function. The same likelihood function was also used by OCR-Stats¹⁰. In the first case study, we found that on average the uncertainty in FCCP-related measurements (0.147 [0.0443,0.270]) was larger than initial (0.0707 [0.0227,0.176]), oligomycin (0.0923 [0.0257,0.403]) and rotenone/antimycin A (0.0972 [0.0242,0.519]) (Supplementary Fig. S1). The variable OCR values could indicate that FCCP possibly induces an unstable physiological state, possibly due to the off-target effects. It has been proposed that other mitochondrial uncouplers such as BAM15¹⁶ would have less off-target effects and would thus generate a more stable cellular physiological state.

In the second case study, we found that on average the measurement uncertainty in initial, oligomycin and rotenone/antimycin A condition was 0.0581 [0.0135, 0.221], 0.0760 [0.0220, 0.262] and 0.0798 [0.0208, 0.301], respectively (Supplementary Fig. S2). These measurement uncertainties were comparable between these two case studies, indicating that OCR values were stable in initial, oligomycin and rotenone/antimycin A scenario.

The second level of Seahorse OCR data is the level of the well. Since the same cell lines with the same treatment were plated in multiple wells, these replicated wells (also called pseudo replication) essentially reflect the same biological signals. In other words, these replicate wells should give the same OCR value assuming that the numbers of cells are identical. Treating these replicated wells as biological replicates in Students' t- test or ANOVA (analysis of variance) deviates from the assumptions that are associated with those procedures, making these statistical analyses not suitable for experimental data based on a single cell line. We notice that a "workaround" is to treat replicated experiments on different days as biological replicates. However, this "workaround" does not solve the issue that there is no true biological replication, although cell proliferation over days may result in small cellular changes but they originate from the same biological sample. In fact, this issue is not unique to Seahorse OCR data analysis, and it also happens to most if not all cell line-based studies. Our Bayesian hierarchical modelling approach provides a way to properly handle this type of experimental data. However, without true biological replication, for example by using multiple cell lines, we still cannot generalize observations towards a certain cell type, let alone to a tissue, without proper validation. Furthermore, since the numbers of cells are comparable but not exactly identical in replicated wells, it is common to see OCR values differ among the pseudo

replication¹⁷. To adjust for the cell number variation, our hierarchical model explicitly incorporated the cell number information of each well (Equation 7) and estimated the $OCR_{\text{per 1k cells}}$, which represented the OCR value of 1000 cells.

The last level of Seahorse OCR data is the experimental group. $OCR_{\text{per 1k cells}}$ reflects OCR values that are determined by a particular cell line, a particular treatment and a particular injection. The cell line, treatment and their combinations are viewed as groups. To find out the difference between groups, regression analysis of $OCR_{\text{per 1k cells}}$ needs to be performed. In our case studies, we therefore constructed and used two different regression models to handle Seahorse XF data for factorial and split-plot designs, respectively. It should be noted that both cases represent a single experiment, without any replication. Although the three controls' and two patients' samples constitute true biological replicates, experimental replication is also needed to draw biological valid conclusions from cell experiments.

Our Bayesian hierarchical modelling approach has several advantages. The first advantage of our approach is that the uncertainty in the OCR measurements was incorporated in the posterior estimation of bioenergetic measures. The second advantage is that our approach is flexible and can be adapted to different experimental designs. The third advantage is that our approach can work with any sample size and unbalanced group sizes. For example, case study 2 has four biological replicates in the control group, whereas two in the patient group. This is especially useful for studies where it is challenging to acquire biological samples.

Material and methods

Patient ethics

Informed consent for research studies was obtained for patients and controls according to the Declaration of Helsinki and following the regulations of the local medical ethics committee.

Cell culture

Human fibroblasts derived from biopsies of healthy subjects and two patients with SIRT5 gene variants were used in this study (obtained from Radboud UMC, see Chapter 3 for details). Control fibroblasts that were included were #13370, #MW28, #14308, and #14321, and the patients' fibroblasts were #13395 and #13706. For routine culture, the fibroblasts were cultured in fibroblast growth medium which consisted of medium 199 (# M3769, Sigma-Aldrich) supplemented with 10% foetal bovine serum (FBS, #06Q3501K, Gibco), 2 mM GlutaMax (#35050038, Gibco), and 1x antibiotic-antimycotic mix (#15240062, Gibco; containing 100 IU/ml

penicillin/streptomycin and 25 µg/ml Amphotericin B). Cells were maintained in 5% CO₂ atmospheric environment at 37°C. Cells were passaged once every 4-5 days when reaching 90% confluency, by trypsinization (#15400054, Gibco). All cells were tested mycoplasma-free using MycoSensor qPCR assay (#302107, Agilent Technologies).

Seahorse extracellular flux assay

Cell seeding and exposure media

In case study 1, one control fibroblast (#14321) was used to investigate the effect of SIRT5 inhibitor DK1-04e (a kind gift of Dr. Hening Lin from Cornell U, see Chapter 3 for details) on mitochondrial respirational characteristics. The fibroblasts were seeded in one XFe96 V3 PS cell culture microplate (#101085-004, Agilent Technologies) at a density of 7000 cells/well and cultured in fibroblast growth medium. After 16 hrs, medium was switched to galactose medium supplemented with either DMSO (#276855, Sigma-Aldrich), SIRT5 inhibitor DK1-04e, or Dk1-04e(O) (“placebo” control drug for SIRT5 inhibitor, a kind gift from Dr. Hening Lin). Galactose medium was prepared by supplementing basic DMEM (#A1443001, ThermoFisher Scientific) with 10 % FBS, 5.5 mM galactose (#G0625, Sigma-Aldrich), and 2 mM L-glutamine (#25030024, Gibco). Drug DK1-04e or its “placebo” control drug DK1-04e(O) stock (50 mM in DMSO) was diluted in this galactose medium, and a serial dilution was performed to reach different concentrations. Since these two drugs both were dissolved in DMSO, a group of galactose_DMSO (final concentration of 0.14%) medium was included as a solvent control.

In case study 2, four controls and two patients’ fibroblasts were plated in one Seahorse plate in the same way as stated in case study 1. Sixteen hours post seeding, growth medium was discarded and switched to either glucose or galactose exposure medium. The preparation of galactose medium was the same as described in case study 1. The glucose medium was prepared similarly, except that 5.5 mM XF glucose (#103577-100, Agilent Technologies), instead of galactose, was added in the basic DMEM medium. The exposure media information is listed in Table 1.

In both case studies, all the pH of exposure media was checked and adjusted to 7.4 with HCl if needed. All the media was filtered through 0.2 µm cellulose acetate membranes after preparation prior to application to the cells. The exposure duration in both studies was 72 hrs.

Seahorse assay media preparation

The cells underwent Seahorse flux analysis after exposure for 72 hrs. Fresh Seahorse assay media (XF media) were prepared on the day of OCR measurement. As a starting point, the XF DMEM (pH 7.4, #27518004, Agilent Technologies) was used and it was supplemented with components in accordance with key components present in the exposure media. After preparation, the pH of the XF media was checked and adjusted to 7.4 with HCl, if needed, and was filtered through 0.2 µm cellulose acetate membranes prior to application to the cells. The detailed composition of XF media is described in Table 1. The L-Gln (#103579-100) used in the XF media was from Agilent Technologies.

Seahorse metabolic flux analyses

Prior to OCR measurement run, exposure media were replaced by XF media and cells were kept in a 37°C in a non-CO₂ incubator with normal air for 1 hr. Then, fresh XF media were applied to cells just before the start of the OCR measurement. The cellular respiratory characteristics were assessed with consecutive injections of mitochondrial complex inhibitors and uncouplers, after basal measurement. The injections strategies in the two cases were distinct. All the compounds for injection were from Sigma-Aldrich.

In case study 1, we performed a classical Mito Stress test based on the Agilent Mito Stress Test user guide (#103015-100) with some adjustments using chemical stocks dissolved in DMSO. The injection strategy was as follow: 1 µM oligomycin (#O4876) final concentration in port A; 1 µM FCCP (#C2920) final concentration in port B; 2.5 µM antimycin A (#A8674) plus 1.25 µM rotenone (#R8875) final concentration in port C. The injection solutions were prepared in XF media without DMSO, DK1-04e or DK1-04e(O).

In case study 2, we performed an ATP rate assay according to Agilent user guide (#103591-100) with some adaptations using chemical stocks in DMSO. 1 µM oligomycin (#O4876, Sigma-Aldrich) final concentration in port A; 2.5 µM antimycin A (#A8674) plus 1.25 µM rotenone (#R8875) final concentration in port B. The injection solutions were prepared in XF media.

During the Seahorse assay, the assay procedure consisted of a 12 min equilibration period followed by 3 measurement cycles for basal respiration, and injection of compounds was followed by 3 measurement cycles as well. Each cycle comprised of a 2 min mixing and a 3 min measurement period. The Seahorse XFe96 Extracellular Flux analyzer was maintained at 37°C for all XF measurements.

Cell number quantification

In both case studies, after the completion of the metabolic flux analysis, cells in plates were stained with 4 μ M of 2'-(4-ethoxyphenyl)-5-(4-methyl-1-piperazinyl)-2,5'-bi-1H-benzimidazole trihydrochloride trihydrate (Hoechst 33342, #B2261, Sigma-Aldrich) dissolved in assay medium, for 1 hr at 37°C in a non-CO₂ incubator. Images were taken by Cytation 1 Imaging Reader (BioTek) and the cell number was determined using ImageJ 1.52 (National Institutes of Health).

Case study 1

In the first study, fibroblast cells derived from a healthy subject were cultured in galactose exposure medium (5.5 mM). A SIRT5 inhibitor, DK1-04e, or the control counterpart, DK1-04e(O) was administrated into the cell culture. Galactose exposure medium with DMSO (0.014 %) was used as the control. In this experiment, four inhibitor concentrations (10 μ M, 40 μ M, 60 μ M and 70 μ M) were used. Respiration of fibroblasts was measured using a Seahorse Extracellular Flux Analyzer and a Mito Stress test was performed as described above.

During the quality control, we removed three wells (2 derived from the 10 μ M DK1-04e(O) group and 1 from the DMSO group) due to negative OCR values. After quality control, the number of wells that contained cells treated with 10 μ M, 40 μ M, 60 μ M and 70 μ M DK1-04e were 10, 10, 10 and 9, respectively. For DK1-04e(O), the number of wells that correspond to 10 μ M, 40 μ M, 60 μ M and 70 μ M were 8, 10, 9 and 9, respectively. There were 11 wells with DMSO exposed fibroblasts.

Case study 2

In the second study, fibroblast cells derived from four healthy subjects and two patients with SIRT5 variant were used for Seahorse XF analysis. Each of the two patients harboured one distinct SIRT5 variant, and SIRT5 protein levels were largely reduced in both patients' fibroblasts (Chapter 3). In this experiment, an ATP rate assay test was performed where two injections were used.

For every fibroblast cell line derived from healthy controls, 8 replicate wells were used for galactose exposure and 7 replicate wells were used for glucose exposure. For each patient-derived fibroblast cell line, 8 replicate wells were used for galactose and glucose exposure, respectively.

Hierarchical model implementation details

The Bayesian hierarchical models were implemented in Stan (version 2.19.3)¹⁸. We fitted the model by running Hamiltonian Markov Chain Monte Carlo. We ran four

Markov chains with 2000 iterations in each chain. Results were presented with the posterior mean with 95% credible interval. The code can be found at <https://github.com/XiangZhangSC/seahorse>.

Calculation of bioenergetic measures

Based on OCR (per 1000 cells), we calculated various bioenergetic measures, such as basal respiration, proton leak, ATP-linked respiration, spare respiratory capacity and maximal respiration. These bioenergetic measures are defined as below:

$$\text{Basal respiration} = \text{OCR}_{\text{per 1k cells, initial}} - \text{OCR}_{\text{per 1k cells, rotenone}} \quad (\text{Equation 1})$$

$$\text{ATP-linked respiration} = \text{OCR}_{\text{per 1k cells, initial}} - \text{OCR}_{\text{per 1k cells, oligomycin}} \quad (\text{Equation 2})$$

$$\text{Proton leak} = \text{OCR}_{\text{per 1k cells, oligomycin}} - \text{OCR}_{\text{per 1k cells, rotenone}} \quad (\text{Equation 3})$$

$$\text{Spare respiratory capacity} = \text{OCR}_{\text{per 1k cells, FCCP}} - \text{OCR}_{\text{per 1k cells, initial}} \quad (\text{Equation 4})$$

$$\text{Maximal respiration} = \text{OCR}_{\text{per 1k cells, FCCP}} - \text{OCR}_{\text{per 1k cells, rotenone}} \quad (\text{Equation 5})$$

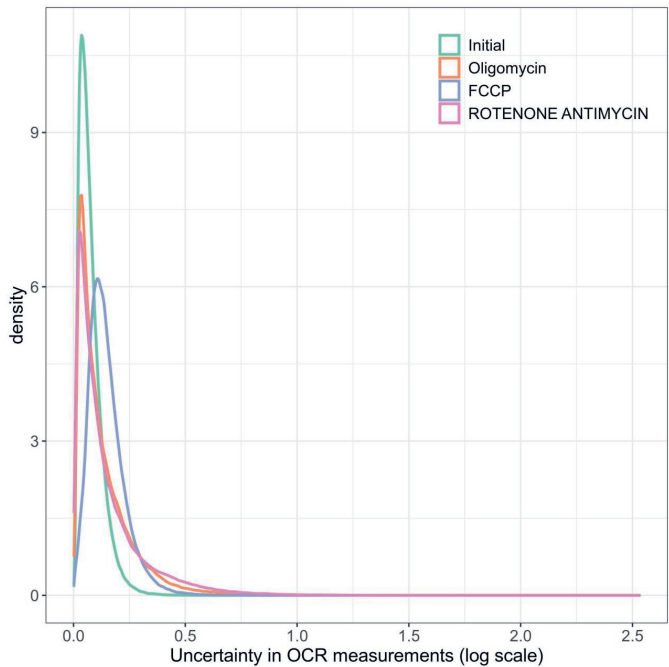
References

1. Ballinger, S.W. Mitochondrial dysfunction in cardiovascular disease. *Free Radic. Biol. Med.* **38**, 1278-1295 (2005).
2. Szendroedi, J., Phielix, E. & Roden, M. The role of mitochondria in insulin resistance and type 2 diabetes mellitus. *Nat. Rev. Endocrinol.* **8**, 92-103 (2011).
3. Johri, A. & Beal, M.F. Mitochondrial dysfunction in neurodegenerative diseases. *J. Pharmacol. Exp. Ther.* **342**, 619-630 (2012).
4. van der Hoek, M.D., *et al.* Intramuscular short-chain acylcarnitines in elderly people are decreased in (pre-)frail females, but not in males. *FASEB J.* **34**, 11658-11671 (2020).
5. Erez, A. & DeBerardinis, R.J. Metabolic dysregulation in monogenic disorders and cancer - finding method in madness. *Nat. Rev. Cancer* **15**, 440-448 (2015).
6. Murphy, M.P. & Hartley, R.C. Mitochondria as a therapeutic target for common pathologies. *Nat. Rev. Drug Discov.* **17**, 865-886 (2018).
7. Wu, M., *et al.* Multiparameter metabolic analysis reveals a close link between attenuated mitochondrial bioenergetic function and enhanced glycolysis dependency in human tumor cells. *Am. J. Physiol. Cell Physiol.* **292**, C125-136 (2007).
8. Gerencser, A.A., *et al.* Quantitative microplate-based respirometry with correction for oxygen diffusion. *Anal. Chem.* **81**, 6868-6878 (2009).
9. Artyomov, M.N. & Van den Bossche, J. Immunometabolism in the Single-Cell Era. *Cell Metab.* **32**, 710-725 (2020).
10. Yepez, V.A., *et al.* OCR-Stats: Robust estimation and statistical testing of mitochondrial respiration activities using Seahorse XF Analyzer. *PLoS One* **13**, e0199938 (2018).
11. Nicholas, D., *et al.* Advances in the quantification of mitochondrial function in primary human immune cells through extracellular flux analysis. *PLoS One* **12**, e0170975 (2017).
12. Chacko, B.K., *et al.* The Bioenergetic Health Index: a new concept in mitochondrial translational research. *Clin Sci (Lond)* **127**, 367-373 (2014).
13. Robinson, M.D., McCarthy, D.J. & Smyth, G.K. edgeR: a Bioconductor package for differential expression analysis of digital gene expression data. *Bioinformatics* **26**, 139-140 (2010).
14. Love, M.I., Huber, W. & Anders, S. Moderated estimation of fold change and dispersion for RNA-seq data with DESeq2. *Genome Biol.* **15**, 550 (2014).
15. Abril, Y.I.N., *et al.* Pharmacological and genetic perturbation establish SIRT5 as a promising target in breast cancer. *Oncogene*, (2021).
16. Kenwood, B.M., *et al.* Identification of a novel mitochondrial uncoupler that does not depolarize the plasma membrane. *Mol. Metab.* **3**, 114-123 (2014).
17. Little, A.C., *et al.* High-content fluorescence imaging with the metabolic flux assay reveals insights into mitochondrial properties and functions. *Commun. Biol.* **3**, 271 (2020).
18. Carpenter, B., *et al.* Stan: A Probabilistic Programming Language. *J. Stat. Softw.* **76**, 1-29 (2017).

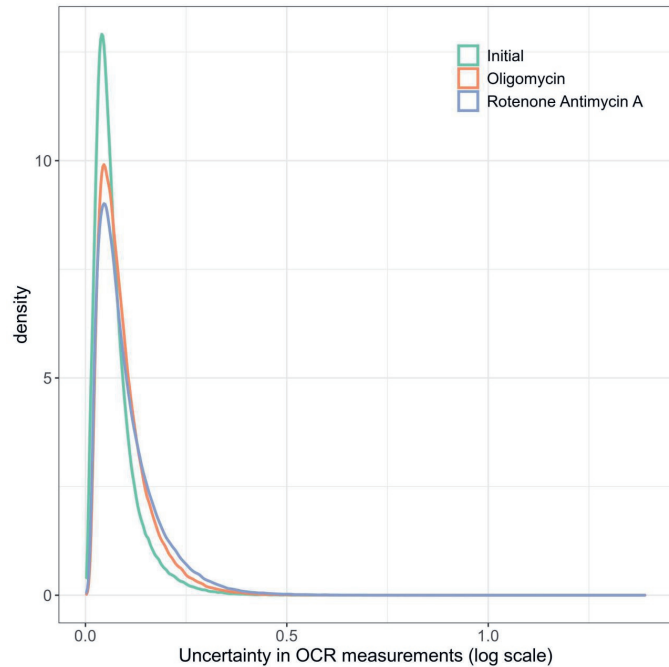
Table 1. Detailed description of exposure as well as Seahorse assay media used in Seahorse assays

Case Study	Exposure media	Exposure media	Seahorse assay (XF) media
1	Galactose_DMSO	DMEM, supplemented with 10% FBS, 2 mM L-Gln, 5.5 mM galactose, and DMSO (0.14%)	XF DMEM, supplemented with 2 mM XF L-Gln, 5.5 mM galactose, and DMSO (0.14%)
1	Galactose_DK1-04e	DMEM, supplemented with 10% FBS, 2 mM L-Gln, 5.5 mM galactose, and a serial concentration of DK1-04e	XF DMEM, supplemented with 2 mM XF L-Gln, 5.5 mM galactose, and a serial concentration of DK1-04e
1	Galactose_DK1-04e(O)	DMEM, supplemented with 10% FBS, 2 mM L-Gln, 5.5 mM galactose, and a serial concentration of DK1-04e(O)	XF DMEM, supplemented with 2 mM XF L-Gln, 5.5 mM galactose, and a serial concentration of DK1-04e(O)
2	Galactose	DMEM, supplemented with 10% FBS, 2 mM L-Gln, and 5.5 mM galactose	XF DMEM, supplemented with 2 mM XF L-Gln, and 5.5 mM galactose
2	Glucose	DMEM, supplemented with 10% FBS, 2 mM L-Gln, and 5.5 mM XF glucose	XF DMEM, supplemented with 2 mM XF L-Gln, and 5.5 mM XF glucose

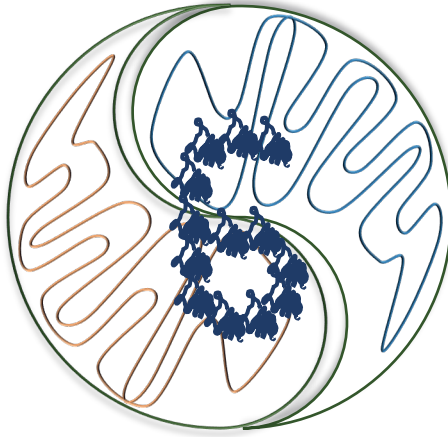
Supplementary Figures



Supplementary Figure S1. Uncertainty in OCR measurements per scenario in the case study 1.



Supplementary Figure S2. Uncertainty in OCR measurements per scenario in the case study 2.



General Discussion

SIRT5 is a robust NAD⁺-dependent desuccinylase, demalonylase and deglutarylase, primarily localized in mitochondria, and is a relatively understudied member of the sirtuin family^{1, 2, 3}. Increasing evidence from mouse and cell-line based studies emphasize the regulatory role of SIRT5 in cellular adaptive responses to environmental stresses^{4, 5, 6}. However, many aspects of the biology of SIRT5 remained elusive and the physiological relevance of SIRT5 in humans was unclear and remained to be answered.

The overall aim of this thesis therefore was to improve our knowledge of the biological function of SIRT5 and to provide evidence for the physiological relevance of SIRT5 in human health and disease. The specific aims of this thesis were: (1) To better understand the biological function of SIRT5 and how human SIRT5 variants relate to human disease. (2) To optimize an enzymatic assay for gaining better insights into cellular SIRT5 biochemical activity under different metabolic conditions. (3) To develop a new statistical model to better analyse effects of SIRT5 on the mitochondrial bioenergetic function assessed by Seahorse extracellular flux analysis.

In this thesis, I reported two novel genetic homozygous *SIRT5* variants in two patients with clinical mitochondrial disease manifestations (**Chapter 3**). Each of the two *SIRT5* variants was demonstrated to cause loss of SIRT5 in the patients-derived primary skin fibroblasts. Consequently, global lysine succinylation levels were significantly increased. Multiple lines of evidence showed redox perturbations in the SIRT5 variant fibroblasts. Redox couple NADPH/NADP⁺ ratios were reduced 2-fold, intracellular ROS levels were significantly increased upon acute exogenous H₂O₂ application, and proton leak rates were significantly increased. Further studies in **Chapter 4** confirmed the redox imbalance in the SIRT5 patients' fibroblasts. Notably, glutathione antioxidant defence system was shown to be impaired in the SIRT5 variant fibroblasts, with strikingly high intracellular GSH abundance, 2-fold lower glutathione reductase activity, and 1.5-fold higher glutathione peroxidase 4 mRNA levels. Moreover, I demonstrated this GSH-system impairment was associated with an imbalanced GSH and thioredoxin antioxidant system in the SIRT5 variant fibroblasts. These results highlight the critical role for SIRT5 in regulation of human redox homeostasis, and the SIRT5 deficiency induced by loss-of-function variants, in turn, may lead to oxidative damage and ultimately contribute to the pathogenesis.

In addition, I aimed to improve the understanding of SIRT5 biological function from the methodological point of view. In **Chapter 2**, I optimized a fluorescence-based (fluor de lys) enzymatic assay to analyse the NAD⁺-dependent desuccinylase activity in crude cell lysates. Using SIRT5 knockout (KO) HEK293T cell line, I showed that SIRT5 was partially responsible for the NAD⁺-dependent desuccinylase activity. A

mismatch between SIRT5 protein level and the desuccinylase activity was observed in proliferative C2C12 and 3T3-L1 cells as compared to their own differentiated counterparts. This supports the notion that it is important to assess the NAD⁺-dependent desuccinylase activity over only analysing the expression of proteins. In the **Chapter 5**, a novel Bayesian hierarchical modelling framework was developed. This model incorporates the complexity of Seahorse data structure and can propagate uncertainty in the oxygen consumption rate (OCR) measurements into the posterior estimation of mitochondrial bioenergetics.

This thesis is the first report about two potential pathogenic *SIRT5* variants in humans and provided the evidence for the relevance of SIRT5 in regulation of human redox homeostasis. Apart from biological insights, progress has been made in optimizing and developing new methods for understanding SIRT5 biological function under different metabolic conditions.

Below, I will first extensively discuss the biological function of SIRT5 and how human *SIRT5* variants relate to human disease (Aim 1). More specifically, I will discuss SIRT5 biology, relations between its different regulatory roles, and the association between SIRT5 variants and the disease pathology. In addition, potential implications of my findings will be discussed. In this context, it is important to realize that recombinant SIRT5 variants were characterized from a biochemical perspective, and the functional impacts of the SIRT5 variants were investigated by a series of molecular and functional analyses on human primary skin fibroblasts. Primary skin fibroblasts are the most common, and in many cases, the only available material from patients. Apart from the primary skin fibroblasts we also used other cell models and CRISPR/Cas9 techniques to entangle the biological impacts of the SIRT5 variant.

Second, I will discuss the fluorescence-based enzymatic method that I optimized to analyse NAD⁺-dependent desuccinylase activity in crude cell lysates (Aim 2), in particular its limitations and advantages.

To answer my third aim, a Bayesian hierarchical statistic model was developed to better characterize mitochondrial respiratory capacity from Seahorse extracellular flux analysis data. The Seahorse XF analyzer monitors the real-time oxygen consumption rate (OCR) of living cells, and several application features make it a powerful tool to examine mitochondrial bioenergetics *ex vivo* and *in vitro*. First, the multi-well (96-well or 24-well) system allows us to test different biological replicates under a number of metabolic conditions. Second, during the assay, multiple measurements under different phases are available because cells can undergo consecutive (maximal four) injections of chemicals of interest, and different injection strategies can be applied across wells in one plate. Third, there are three

measurement cycles for each measurement phase. As a result, the Seahorse data structure is very complex in most of the studies, with measurements nested within injection scenarios, scenarios crossed with wells, and wells nested in experiment groups. However, current Seahorse data analysis methods do not take this complex experimental setup into account for data analysis, which can weaken the robustness of statistical inference. In the **Chapter 5**, I showed that a Bayesian hierarchical modelling can be used to assess Seahorse OCR data, incorporating uncertainty in the OCR measurements into the posterior distribution of the bioenergetics. This model allows for better use of the data that are available in an assay. Because datapoints from all the measurements of the assay plate are used to determine OCR values, a more robust determination of the values can be achieved. Furthermore, this model can be readily adapted to other studies with different experiment setups by incorporating different level of factors. Given the world-wide use of Seahorse analysis platform in biological research, I believe this model, providing a rigorous approach to gain the mitochondrial bioenergetic characteristics especially under complicated experimental setup, can be relevant for all Seahorse users.

Physiopathological relevance of SIRT5 in humans

***SIRT5* loss-of-function variants**

I reported two loss-of-function *SIRT5* variants identified in two independent patients (**Chapter 3**). The two patients presented severe clinical symptoms highly suggestive of genetic mitochondrial disorders, such as global developmental delay, abnormally high plasma alanine levels, hearing loss, dystonia, neuroregression, etc. Genetic variants in more than 250 nuclear genes that encode mitochondrial proteins and 37 mitochondrial genes have been established to cause mitochondrial diseases⁷. Exome sequencing analysis revealed that each of the two identified patients harboured one different homozygous *SIRT5* variant, i.e. 340C>A and 382C>G, respectively. Both altered amino acids are evolutionarily conserved among the human sirtuin family, i.e., among SIRT1-7, as well as among various animal species, indicating their importance in the biochemical characteristics of the SIRT5 protein. I was able to show decreased thermal stabilities of recombinant SIRT5 P114T as well as L128V proteins. This suggested an impaired protein structure of both SIRT5 variants, consequently leading to strikingly reduced protein levels in both patients and was also confirmed in another human cell line HEK293T in which CRISPR/Cas9 was used to introduce the SIRT5 variant P114T. This loss of SIRT5 protein was likely (partially) due to degradation of misfolded SIRT5 variants by the proteasome *in vivo*^{8, 9}. The availability of the patients' cells with SIRT5 variants which consequently have severely reduced SIRT5 protein levels, not only provides the opportunity to

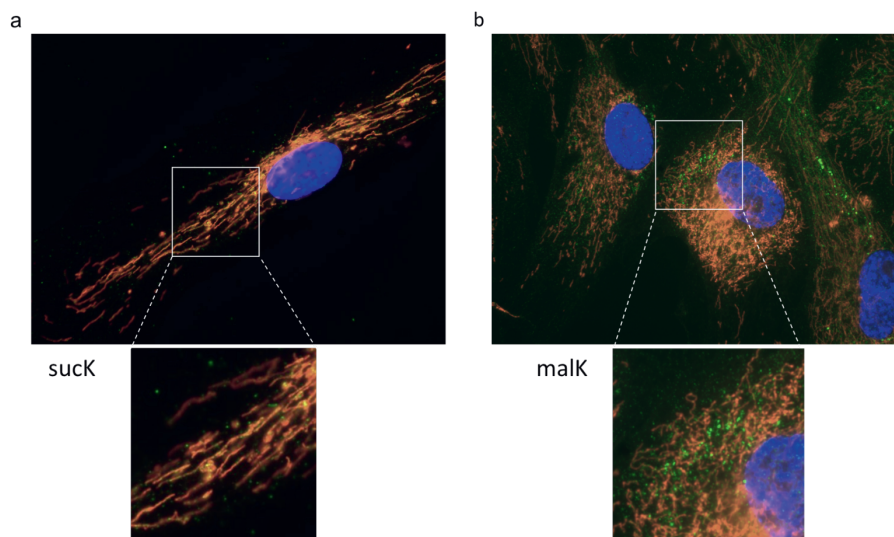


Figure 1. lysine succinylation and malonylation displays distinct subcellular localization in human fibroblasts. (a) A representative immunofluorescence image of lysine succinylation in human fibroblasts. Green fluorescence indicates lysine succinylation, mitochondria were stained as orange, and blue indicates nuclei. The overlay of lysine succinylation (green) and mitochondria (orange) can display colour of yellow. The majority of succinylation signals were overlapping with mitochondria. (b) A representative immunofluorescence image of lysine malonylation in human fibroblasts. Green fluorescence represents lysine malonylation, orange represents mitochondria and blue indicates nuclei. The malonylation signals were largely separated from mitochondria.

understand what the pathological cause of the disease symptoms are, but also will generate insights in the biological role of SIRT5 in humans.

SIRT5 is known as a robust NAD⁺-dependent desuccinylase, demalonylase, and deglutarylase^{1, 2}. As a result of reduced SIRT5 protein levels, evident increase in global lysine succinylation levels were detected in the patients' fibroblasts by both Western blotting and immunofluorescence staining, whereas no clear difference was shown in lysine malonylation or glutarylation level (**Chapter 3**). Interestingly, we observed that lysine succinylation exhibited a distinct subcellular localization from lysine malonylation in human fibroblasts. With the co-staining of mitochondrial marker mitoTracker as well as the nuclear marker DAPI, we found that the majority of succinylation fluorescence signals were overlapping with mitochondria, whereas malonylation was largely present in cytosol (Fig. 1a and 1b). These observations were in line with previous reports in mouse studies, where succinylation was shown to be enriched in mice liver mitochondrial proteins^{10, 11}. Less is known about lysine malonylation and Nishida *et al.* identified a set of malonylated proteins in liver largely belonging to cytoplasm¹². The distinct subcellular locations of succinyl-lysine and

malonyl-lysine that I observed correspond to SIRT5 being present both inside and outside mitochondria³. Based on this and the fact that the patients were clinically diagnosed with symptoms associated with mitochondrial disease, it can even be speculated that mitochondria-localized SIRT5 is primarily affected in the patients. Given the different sets of substrate targets in different subcellular compartments, SIRT5 is likely to play a regulatory role in a compartmentalized manner. However, not much is known about how cytosolic and mitochondrial SIRT5 are coordinated and work along with each other in response to metabolic stress, which would be an interesting topic for future research.

Redox homeostasis is more sensitive to SIRT5 deficiency than bioenergetics in humans

After establishing instability, I aimed to understand whether the two SIRT5 variants were associated with functional defects. To this end, the patients' fibroblasts were subjected to different metabolic conditions, including stress challenges, and were characterized with a wide range of cellular and molecular analyses, including mitochondrial bioenergetics, cell growth, cellular redox environment and thiol-dependent antioxidant systems (**Chapter 3** and **4**). Among all the functional assessments, redox perturbation and decreased cell growth rates were the most prominent phenotypes, while mitochondria bioenergetics was marginally affected.

GSH is the most abundant antioxidant *in vivo*, it works along with glutathione peroxidase, glutathione reductase and NADPH, to maintain the mitochondrial redox environment¹³. We found multiple evident alterations in either expression level or activity of antioxidants in GSH-dependent system (**Chapter 4**). Intracellular GSH levels were strikingly high in the patients' fibroblasts (150% of control), while both gene expression level and activity of glutathione reductase, the enzyme maintaining GSH pool via reducing oxidized glutathione (GSSG) back to GSH, was decreased by 50%. These results showed an impaired GSH-system with disruption in the downstream use of GSH. In support of this, total GSH level was significantly higher in cells with an inactive glutathione peroxidase 4 (GPx4) mutant¹⁴. GPx4 is one member in the glutathione peroxidase family. It can detoxify free radicals with preference for lipid peroxides at the cost of oxidizing GSH to GSSG and plays a critical role to protect membranes against oxidative stress¹⁵. In my study, I showed a 1.5-fold higher gene expression level of *GPx4*, and I interpreted this gene expression increase as a compensatory response to the inhibited activity by high succinylation level. This reasoning is supported by the fact that large number of studies have shown that increased succinylation has a general inhibitory effect on enzymatic activities of modified proteins^{4, 5, 11, 16, 17}. Follow-up studies on determining GPx4 enzymatic

activity and lipid peroxidation, especially peroxidation of cardiolipin, an inner mitochondrial membrane specific phospholipid, would be helpful to identify the involvement of GPx4 as well as lipid peroxidation in the observed redox perturbation phenotypes.

As a result of the disrupted GSH-dependent antioxidant system, dependence of the patients' fibroblasts on thioredoxin system was increased, as evidenced by their enhanced sensitivity to auranofin-induced thioredoxin reductase inhibition (**Chapter 4**). Moreover, under galactose culture conditions, where cellular ROS production is increased due to the fact cells generate energy almost exclusively from mitochondria, we observed that patients' cells were in a more oxidized cellular environment as shown by a 2-fold lower intracellular NADPH/NADP⁺ ratios. However, no clear difference in the DCFDA-oxidizing ROS levels between control and patients' fibroblasts under basal (galactose) condition was observed (**Chapter 3**). This can be explained by a counteract effecting of an increased proton leak. Indeed, proton leak was significantly increased in the patients' cells. An increased proton leak can diminish oxidative stress by decreasing the mitochondrial membrane potential¹⁸. Furthermore, in line with the decreased NADPH/NADP⁺ ratios, I found significantly higher DCFDA-oxidizing ROS accumulation rates in patients' fibroblasts compared to controls' cells upon acute application of exogenous H₂O₂, which strongly suggested antioxidant defence was dysfunctional in the patients' fibroblasts. Together, I demonstrated SIRT5 is critical for human redox homeostasis and the data point to a regulatory role in GSH-dependent antioxidant defence.

Multiple large-scale proteomics studies on SIRT5 KO mice have revealed that SIRT5 targets a number of metabolic enzymes for deacylation (desuccinylation, demalonylation, and deglutarylation), many of which are key enzymes in energy metabolism pathways, such as fatty acid oxidation, TCA cycle, and electron transport complexes^{4, 5, 10, 11, 12}. The acylation modifications are believed to play a regulatory role on proteins functions and SIRT5 KO mice displayed decreased ATP production under fasting conditions in some, but not all studies^{4, 10}. In this thesis, I characterized the cellular bioenergetics capacity by analysing the activities of OXPHOS complexes as well as the real-time glycolysis/OXPHOS flux rate, with the Seahorse XF analyzer (**Chapter 3**). Clinically, neither of the two patients exhibited lactic acidosis, a common phenotype in OXPHOS deficiency-induced mitochondrial disease patients¹⁹. Biochemical analysis of the enzymatic activities of all five complexes in fibroblasts (two patients) and skeletal muscle biopsy (only available in one patient) were within the normal range of control subjects. We then further checked the cellular glycolytic as well as mitochondrial respiratory capacities under stressed conditions. The fibroblasts were forced to strongly rely on either glycolysis, by applying CoCl₂ as a

HIFA mediated inducer of glycolysis²⁰, or on OXPHOS, by applying galactose and low glucose conditions. Integration of bioenergetics data showed that both SIRT5 patients' fibroblasts exhibited consistent and evident alterations on OXPHOS-related parameters in all galactose conditions tested, with 2-fold higher proton leak rates as a pronounced phenotype which I interpreted as an indicator of oxidative stress as discussed above. Additionally, basal OCR were slightly elevated in the SIRT5 variant fibroblasts, which was very likely caused by the increased proton leak rates. Glycolytic parameters were also altered in glycolysis-stimulated conditions, which could indicate an impaired mitochondrial respiration, but only evident in patient 1. Otherwise, I found no difference in other aspects of bioenergetics including mitochondrial ATP-linked OCR, maximal OCR, and contribution of mitochondrial ATP to total cellular ATP generation.

Importantly, cellular oxidative stress can be a result of dysfunctional mitochondria such as impaired OXPHOS^{21, 22}, however, we observed the redox perturbations with only mild alterations of bioenergetics, which could support the concept that disrupted redox balance is directly caused by SIRT5 deficiency, rather than a secondary effect. Taken together, we show that SIRT5 plays a critical role on redox homeostasis in humans.

A proposed pathological model: SIRT5/GSH system/oxidative stress

In this thesis, I established a critical role for SIRT5 in the human redox homeostasis. This is also in line with the findings about other sirtuins. Every mammalian sirtuin has directly or indirectly been shown to be associated with redox regulation in mice or cell-based studies^{23, 24}. For example, SIRT1, the first identified member in sirtuin family, was shown to reduce amount of superoxide produced from uncoupled endothelial nitric oxide synthase (eNOS) and protect cells from oxidative stress by increasing protein levels of multiple antioxidant enzymes such as SOD2 and thioredoxin^{25, 26, 27}. Similarly, SIRT3 was shown to protect mice hearts by suppressing cellular ROS levels. SIRT3-deficient mice developed a severe ROS-mediated cardiac hypertrophic response when challenged by hypertrophy agonist, whereas SIRT3 overexpression protected mice from similar stimuli²⁸. So far, the actions of the sirtuins on antioxidant defence systems appear to be largely indirect, when assessed at molecular level²³. It has been demonstrated that sirtuins (SIRT1-3, SIRT6) deacetylate and regulate key redox-related transcription factors including forkhead box O (FOXO), nuclear factor erythroid 2-related factor 2 (NRF2) and p53. The changes in these transcription factors subsequently induce increase antioxidant enzymes at the gene as well as protein levels^{23, 26, 28, 29}. Another mechanism is by increasing the level of the antioxidant cofactor NADPH by activating a NADPH-

producing enzyme. For instance, SIRT3 and SIRT5 activate isocitrate dehydrogenase (IDH2) and glucose-6-phosphate dehydrogenase (G6PD)^{30, 31}. SIRT5 was also shown to desuccinylate SOD1 in HEK293T cells. Notably, my data in this thesis points to a regulatory role for SIRT5 towards the GSH-dependent antioxidant defence system. This expands our understanding about the biological function of SIRT5. It also provides a new mechanism by which sirtuins contribute to redox balance.

Although I did not have enough data to depict a clear picture of the pathogenic mechanism of the disease caused by SIRT5, current findings directed me to the SIRT5/GSH system/oxidative stress axis. Given the high metabolic activity of several organs such as brain and skeletal muscle, disease due to oxidative stress could happen *in vivo*, as a result of impaired GSH-dependent system. Although physiological levels of ROS may serve as signaling molecules, it is well documented that excessive ROS cause oxidative damage^{32, 33}. Fundamental intracellular macromolecules, such as DNA, protein and lipids, can be attacked by the free radicals within cells, leading to biological dysfunctions. For instance, DNA bases are susceptible to ROS, leading to mutations, nucleotide cyclization and strand crosslinking^{34, 35, 36}. Proteins can undergo a diversity of oxidative modifications by ROS and generate modified proteins, such as protein carbonyl- and hydroxyl-derivatives, protein disulfide bonds and protein nitrotyrosines^{37, 38, 39, 40}. Many of these modifications result in loss of protein structure, enzymatic activities and/or interfere with protein-protein interactions^{40, 41}. Lipids, especially poly unsaturated fatty acids (PUFAs), are easily oxidized by ROS and undergo lipid peroxidation via enzymatic and nonenzymatic routes^{42, 43, 44}. Biological membranes, containing PUFAs, are therefore affected by lipid peroxidation, disturbing the assembly and fluidity of the membranes^{45, 46}. In addition, lipid peroxidation products can diffuse across membranes and react with proteins and results in protein carbonyl adducts^{47, 48, 49}. Since disrupted redox homeostasis has been reported to be associated with many diseases, including mitochondrial disease, cardiovascular and neurodegenerative diseases⁵⁰, it is reasonable to infer that oxidative stress at least partially contributes to the pathogenesis in the SIRT5 patients.

More importantly, the altered *GPx4* gene expression levels in two patients' fibroblasts suggests that lipid peroxidation and its triggered ferroptosis may play a significant role in the pathogenesis, although we cannot exclude the possibility that other proteins involved in other pathways can also be affected by the SIRT5 variants and contributed to the pathogenesis, GPx4 is an interesting target to follow-up in this context. GPx4 is known for its protective role against ferroptosis, an iron- and lipid peroxidation-dependent non-apoptotic form of cell death^{14, 51}. Among glutathione peroxidases family, GPx4 is unique as it can directly reduce phospholipid

peroxides⁵². GPx4 ablation has been shown to lead to a significant increase in phospholipids oxidation in mice kidneys, associated with acute renal failure and early ferroptotic death⁵¹. Collectively, it is attractive to postulate that GPx4 deficiency leads to accumulation of lipid peroxides and cardiolipin oxidation in mitochondria. Cardiolipin is a mitochondria-specific phospholipid as well as a preferred GPx4 substrate⁵³, and its oxidation can lead to mitochondrial dysfunction. Finally, the most pronounced clinical manifestation in the two SIRT5 patients is a mitochondrial encephalopathy, indicating that the brain is likely mostly affected by the SIRT5 variants. Since the brain has a high content of PUFAs, it is highly susceptible to lipid peroxidation, which may be induced by loss of SIRT5.

The observation of significantly increased global lysine succinylation levels in SIRT5 variant fibroblasts is a direct evidence for the SIRT5 deficiency caused by the variants. In addition, multiple clear biological impairments were seen in the patients' fibroblasts, SIRT5 inhibitor phenocopied the increased proton leak rates in human control fibroblasts, and loss of SIRT5 was induced by the same variant in another human cell line, all these findings strengthen the possibility that variants being pathogenic. Nevertheless, the gold standard for establishing the pathogenicity is to show a rescue effect upon complementation of wild-type (WT) *SIRT5* gene in the patients' fibroblasts⁵⁴. I, unfortunately, did not observe conclusive rescue effects in the SIRT5 complemented patients' fibroblasts. This is not completely surprising, as functional complementation of SIRT5 is challenging in many laboratories. The reason for the failed functional rescue is suspected to be inefficient import of SIRT5 WT to mitochondrial matrix in the patients' fibroblasts. One mitochondrial targeting signal was present in the inserted *SIRT5* WT gene, and little or no mitochondrial import of proteins with only one target signal have been reported previously⁵⁵. While in-tandem use of duplicate or multiple mitochondrial targeting signals have been shown to largely improve the mitochondria-import efficiency^{55, 56}, thus, it is worthwhile to try this strategy for the new SIRT5 complementation experiments in the future.

SIRT5 orchestrates the stress response with its regulatory roles in redox as well as in bioenergetics

Although we did not find evidence of major negatively affected bioenergetic phenotypes in the SIRT5 variant fibroblasts, the regulatory role for SIRT5 in energy metabolism has been substantiated in multiple genetically modified mice studies. SIRT5 has been demonstrated to deacylate and activate the enzymes in glycolysis, such as glyceraldehyde 3-phosphate dehydrogenase (GAPDH) and in fatty acid oxidation, such as mitochondrial trifunctional enzyme α -subunit (ECHA)^{5, 12}. This

agrees with *in vivo* data. SIRT5 deficiency led to decreased cardiac fatty acid oxidation, decreased ATP levels under fasting conditions, and ultimately cardiomyopathy in the aged mice⁵. Brown adipose tissue specific SIRT5 KO fasted mice failed to sustain core temperature during acute cold challenge (from 22°C to 7°C), associated with impaired fatty acid oxidation. Together these data indicate that a regulatory role for SIRT5 in the energy metabolism is essential for the organism's metabolic flexibility in response to stress conditions.

Increased fatty acid β -oxidation and glycolysis can be important for cellular energy homeostasis under certain metabolic conditions. However, they can increase ROS levels at the same time. Electrons generated from different enzymatic reaction step of β -oxidation enter respiratory chain at multiple sites, apart from being donated to complex I, they can also feed directly into coenzyme Q via electron transferring flavoprotein (ETF) and ETF-ubiquinone oxidoreductase^{57, 58, 59}. The high reduced to oxidized Q ratio and possible electron leaks at several sites ultimately lead to high ROS production at complex I, II and III^{60, 61, 62, 63, 64}. Similarly, a high glycolytic flux can result in an increased TCA cycle flux, a subsequent accumulation of NADH and FADH₂ and elevated NADH/NAD⁺ as well as FADH₂/FAD ratios. This consequently causes a high reducing state of electron transport complexes, which potentially stimulates superoxide production and favours reverse electron transfer which also increase superoxide production^{65, 66, 67, 68}. Under these circumstances, the regulatory role for SIRT5 on the GSH antioxidant defence system could play a significant role to counteract the increased ROS production from SIRT5 involved changes in energy metabolism, and ultimately contribute to the cellular energy as well as redox homeostasis.

Methodology

Fluor de Lys assay is more suitable for analysing SIRT5 activity of recombinant SIRT5 over in crude cell lysate

One of the aims of my thesis research was to optimize an enzymatic assay to better understand SIRT5 biological function in the context of crude cell lysates (Aim 2), because SIRT5 has been shown to exert its biological functions in a highly context-dependent manner⁶. I therefore optimized a fluorescence-based enzymatic method to analyse NAD⁺-dependent desuccinylase activity, the most robust deacylation activity of SIRT5, in the crude cell lysate. I further verified the contribution of SIRT5 to the cellular desuccinylase activity using SIRT5 KO HEK293T cell line.

I used a commercially available fluor de lys-succinyl substrate, which was conjugated with a fluor-group. The removal of succinyl-group from the substrate sensitizes it to

the 'Developer' reagent and releases the fluorophore, which can be detected with excitation at 360 nm and emission at 460 nm. I first verified this assay using recombinant SIRT5, substantial desuccinylase activity was detected in WT SIRT5 but not in enzymatic inactive mutant SIRT5 H158Y³ (Fig. 2).

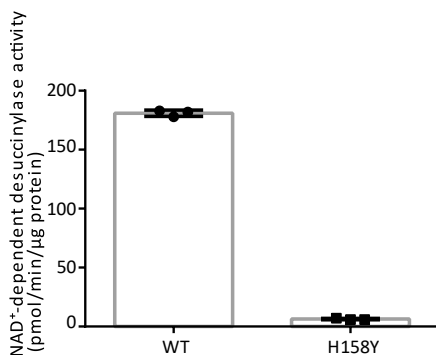


Figure 2. Fluor de lys assay is sensitive and specific for desuccinylase activity of recombinant SIRT5. His-SIRT5 (0.03 μg) was incubated with 10 μM succinyl-substrate and 500 μM NAD⁺. The activity was subtracted from negative control wells (His-SIRT5 was incubated with succinyl-substrate and without NAD⁺). WT, wild type SIRT5 protein. H158Y, enzymatic inactive SIRT5 mutant H158Y.

During the optimization of this assay in crude cell lysates, I noticed an initial high activity, for the first 15 min, followed by a second slower one. This demonstrated that a critical reaction time is needed to assess the initial reaction rate in the complex cell lysate context, which has not been established in similar studies^{69, 70}. Next, I further verified whether the cellular desuccinylase activity detected was solely attributed to SIRT5. Although I specifically determined NAD⁺-dependent activity, which is believed to be a unique feature of sirtuins over other classes of deacylases, I still observed NAD⁺-dependent desuccinylase activity in SIRT5 KO HEK293T cells. This result demonstrated that SIRT5 was not the only enzyme present in the cell lysate being able to remove the succinyl-group from the fluor de lys succinylated-substrate. I therefore conclude that this substrate is probably not the best option for determining SIRT5-mediated desuccinylase activity in the setting of crude cell lysates, because other proteins than SIRT5 can still NAD⁺-dependently produce the fluorogenic signal. Very recently, Yang *et al.* (2020), developed a novel succinylated peptide precursor which can be transformed into self-assembling building blocks upon removal of succinyl-group, leading to fluorescent supramolecular nanofibers in living cells⁷¹. The authors showed the fluorescence signals were mostly detected in mitochondria and that fluorescence signals diminished in cells with knockdown of SIRT5, which strongly indicated that the removal of succinylation in the peptide was very likely catalysed by SIRT5. Thus, this novel succinylated-peptide represents a very promising substrate to assess SIRT5 desuccinylase activity *in vivo*, although the permeability to primary cells, such as human fibroblasts, still needs to be established.

Although a better assay has recently become available for assessing cellular SIRT5 activity, the fluor de lys assay I use was sensitive enough for detecting alterations in the NAD⁺-desuccinylase activity in C2C12 and 3T3-L1 cells under different metabolic conditions (**Chapter 2**). Furthermore, the activity of recombinant SIRT5 proteins can be appropriately assessed. In this thesis, I determined the enzymatic kinetics of WT and SIRT5 variants using the fluor de lys assay. I found that two recombinant SIRT5 variants were overall mildly altered biochemically, with desuccinylase activity being decreased 30% under substrate-limiting conditions (**Chapter 3**). I also further tested the action of recombinant SIRT5 variants on a more physiological substrate: succinylated fibroblasts cell lysates. The cell lysates were succinylated with succinic

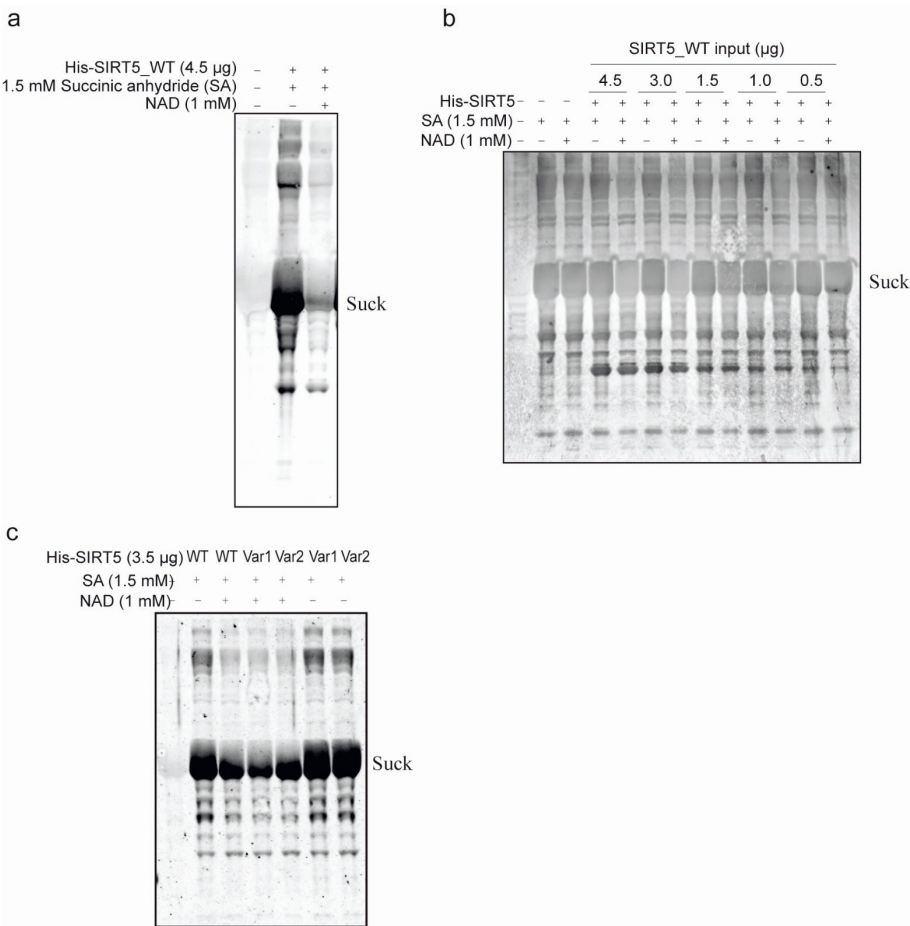


Figure 3. NAD⁺-dependent desuccinylase activity of recombinant SIRT5 on succinylated fibroblasts cell lysates. (a) Desuccinylation of His-SIRT5 WT on succinylated fibroblasts. (b) Titration of His-SIRT5 input in the desuccinylation assay. (c) Desuccinylation of His-SIRT5 WT and two variants on succinylated fibroblasts

anhydride, incubated with recombinant SIRT5 together with NAD⁺, finally the lysine succinylation levels, detected with Western blotting, was used to indicate the desuccinylase activity of the SIRT5⁷². I observed robust desuccinylase activity of SIRT5 WT under abundant (co)enzyme input (4.5 µg SIRT5, 1 mM NAD⁺) (Fig. 3a). A titration assay showed that around 3 µg SIRT5 input was required for an evident desuccinylation (Fig. 3b), which was still 100-fold of the input used in fluor de lys assay (0.03 µg). We then tested WT and SIRT5 variants desuccinylation activity, and a mild desuccinylation was observed in both WT and SIRT5 variants without clear difference between them (Fig. 3c). On the one hand, this observation supports the results from fluor de lys assay that the impact of SIRT5 variant on its enzymatic activity is subtle. On the other hand, it also shows the sensitivity of fluor de lys assay to detect clear desuccinylase activity with limited input of substrates.

The implications of this research and recommendations for future research

Because the strong association between redox imbalance and mitochondrial diseases⁷³, major and ongoing efforts have been made on developing and testing antioxidant treatments for this disorder^{74, 75, 76, 77, 78}. Some antioxidants hold great promise based on clinical outcomes and some were approved for treatment of certain type of mitochondrial disease. For instance, KH176, a derivative of water-soluble form of vitamin E, acts as a potent ROS modulator in patients' fibroblasts. In a phase II clinical trial, although no primary functional improvements were observed, it was reported to be safe and to have a positive effect on alertness and mood in patients with mitochondrial m.3243A>G disorders⁷⁵. Idebenone, an analogue of coenzyme Q, is a potent antioxidant and can serve as an inhibitor for lipid peroxidation by facilitating electrons to pass through complex I rather than escape⁷⁹. Clinical trials have provided evidence for persistent beneficial effects of idebenone on visual acuity in Leber's hereditary optic neuropathy (LHON) patients with discordant visual acuities^{76, 80}. Recently, idebenone has been approved for treatment in adolescent and adult patients with LHON⁸¹. Here, given the clear redox interruption observed in the two SIRT5 patients' fibroblasts, restoration of redox homeostasis with some approved antioxidants could be a direction for mitigating the symptoms of the two patients.

Beyond the involvement in genetic mitochondrial diseases, or other metabolic disorders, redox imbalance also occurs during natural ageing process, which, in turn, is associated with multiple age-related diseases, such as cancer, diabetes, and neurodegenerative diseases^{82, 83}. Sirtuins have gained much attention for their involvement in ageing and ageing-related disease. This has in fact largely started sirtuin research following the reports that Sir2 overexpression extended life span,

first in *S. cerevisiae* and then in *C. elegans* and *Drosophila*^{84, 85, 86}. However, a big debate subsequently ensued because studies in both *C. elegans* and *Drosophila* have challenged the life-extending effects of sirtuins. The longevity phenotype was still present in the setting of Sir2 knockdown and other genes were suggested to be responsible for the life-extending effect⁸⁷. Nevertheless, some mammalian sirtuins have shown longevity-associated effects. Overexpression of SIRT1 and SIRT6 increased lifespan in male mice^{88, 89}. Furthermore, sirtuins have been suggested to modulate health span via playing protective roles in age-related diseases⁹⁰. SIRT1 was demonstrated to play a neuroprotective role in the setting of neurodegenerative diseases. Mutant huntingtin-induced abnormal phenotypes were attenuated in SIRT1-overexpressed Huntington's disease mice, and knockdown of SIRT1 in cell line models exacerbated the mutant huntingtin toxicity⁹¹. Cardiovascular disease is another common disease of which occurrence increases with age⁹². SIRT3-ablated mice developed cardiac hypertrophy at age of 13 months, whereas SIRT3 overexpression blocked hypertrophic stimuli via upregulation on antioxidant systems^{28, 93}. These findings reveal that mammalian sirtuins are strongly associated with age-related disease as well as emphasize the potential therapeutic targets of the sirtuins for age-related disease. So far, less is known about the role for SIRT5 in these age-related diseases. Given the strong involvement of SIRT5 in redox homeostasis supported by our findings as well as reports from other studies, for future studies, it is worthwhile to investigate the relationship between SIRT5 and metabolic health during process of ageing, which can be considered as a stressor in this context.

Sirtuins have been inferred to play an important role in human metabolic health for long time since their deacylase activities were discovered to be NAD⁺-dependent. In spite of this, direct evidence showing physiological relevance for sirtuins is very limited. To date, SIRT6 was the only one in the mammalian sirtuin family supported by clear evidence for its essential role in humans. A homozygous *SIRT6* variant (187G>C) was demonstrated to be prenatally lethal in four affected fetuses from one family⁹⁴. This SIRT6 variant resulted in virtually complete loss of deacetylase and demyristoylase activities of SIRT6 and led to differentiation defects in both mouse embryonic stem cells and human induced pluripotent stem cells (iPSCs). Importantly, constitution of SIRT6 WT in iPSCs rescued the differentiation phenotypes, which strongly indicated the pathogenesis of the SIRT6 variant. In addition, there is some evidence suggesting the association of SIRT3 in human health. Single nucleotide polymorphisms (SNP) of SIRT3 have been suggested to be correlated with metabolic syndrome in humans⁹⁵ or be relevant with longevity in the Italian population⁹⁶. Here, my findings in this thesis add a new promising candidate, SIRT5, in the list.

Although the severe clinical anomalies observed in the SIRT5 patients suggested that SIRT5 is required for human normal health, overexpression of SIRT5 has also been shown to be associated with different types of human cancers, such as breast tumors, colorectal carcinoma, hepatocellular carcinoma^{6, 97, 98, 99}. This high SIRT5 expression was generally associated with poor survival rates. Very recently, SIRT5 was shown to be a promising therapeutic target for breast cancer. Either genetic deletion or chemical inhibition of SIRT5 reduced tumorigenesis and mammary tumor growth mouse models as well as in breast cancer cell lines¹⁰⁰. Clearly, biological role for SIRT5 is complex *in vivo* and its expression and function must be tightly controlled to maintain human health. More research is required to fully understand SIRT5 biology and its modulation *in vivo*. This will also provide a fundamental basis for targeting it as a therapeutic strategy.

References

1. Du, J., *et al.* Sirt5 is a NAD-dependent protein lysine demalonylase and desuccinylase. *Science* **334**, 806-809 (2011).
2. Tan, M., *et al.* Lysine glutarylation is a protein posttranslational modification regulated by SIRT5. *Cell Metab.* **19**, 605-617 (2014).
3. Nakagawa, T., Lomb, D.J., Haigis, M.C. & Guarente, L. SIRT5 Deacetylates carbamoyl phosphate synthetase 1 and regulates the urea cycle. *Cell* **137**, 560-570 (2009).
4. Wang, G., *et al.* Regulation of UCP1 and Mitochondrial Metabolism in Brown Adipose Tissue by Reversible Succinylation. *Mol. Cell* **74**, 844-857 e847 (2019).
5. Sadhukhan, S., *et al.* Metabolomics-assisted proteomics identifies succinylation and SIRT5 as important regulators of cardiac function. *Proc. Natl. Acad. Sci. U. S. A.* **113**, 4320-4325 (2016).
6. Kumar, S. & Lombard, D.B. Functions of the sirtuin deacylase SIRT5 in normal physiology and pathobiology. *Crit. Rev. Biochem. Mol. Biol.* **53**, 311-334 (2018).
7. Alston, C.L., Rocha, M.C., Lax, N.Z., Turnbull, D.M. & Taylor, R.W. The genetics and pathology of mitochondrial disease. *J. Pathol.* **241**, 236-250 (2017).
8. Labbadia, J. & Morimoto, R.I. The biology of proteostasis in aging and disease. *Annu. Rev. Biochem.* **84**, 435-464 (2015).
9. Ciechanover, A. Proteolysis: from the lysosome to ubiquitin and the proteasome. *Nat. Rev. Mol. Cell Biol.* **6**, 79-87 (2005).
10. Park, J., *et al.* SIRT5-mediated lysine desuccinylation impacts diverse metabolic pathways. *Mol. Cell* **50**, 919-930 (2013).
11. Rardin, M.J., *et al.* SIRT5 regulates the mitochondrial lysine succinylome and metabolic networks. *Cell Metab.* **18**, 920-933 (2013).
12. Nishida, Y., *et al.* SIRT5 Regulates both Cytosolic and Mitochondrial Protein Malonylation with Glycolysis as a Major Target. *Mol. Cell* **59**, 321-332 (2015).
13. Mari, M., Morales, A., Colell, A., Garcia-Ruiz, C. & Fernandez-Checa, J.C. Mitochondrial glutathione, a key survival antioxidant. *Antioxid. Redox Signal.* **11**, 2685-2700 (2009).
14. Ingold, I., *et al.* Selenium Utilization by GPX4 Is Required to Prevent Hydroperoxide-Induced Ferroptosis. *Cell* **172**, 409-422 e421 (2018).
15. Savaskan, N.E., Ufer, C., Kuhn, H. & Borchert, A. Molecular biology of glutathione peroxidase 4: from genomic structure to developmental expression and neural function. *Biol. Chem.* **388**, 1007-1017 (2007).
16. Yang, Y. & Gibson, G.E. Succinylation Links Metabolism to Protein Functions. *Neurochem. Res.* **44**, 2346-2359 (2019).
17. Gut, P., *et al.* SUCLA2 mutations cause global protein succinylation contributing to the pathomechanism of a hereditary mitochondrial disease. *Nat. Commun.* **11**, 5927 (2020).
18. Brookes, P.S. Mitochondrial H(+) leak and ROS generation: an odd couple. *Free Radic. Biol. Med.* **38**, 12-23 (2005).
19. Koenig, M.K. Presentation and diagnosis of mitochondrial disorders in children. *Pediatr. Neurol.* **38**, 305-313 (2008).
20. Ullah, M.S., Davies, A.J. & Halestrap, A.P. The plasma membrane lactate transporter MCT4, but not MCT1, is up-regulated by hypoxia through a HIF-1alpha-dependent mechanism. *J. Biol. Chem.* **281**, 9030-9037 (2006).
21. Esposito, L.A., Melov, S., Panov, A., Cottrell, B.A. & Wallace, D.C. Mitochondrial disease in mouse results in increased oxidative stress. *Proc. Natl. Acad. Sci. U. S. A.* **96**, 4820-4825 (1999).
22. Kirkinezos, I.G. & Moraes, C.T. Reactive oxygen species and mitochondrial diseases. *Semin. Cell Dev. Biol.* **12**, 449-457 (2001).

23. Singh, C.K., *et al.* The Role of Sirtuins in Antioxidant and Redox Signaling. *Antioxid. Redox Signal.* **28**, 643-661 (2018).
24. Radak, Z., *et al.* Redox-regulating sirtuins in aging, caloric restriction, and exercise. *Free Radic. Biol. Med.* **58**, 87-97 (2013).
25. Hsu, C.P., *et al.* Silent information regulator 1 protects the heart from ischemia/reperfusion. *Circulation* **122**, 2170-2182 (2010).
26. Brunet, A., *et al.* Stress-dependent regulation of FOXO transcription factors by the SIRT1 deacetylase. *Science* **303**, 2111-2115 (2004).
27. Mattagajasingh, I., *et al.* SIRT1 promotes endothelium-dependent vascular relaxation by activating endothelial nitric oxide synthase. *Proc. Natl. Acad. Sci. U. S. A.* **104**, 14855-14860 (2007).
28. Sundaresan, N.R., *et al.* Sirt3 blocks the cardiac hypertrophic response by augmenting Foxo3a-dependent antioxidant defense mechanisms in mice. *J. Clin. Invest.* **119**, 2758-2771 (2009).
29. Hasegawa, K., *et al.* Sirt1 protects against oxidative stress-induced renal tubular cell apoptosis by the bidirectional regulation of catalase expression. *Biochem. Biophys. Res. Commun.* **372**, 51-56 (2008).
30. Yu, W., Dittenhafer-Reed, K.E. & Denu, J.M. SIRT3 protein deacetylates isocitrate dehydrogenase 2 (IDH2) and regulates mitochondrial redox status. *J. Biol. Chem.* **287**, 14078-14086 (2012).
31. Zhou, L., *et al.* SIRT5 promotes IDH2 desuccinylation and G6PD deglutarylation to enhance cellular antioxidant defense. *EMBO Rep.* **17**, 811-822 (2016).
32. Schieber, M. & Chandel, N.S. ROS function in redox signaling and oxidative stress. *Curr. Biol.* **24**, R453-462 (2014).
33. D'Autreaux, B. & Toledano, M.B. ROS as signalling molecules: mechanisms that generate specificity in ROS homeostasis. *Nat. Rev. Mol. Cell Biol.* **8**, 813-824 (2007).
34. Box, H.C., *et al.* Radiation-induced formation of a crosslink between base moieties of deoxyguanosine and thymidine in deoxygenated solutions of d(CpGpTpA). *Radiat. Res.* **145**, 641-643 (1996).
35. Fuciarelli, A.F., Shum, F.Y. & Raleigh, J.A. Stereoselective intramolecular cyclization in irradiated nucleic acids: R- and S-8,5'-cycloadenosine in polyadenylic acid. *Biochem. Biophys. Res. Commun.* **134**, 883-887 (1986).
36. Dizdaroglu, M. & Jaruga, P. Mechanisms of free radical-induced damage to DNA. *Free Radic. Res.* **46**, 382-419 (2012).
37. Amici, A., Levine, R.L., Tsai, L. & Stadtman, E.R. Conversion of amino acid residues in proteins and amino acid homopolymers to carbonyl derivatives by metal-catalyzed oxidation reactions. *J. Biol. Chem.* **264**, 3341-3346 (1989).
38. Bartsaghi, S. & Radi, R. Fundamentals on the biochemistry of peroxynitrite and protein tyrosine nitration. *Redox Biol.* **14**, 618-625 (2018).
39. Cremers, C.M. & Jakob, U. Oxidant sensing by reversible disulfide bond formation. *J. Biol. Chem.* **288**, 26489-26496 (2013).
40. Sitte, N. Oxidative Damage to Proteins. In: *Aging at the Molecular Level* (ed von Zglinicki T). Springer Netherlands (2003).
41. Starke, P.E., Oliver, C.N. & Stadtman, E.R. Modification of hepatic proteins in rats exposed to high oxygen concentration. *FASEB J.* **1**, 36-39 (1987).
42. Xu, L., Davis, T.A. & Porter, N.A. Rate constants for peroxidation of polyunsaturated fatty acids and sterols in solution and in liposomes. *J. Am. Chem. Soc.* **131**, 13037-13044 (2009).
43. Kanner, J., German, J.B. & Kinsella, J.E. Initiation of lipid peroxidation in biological systems. *Crit. Rev. Food Sci. Nutr.* **25**, 317-364 (1987).

44. Massey, K.A. & Nicolaou, A. Lipidomics of polyunsaturated-fatty-acid-derived oxygenated metabolites. *Biochem. Soc. Trans.* **39**, 1240-1246 (2011).
45. Pamplona, R. Membrane phospholipids, lipoxidative damage and molecular integrity: a causal role in aging and longevity. *Biochim. Biophys. Acta* **1777**, 1249-1262 (2008).
46. Chen, J.J. & Yu, B.P. Alterations in mitochondrial membrane fluidity by lipid peroxidation products. *Free Radic. Biol. Med.* **17**, 411-418 (1994).
47. Refsgaard, H.H., Tsai, L. & Stadtman, E.R. Modifications of proteins by polyunsaturated fatty acid peroxidation products. *Proc. Natl. Acad. Sci. U. S. A.* **97**, 611-616 (2000).
48. Esterbauer, H., Schaur, R.J. & Zollner, H. Chemistry and biochemistry of 4-hydroxynonenal, malonaldehyde and related aldehydes. *Free Radic. Biol. Med.* **11**, 81-128 (1991).
49. Burcham, P.C. & Kuhan, Y.T. Introduction of carbonyl groups into proteins by the lipid peroxidation product, malondialdehyde. *Biochem. Biophys. Res. Commun.* **220**, 996-1001 (1996).
50. Chinta, S.J. & Andersen, J.K. Redox imbalance in Parkinson's disease. *Biochim. Biophys. Acta* **1780**, 1362-1367 (2008).
51. Friedmann Angeli, J.P., *et al.* Inactivation of the ferroptosis regulator Gpx4 triggers acute renal failure in mice. *Nat. Cell Biol.* **16**, 1180-1191 (2014).
52. Imai, H. & Nakagawa, Y. Biological significance of phospholipid hydroperoxide glutathione peroxidase (PHGPx, GPx4) in mammalian cells. *Free Radic. Biol. Med.* **34**, 145-169 (2003).
53. Nomura, K., Imai, H., Koumura, T., Kobayashi, T. & Nakagawa, Y. Mitochondrial phospholipid hydroperoxide glutathione peroxidase inhibits the release of cytochrome c from mitochondria by suppressing the peroxidation of cardiolipin in hypoglycaemia-induced apoptosis. *Biochem. J.* **351**, 183-193 (2000).
54. Thompson, K., *et al.* Recent advances in understanding the molecular genetic basis of mitochondrial disease. *J. Inherit. Metab. Dis.* **43**, 36-50 (2020).
55. Galanis, M., Devenish, R.J. & Nagley, P. Duplication of leader sequence for protein targeting to mitochondria leads to increased import efficiency. *FEBS Lett.* **282**, 425-430 (1991).
56. Chin, R.M., Panavas, T., Brown, J.M. & Johnson, K.K. Optimized Mitochondrial Targeting of Proteins Encoded by Modified mRNAs Rescues Cells Harboring Mutations in mtATP6. *Cell Rep.* **22**, 2818-2826 (2018).
57. Mackenzie, J., Pedersen, L., Arent, S. & Henriksen, A. Controlling electron transfer in Acyl-CoA oxidases and dehydrogenases: a structural view. *J. Biol. Chem.* **281**, 31012-31020 (2006).
58. Ruzicka, F.J. & Beinert, H. A new iron-sulfur flavoprotein of the respiratory chain. A component of the fatty acid beta oxidation pathway. *J. Biol. Chem.* **252**, 8440-8445 (1977).
59. Ramsay, R.R., Steenkamp, D.J. & Husain, M. Reactions of electron-transfer flavoprotein and electron-transfer flavoprotein: ubiquinone oxidoreductase. *Biochem. J.* **241**, 883-892 (1987).
60. Anderson, E.J., Yamazaki, H. & Neuffer, P.D. Induction of endogenous uncoupling protein 3 suppresses mitochondrial oxidant emission during fatty acid-supported respiration. *J. Biol. Chem.* **282**, 31257-31266 (2007).
61. Seifert, E.L., Estey, C., Xuan, J.Y. & Harper, M.E. Electron transport chain-dependent and -independent mechanisms of mitochondrial H₂O₂ emission during long-chain fatty acid oxidation. *J. Biol. Chem.* **285**, 5748-5758 (2010).
62. St-Pierre, J., Buckingham, J.A., Roebuck, S.J. & Brand, M.D. Topology of superoxide production from different sites in the mitochondrial electron transport chain. *J. Biol. Chem.* **277**, 44784-44790 (2002).
63. Perevoshchikova, I.V., Quinlan, C.L., Orr, A.L., Gerencser, A.A. & Brand, M.D. Sites of superoxide and hydrogen peroxide production during fatty acid oxidation in rat skeletal muscle mitochondria. *Free Radic. Biol. Med.* **61**, 298-309 (2013).

64. Quinlan, C.L., Perevoshchikova, I.V., Hey-Mogensen, M., Orr, A.L. & Brand, M.D. Sites of reactive oxygen species generation by mitochondria oxidizing different substrates. *Redox Biol.* **1**, 304-312 (2013).
65. Kussmaul, L. & Hirst, J. The mechanism of superoxide production by NADH:ubiquinone oxidoreductase (complex I) from bovine heart mitochondria. *Proc. Natl. Acad. Sci. U. S. A.* **103**, 7607-7612 (2006).
66. Turrens, J.F., Alexandre, A. & Lehninger, A.L. Ubisemiquinone is the electron donor for superoxide formation by complex III of heart mitochondria. *Arch. Biochem. Biophys.* **237**, 408-414 (1985).
67. Batandier, C., *et al.* The ROS production induced by a reverse-electron flux at respiratory-chain complex 1 is hampered by metformin. *J. Bioenerg. Biomembr.* **38**, 33-42 (2006).
68. Murphy, Michael P. How mitochondria produce reactive oxygen species. *Biochem. J.* **417**, 1-13 (2009).
69. Pacella-Ince, L., Zander-Fox, D.L. & Lane, M. Mitochondrial SIRT5 is present in follicular cells and is altered by reduced ovarian reserve and advanced maternal age. *Reprod. Fertil. Dev.* **26**, 1072-1083 (2014).
70. Polletta, L., *et al.* SIRT5 regulation of ammonia-induced autophagy and mitophagy. *Autophagy* **11**, 253-270 (2015).
71. Yang, L., *et al.* Desuccinylation-Triggered Peptide Self-Assembly: Live Cell Imaging of SIRT5 Activity and Mitochondrial Activity Modulation. *J. Am. Chem. Soc.* **142**, 18150-18159 (2020).
72. Pougovkina, O.A. Functional interplay between protein acylation and cellular metabolism in metabolic disorders.) (2016).
73. Hayashi, G. & Cortopassi, G. Oxidative stress in inherited mitochondrial diseases. *Free Radic. Biol. Med.* **88**, 10-17 (2015).
74. Russell, O.M., Gorman, G.S., Lightowlers, R.N. & Turnbull, D.M. Mitochondrial Diseases: Hope for the Future. *Cell* **181**, 168-188 (2020).
75. Janssen, M.C.H., *et al.* The KHENERGY Study: Safety and Efficacy of KH176 in Mitochondrial m.3243A>G Spectrum Disorders. *Clin. Pharmacol. Ther.* **105**, 101-111 (2019).
76. Klopstock, T., *et al.* Persistence of the treatment effect of idebenone in Leber's hereditary optic neuropathy. *Brain* **136**, e230 (2013).
77. Karaa, A., *et al.* Randomized dose-escalation trial of elamipretide in adults with primary mitochondrial myopathy. *Neurology* **90**, e1212-e1221 (2018).
78. Koopman, W.J., *et al.* Mitigation of NADH: ubiquinone oxidoreductase deficiency by chronic Trolox treatment. *Biochim. Biophys. Acta* **1777**, 853-859 (2008).
79. Haefeli, R.H., *et al.* NQO1-dependent redox cycling of idebenone: effects on cellular redox potential and energy levels. *PLoS One* **6**, e17963 (2011).
80. Klopstock, T., *et al.* A randomized placebo-controlled trial of idebenone in Leber's hereditary optic neuropathy. *Brain* **134**, 2677-2686 (2011).
81. Lyseng-Williamson, K.A. Idebenone: A Review in Leber's Hereditary Optic Neuropathy. *Drugs* **76**, 805-813 (2016).
82. Go, Y.M. & Jones, D.P. Redox theory of aging: implications for health and disease. *Clin Sci (Lond)* **131**, 1669-1688 (2017).
83. Szentesi, P., Csernoch, L., Dux, L. & Keller-Pinter, A. Changes in Redox Signaling in the Skeletal Muscle with Aging. *Oxid. Med. Cell. Longev.* **2019**, 4617801 (2019).
84. Tissenbaum, H.A. & Guarente, L. Increased dosage of a sir-2 gene extends lifespan in *Caenorhabditis elegans*. *Nature* **410**, 227-230 (2001).
85. Viswanathan, M., Kim, S.K., Berdichevsky, A. & Guarente, L. A role for SIR-2.1 regulation of ER stress response genes in determining *C. elegans* life span. *Dev. Cell* **9**, 605-615 (2005).

86. Rogina, B. & Helfand, S.L. Sir2 mediates longevity in the fly through a pathway related to calorie restriction. *Proc. Natl. Acad. Sci. U. S. A.* **101**, 15998-16003 (2004).
87. Burnett, C., *et al.* Absence of effects of Sir2 overexpression on lifespan in *C. elegans* and *Drosophila*. *Nature* **477**, 482-485 (2011).
88. Kanfi, Y., *et al.* The sirtuin SIRT6 regulates lifespan in male mice. *Nature* **483**, 218-221 (2012).
89. Satoh, A., *et al.* Sirt1 extends life span and delays aging in mice through the regulation of Nk2 homeobox 1 in the DMH and LH. *Cell Metab.* **18**, 416-430 (2013).
90. Imai, S. & Guarente, L. NAD⁺ and sirtuins in aging and disease. *Trends Cell Biol.* **24**, 464-471 (2014).
91. Jiang, M., *et al.* Neuroprotective role of Sirt1 in mammalian models of Huntington's disease through activation of multiple Sirt1 targets. *Nat. Med.* **18**, 153-158 (2011).
92. Favero, G., Franceschetti, L., Rodella, L.F. & Rezzani, R. Sirtuins, aging, and cardiovascular risks. *Age (Dordr)* **37**, 9804 (2015).
93. Hafner, A.V., *et al.* Regulation of the mPTP by SIRT3-mediated deacetylation of CypD at lysine 166 suppresses age-related cardiac hypertrophy. *Aging* **2**, 914-923 (2010).
94. Ferrer, C.M., *et al.* An inactivating mutation in the histone deacetylase SIRT6 causes human perinatal lethality. *Genes Dev.* **32**, 373-388 (2018).
95. Hirschey, M.D., *et al.* SIRT3 deficiency and mitochondrial protein hyperacetylation accelerate the development of the metabolic syndrome. *Mol. Cell* **44**, 177-190 (2011).
96. Albani, D., *et al.* Modulation of human longevity by SIRT3 single nucleotide polymorphisms in the prospective study "Treviso Longeva (TRELONG)". *Age (Dordr)* **36**, 469-478 (2014).
97. Wang, Y.Q., *et al.* Sirtuin5 contributes to colorectal carcinogenesis by enhancing glutaminolysis in a deglutarylation-dependent manner. *Nat. Commun.* **9**, 545 (2018).
98. Chang, L., *et al.* SIRT5 promotes cell proliferation and invasion in hepatocellular carcinoma by targeting E2F1. *Mol. Med. Rep.* **17**, 342-349 (2018).
99. Greene, K.S., *et al.* SIRT5 stabilizes mitochondrial glutaminase and supports breast cancer tumorigenesis. *Proc. Natl. Acad. Sci. U. S. A.*, (2019).
100. Abril, Y.L.N., *et al.* Pharmacological and genetic perturbation establish SIRT5 as a promising target in breast cancer. *Oncogene* **40**, 1644-1658 (2021).

Summary

Mitochondria play a central role in cellular function and ultimate in organism health through their distinct bioenergetic, biosynthetic, and intracellular signaling functions. A number of human diseases are associated with mitochondrial dysfunctions, among them, genetic mitochondrial diseases. These disorders are caused by genetic variants in mitochondrial or nuclear DNA that encode the mitochondrial proteins. Sirtuin 5 (SIRT5) is a mitochondrial protein with a role in post-translational modifications homeostasis. It is a versatile NAD⁺-dependent desuccinylase, demalonylase and deglutarylase, with robust activities removing lysine succinyl-, malonyl- and glutaryl- groups on many metabolic enzymes. Using genetically modified mouse models, it was shown that SIRT5 is involved in various major metabolic pathways and that it plays an important role in metabolic response to environmental stress. Inconsistency in its regulatory roles of enzymatic activities and the fact that tissue specific SIRT5 knockout mice failed to produce the phenotypes observed in whole-body knockout mice illustrate the complexity of SIRT5 biology. More importantly, all studies addressing the biological function of SIRT5 were performed in animals or cell lines. It is therefore unclear, whether or not SIRT5 has an essential role in maintaining human metabolic health.

In this thesis, I reported two novel homozygous *SIRT5* variants in two independent patients with clinical mitochondrial disease manifestations, especially mitochondrial encephalopathy. The availability of primary skin fibroblasts from these patients provided me the opportunity to explore the physiopathological relevance of SIRT5 in humans and to gain insight in the SIRT5 biological function in humans.

The overall aim of this thesis was to improve our knowledge of the biological function of SIRT5 and to provide evidence for the physiological relevance of SIRT5 in human health and disease. The specific aims were: (1) To better understand the biological function of SIRT5 and how human SIRT5 variants relate to human disease. (2) To optimize an enzymatic assay for gaining better insight into cellular SIRT5 biochemical activity under different metabolic conditions. (3) To develop a new statistical model to better analyse effects of SIRT5 on the mitochondrial bioenergetic function assessed by Seahores extracellular flux analysis.

SIRT5 has been shown to play its biological roles in a highly context-dependent fashion, and different intracellular metabolic conditions may significantly affect its enzymatic activity. In **Chapter 2** of this thesis, I optimized a fluorescence (fluor de lys) based desuccinylase activity assay to analyse the intracellular NAD⁺-dependent desuccinylase activity in whole cell lysates. I discovered distinct NAD⁺-dependent desuccinylase activities, for which SIRT5 was partially responsible. In addition, SIRT5 protein level was higher in differentiated C2C12 and 3T3-L1 cells as compared to

their proliferative counterparts, whereas the desuccinylase activity was lower. Thus, NAD⁺-dependent desuccinylase activity in crude cell lysates varied between different metabolic conditions. The mismatch between SIRT5 protein level and the desuccinylase activity highlights the importance of analysing NAD⁺-dependent desuccinylase activity, over only analysing expression of proteins.

In **Chapter 3**, I aimed to understand whether the *SIRT5* variants identified in patients were associated with biological defects by studying the biochemistry of the SIRT5 variants as well as their biological impacts. Enzymatic kinetics of recombinant SIRT5 variants were mildly affected as compared to SIRT5 wild-type (WT), and thermal stabilities of SIRT5 variants were evidently decreased. It reflected at cellular level with strikingly reduced SIRT5 protein levels in the patients-derived SIRT5 variant fibroblasts as compared to controls. As a result, global succinylation levels were significantly increased in the patients' fibroblasts. Among an array of mitochondrial functional analyses under different stress conditions, increased proton leak rates were the most consistent and pronounced phenotype under galactose culture medium, a metabolic challenging condition where fibroblasts were forced to strongly rely on mitochondrial respiration and consequently led to higher cellular ROS level. Further analysis showed that redox couple NADPH/NADP⁺ was decreased by 50% in patients under galactose condition. Although no difference was observed under basal condition, intracellular ROS accumulation rates were significantly higher in the SIRT5 variant fibroblasts upon exogenous H₂O₂ challenge. Also, the H₂O₂-induced intracellular ROS accumulation rates were positively related to intracellular NADPH/NADP⁺ ratios ($R^2 = 0.9476$), suggesting a mechanistic link between the two phenotypes. To conclude, this study showed that each of the two *SIRT5* variants was a loss-of-function variant and that redox homeostasis was significantly perturbed in the SIRT5 variant human fibroblasts. It highlights the important role for SIRT5 in maintaining human redox homeostasis.

Next, in **Chapter 4**, I further looked into redox system to understand how the redox balance was affected by the SIRT5 variants. As shown in **Chapter 3**, the redox perturbation phenotypes were evident under oxidants-stimulating conditions such as galactose medium and exogenous H₂O₂ application. I, therefore, hypothesized that antioxidant systems were impaired and led to the redox imbalance in the patients. To test this, I focused on the glutathione (GSH)- and thioredoxin-dependent systems, two important antioxidant defense systems in mitochondria. In the SIRT5 variant fibroblasts, intracellular GSH levels were significantly higher, 1.5-fold of controls, while glutathione reductase (GR) was surprisingly 2-fold lower than controls at gene expression as well as enzymatic activity level. In contrast, glutathione peroxidase 4 (GPx4) was significantly increased by 1.5-fold at transcriptional level in the SIRT5

variant fibroblasts. These changes showed an impairment in the GSH-dependent antioxidant system, which, in turn, made the patients' fibroblasts less dependent on GSH-antioxidant defense system, as supported by the observation of blunted response to BSO-induced GSH deprivation. In contrast to evident decrease in cell viability associated with increased ROS levels observed in control fibroblasts subjected to BSO, no apparent changes were detected in the SIRT5 variant fibroblasts. In addition, longer time was needed for the SIRT5 variant fibroblasts to show BSO-induced cell morphological damage as compared to controls. As a result of decreased dependence on impaired GSH antioxidant system, the SIRT5 fibroblasts were more sensitive to inhibition of thioredoxin system, as evidenced by the morphological changes and increased ROS levels upon auranofin treatment, a well-established thioredoxin reductases inhibitor. Collectively, this study showed that SIRT5 variant fibroblasts displayed an impaired GSH-dependent antioxidant system associated with a disrupted glutathione-thioredoxin balance.

Mitochondria play a central role in metabolic health and the bioenergetic capacity is one of the important parameters for indicating their functions. Seahorse extracellular flux analyzer, a widely-used platform, monitors real-time oxygen consumption rate (OCR) in living cells. Several application features make the Seahorse analyzer a powerful tool to assess the mitochondrial bioenergetics with sophisticated experimental setup. As a result, a complex structure is hidden in Seahorse data, which has received little attention in the current Seahorse analysis methods and can weaken the robustness of the statistical inference.

Chapter 5 describes a novel Bayesian hierarchical statistical model incorporating the complex Seahorse data structure. The complexity of Seahorse data structure arises from factors at several levels embedded in the most assay settings. The multi-well (96- or 24-well) system provides the possibility to test different biological samples subjected to a number of metabolic conditions (factor of experimental groups); there are several distinct measurement phases with typically three measurement cycles for each phase over the assay (factor of measurements), because consecutive injections of chemicals of interest can be applied to cells across wells in one plate (factor of wells). In the fully Bayesian model, these factors at the different levels were taken into account. In addition, the model was applied to two assays where I investigated the effects of a SIRT5 variant as well as a novel SIRT5 inhibitor on the human fibroblasts' bioenergetics. The results showed that this model can propagate uncertainty in the OCR measurements into the posterior estimation of the mitochondrial respiration. Importantly, this Bayesian hierarchical model can be applied to other studies by incorporating different level of factors.

In **Chapter 6**, the findings of this thesis are discussed. In conclusion, this thesis highlights the critical role for SIRT5 in regulating human redox homeostasis and shows that SIRT5 loss-of-function variants are associated with mitochondrial disease. In **Chapter 6**, it is argued that the pathological mechanism by which SIRT5 deficiency caused the disease is likely via the SIRT5/GSH system/oxidative stress axis. Given the evident redox perturbation in the SIRT5 variant fibroblasts, approved antioxidant treatments hold promise to restore redox homeostasis and ultimately alleviate the symptoms of the SIRT5 patients. Redox imbalance also occurs in other physiological contexts such as ageing, and it would be worthwhile to study SIRT5 in that context. Future studies on the interplay between SIRT5 and redox biology are likely to contribute to our understanding of the role for SIRT5 in human health and disease.

Acknowledgements

At the end of my thesis, I would like to take the opportunity to thank my supervisors, colleagues, friends and family who have helped me make this thesis possible and supported me in any way.

First of all, I would like to thank my (co)promoters Jaap and Vincent. Jaap, I still clearly remember our first skype meeting, the interview talk and thank you for providing me the opportunity to conduct a PhD research at HAP. Thank you for all the nice ideas and providing different perspectives to tackle challenges. I appreciate your great support especially in the last phase of my PhD, which was a quite difficult period. Besides scientific discussion, thank you for being available to provide personal support as well as suggestions for my future development. Vincent, you were the first HAP colleague I met in live the first day I was at Zodiac, although we did not know each other at that time. Thank you for the opportunity you gave me to work on the SIRT5 patients project. This project led me to a very molecular biology field which was quite different from my background when I started, but I did find it interesting and had fun with it. I learned critical thinking from our discussions which helped me grow as a scientist. I am also very grateful for all your help in the past years.

Next, I would like to thank Dr. Rodenburg and Dr. Spelbrink for identifying the human SIRT5 variants in patients and for data discussion. My gratitude also goes to Werner, thank you for all the open scientific discussions, nice suggestions on my experiments, and for providing me the opportunity to try the ROS measurement in your lab in Nijmegen. I also want to thank Xiang for the help in Chapter 5 with developing the Bayesian model and data analysis.

I would like to acknowledge China Scholarship Council (CSC) for the financial support which allows me to perform a PhD research in the Netherlands.

I would also like to express my gratitude to the technicians who provided the technical support for my project. Annelies, thank you for your willingness to help and generate all the nice constructs in my project. Inge, thank you for the help in the qPCRs experiments and discussion on the results. Hans and Marcel, thank you for all your help in the histological work. Melissa, thank you for showing me the first qPCR experiment when I just arrived at HAP, I still remember it was about genotyping NNT knockout mice. Besides the specific help in my own project, I also would like to thank the technician team to keep the HAP lab organized.

Next, I would like to thank all the students and guest researchers who worked on my PhD project: Julia, Qing, Yi, Beshar, Erwin, Nick and Danjun. Thanks for your help in

setting up methods, data collection, and for everything I learned while working with you.

In addition, my gratitude goes to all other staff at HAP as well. Katja, I appreciate that you were always available for histological questions. Also, at personal level, thanks for all the talks and support in the last period of my PhD. Arie, Claudia, Deli, Evert, Sander, Sandra, and Silvie, thanks for your comments and suggestions from department scientific meetings. Furthermore, I would like to acknowledge our secretariat: Corine, Irene, Annet and Annika, for your important practical support.

And thanks to all HAPpy (former) PhD colleagues: Li, Lonneke, Wenbiao, Jeske, Marjanne, Jose, Lianne, Natasja, Bart, Miranda, Anna, Joëlle, Jingyi, Liangyu, Cresci-Anne, Peixin, Ferran, Qi, and Sarmad. I had many nice memories about all the Happy dinners, Halloween/SinterKlass activities, mudflat walking, filming movies and lunch break walks. I am very happy and feel lucky to have you guys as my fellow-PhDs.

Specially, I would like to thank Mr. and Mrs. Bekebrede, Anna's parents. Anna, thank you for inviting me to your parents' place, where I have always been welcome, and treated with nice food and surrounded with a lovely family atmosphere. These are really my sweet and special memories about the Netherlands 😊.

Anna and Jingyi, thank you for being willing to be my paranymphs and take the time to help me with the defence. I am very happy to have you supporting me on the stage on the day of my defence.

I also would like to thank my friendly roommates in 187, Zhaolin, Joke, Jiaru, Martijn, Dymphy, Cornine, Bram, Nico, Feline. You guys expanded my cooking knowledge as well as Dutch.

感谢我的中国小伙伴们，文彩芳，刘琅青，干劲，熊玲，邓亚乐，岳笑梅，李静，刘奇，徐蔚，夏淑雯，王芳，以及冯涛老师和张景艳老师。特别地，温柔的包曼师姐，感谢你在我刚来瓦村时对我的照顾，期待有一天我们可以再相遇。喳喳妹，转眼间我们已认识十多年！我很开心这段异国求学之路上有你。希望你的爱丁堡博后之旅开心顺利。曼琪，不知不觉我们也认识四年多了！我的哈外好邻居，感谢你的陪伴。曹露，在荷兰能再次相遇也是极大的缘分，你一直都很温柔，给人温暖，我相信不久的将来我们会再见的。

十分感谢我的家人。爸爸，您支撑起了整个家；妈妈，谢谢您对我无条件的呵护和支持，您永远都是我温暖的港湾；姐姐和哥哥，一直以来你们都为我树立了良好的榜样，回首我过去二十多年的求学之路，我一直都在追寻你们的足迹。我很珍惜你们，我也非常期待和你们团聚。

About the author

Curriculum Vitae

Taolin Yuan (袁桃林) was born on the 22nd of December 1992 in Anhui, the People's Republic of China. She started her BSc study in Animal Science in China Agricultural University in 2010 and graduated with honour in 2014. She developed interest in science during her BSc study. In the third year of her undergraduate study, she was funded with a one-year undergraduate research project in collaboration with the other fellow student. In this project, she investigated the potential interactive proteins of β -conglycinin in intestinal porcine enterocytes. After BSc, she was recommended for a master study (free from National Postgraduate Entrance Examination) and she decided to continue studying in Animal Nutrition and Feed Technology in China Agricultural University. During her MSc thesis, she investigated the effects of glucosamine supplementation on within-litter birthweight variation using the model of Sprague Dawley rat. She completed her MSc education and graduated in 2016. In the same year, she was granted by the China Scholarship Council (CSC) to pursue her PhD study outside of China. She decided to perform her PhD research in the Netherlands, and in September 2016, Taolin started her PhD at Human and Animal Physiology, Wageningen University & Research. During her PhD research, she focused on understanding sirtuin5 biology and investigating the physiopathological relevance of two *SIRT5* gene variants in human. The results of her PhD research are presented in this thesis.

Overview of completed training activities

Discipline specific activities

Course Laboratory animal science	(Utrecht, NL, 2016)
Course Advanced Statistics: Design of Experiments	(Wageningen, NL, 2016)
Course Epigenesis and epigenetics	(Wageningen, NL, 2017)
Course Shaping future animal systems	(Wageningen, NL, 2017)
Course International Advanced proteomics	(Wageningen, NL, 2017)
Mipschool on Mitochondrial Physiology	(Oberurg, AT, 2017)
Netherlands Mitochondrial Meeting	(Amsterdam, NL, 2018)
Conference The reversible protein acylation in health and in disease, <i>oral & poster presentation</i>	(Lisbon, PT, 2019)

General courses

VLAG PhD week	(VLAG, Baarlo, NL, 2016)
Course Project and time management	(WGS, Wageningen, NL, 2017)
Course Introduction to R	(VLAG, Wageningen, NL, 2017)
Course PhD Workshop Carousel	(WGS, Wageningen, NL, 2017)
Course Applied statistics	(VLAG, Wageningen, NL, 2017)
Course Presenting with Impact	(WGS, Wageningen, NL, 2019)
Course Critical thinking and Argumentation	(WGS, Wageningen, NL, 2020)
Course Brain-friendly working and writing	(WGS, Wageningen, NL, 2020)
Course Research Data Management	(Library, Wageningen, NL, 2020)
Course Supervising BSc & MSc thesis students	(WGS, Wageningen, NL, 2020)
Course Career Orientation	(WGS, Wageningen, NL, 2020)
Course RMarkdown	(VLAG, Wageningen, NL, 2020)

Other activities

Preparation of research proposal	(Wageningen, NL, 2016)
Weekly HAP group meetings	(Wageningen, NL, 2016-2019)
Journal Club HAP	(Wageningen, NL, 2017-2018)
Research progress day	(Wageningen, NL, 2018-2019)

Teaching activities

Development and Healthy Aging (HAP-31306)
Nutritional Physiology (HAP-30306)
Molecular Regulation of Health and Disease (HAP-31806)
Supervision of BSc and MSc thesis students (x 6)

Colophon

The research described in this thesis and printing of the thesis were financially supported by Human and Animal Physiology. China Scholarship Council (CSC) is acknowledged for providing the financial contribution to the author of this thesis.

Layout by: Taolin Yuan

Cover design by: Taolin Yuan & Jingyi Song

Printed by: ProefschriftMaken | DigiForce

